



**University of
Nottingham**

UK | CHINA | MALAYSIA

**Chemical and *in silico*
exploration of novel
5-hydroxytryptamine 2A receptor
(5-HT_{2A}R) ligands**

Luke Damerum

BSc., BSc., MRes., MRSC

Student ID: 20213169

**School of Pharmacy
University of Nottingham
Nottingham, UK**

**Thesis submitted to the University of Nottingham
for the degree of Doctor of Philosophy**

March 2024

Abstract

The 5-HT_{2A}R is a target in neuropsychiatric conditions such as psychosis, which is commonly managed with atypical antipsychotics. These have associated side effects due to off-target interactions. Consequently, there is a demand to develop therapeutics that exhibit no affinity for these off-target sites. Moreover, in recent 5-HT_{2A}R X-ray crystal structures, a unique hydrophobic pocket or passage between transmembrane helices 4 and 5 sets it apart from other 5-HT₂ receptor subtypes. This structural feature is implicated in the selectivity demonstrated by therapeutic pimavanserin towards the 5-HT_{2A}R, owing to its binding conformation. Thus, presenting it as a target to interrogate for enhancing 5-HT_{2A}R binding.

A structure-based approach was used to design a pimavanserin analogue series targeting transmembrane helices 4 and 5. *In silico* studies involving docking and MM-GBSA calculations using a 5-HT_{2A}R homology model (RMSD 0.09 Å) predicted several analogues to demonstrate improved binding compared to pimavanserin. Synthesis of the series yielded low to moderate yields. To evaluate the binding of the series experimentally a cell membrane-based fluorescent time-resolved Förster resonance energy transfer (TR-FRET) methodology was chosen. This led to the development of a high-affinity 5-HT_{2A}R fluorescent probe, and determination of kinetic rates, (K_d 1.74 ± 0.46 nM, K_{on} $1.96 \pm 0.13 \times 10^8$ M⁻¹ min⁻¹, and K_{off} 0.42 ± 0.02 min⁻¹) characterised at SNAP-tagged human 5-HT_{2A}R expressed in Chinese hamster ovary membranes.

Acknowledgement

I would like to give my greatest thankyou and appreciation to Associate Professor Shailesh Mistry and Professor Charles Laughton for their support in developing my PhD project, and their invaluable mentorship, contributions, and guidance throughout this journey. I am equally grateful to Associate Professor Rob Lane for his mentorship and contributions to my research.

I am deeply indebted to Lee Hibbett and technical staff, for their comprehensive laboratory guidance and support, which significantly enriched my PhD training and the outcome of this research.

I am profoundly grateful to all my friends and colleagues whom I have had the great honour to work alongside. Their support, teachings, and camaraderie have been invaluable in sustaining and enriching my academic journey.

Finally, Mum and Dad, I express my deepest love and gratitude for your unwavering support and constant encouragement throughout this journey. Yselkla, your care, support, and understanding have been a constant source of respite and grounding and have been instrumental in helping me overcome the last challenges.

This work was funded by the Biotechnology and Biological Sciences Research Council.



Table of contents

1. Introduction	1
1.1 5-HT receptor family	1
1.2 Therapeutic basis for targeting the 5-HT_{2A}R	2
1.3 5-HT_{2A}R signal transduction	4
1.3.1 5-HT _{2A} R signalling modulation	7
1.4 Therapeutics for 5-HT_{2A}R-associated neuropsychiatric disorders	9
1.5 5-HT_{2A}R X-ray crystal structures	12
1.6 5-HT_{2A}R molecular structure	14
1.6.1 5-HT _{2A} R structural transitions during activation	17
1.6.2 The 5-HT _{2A} R TM4-TM5 hydrophobic pocket	21
1.6.2.1 5-HT _{2A} R transmembrane helix 4	29
1.7 Selectively targeting the 5-HT_{2A}R	30
1.8 5-HT_{2A}R selective ligands	31
1.9 Pimavanserin	34
1.10 Pimavanserin structure-activity relationships	37
1.10.1 Ring A analogues	39
1.10.2 Ring B analogues	43
1.10.3 Ring C analogues	45
1.10.3.1 Extension of ring C	50
1.10.4 Pimavanserin scaffold core	51
1.11 Fluorescence-based methods to interrogate the 5-HT_{2A}R	52
1.12 <i>In silico</i> tools for exploration of the 5-HT_{2A}R	56
1.12.1 Homology modelling: building protein structure	57
1.12.2 Homology model assessment	59
1.12.3 Modelling ligand binding: molecular docking	61
1.12.3.1 Glide docking process summary	63
1.12.4 <i>In silico</i> calculations of binding free energy	67
1.12.4.1 MM-PBSA/GBSA methodology	67
1.12.4.2 Entropy and Enthalpy	73
1.12.5 Alternative <i>in silico</i> approaches to develop 5-HT _{2A} R ligands	74
1.13 Research aims and objectives	77
2. <i>In silico</i> exploration of pimavanserin analogues at the human 5-HT_{2A}R	78
2.1 Introduction	78
2.2 Aims	78
2.3 Designing the pimavanserin analogue series	78

Table of contents

2.4	5-HT_{2A}R homology model	82
2.4.1	Template search	82
2.4.2	Model Building	83
2.4.3	Ligand Modelling	84
2.4.4	Model quality assessment	84
2.5	Molecular docking protocol	87
2.5.1	Ligand preparation	87
2.5.2	Protein preparation	87
2.5.3	Receptor grid generation method	88
2.5.3.1	Receptor grid generation for pimavanserin	88
2.5.3.2	Receptor grid generation for pimavanserin analogues	89
2.5.4	Docking protocol	90
2.6	Molecular docking results and discussion	91
2.6.1	Glide results	91
2.6.2	Glide binding pose assessment	93
2.6.3	Glide discussion	99
2.6.4	MM-GBSA assessment	101
2.6.4.1	Ligand-5-HT _{2A} R complex refinement	102
2.6.5	MM-GBSA calculation discussion	107
2.7	Conclusion of pimavanserin analogue docking	109
3.	Design, synthesis, characterisation of 5-HT_{2A}R fluorescent probes	113
3.1	Introduction	113
3.1.1	5-HT ₂ receptor fluorescent probes	115
3.2	Aims	121
3.3	5-HT_{2A}R fluorescent probe design	121
3.3.1	The receptor targeting moiety	123
3.3.2	Linker region	126
3.3.3	Fluorophore	129
3.4	Proposed 5-HT_{2A}R fluorescent probes	132
3.4.1	Reterosynthetic analysis of proposed 5-HT _{2A} R fluorescent probes	133
3.5	Synthetic route to 5-HT_{2A}R fluorescent probes	135
3.6	Pharmacological characterisation of fluorescent probes binding to the human 5-HT_{2A}R	139
3.7	5-HT_{2A}R fluorescent probe pharmacology discussion	142
3.8	Conclusion of pharmacological characterisation of fluorescent probes binding to the human 5-HT_{2A}R	145

Table of contents

4. Synthesis and pharmacological evaluation of pimavanserin analogues	147
4.1 Introduction	147
4.2 Aims	149
4.3 Synthesis of structure-based pimavanserin analogues	150
4.3.1 Pimavanserin analogues synthesis route 1	150
4.3.2 Pimavanserin analogues synthesis route 2	151
4.4 Pharmacological characterisation of pimavanserin analogues binding to the human 5-HT_{2A}R	154
4.5 Conclusions of pimavanserin analogues binding to the human 5-HT_{2A}R	155
5. Future work	157
5.1.1 Binding affinity evaluation of the pimavanserin analogue series at the 5-HT ₂ receptor subtypes	157
5.1.2 Characterize fluorescent probes at 5-HT _{2C} R and 5-HT _{2B} R	158
5.1.3 Pimavanserin-based 5-HT _{2A} R fluorescent probe	159
5.1.4 Optimize Synthetic Route	161
6. Experimental	163
6.1 Pharmacology methods	163
6.1.2 Terbium labelling of SNAP-tagged cells	163
6.1.3 Fluorescent probe-binding assays	165
6.1.4 Determination of fluorescent probe binding kinetics	165
6.1.5 Unlabelled ligand-binding assays	166
6.1.6 Signal detection and data analysis	166
6.2 General chemistry	168
6.3 Fluorescent probe synthesis methods	171
6.4 Pimavanserin analogues synthesis methods	186
7. References	265

Table of Figures

Figure 1.3 1: Schematic of the G protein-coupled signalling pathways of the 5-HT receptor subtypes. **6**

Figure 1.3.1-1: Cubic ternary complex model of GPCR activation. A: agonist; G: G protein; Ri : inactive form of receptor; Ra: active form of receptor. Source: adapted from Kenakin 2002 ⁴⁷ **8**

Figure 1.4-1: Example of typical antipsychotic drugs haloperidol (1) and chlorpromazine (2). **9**

Figure 1.4-2: Example of atypical antipsychotic drugs clozapine (3), risperidone (4), olanzapine (5), ziprasidone (6), paliperidone (7), and asenapine (8). **10**

Figure 1.6-1: The inactive 5-HT_{2A}R XRC structure (PDB: 6A93), highlighting location of key binding residues. D155^{3.32} and toggle switch W336^{6.48} proximity to the non-conserved PIF motif. Additionally, the conserved EDRY and NPxxY motifs are highlighted. The ICL3 between TM5-TM6 (Thr266^{5.70}–Met312^{6.24}) was not resolved, as well as the allosteric Na⁺ ion associated to ligand receptor signalling. **15**

Figure 1.6-2: 5-HT_{2A}R (i) ECL2 displaying a folded conformation; and (ii) the ICL2 displaying looped conformation or helical conformation when bound to antagonist risperidone (PDB: 6A93, teal) and partial agonist LSD (PDB: 6WGT, orange). **16**

Figure 1.6.1-1: 5-HT_{2A}R NPxxY motif conformation between inactive and active receptor state when bound to antagonist risperidone (PDB: 6A93, teal), partial agonist LSD (PDB: 6WGT, orange), and full agonist 25CN-

Table of Figures

NBOH (PDB: 6WHA, green). Direction of movement depicted by black arrows **18**

Figure 1.6.1-2: 5-HT_{2A}R E/DRY motif conformation between inactive and active receptor state when bound to antagonist risperidone (PDB: 6A93, teal), partial agonist LSD (PDB: 6WGT, orange), and full agonist 25CN-NBOH (PDB: 6WHA, green). Direction of movement depicted by black arrows **19**

Figure 1.6.1-3: 5-HT_{2A}R W336^{6.48} “toggle switch” and PIF motif conformation between inactive and active receptor state when bound to antagonist risperidone (PDB: 6A93, teal), partial agonist LSD (PDB: 6WGT, orange), and full agonist 25CN-NBOH (PDB: 6WHA, green). Direction of movement depicted by black arrows **20**

Figure 1.6.2-1: Molecular surface slice-through of the 5-HT_{2A}R displaying location of the central binding pocket, hydrophobic cleft, and TM4-TM5 hydrophobic pocket/passage (HP). Local environments coloured by residue type; green, hydrophobic; cyan, polar; red, negative; purple, positive; yellow, solvent accessible surface area per-atom. **22**

Figure 1.6.2-2: 5-HT_{2A}R active and inactive displaying TM4-TM5 HP residues P211^{4.61}, I210^{4.60}, and F213^{4.63} conformations during binding of antagonist risperidone (PDB: 6A93, teal) and partial agonist LSD (PDB: 6WGT, orange) which form an opening into the TM helices bundle. ECL2 not displayed. **23**

Table of Figures

- Figure 1.6.2-3:** (i) Superimposition of 5-HT_{2A}R active (PDB: 6WGT) and inactive (PDB: 6A93) state in comparison to (ii) the 5-HT_{2C}R active state (PDB: 6BQH) displaying K220^{ECL2}/K199^{ECL2} forming electrostatic interactions (dashed line), between D^{4.67}, D^{5.35}, and N^{5.37} Source: adapted from Casey et al 2022⁸⁷ **26**
- Figure 1.6.2.1-1:** 5-HT_{2A}R XRC inactive state structure (PDB: 6A93) with an observable TM4 α -helix kink (dashed line). **30**
- Figure 1.8-1:** 5-HT_{2A}R selective ligands, spiperone (9), ketanserin (10), and volinanserin (11), 4-phenyl-2-dimethylaminotetralin cis-(2R,4R)-diastereomer (12). **31**
- Figure 1.9-1:** Pimavanserin (13). **35**
- Figure 1.10-1:** SAR map of the pimavanserin scaffold depicted by 3 ring regions and tri-substituted urea core. **38**
- Figure 1.10.4-1:** Structural cores of 5-HT_{2A}R selective ligands : (i) 13, (ii) 10, and (iii) general structure of 1,3- disubstituted thiourea ligands. **52**
- Figure 1.11-1:** Labelling protocol of GPCR N-terminus and fluorescent probe binding during cell membrane-based fluorescent TR-FRET assay **54**
- Figure 1.11-2:** 4-(4-fluorobenzoyl)-1-(4-phenylbutyl)piperidine (4F4PP) (16). **56**

Table of Figures

- Figure 1.12.3-1:** Molecular docking workflow schematic, (i) ligand preparation, (ii) protein preparation of XRC structure or homology model (iii) grid-box generation, (iv) setting docking constraints and protocol, (v) docking of prepared ligands using docking protocol. Predicted binding poses ranking docked ligands by Gscore. **63**
- Figure 1.12.4.1-1:** Diagram representing MM-PBSA/GBSA receptor-ligand binding free energy calculation method. **71**
- Figure 2.3-1:** Pimavanserin (13). **79**
- Figure 2.3-2:** Structure-based designed pimavanserin ring C analogues (17a-c). **80**
- Figure 2.3-3:** Structure-based designed pimavanserin ring C amino alcohol analogues (18a-j). **81**
- Figure 2.5.3.2-1:** Superimposition of 13 self-docking pose (purple) via pimavanserin analogue receptor grid generation protocol and the docked pose of 13 (grey) via the receptor grid generation protocol for 13. **90**
- Figure 2.6.2-1:** (i) 13 and (ii) S-18a docked into 5-HT_{2A}R homology model. Reduced hydrophobic interactions with the TM4-TM5 HP by the amino alcohol moiety of the latter, which features a primary amine, is associated to weaker Gscore in comparison to 13. **94**
- Figure 2.6.2-2:** (i) S-18j docked into 5-HT_{2A}R homology model, showing the amino alcohol moiety within the TM4-TM5 HP. Compared to pimavanserin, increased hydrophobic interactions by the amino alcohol

Table of Figures

moiety's 4-phenyl-piperdiny ring is associated to a better Gscore. (ii) S-18c docked into 5-HT_{2A} SWISS-MODEL homology model, illustrating a "reversed" pose. **94**

Figure 2.6.2-3: Ligand interaction diagram (i) 13, (ii) S-18a, and (iii) S-18j **98**

Figure 3.1.1-1: DOI based fluorescent probes featuring acid functionalised propoxy linker tethered to; dansyl (19a), NBD (19b), or rhodamine-based (19c) fluorophores. **115**

Figure 3.1.1-2: 5-HT-based fluorescent probes tethered to fluorophores; Cyannie3B (Cy3B) (20a-f), tetramethylrhodamine (TMR) (20g-h), and EVOBlueTM (20i) **117**

Figure 3.1.1-3: Molecular structure of 5-HT_{2A}R and 5-HT_{2C}R antagonist 4F4PP (16). **120**

Figure 3.3-1: Functionalised congener schematic. **122**

Figure 3.3.1-1: Compound 16 docked into the human 5-HT_{2A}R. Residues surrounding central pocket and TM4-TM5 hydrophobic SEP displayed. Key binding interactions; H-bond (purple), salt bridge (yellow), and π -CH (blue). **124**

Figure 3.3.1-2: Superimposition sideview of 16 (grey) docked and 4 (red-orange) co-crystalised ligand in the human 5-HT_{2A}R. Molecular surface displayed. No TM4-TM5 HP binding predicted by 16 or 4. **125**

Table of Figures

- Figure 3.3.1-3:** Proposed phenol substitution on 4F4PP molecular structure. **126**
- Figure 3.3.2-1:** Proposed linker regions for the modified 4F4PP-based fluorescent probes. (i) ethanamine linker (ii) amino propanamide linker. **127**
- Figure 3.3.2-2:** Proposed *N*-Boc protected 4F4PP congener (22) with 2 carbon amino-alkyl linker. **127**
- Figure 3.3.2-3:** *N*-Boc protected congener (22) docked into the human 5-HT_{2A}R. Residues surrounding central pocket and TM4-TM5 HP displayed. **128**
- Figure 3.3.2-4:** *N*-Boc protected congener (22) docked the human 5-HT_{2A}R. Molecular surface displayed. No TM4-TM5 HP binding predicted by 22. **129**
- Figure 3.3.3-1:** BODIPY 630/650 carboxylic acid (23) and 630/650 X NHS variants (24). **132**
- Figure 3.4-1:** Proposed 5-HT_{2A}R fluorescent probes (25) and (26). **132**

Table of Graphs

Graph 2.4.4-1: Ramachandran plot analysis of SWISS-MODEL 5-HT_{2A}R homology mode displaying 94.8% (310/327) of all residues were in favoured (98%) regions. **86**

Graph 2.6.4-1: MM-GBSA ΔG plotted against the HAC of *R/S-15a-d*, *R/S-18a-e*, *R-18c*, *R/S-18e-h*, *S-18i*, and *R/S-18j*. **106**

Graph 2.6.4-2: MM-GBSA ΔG plotted against the cLogP for *R/S-15a-d*, *R/S-18a-e*, *R-18c*, *R/S-18e-h*, *S-18i*, and *R/S-18j*. **106**

Graph 3.6-1: Saturation binding experiment employing endpoint analysis for derivation of 26 affinity to the human 5-HT_{2A}R expressed in CHO-cell membranes (4 μ g per well) incubated for 30 min with gentle agitation, with increasing concentrations of 26. Assay was performed in the presence of GppNHp (0.1mM) with non-specific binding levels determined by the inclusion of sertindole (10 μ M). Data presented is a single representative from $n=3$ performed in singlet. **140**

Graph 3.6-2: Saturation time course binding experiment employing kinetic analysis for derivation of 26 affinity to the human 5-HT_{2A}R expressed in CHO-cell membranes (4 μ g per well) incubated for 30 min with gentle agitation with increasing concentrations of 26. Assay was performed in the presence of GppNHp (0.1mM) with non-specific binding levels determined by the inclusion of sertindole (10 μ M). Data presented is a single representative from $n=3$ performed in singlet. **140**

Table of Graphs

Graph 3.6-3: Saturation time course binding experiment employing kinetic analysis for derivation of 25 affinity to the human 5-HT_{2A}R expressed in CHO-cell membranes (4 µg per well) incubated for 30 min with gentle agitation with increasing concentrations of 25. Assay was performed in the presence of GppNHp (0.1mM) with non-specific binding levels determined by the inclusion of sertindole (10 µM). Data presented is a single representative from $n=3$ performed in singlet. **142**

Table of Tables

Table 1.1-1: List of 5-HTR family and corresponding signal transduction pathway, (-) no receptor subtypes.	1
Table 1.5-1: Experimentally resolved 5-HT ₂ receptor subtype XRC and cryo-em structures available from the PDB. Resolution (Å), agonist (Ago), antagonist (Antag), and inverse agonist (Iago).	14
Table 1.6.2-1: Sequence based alignment of 5-HT _{2A} R TM4-TM5 HP residues against equivalent residue positions of other clinically relevant GPCRs. Non-conserved residues (green).	27
Table 1.6.2-2: 5-HT _{2A} R TM4 residue alignment against equivalent residue positions on the 5-HT _{2B} R and 5-HT _{2C} R subtypes, displaying conserved residues (green) and non-conserved residues (red).	28
Table 1.8-1: Binding affinity of 5-HT _{2A} R selective ligands (9-12).	32
Table 1.9-1: 5-HT _{2A} R residue point mutations and associated binding affinities show G238 ^{5.42} is implicated in the binding mode of 13 in comparison to 4.	36
Table 1.10.1-1: Pimavanserin ring A analogues (14a-n)	41
Table 1.10.2-1: Pimavanserin ring B analogues (14o-v).	44
Table 1.10.3-1: Pimavanserin ring C analogues (14x-av).	46
Table 1.10.3.1-1: Pimavanserin ring C amino alcohol analogues (15a-d).	51

Table of Tables

Table 2.6.1-1: Gscore for 13, *R/S*-15a-d, and *R/S*-18a-j. Reversed pose ([†]), Gscore lower (green) or higher (red) than pimavanserin. Top Gscore (blue highlight). (*) denotes compounds were tested as racemic mixtures. No detectable binding (ND). Compounds not tested experimentally (-). **92**

Table 2.6.3-1: Experimental potency of 13 and 15a-d compared to their individual enantiomer Gscores, shows an increasing trend between both. No detectable binding (ND). **99**

Table 2.6.4-1: Predicted ΔG via MM/GBSA, cLogP, and heavy atom count (HAC) of docked complexes 13, *R/S*-15a-d, and *R/S*-18a-j, reversed pose ([†]), MM-GBSA ΔG lower (green) or higher (red) than 13. Highest Gscore pimavanserin amino alcohol analogue (blue shaded). **103**

Table 2.6.5-1: Experimental potency of 13 and 15a-d compared to their individual enantiomer MM-GBSA ΔG values showing no ranking order correlation between binding strength. **107**

Table 3.3.3-1: List of fluorophore excitation and emission wavelength. **131**

Table 3.6-1: Binding affinities and kinetic rate parameters of 25 and 26 in 5-HT_{2A}R membranes determined by saturation binding assays. All values represent mean \pm SEM of *n*=3, not determined (ND). **141**

Table of Schemes

Scheme 3.4.1-1: Retrosynthesis of 25.	133
Scheme 3.4.1-2: Retrosynthesis of 26.	134
Scheme 3.5-1: Synthesis pathway for 25 and 26.	135
Scheme 4.3.1-1: 17a-c and 18a-j synthesis route 1.	150
Scheme 4.3.2-1: 18a-t synthesis route 2.	152
Scheme 5.1.3-1: Synthetic route to pimavanserin-based fluorescent probe (48).	160
Scheme 5.1.4-1: Proposed optimised synthetic route to fluorescent probe deprotected congeners via nitrile reduction.	162

Abbreviations

δ	Chemical shift
ΔG	Binding free energy
4-DMAP	<i>N,N</i> -dimethylaminopyridine
5-HT	5-Hydroxytryptamine, serotonin
25CN-NBOH	4-[2-[[2-Hydroxyphenyl)methyl]amino]ethyl]-2,5-dimethoxybenzonitrile
α AR	Alpha adrenoreceptor
β AR	Beta adrenoreceptor
BBSRC	Biotechnology and Biological Sciences Research Council
A AR	Adenosine receptor
ADHD	Attention deficit–hyperactivity disorder
Ar	Aryl
ATP	Adenosine 5'-triphosphate
bp	Boiling point
br	Broad (spectra)
cAMP	Cyclic adenosine monophosphate
CDCl ₃	Deuterated chloroform
conc	Concentrated
COSY	Correlation spectroscopy
Cryo-em	Cryogenic electron microscopy
DAG	Diacylglycerol
DCM	Dichloromethane
DMF	<i>N,N</i> -Dimethylformamide
DMSO	Dimethyl sulfoxide
DMSO- <i>d</i> ₆	Deuterated DMSO
d	Doublet (spectra)
dd	Doublet of doublets (spectra)
dq	Doublet of quartet (spectra)
dt	Doublet of triplets (spectra)

Abbreviations

DR	Dopamine receptor
ECD	Extracellular domain
ECL	Extracellular loop
EPS	Extrapyramidal side effects
eq	Equivalent
ER	Endoplasmic reticulum
ES	Electron spray
FASTA	Text-based format for representing amino acid (protein) sequences
G $\alpha_{i/o}$	G _i alpha subunit
G $\alpha_{q/11}$	G _{q/11} alpha subunit
G α_s	G _s alpha subunit
GDP	Guanine diphosphate guanine
Gemodel	Glide Emodel score
Genergy	Glide energy score
GPCR	G protein-coupled receptor
Gscore	Glide score
GTP	Guanine triphosphate
H R	Histamine receptor
HRMS	High resolution mass spectrometry heteronuclear
ICD	Intracellular domain
IMS	Industrial methylated spirits
IR	Infrared spectroscopy
IP ₃	Inositol 1,4,5-triphosphate
<i>J</i>	Coupling constant
kcal·mol ⁻¹	Kilocalorie per mole
<i>K_i</i>	Inhibitory constant
LC-MS	Liquid chromatography-mass spectrometry
LSD	Lysergic acid diethylamide

Abbreviations

m	Multiplet (spectra)
<i>m/z</i>	Mass to charge ratio
MAO	Monoamine oxidase
MMPA	Molecular match pair analysis
mp	Melting point
MS	Mass spectroscopy
MW	Microwave
NMR	Nuclear magnetic Resonance spectroscopy
PDB	Protein databank
r.t	Room temperature
s	Singlet (spectra)
	(10 <i>R</i> ,15 <i>S</i>)-12-[3-(2-Methoxyphenyl)propyl]-4-methyl-1,4,12- triazatetracyclo[7.6.1.0 ^{5,16} .0 ^{10,15}]-hexadeca-5,7,9(16)-triene
THT	
TM	Transmembrane helices
TOF	Time of flight
TpH	Tryptophan hydroxylase
tt	Triplet of triplets (spectra)
vdW	Van der Waals
wt	Wild type
XRC	X-ray crystal

1. Introduction

1.1 5-HT receptor family

Serotonin/5-hydroxytryptamine (5-HT) G protein-coupled receptors (GPCR) are a family of membrane proteins¹ which are signal transducers, able to transmit the binding of an extracellular ligand, such as 5-HT, into an intracellular response.^{2,3} These receptors modulate several physiological processes, including mood, digestion, cardiovascular function, cognition, and neurogenesis.⁴ The 5-HT receptors are classified into seven subfamilies (5-HT₁₋₇R) based on their structural and functional characteristics **Table 1.1-1**.

Family	Subtype	Signal transduction	Cellular response
5-HT ₁	A, B, D, E, F	Gα _i -protein-coupled	Decrease cellular levels of cAMP
5-HT ₂	A, B, C	Gα _q /Gα ₁₁ protein-coupled	Increase cellular levels of IP ₃ and DAG
5-HT ₃	-	Ligand gated Na ⁺ and K ⁺ channel	Depolarization of plasma membrane
5-HT ₄	-	Gα _s protein-coupled	Increase cellular levels of cAMP
5-HT ₅	A	Gα _{i/o} protein-coupled	Decrease cellular levels of cAMP
5-HT ₆	-	Gα _s -protein-coupled	Increase cellular levels of cAMP
5-HT ₇	-	Gα _s -protein-coupled	Increase cellular levels of cAMP

Table 1.1-1: List of 5-HTR family and corresponding signal transduction pathway, (-) no receptor subtypes.

Among them, the 5-HT₁R, 5-HT₂R, and 5-HT₅R subfamilies are further divided into subtypes (e.g. 5-HT_{1A}R, 5-HT_{2A}R, and 5-HT_{5A}R)

1. Introduction

according to their pharmacological profiles and molecular structures.⁵ The 5-HT₃R is a ligand-gated ion channel with a distinct structure and mechanism of action.⁶

There is interest into targeting the 5-HT_{2A}R due to its implication in several neuropsychiatric disorders such as schizophrenia, depression, obsessive compulsive disorder (OCD), and attention-deficit/hyperactivity disorder (ADHD).⁷⁻⁹ The receptor is the target of many drugs, ranging from antipsychotics to psychedelics, e.g. risperidone and psilocybin respectively.¹⁰

Dysregulation of 5-HT_{2A}R signalling has been linked to schizophrenia, depression, and anxiety.¹¹⁻¹⁴ However, the development of effective 5-HT_{2A}R therapeutics is challenging due to high sequence homology between receptor subtypes across the aminergic GPCR families. Consequently this leads to off-target side effects and impedes development of therapeutics.¹⁵

1.2 Therapeutic basis for targeting the 5-HT_{2A}R

The 5-HT_{2A}R is highly expressed in brain regions involved in cognitive and social functions, such as the cortex, hippocampus, basal ganglia, and forebrain.¹⁶ This receptor is targeted by different types of therapeutics such as antipsychotics or psychedelics that act as antagonists¹⁷ or agonists,¹⁸ respectively.

Several neuropsychiatric disorders have been associated with altered 5-HT_{2A}R expression in the brain.¹⁹ For example, major depressive

1. Introduction

psychiatric conditions have been linked to decreases in 5-HT_{2A}R expression, as evidenced by positron emission tomography studies.²⁰ Depression was linked to reduced 5-HT_{2A}R expression in the cortex, however this may result from chronic treatment with tricyclic antidepressants.²¹ Anxiety has also been associated to the 5-HT_{2A}R, For example, 5-HT_{2A}R knockout mice were reported to exhibit less anxiety-like behaviour in behavioural tests than wild-type mice.²² OCD has too been associated with increased 5-HT_{2A}R expression in the brain.²³ ADHD, a neurodevelopmental disorder, does not seem to involve changes in 5-HT_{2A}R expression,²⁴ but rather genetic variations in the 5-HT_{2A}R gene, such as the H452W and T102C^{1.60} (Ballesteros–Weinstein numbering)²⁵ polymorphisms at the C-terminal domain that may affect the receptor function and signalling.^{26,27}

These reports demonstrate that the 5-HT_{2A}R is implicated in many conditions associated to mental health. Consequently, there is an importance in treatment development, thus the receptor presents itself as a prominent therapeutic target.

Moreover, there are important physiological and psychological side-effects to consider for targeting the 5-HT_{2A}R over other 5-HT₂ receptor subtypes. 5-HT_{2B}R antagonism has been related to psychotic conditions²⁸ and impulsiveness.²⁹ Whereas 5-HT_{2B}R agonism has been linked to valvular heart disease.^{30,31} Therefore ligands binding at this 5-HT₂ receptor subtype is undesirable currently.

1. Introduction

Further importance is necessary for the 5-HT_{2c}R. 5-HT_{2c}R antagonism is known to increase the release of dopamine and norepinephrine in the brain. Although this effect could potentially counteract the reduction in dopamine release mediated by 5-HT_{2a}R antagonists, which are commonly used in antipsychotic medications. In brain regions where both 5-HT_{2a}R and 5-HT_{2c}R are expressed, the opposing actions of 5-HT_{2a}R and 5-HT_{2c}R antagonism on dopamine levels may diminish the overall efficacy of 5-HT_{2a}R-targeting therapeutics.³² The increased dopamine and norepinephrine release resulting from 5-HT_{2c}R blockade can contribute to off-target side effects associated with these therapeutics as well. Thus, being capable to modulate either receptor individually sought after in therapeutic design approaches. Moreover, 5-HT_{2c}R inverse agonism may benefit psychiatric treatment although this is less well known.^{33,34}

1.3 5-HT_{2a}R signal transduction

Binding of endogenous or exogenous agonists at the different 5-HT receptor triggers different cellular responses, which are associated to the receptor conformation and coupled G protein.³⁵ Agonist binding causes a conformational change in the receptor. This conformational change is transmitted to the bound heterotrimeric G protein. The G protein's α subunit exchanges GDP for GTP, which triggers the dissociation of the G protein subunits. The GTP-bound $G\alpha$ subunit dissociates from the receptor and from the $G\beta\gamma$ dimer. The $G\beta\gamma$ dimer also dissociates from

1. Introduction

the receptor. The dissociated G α -GTP and G $\beta\gamma$ subunits go on to interact with other intracellular proteins and initiate signalling cascades. Some 5-HT receptors can also recruit β -arrestin, a protein that mediates receptor desensitization and internalization.³⁶ An overview of the main signalling pathway of each 5-HT receptor type and subtype is provided **Figure 1.3-1**.

5-HT receptors, except the 5-HT₂R and 5-HT₃R, have opposing effects on the cellular level of cyclic adenosine monophosphate (cAMP), a second messenger that regulates various cellular process. The 5-HT₁R and 5-HT₅R families are coupled to G α_i /G α_o proteins, which reduce the activity of cAMP-dependent protein kinase A (PKA) by inhibiting adenylyl cyclase, the enzyme that produces cAMP from ATP. This leads to a decrease in the cellular concentration of cAMP and has an inhibitory effect on the postsynaptic neuron.³⁷ Conversely, the 5-HT₄R, 5-HT₆R, and 5-HT₇R families are coupled to G α_s proteins, which activate adenylyl cyclase and increase the production of cAMP. This leads to an increase in the cellular concentration and activity of cAMP-dependent PKA, and has an excitatory effect on postsynaptic neurons.³⁸⁻⁴⁰ The 5-HT₃R family is a ligand-gated cation channel which in the presence of serotonin, opens and depolarises the plasma membrane, allowing the influx of Na⁺ and K⁺ ions. This has an excitatory effect on postsynaptic neurons.⁶

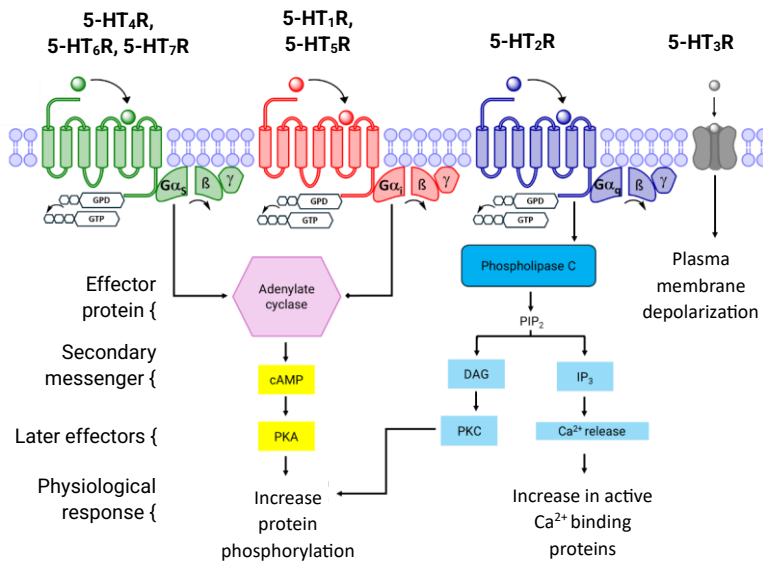


Figure 1.3-1: Schematic of the G protein-coupled signalling pathways of the 5-HT receptor subtypes. Binding of agonist triggers a receptor conformational change and signalling cascade. Coupled heterotrimeric G proteins consisting of $G\alpha$, $G\beta$, and $G\gamma$ subunits leads to G protein coupling-induced nucleotide exchange from GDP to GTP in the $G\alpha$ subunit. Dissociation of the heterotrimer into $G\alpha$ and $G\beta\gamma$ subunits occurs. $G\alpha$ subunits then either activate ($G\alpha_s$ - green) or inhibit ($G\alpha_i$ - red) adenylate cyclase, and activate phospholipase C ($G\alpha_q/G\alpha_{11}$, blue). Not depicted in this illustration; $G\beta\gamma$ subunits modulation of inward rectifying potassium (GIRK) channels, phosphoinositide 3-kinase (PI3K), and phospholipase C (PLC). Phosphorylation by G protein-coupled receptor kinases (GRKs) leading to arrestin recruitment and activation.

The 5-HT_{2R} subtypes are unique in that they are coupled to $G\alpha_q/G\alpha_{11}$ -proteins which activate phospholipase C (PLC- β). This hydrolyses the membrane phospholipid phosphatidylinositol 4,5-bisphosphate (PIP₂) into inositol 1,4,5-trisphosphate (IP₃) and diacylglycerol (DAG).⁴¹ The secondary messenger IP₃ dissociates and binds to its receptors in the endoplasmic reticulum. This process triggers the release of Ca⁺ ions into the cytoplasm. DAG stays within the plasma membrane and activates protein kinase C (PKC), causing downstream

effects such as phosphorylation of target proteins, modulation of gene expression, regulation of cell growth and differentiation, and cell survival.⁴²

1.3.1 5-HT_{2A}R signalling modulation

Agonists, antagonists, and inverse agonists are pharmacological agents that interact with and modulate signalling of receptors, such as the 5-HT_{2A}R. Agonists bind to and activate the receptor, enhancing its signalling activity above baseline levels. Antagonists bind to the receptor without activating it, effectively blocking the actions of both agonists and inverse agonists. Inverse agonists, upon binding, reduce the receptor's activity below basal levels, producing effects opposite to those of agonists.^{3,43} In the context of 5-HT_{2A}R, agonists increase serotonergic signalling, antagonists inhibit serotonin-mediated effects, and inverse agonists suppress serotonin signalling to sub-baseline levels, resulting in opposite effects to agonist.

The activation of 5-HT_{2A}R by endogenous (e.g. 5-HT) or exogenous (e.g. psilocybin) agonists, can modulate neuronal excitability, synaptic plasticity, cognitive functions, mood, inflammation, and vascular tone.⁴⁴

The cubic ternary complex (CTC) model **Figure 1.3.1-1** illustrates various complexes formed during the interaction between agonist, receptor, and G protein. Different conformational states, such as inactive (R_i) and active (R_a), can facilitate G protein dissociation and downstream

1. Introduction

signalling cascades. Different ligands can stabilize these conformations to different extents, which is the basis for their efficacy.⁴⁵

The CTC model includes the 2 receptor states, active (R_a) and inactive (R_i). Only R_a can activate the relevant G protein (G). The agonist (A) binds with both R_i and R_a , with higher affinity for R_a (in the case of inverse agonists, affinity would be higher for R_i). Additionally, binding of A to R_i to form AR_i promotes the conversion to AR_a , stabilising an active conformation of the receptor. Finally, the G protein can be activated when AR_aG is formed (agonist binding and receptor activity) or when R_aG is formed (representing constitutive activity).⁴⁶

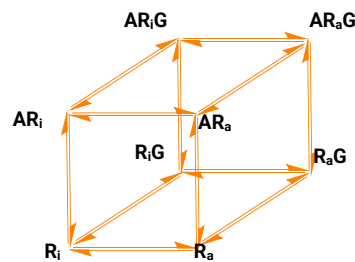


Figure 1.3.1-1: Cubic ternary complex model of GPCR activation, A: agonist; G: G protein; R_i : inactive form of receptor; R_a : active form of receptor.
Source: adapted from Kenakin 2002⁴⁶

An advanced extension of the model proposes the existence of multiple receptor active conformations, each with varying ligand affinities. These conformations may signal through different G-proteins and initiate distinct signalling cascades.^{45,47}

1.4 Therapeutics for 5-HT_{2A}R-associated neuropsychiatric disorders

Typical antipsychotics **Figure 1.4-1**, such as haloperidol (1) and chlorpromazine (2) were implemented in 1950s target the dopamine D₂ receptors (D₂R) and function as antagonists. This mode of action contributes to their efficacy in treating psychiatric conditions. However, the interaction of typical antipsychotics with D₂R can lead to the development of extrapyramidal symptoms (EPS) and other unwanted side effects.

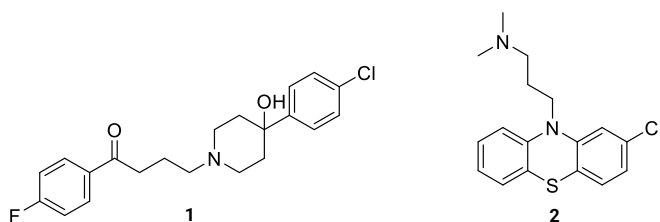


Figure 1.4-1: Example of typical antipsychotic drugs haloperidol (1) and chlorpromazine (2).

The polypharmacology of haloperidol and chlorpromazine also involves interactions with various receptors beyond dopamine receptors, such as cholinergic or histaminergic receptors, resulting in a higher incidence of side effects involving sedation, weight gain, and hypotension.⁴⁸ Hence, while effective in treating psychiatric conditions, the broader receptor interactions and associated side effects of haloperidol and chlorpromazine warranted caution when selecting these

1. Introduction

medications as treatment. Therefore, improved therapeutics were desired.

Atypical antipsychotics **Figure 1.4-2** are a class of therapeutics introduced from the 1970s, implemented to treat various neuropsychiatric conditions, such as schizophrenia, bipolar disorder, and major depressive disorder, and are still used in clinical settings.⁴⁹ Atypical antipsychotics function through dual receptor antagonism, primarily targeting 5-HT_{2A}R, as well as D₂R.⁵⁰

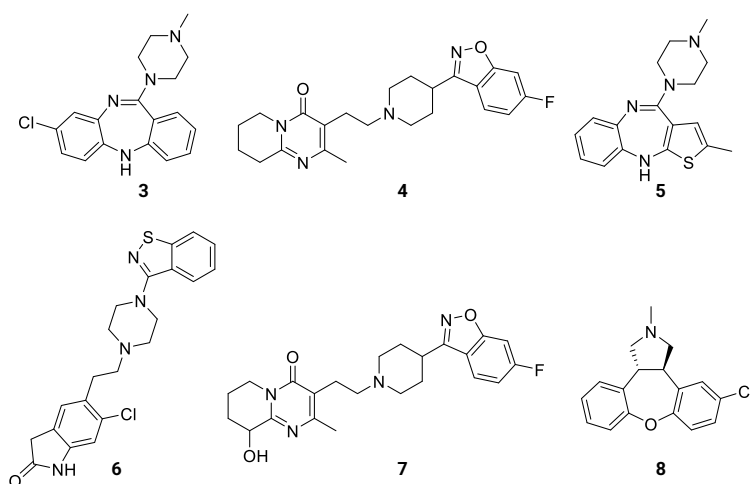


Figure 1.4-2: Example of atypical antipsychotic drugs
clozapine (3), risperidone (4), olanzapine (5), ziprasidone (6), paliperidone (7), and asenapine (8).

Atypical antipsychotics are thought to be improved therapeutics in comparison to their predecessors. A lower risk of causing EPS associated to their mechanism of action is reported, as well as have reduced off-target interactions related to their improved binding profiles. However, newer atypical antipsychotics are still reported to demonstrate

1. Introduction

affinity at several GPCRs as their predecessors, and have comparable side effects.⁵¹

First was the discovery of clozapine (**3**), a dibenzodiazepine that showed improved efficacy such as improved response rate and lower risk of EPS than conventional antipsychotics.⁵² However, clozapine may cause the blood disorder agranulocytosis, thus limiting its clinical use.⁵³ It also increases prolactin levels, and is associated with weight gain and metabolic disturbances.⁵⁴ A second generation of atypical antipsychotics emerged, such as risperidone (**4**), a benzisoxazole with a better EPS profile than clozapine. Olanzapine (**5**), a thienobenzodiazepine derived from clozapine, offered a similar efficacy and EPS advantage, but with less risk of agranulocytosis.^{55,56} However, olanzapine is also associated with hepatotoxicity and severe weight gain.^{57,58} Further atypical antipsychotics developed included ziprasidone (**6**), a benzothiazolylpiperazine that caused the lowest weight gain and EPS among the atypical antipsychotics.^{58,59} This was attributed to its weak or negligible antagonism of α_{1A} -adrenergic receptor, histamine H₁ receptor (H₁R), and M₁ muscarinic acetylcholine receptor (M₁ AChR).⁶⁰

Newer atypical antipsychotics have been approved for schizophrenia and bipolar disorders, such as paliperidone (**7**) and asenapine (**8**).^{61,62} However, **7** is an active metabolite of its predecessor **4**, thus sharing similar pharmacological and adverse effects profiles and ⁶³ **8** is an under development atypical antipsychotic with a high affinity

1. Introduction

for multiple receptors including the D₂R, α_{2A}-AR, H₁R, and M₁R. Its clinical efficacy and safety are still under investigation.⁶²

Although atypical antipsychotics pose a lower risk of causing EPS compared to typical antipsychotics and the incidence is typically lower than that observed with typical antipsychotics, there is still the risk of it.⁶⁴ Moreover, affinity of the atypical antipsychotics at off-targets results in unwanted activation or inhibition of several different cell signalling pathways implicated with displayed side-effects.^{49,51,65-67} Thus compounds with improved subtype selectivity are desired.

1.5 5-HT_{2A}R X-ray crystal structures

X-ray crystal (XRC) structures have become available for the 5-HT_{2A}R via the Protein Data Bank (PDB), **Table 1.5-1**. These provide high-resolution structural details of several types of molecules binding at the receptor and the associated receptor conformation at the atomistic scale. Several cryogenic electron microscopy (cryo-em) structures have also become available. The first high-resolution XRC structures of the 5-HT_{2A}R (PDB: 6A93 and PDB: 6A94) were available in 2019, in complex with risperidone and zotepine respectively.¹⁷ This provided the first opportunity to undertake a comparative structural analysis of each 5-HT₂ receptor subtype by their available XRC structures.

Unsurprisingly, the resolved 5-HT_{2A}R structures have unveiled new structural details. The central binding pocket of the 5-HT_{2A}R can be seen to extend further between transmembrane helices (TM) 4 and 5 than

1. Introduction

what is observed in the available XRC structures of the 5-HT_{2B}R and 5-HT_{2C}R subtypes, **Table 1.5-1**. This creates a membrane-exposed opening into the channel or pocket, depending on the receptor conformation, connecting the transmembrane environment to the central binding pocket within the receptor helices bundle. This difference observed in the binding pockets of the 5-HT₂ receptor subtypes XRC structures may be an opportunity to achieve improved affinity towards the 5-HT_{2A}R only.

GPCR	PDB	Type	Å	Ligand	Type	Date
5-HT _{2A} R	UP ₆₈	Cryo-em	3.0	Z7757	Agot	2024
	7WC4 ₆₉	X-ray	3.2	5-HT	Ago	2022
	7WC6 ₆₉	X-ray	2.6	LSD	Ago	2022
	7WC5 ₆₉	X-ray	3.2	Psilocin	Ago	2022
	7WC7 ₆₉	X-ray	2.6	Lisuride	Ago	2022
	7WC8 ₆₉	X-ray	2.5	Lumateperone	Antag	2022
	7WC9 ₆₉	X-ray	2.5	THT	Ago	2022
	7RAN ₇₀	Cryo-em	3.5	TPP	Ago	2022
	7VOD ₇₁	X-ray	3.3	Cariprazine	Antag	2021
	7VOE ₇₁	X-ray	2.9	Aripiprazole	Antag	2021
	6WGT ₄₁	X-ray	3.4	LSD	Ago	2020
	6WHA ₄₁	Cryo-em	3.4	25-CN-NBOH	Ago	2020
	6WH4 ₄₁	X-ray	3.4	Methiothepin	Antag	2020
	6A93 ₁₇	X-ray	3.0	Risperidone	Antag	2019

1. Introduction

	6A94 ₁₇	X-ray	2.9	Zotepine	Antag	2019
5-HT _{2B} R	6DRX ₇₂	X-ray	3.1	Lisuride	Antag	2018
	6DS0 ₇₂	X-ray	3.2	LY266097	Antag	2018
	6DRZ ₇₂	X-ray	3.1	Methysergide	Antag	2018
	6DRY ₇₂	X-ray	2.9	Methylegonovine	Ago	2018
	5TUD ₇₃	X-ray	3.0	Ergotamine	Ago	2017
	5TVN ₇₄	X-ray	2.9	Lysergide	Ago	2017
	4NC3 ₇₅	X-ray	2.8	Ergotamine	Ago	2013
	4IB4 ⁷⁶	X-ray	2.7	Ergotamine	Ago	2013
5-HT _{2C} R	6BQH ₇₇	X-ray	2.7	Ritanserin	Iago	2018
	6BQG ₇₇	X-ray	3.0	Ergotamine	Ago	2018

Table 1.5-1: Experimentally resolved 5-HT₂ receptor subtype XRC and cryo-em structures available from the PDB. Resolution (Å), agonist (Ago), antagonist (Antag), and inverse agonist (Iago).

1.6 5-HT_{2A}R molecular structure

5-HT_{2A}R XRC structures display a classic GPCR transmembrane architecture, as represented by **Figure 1.6-1**. The receptor structure is characterized by seven transmembrane α -helices that spans from the extracellular matrix at the N-terminus to the cytoplasm at the C-terminus. An additional intracellular helix 8 runs parallel to the cell membrane. Conserved Class A aminergic GPCR amino acid residues: E318^{6,30}, D172^{3,49}, R173^{3,50}, Y174^{3,51}, and N376^{7,49}, P377^{7,50}, and Y380^{7,35}, represent the conserved motifs respectively. E/DRY,⁷⁸ and NPxxY⁷⁹ have been resolved in all 5-HT_{2A}R XRC structures.^{17,41,69–71}

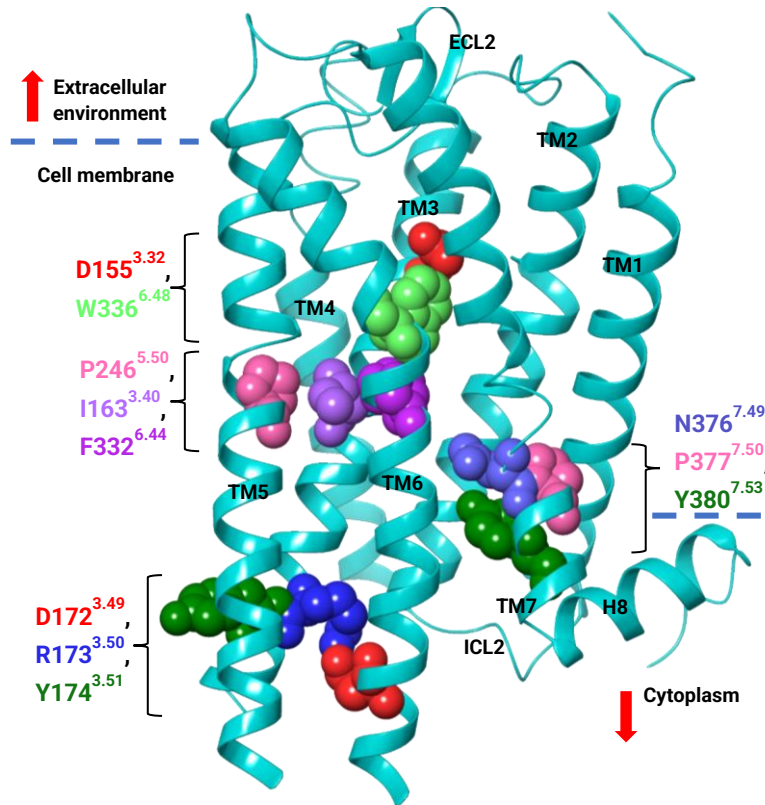


Figure 1.6-1: The inactive 5-HT_{2A}R XRC structure (PDB: 6A93). highlighting location of key binding residues. D155^{3.32} and toggle switch W336^{6.48} proximity to the non-conserved PIF motif. Additionally, the conserved EDRY and NPxxY motifs are highlighted. The ICL3 between TM5-TM6 (Thr266^{5.70}-Met312^{6.24}) was not resolved, as well as the allosteric Na⁺ ion associated to ligand receptor signalling.

The residue D155^{3.32}, critical for ligand binding is located at the centre of the helices bundle.⁸⁰ This is in the region of the residue W336^{6.48} known as the toggle switch.^{17,81} Beneath this, a hydrophobic triad of residues P246^{5.50}, I163^{3.40}, and F332^{6.44} form a hydrophobic region/cleft which extends the binding pocket deeper within the helices bundle. A direct interaction between F332^{6.44} and W336^{6.48} form the base of the pocket.⁸²

1. Introduction

This hydrophobic cleft appears well defined when the 5-HT_{2A}R is bound to an antagonist. It appears as a crucial binding mode associated to the ligands antagonistic effect thus far. Whereas when the 5-HT_{2A}R is agonist-bound, the hydrophobic cleft is less well defined and the central binding pocket volume increases,^{41,77,83} highlighting the dynamic nature of the TM helices bundle to accommodate different classes of molecules. The hydrophobic cleft is conserved across structurally similar GPCRs: 5-HT_{2C}R⁷⁷, D₂R⁸⁴, 5-HT_{1B}R⁸⁵, and H₁R⁸⁶ when bound to antagonists and inverse-agonists.

In the 5-HT_{2A}R XRC structures, the extracellular loop 2 (ECL2) was resolved in a loop conformation, **Figure 1.6-2**. This appears to form a lid between the TM helices bundle at the face of the extracellular environment.⁸³ This appears to secure a ligand into the binding pocket via hydrophobic interactions with side chain residue L299^{ECL2}, as demonstrated by mutation of L299A^{ECL2} which impacted ligand residence time at 5-HT_{2A}R.^{17,41,69}

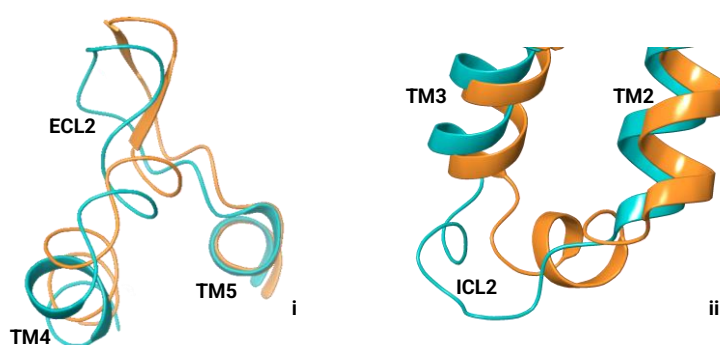


Figure 1.6-2: 5-HT_{2A}R (i) ECL2 displaying a folded conformation; and (ii) the ICL2 displaying looped conformation or helical conformation when bound to antagonist risperidone (PDB: 6A93, teal) and partial agonist LSD (PDB: 6WGT, orange).

1. Introduction

The intracellular loop 2 (ICL2) exhibits different conformations during the binding of antagonists and agonists. In the high energy active state, it adopts a helical conformation, whereas in its lower energy state of the inactive conformation, it appears looped, **Figure 1.6-2**. The ICL3 also plays a significant role in the dynamics of the TM6 helices during receptor activation. However in the available 5-HT_{2A}R XRC structures this was engineered to enhance the stability of the receptor for crystallisation purposes.^{17,41} Future XRC structures of 5-HT_{2A}R in complex with different types of ligands will reveal further insights into receptor and residue motif conformation, and their binding interactions.

1.6.1 5-HT_{2A}R structural transitions during activation

Upon receptor activation the agonist induced signal transduction leads to conformational changes and repacking of TM α -helices and motif side chains. The structural conformational changes associated with 5-HT_{2A}R activation are shown in **Figure 1.6.1-1** - **Figure 1.6.1-3**. Binding of an agonist at D155^{3,32,80} in between the TM bundle occurs via an ionic/salt bridge interaction between the carboxylate anion of D155^{3,32} and the ammonium ion of the ligand. This can be considered as the main anchor between both.^{17,41,80} Displacement of the allosteric Na⁺ ion results in collapse of the ion pocket, which triggers the inward movement of the NPxxY motif **Figure 1.6.1-1**, where x represents a variable residue among aminergic GPCRs. This leads to the

1. Introduction

rearrangement of R173^{3.50} and the disruption of the ionic interaction between E318^{6.30}, **Figure 1.6.1-2**.

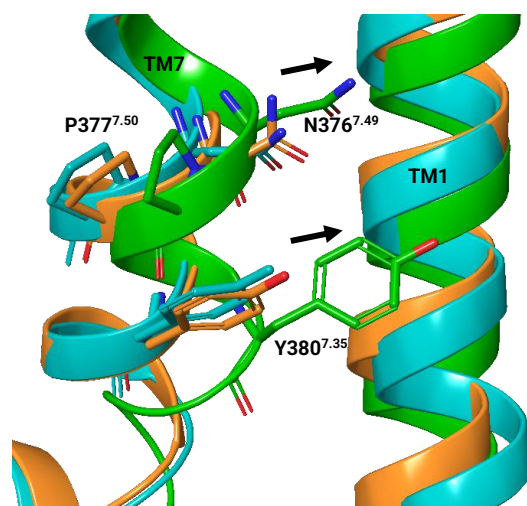


Figure 1.6.1-1: 5-HT_{2A}R NPxxY motif conformation between inactive and active receptor state when bound to antagonist risperidone (PDB: 6A93, teal), partial agonist LSD (PDB: 6WGT, orange), and full agonist 25CN-NBOH (PDB: 6WHA, green). Direction of movement depicted by black arrows.

The structural conformation differences in different 5-HT_{2A}R XRC structures can be correlated with the pharmacological profile of the ligand. For instance, the increase in distance between residues E318^{6.30} and R173^{3.50} of the E/DRY motif that are associated with active state complexes, **Figure 1.6.1-2**.

The distance between the side chains was at its shortest when the 5-HT_{2A}R was bound to the antagonist risperidone (7.10 Å) but resolved at the greatest distance away from one another when bound to the full agonist 25CN-NBOH (14.14 Å). This represents a fully broken ionic lock and active receptor state.⁴¹ However, in the 5-HT_{2A}R active state

1. Introduction

structure bound to the partial agonist LSD, the lock appears to appear to be intact as E318^{6.30} and R173^{3.50} are at the shortest distance from each other (3.52 Å).

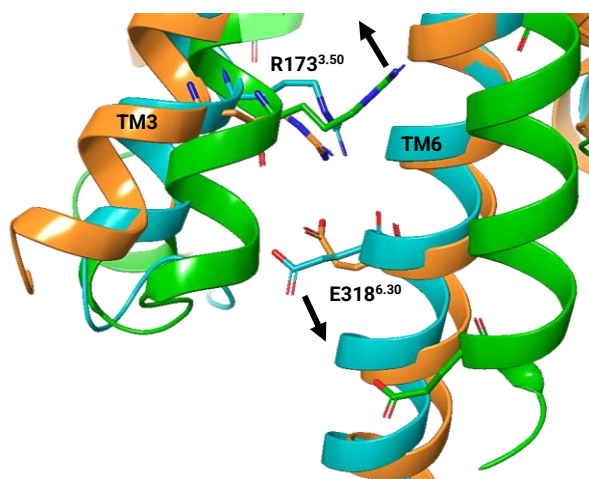


Figure 1.6.1-2: 5-HT_{2A}R E/DRY motif conformation between inactive and active receptor state when bound to antagonist risperidone (PDB: 6A93, teal), partial agonist LSD (PDB: 6WGT, orange), and full agonist 25CN-NBOH (PDB: 6WHA, green). Direction of movement depicted by black arrows.

Receptor activation is shown by the W336^{6.48} side chain conformation resolved in the 5-HT_{2A}R structures when bound to either a partial agonist, full agonist, and antagonist. For example, when bound to the full agonist a 25CN-NBOH, **Figure 1.6.1-3**, W336^{6.48} is facing downwards towards the bottom of the central binding pocket. Whereas in the 5-HT_{2A}R inactive state structures W336^{6.48} is resolved in-line with the TM6 helix, facing towards the central binding pocket and TM4-TM5. Residue W336^{6.48} is also known as a toggle switch, that forms part of the cWxP motif.⁷⁸

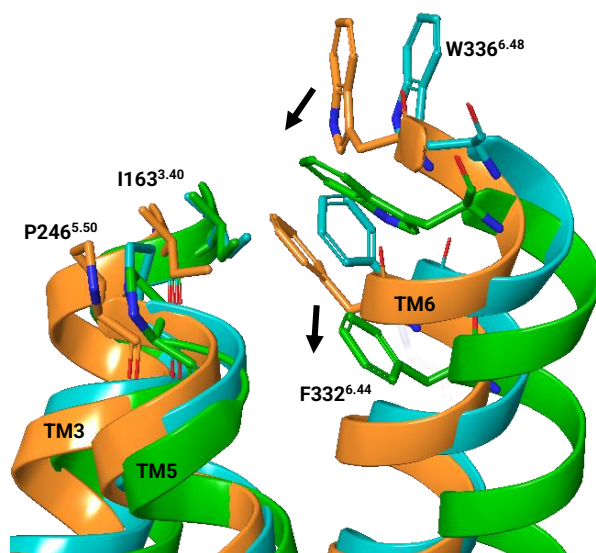


Figure 1.6.1-3: 5-HT_{2A}R W336^{6.48} "toggle switch" and PIF motif conformation between inactive and active receptor state when bound to antagonist risperidone (PDB: 6A93, teal), partial agonist LSD (PDB: 6WGT, orange), and full agonist 25CN-NBOH (PDB: 6WHA, green). Direction of movement depicted by black arrows.

A change in the side chain conformations of F332^{6.44} forming part of the PIF motif can be observed, **Figure 1.6.1-3**. This reduces the size of the hydrophobic cleft. The conformation changes observed in the PIF and cWxP motifs during activation are considered part of a larger receptor motif known as the transmission switch. This switch includes residues I^{3.40}, P^{5.50}, L^{5.51}, F^{6.44}, and W^{6.48,81,87}. The motif is proposed to facilitate conformational alterations in the ligand-binding pocket which results in a significant displacement of the intracellular ends of TM5 and TM6. This also results in rearrangements in the interface between TM3 and TM5 to enabling G protein-coupling.⁴¹ Considered together, the available 5-HT_{2A}R XRC structures are useful in highlighting specific

differences in the arrangements of conserved motifs and associated side-chain conformations when bound with different classes of ligands.

1.6.2 The 5-HT_{2A}R TM4-TM5 hydrophobic pocket

A unique hydrophobic pocket/passage (HP) has been resolved between TM4-TM5 helices in the 5-HT_{2A}R XRC structures, represented via **Figure 1.6.2-1**. This feature has been identified as a side-extended pocket,¹⁷ or cavity⁸⁸ which appears to form a passage connecting the pocket in the centre of the TM helices bundle to the TM bilayer.

The TM4-TM5 HP has been resolved as a passage between both α -helices when an antagonist such as risperidone and zotepine is bound to the 5-HT_{2A}R.¹⁷ The HP has also been resolved as either a pocket when the 5-HT_{2A}R is bound to agonists such as LSD, psilocin, and 5-HT, or as a passage, were it was occupied by a lipid.^{41,69} The TM4-TM5 HP is not seen in the available XRC structures of the 5-HT_{2B}R and 5-HT_{2C}R subtypes, **Section 1.5, Table 1.5-1**. This structural difference presents an opportunity to explore the TM4-TM5 HP as a potential molecular target for enhanced ligand binding and selectivity towards the 5-HT_{2A}R.

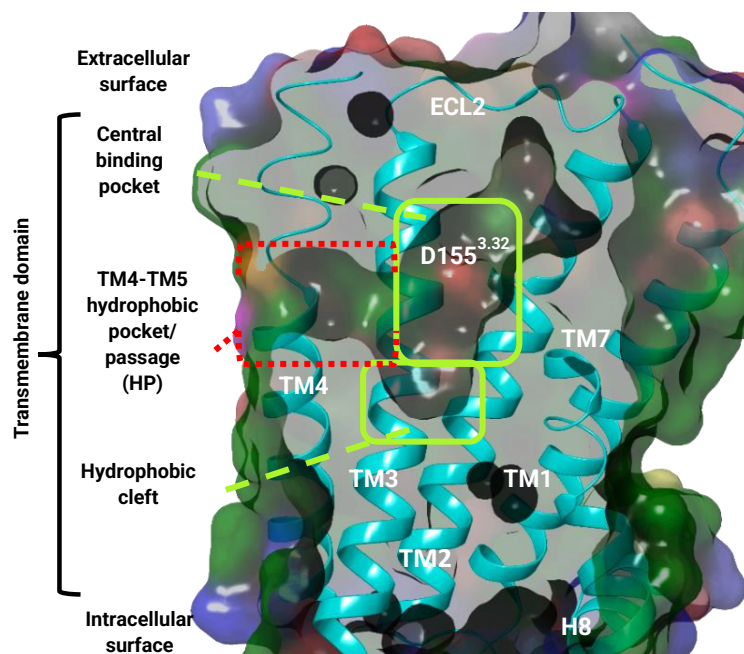


Figure 1.6.2-1: Molecular surface slice-through of the 5-HT_{2A}R displaying location of the central binding pocket, hydrophobic cleft, and TM4-TM5 hydrophobic pocket/passage (HP). Local environments coloured by residue type; green, hydrophobic; cyan, polar; red, negative; purple, positive; yellow, solvent accessible surface area per-atom.

The 5-HT_{2A}R HP is a significantly lipophilic region between TM4 and TM5 helices, enclosed by less conserved amphipathic and hydrophobic residues on TM3, TM4, TM5, and ECL2. It creates a pocket/passage from the membrane-exposed residues to the centre region of the TM helices bundle, directly opposite the conserved residue D155^{3,32}.

The available XRC structures highlight the differences between the conformation of residue side chains forming the TM bilayer interface/opening and channel of the HP between the 5-HT_{2A}R active and inactive states, **Figure 1.6.2-2**.

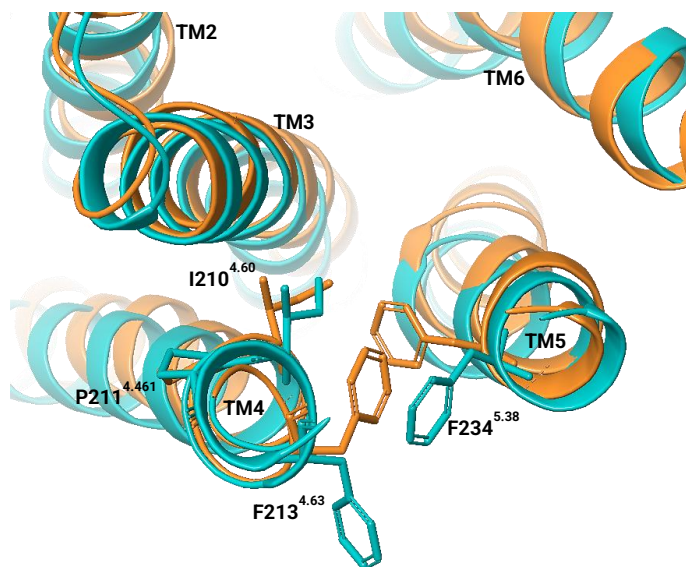


Figure 1.6.2-2: 5-HT_{2A}R active and inactive displaying TM4-TM5 HP residues P211^{4.61}, I210^{4.60}, and F213^{4.63} during binding of antagonist risperidone (PDB: 6A93, teal) and partial agonist LSD (PDB: 6WGT, orange) which form an opening into the TM helices bundle. ECL2 not displayed.

Comparison of the active and inactive states have resolved F213^{4.63} and F234^{5.38} hydrophobic side chains are outward-facing from the TM helices bundle associated to the inactive state (PDB: 6A93)¹⁷ bound to an antagonist. This appears to increase the size of the TM4-TM5 HP. The F213^{4.63} and F234^{5.38} rotamers appear to be forming a T-stacking interaction with their aromatic rings.

In contrast, the active state XRC structure (PDB: 6WGT)⁴¹ showed both rotamers resolved inward-facing in an off-set stacked formation towards the TM helix bundle. In a high energy active state, the size of the TM4-TM5 HP appears reduced. The interaction and associated rotamer

1. Introduction

conformation changes of F213^{4.63} and F234^{5.38} between the active and inactive states are common, as these facilitate the most favourable interactions between residue side chains.^{89–91} A conformational change is also observed by I210^{4.60} towards F234^{5.47} on TM5 between inactive and active states, which may also restrict the size of the HP. This change in side chain conformation is comparable to that of I163^{3.40} and F332^{6.44} in the PIF motif upon GPCR activation.

In recent agonist-bound 5-HT_{2A}R active state XRC structures, e.g. (PDB: 7WC6),⁶⁹ the lipid monoolein was resolved binding through the TM4-TM5 HP. Interactions were reported between the glycerol moiety of monoolein and S239^{5.43}, and S242^{5.46}.⁶⁹ Thereby suggesting contribution to ligand binding. F213^{4.63} and F234^{5.38} were resolved adopting side chain conformations to accommodate the lipid comparable to those resolved in low energy antagonist-bound 5-HT_{2A}R XRC structures, e.g. risperidone (PDB: 6A93) and zotepine (PDB: 6A94).¹⁶ However it is unclear if the presence of monoolein in the TM4-TM5 HP was associated with the crystallisation process.⁶⁹ Moreover, monoolein may not be the endogenous lipid to bind at the 5-HT_{2A}R.⁹²

Unlike the 5-HT_{2A}R, where F213^{4.63} and F234^{5.38} face outward and increase the size of the TM4-TM5 HP. F217^{5.38} and F214^{5.38} at equivalent positions in 5-HT_{2B}R and 5-HT_{2C}R face inward and restrict the pocket size. With the presence of K193^{4.63} and I192^{4.63} at the equivalent of F213^{4.63} in the 5-HT_{2A}R, neither residue can participate in aromatic-aromatic interactions which would stabilise either side chain.

1. Introduction

Additionally, K193^{4.63} in the 5-HT_{2B}R, and I192^{4.63} or D211^{5.35} in the 5-HT_{2C}R could sterically hinder F^{5.38} rotation.

The influence of the rotamer pair F213^{4.63} and F234^{5.38} on the affinity of 5-HT_{2A}R antagonists has been reported.⁹³ The F213K^{4.63} mutation was introduced to mimic the corresponding residue in 5-HT_{2B}R. Then the affinity of several 5-HT_{2A}R antagonists was then interrogated and demonstrated no significant difference compared to the wt 5-HT_{2A}R.⁹³

The role of F234^{5.38} in modulating 5-HT_{2A}R affinity was investigated by attempting to perturb its side chain with mutation of D231F^{5.35}, one helical turn away. However, the point mutation D231F^{5.35} was thought to have perturbed membrane folding, thus binding affinity could not be determined.⁸⁸ Moreover, the F234^{5.38}-D231F^{5.35} interactions introduced by the point mutation could disrupt interactions between the adjacent F213^{4.63} rotamer on TM4, thus impacting 5-HT_{2A}R stability and helix packing.⁹⁴ This aligned with the lack of detectable binding affinity demonstrated by the D231F^{5.35} mutation.⁸⁸

The TM helix bundle in the 5-HT_{2A}R XRC structures, shows K220^{ECL2} forms a cover or lid over the TM4-TM5 HP residues nearest the extracellular surface. An ensemble of interactions: hydrophobic, charged, or polar, with either F234^{5.38}, D217^{4.67}, D231^{5.35}, N233^{5.37}, K220^{ECL2}⁸⁸ and S219^{ECL2} may be permitted, **Figure 1.6.2-3**. These interactions may restrict the ECL2 mobility but enhance receptor stability, which are thought to have a role in a network of electrostatic interactions

1. Introduction

required for ligand binding.⁸⁸ Supporting evidence includes altered binding kinetics of LSD following the point mutation K229A^{ECL2} which was carried out to increase loop mobility.⁸³ This demonstrates the importance of an electrostatic network of interactions between the TM and ECL2 in ligand binding.

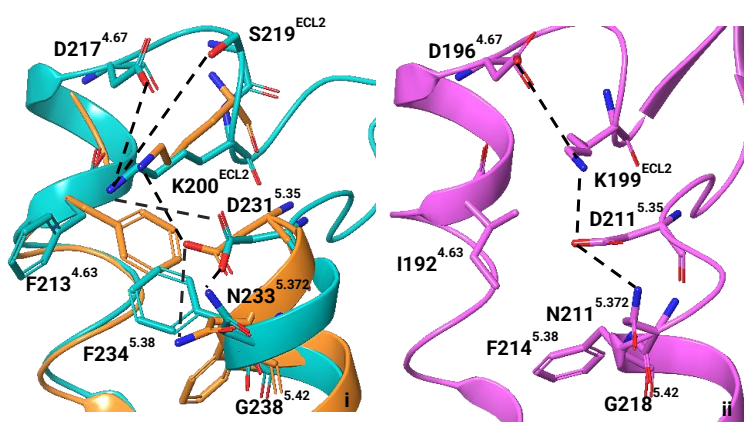


Figure 1.6.2-3: (i) Superimposition of 5-HT_{2A}R active (PDB: 6WGT) and inactive (PDB: 6A93) state in comparison to (ii) the 5-HT_{2C}R active state (PDB: 6BQH) displaying K220^{ECL2}/K199^{ECL2} forming electrostatic interactions (dashed line), between D^{4.67}, D^{5.35}, and N^{5.37}. Source: adapted from Casey et al 2022⁸⁸

A similar network of interactions can be observed in the ritanserin-5-HT_{2C}R XRC structure (PDB: 6BQH), where K199^{ECL2} is surrounded by the negative charges of D196^{4.67} and D211^{5.35}.⁷⁷ This may account for the higher binding affinity of ligands for the 5-HT_{2A}R and 5-HT_{2C}R subtypes compared to 5-HT_{2B}R, e.g. (PDB: 6DRZ) which lacks the K^{ECL2} equivalent residue.⁸⁸

Residue alignment of the TM4-TM5 HP residues with the other 5-HT₂ receptor subtypes and clinically relevant GPCRs, **Table 1.6.2-1**, shows the 5-HT_{2C}R has the highest residue homogeneity at the position

1. Introduction

of the TM4-TM5 HP. G238^{5,42}, located at the intrahelical side of the HP, stands out as non-conserved in the 5-HT₂ receptor subtypes as compared to other aminergic receptors that feature Ala, Ser, Cys, or Thr at equivalent positions. G238^{5,42} role in ligand binding has been investigated by the mutation G238S^{5,42} in the 5-HT_{2A}R and 5-HT_{2C}R. This resulted in reduced binding affinity at the 5-HT_{2A}R, thereby implicating G238^{5,42} in ligand binding.⁷⁷

GPCR	Residue														
5-HT _{2A} R	V156 ^{3,33}	I206 ^{4,56}	S207 ^{4,57}	P209 ^{4,59}	I210 ^{4,60}	P211 ^{4,61}	V212 ^{4,62}	F213 ^{4,63}	L229 ^{5,62}	F234 ^{5,38}	V235 ^{5,39}	I237 ^{5,41}	G238 ^{5,42}	V241 ^{5,46}	S242 ^{5,46}
5-HT _{2B} R	V	I	A	P	V	P	I	K	L	F	M	F	G	A	A
5-HT _{2C} R	V	V	S	P	I	P	V	I	L	F	V	I	G	V	A
D ₂ R	V	I	S	P	L	L	F	G	I	F	V	Y	S	V	S
H ₁ R	Y	L	W	P	I	L	G	-	T	F	K	M	T	I	N
5-HT _{1A} R	V	I	S	P	M	L	G	W	I	Y	T	Y	S	G	A
5-HT _{1B} R	I	I	S	P	F	F	W	-	V	Y	T	Y	S	G	A
5-HT _{1D} R	I	I	S	P	L	F	W	R	V	Y	T	Y	S	G	A
5-HT _{1E} R	M	I	S	P	L	F	W	-	I	Y	T	Y	S	G	A
5-HT _{1F} R	I	I	S	P	L	F	W	R	I	S	T	Y	S	G	A
5-HT ₄ R	V	I	S	P	I	M	Q	G	F	Y	A	T	C	V	A
5-HT _{5A} R	V	I	S	P	L	L	F	G	V	Y	A	F	S	G	A
5-HT ₆ R	V	A	S	P	L	L	L	G	L	F	V	V	A	L	T
5-HT ₇ R	V	I	T	P	L	F	G	-	I	Y	T	Y	S	V	A
M ₁ R	Y	L	W	A	I	L	M	H	I	I	T	G	T	A	A
A _{2A} R	V	I	S	P	L	L	G	-	I	Y	V	F	S	G	S
β ₁ AR	V	V	S	P	I	L	M	H	F	Y	A	A	S	V	S
β ₂ AR	V	T	S	P	I	Q	M	H	F	Y	A	A	S	V	S

Table 1.6.2-1: Sequence based alignment of 5-HT_{2A}R TM4-TM5 HP residues against equivalent residue positions of other clinically relevant GPCRs. Non-conserved residues (green).

1. Introduction

Notably, several lipids, such as monoolein, oleamide, oleoylethanolamide, and 2-oleoyl glycerol, were shown to activate the wt 5-HT_{2A}R, but not the G238S^{5,42} mutant which may have perturbed the TM4-TM5 HP.⁶⁹ Moreover I237^{5,41} also stands out as a non-conserved residue to the 5-HT_{2A}R and 5-HT_{2C}R subtypes only. Ile flexible hydrophobic side chain has good mobility and may also be a requirement to the TM4-TM5 HP in combination with G238^{5,42}. The role of I237^{5,41} in ligand binding has not yet been investigated.

Previously Gly residues have demonstrated to function as a molecular hinge for ion channels.⁷⁰ Therefore a hinge-type mechanism may also be capable on the TM5, which may be supported by studies on the β_2 AR,^{97,98} cannabinoid,⁹⁹ sphingosine-1-phosphate,¹⁰⁰ and opsin receptors.¹⁰¹

Furthermore, it was demonstrated via the binding of a phenylethylamine series at the 5-HT_{2A}R substituted at a single position, the associated increased lipophilicity of the ligands favoured receptor activation and recruitment of miniG α_q protein.¹⁰²⁻¹⁰⁴ This was rationalised via docking, which predicted the ligands to bind into the TM4-TM5 HP via their substituted moieties.¹⁰⁴

Together, resolved 5-HT_{2A}R structures, cell-based assays, and *in silico* techniques have provided insight into 5-HT_{2A}R TM4-TM5 HP influence on ligand binding and signalling pathways. These provide a

foundation to build upon: targeting the TM4-TM5 HP through a structure-based design strategy.

1.6.2.1 5-HT_{2A}R transmembrane helix 4

Residue alignment of 5-HT_{2A}R TM4 against other clinically relevant GPCRs reveals the sequences of residues P209^{4.59}, I210^{4.60}, P211^{4.61}, and V212^{4.62} adjacent to the TM4-TM5 HP. Notably P211^{4.61} appears to be a non-conserved residue belonging to the 5-HT₂ receptor subtypes. Pro residues induce helical kinks by sterically hindering neighbouring carbonyl oxygens.¹⁰⁵ Therefore, P209^{4.59} and P211^{4.61} may be associated with a TM4 helical kink observed in available 5-HT_{2A}R XRC structures, represented by **Figure 1.6.2.1-1**. The distortion enhances helical flexibility, enabling kinking and swivel motions.¹⁰⁶ This has been observed in molecular dynamic simulations demonstrating the helical anisotropy associated with Pro residues.¹⁰⁷⁻¹⁰⁹ Additionally, Pro residues like Gly residues can affect interhelical packing.^{110,111,112}

It is common Val and Ile residues are also present in conjunction with Pro and Gly residues. Both Val and Ile residues can influence helical anisotropy depending on their motif position. The flexible, non-planar side chains may be crucial to the remaining α -helix for the hinge kink and swivel motions against the Pro ring.

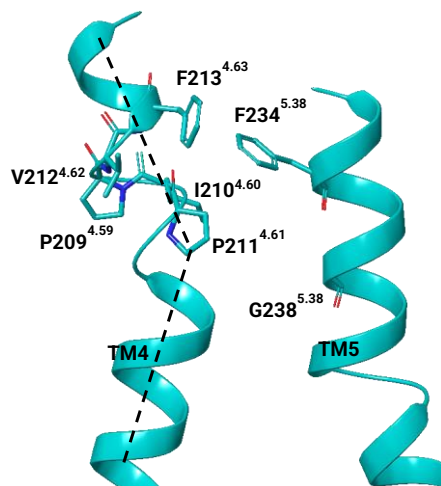


Figure 1.6.2.1-1: 5-HT_{2A}R XRC inactive state structure (PDB: 6A93) with an observable TM4 α -helix kink (dashed line).

The side chain of Val is short with little steric bulk, and the Ile side chain has good flexibility. Therefore, the sequence P209^{4.59}, I210^{4.60}, P211^{4.61}, and V212^{4.62} **Table 1.6.2-1**, may play a role in the dynamics of TM4-TM5 and HP.

1.7 Selectively targeting the 5-HT_{2A}R

The World Health Organization recognizes deteriorating mental health as a global health crisis.^{113,114} In several neuropsychiatric disorders, the 5-HT_{2A}R is implicated,^{8,9} making it a target of interest for various drugs, from antipsychotics to psychedelics.¹⁰ Dysregulation of 5-HT_{2A}R signalling has been linked to conditions such as schizophrenia, depression, and anxiety.¹¹⁻¹⁴ Moreover, 5-HT_{2B}R modulation is associated to psychotic conditions,²⁸ impulsiveness,²⁹ and valvular heart disease.^{30,31} Whereas 5-HT_{2C}R mediated dopamine release has

1. Introduction

opposing effects to 5-HT_{2A}R mediated dopamine release. However, developing subtype selective and effective 5-HT_{2A}R modulators is challenging due to the structural similarities between receptor 5-HT₂ subtypes and closely related receptor families.

This challenge impedes the development of therapeutics due to off-target side effects,¹⁵ as many therapeutics can bind to more receptors than the one distinctly associated with the disease signalling pathway. Therefore, there is a desire for ligands with reduced or no affinity at related receptor subtypes as an approach to minimize unwanted off-target side effects.

1.8 5-HT_{2A}R selective ligands

Therapeutics initially developed as 5-HT_{2A}R selective, **Figure 1.8-1**, e.g. spiperone (**9**), ketanserin (**10**), and volinanserin (**11**) also demonstrate high affinity at other GPCRs, **Table 1.8-1**.

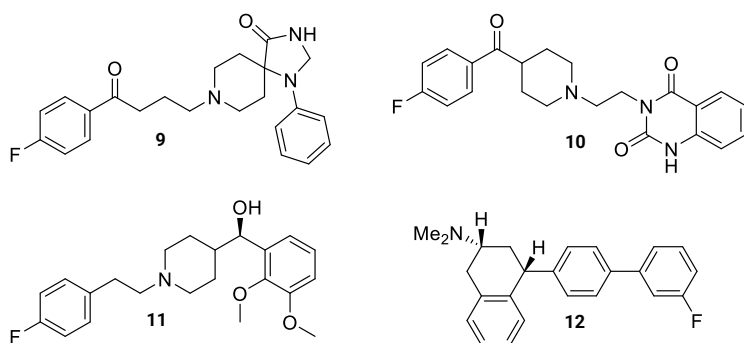


Figure 1.8-1: 5-HT_{2A}R selective ligands, spiperone (**9**), ketanserin (**10**), and volinanserin (**11**), 4-phenyl-2-dimethylaminotetralin *cis*-(2*R*,4*R*)-diastereomer (**12**).

GPCR	Compound pK _i (nM)			
	9	10	11	12
5-HT _{2A} R	7.8	8.5	8.7	9.5
5-HT _{2B} R	5.8	6.2	6	6.77
5-HT _{2C} R	6	6.7	7.5	7.9
5-HT _{1A} R	8.8	5	ND	3
5-HT _{7A} R	7.6	6.3	ND	ND
D ₂ R	8.4	ND	ND	3
α _{1A} R	8.3	8.2	ND	3
α _{1B} R	9.2	8.2	ND	ND
α _{2B} AR	ND	ND	ND	ND
α _{1D} R	8.1	7.8	ND	ND
H ₁ R	ND	ND	ND	6.3

Table 1.8-1: Binding affinity of 5-HT_{2A}R selective ligands (9-12).

Spiperone (**9**) is a butyrophenone antipsychotic and binds at the D₂R¹¹⁵ and 5-HT₂R subtypes,^{116,117} with high affinity. Notably, **9** exhibited > 500-fold higher affinity at the human 5-HT_{2A}R over the 5-HT_{2B}R and 5-HT_{2C}R.¹¹⁸ However, moderate affinity is also reported at the α_{1A}R, α_{1B}R, α_{1D}R,¹¹⁹ 5-HT_{1A}R,¹²⁰ and 5-HT₇R.¹²¹ The radio-labelled analogue, [³H]-spiperone has also been developed and proved useful in the clear labelling and distinguishing of the 5-HT₂ subtypes.¹²² Analogues of **9** were substituted from the *N*1-phenyl 1,3,8-triazaspiro[4.5]decanone moiety to an *N*1-methyl moiety were reported to achieve high selectivity between the 5-HT₂R subtypes. This however still resulted in modest affinity at the D₂R.¹²³

The subsequent development was ketanserin, (**10**) a selective 5-HT_{2A}R and 5-HT_{2C}R antagonist.¹²⁴ Initially it was employed as an antihypertensive agent¹²⁴ and treatment for Raynaud's phenomenon¹²⁵ and recently has been explored as treatment for visual hallucinations.¹²⁶

1. Introduction

The use of **10** as a subtype selective ligand for the 5-HT_{2A}R activity is limited, as it demonstrates high affinity at several aminergic receptors, such as α_{1A} R, α_{1B} R, α_{1D} R,¹¹⁹ moderate affinity at the 5-HT_{2C}R,^{119,122,127,128} and low affinity at the 5HT_{1A}R,¹²⁰ and 5-HT₇R.¹²¹ This is evidenced in the striatum where dopaminergic or adrenergic antagonists could not displace [³H]-ketanserin at the 5-HT_{2A}R. This antagonist also has moderate affinity for the vesicular monoamine transporter 2.^{129,130}

The radioligand, [³H]-ketanserin, is a frequently employed probe used to study 5-HT_{2A}R pharmacology in preclinical research developed from **10**. It has become the primary antagonist based isotopic probe for investigating the serotonergic activity of psychedelics in humans.^{131,132} Thus there is need for 5-HT_{2A}R probes to interrogate the pharmacological profiles of classical and next-generation therapeutics.¹³³

Following the development of **9** and **10** was volinanserin (**11**) which demonstrated sub-nanomolar affinity, and over 100-fold selectivity at the 5-HT_{2A}R compared to off-target GPCR and ion channels.^{134,135} The pharmacological and selectivity profile was derived using a variety of animal species, tissue sources, and radioligands. The recorded affinity appears influenced by differences in: the ligand binding pocket across species,¹³⁶ plasma membrane physiology,¹³⁷ and radiolabelling. For example, studies investigating the behavioural pharmacological profile of **11** appear conflicting. It was not found to be a potent modulator of mouse locomotor activity in some studies,¹³⁸ while in others, strong locomotor-suppressing effects were demonstrated.¹³⁹

1. Introduction

Initially, pre-clinical studies of **11** demonstrated good antipsychotic effects in rodent models with a reduced side effect profile.¹⁴⁰ Positron emission tomography (PET) investigations of the human cortex demonstrated an abundance of **11**-5-HT_{2A}R binding that significantly outlasted the presence of plasma over 24 hours,¹⁴¹ thus suggesting good efficacy. However clinical trials were halted due to challenges in translation of pharmacological results from *in vitro* to *in vivo*.¹⁴²

Recently a series of 4-phenyl-2-dimethylaminotetralin (4-PAT) analogues were reported as selective ligands for 5-HT_{2A}R and 5-HT_{2C}R. The *cis*-(2*R*,4*R*)-diastereomer (**12**) showed stereospecific selectivity, being 40-fold selective for 5-HT_{2A}R over 5-HT_{2C}R,⁹³ and 100-fold selectivity over 5-HT_{2B}R.¹⁴³ *In silico* studies predicted the ligand binding conformation engaged the 5-HT_{2R} TM4-TM5 HP.¹⁷ This was consistent with the associated mutagenesis studies. A significantly reduced binding affinity was observed with a 5-HT_{2A}R G238S^{5,42} mutant, which may impact the TM4-TM5 HP, and perturb ligand binding conformation.⁹³

1.9 Pimavanserin

At current there are no recognised 5-HT_{2A}R subtype-selective ligands or therapeutics. However, pimavanserin (**13**), is a significant advancement towards achieving 5-HT_{2A}R subtype-selectivity. It is a clinically approved therapeutic in the USA, as a treatment for hallucinations and delusions associated with Parkinson's disease psychosis. By employing high-throughput, selectivity screening, followed

1. Introduction

by lead optimization processes, **13** was developed by Acadia Pharmaceuticals.^{143,144} Notably, **13** selectively binds with 1000-fold greater selectivity at the 5-HT_{2A}R ($K_i = 0.4$ nM) in comparison to other the receptors it has been screened against, except for the 5-HT_{2C}R ($K_i = 16$ nM) where only 12-fold greater selectivity is exhibited.¹⁷

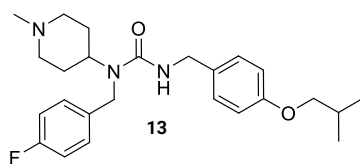


Figure 1.9-1: Pimavanserin (**13**).

Good attenuation of motor and cognitive side effects in humans compared to typical and atypical antipsychotics is reported by **13**.^{144–147} This is currently rationalised by having negligible affinity at the D₂R.¹⁴³ It also has no affinity for the H₁R, the muscarinic, or the α -adrenergic receptor subtypes, which are associated with sedation and weight gain caused by some atypical antipsychotics.^{65–67} Therefore, the pharmacological profile of **13** has the potential to treat other neuropsychiatric disorders involving psychosis and hallucinations.

Species-dependent affinity by 5-HT_{2A}R ligands such as **13** has been demonstrated, and should be considered translating data.^{148,149} For example at modified 5-HT_{2A}R coupled to G_q/G₁₁ proteins expressed in a Sf9 moth cell line, **13** acted as an inverse agonist. The wt 5-HT_{2A}R was not used due to challenges in protein expression.¹⁷ Conversely, in human

1. Introduction

and mouse brain cortex tissue, **13** acted as a neural antagonist towards 5-HT_{2A}R coupled to G_{αq}/G_{α11} proteins *in vivo*.¹⁵⁰

Mutagenesis studies^{17,88} **Table 1.9-1** support *in silico* docking,^{17,88,93} which predicts **13** binding into the TM4-TM5 HP using the 4-isobutoxy moiety. Binding affinity and antagonist activity was significantly attenuated in the mutated G238S^{5,42,17,93,151} A future XRC structure of a **13**-5-HT_{2A}R complex will provide structural confirmation of a binding pose.

Residue mutation	Risperidone K_i (nM)	Pimavanserin K_i (nM)
wt 5-HT _{2A} R	6.9 ¹⁷	9.5 ¹⁷
I206V ^{4,56}	2.8 ¹⁷	2.4 ¹⁷
G238S ^{5,42}	9.2 ¹⁷	184 ¹⁷
W336F ^{6,48}	>1000 ¹⁷	>1000 ¹⁷
wt D ₂ R	9.4 ¹⁵²	0 ^{143,144}

Table 1.9-1: 5-HT_{2A}R residue point mutations and associated binding affinities show residue G238^{5,42} is implicated in the binding mode of **13 in comparison to **4**.**

In comparison to the risperidone-5-HT_{2A}R XRC structure, **4** binds in the hydrophobic cleft, and is absent from the TM4-TM5 HP.¹⁷ Subsequently the binding affinity for **4** is reported to not be significantly affected by point mutation G238S^{5,42,17}.

No XRC structures are available for **13** in complex with the 5-HT_{2C}R either. However, molecular docking suggests the 5-HT_{2C}R residue F214^{5,38} may adopt an outward facing rotamer orientation, similar to F234^{5,38} resolved in the 5-HT_{2A}R, thereby accommodating the ligand.⁸⁸

Better insight into the effect of **13** on the 5-HT_{2C}R is still required as the receptor is widely expressed in the brain where it modulates various

1. Introduction

functions, including dopamine release in the midbrain. Dopamine is a key neurotransmitter involved in motor control, reward, cognition, and emotion.¹⁵³

The 5-HT_{2A}R and 5-HT_{2C}R have opposing effects to post-synaptic dopamine release. 5-HT_{2A}R receptor inhibition decreases dopamine release whereas 5-HT_{2C}R inhibition increases dopamine release.¹⁵⁴ Therefore, the activity of **13** at 5-HT_{2C}R may counter its desired effects at 5-HT_{2A}R, thus potentially diminishing both its efficacy and potency.

Non-GPCR off-targets of **13** also include the α -1 subunit of L-type calcium channels, a voltage-gated ion channel that mediates calcium influx into neurons.¹⁵⁵ Metabolism of **13** is carried out by cytochrome P450 enzymes; 3A4, 3A5, and 2J2.¹⁵⁶ However, ketoconazole, a potent P450 3A4 inhibitor, can indirectly increase the plasma concentration of **13** by 4-fold. Rifampin, a strong P450 3A4 inducer, can indirectly decrease it by 90%.¹⁵⁶ Therefore, dose adjustment and monitoring is required when co-administering **13** with drugs or foods that modulate P450 3A4 activity, such as opioids, calcium channel blockers,¹⁵⁷ and grapefruit juice.¹⁵⁸

1.10 Pimavanserin structure-activity relationships

A primary goal in medicinal chemistry is to comprehend how the structural features of molecules influence their pharmacological properties. Structure-activity relationships (SARs) maps the effects of specific structural modifications on the biological activity of a

1. Introduction

compound. The SARs of various classes of molecules targeting the serotonin 5-HT_{2A}R has been extensively studied.^{93,151,159,160} These molecules commonly share structural features contributing to binding affinity for the 5-HT_{2A}R. Structure-activity relationship (SAR) analysis becomes more reliable when focusing on a series of similar compounds with a shared scaffold.

Pimavanserin (**13**) serves as a promising model scaffold for exploring 5-HT_{2A}R binding affinity and subtype selectivity. A previously reported ring labelling system **Figure 1.10-1** has been adapted and facilitates the delineation of SAR.¹⁵¹ Modification to the ring moieties attached to the urea core have led to the development of pimavanserin analogues for the 5-HT_{2A}R. The SAR for ring modifications tabulated below has been derived from functional assays of separate experiments.

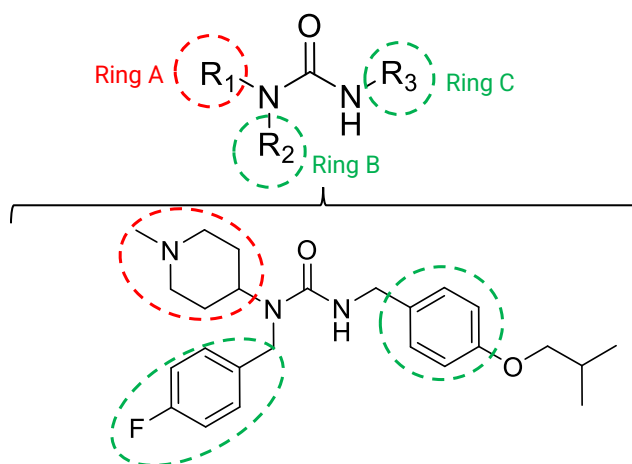
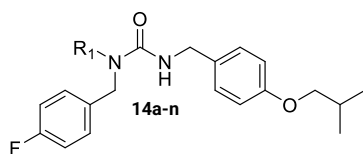


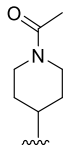
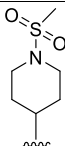
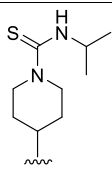
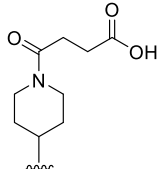
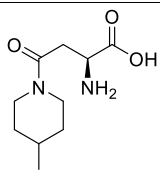
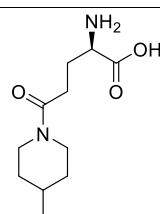
Figure 1.10-1: SAR map of the pimavanserin scaffold depicted by 3 ring regions and tri-substituted urea core. Source: Adapted from Ma et al 2022¹⁵¹

1.10.1 Ring A analogues



Compound	R ₁	IC ₅₀ (nM)
13		22, ¹⁶¹ 27.3 ¹⁵¹
14a		75.40 ¹⁵¹
14b		252.00 ¹⁵¹
14c		138.00 ¹⁵¹
14d		110.20 ¹⁵¹
14e		500.00 ¹⁵¹

1. Introduction

14f	 <chem>CC(=O)N1CCN(C1)C2=CN=C(C=O)N2</chem>	ND ¹⁶¹
14g	 <chem>CC(=O)N1CCN(C1)C2=CN=C(C=O)N2S(=O)(=O)N</chem>	2018.00 ¹⁶¹
14h	 <chem>CC(=O)N1CCN(C1)C2=CN=C(C=O)N2C(=S)NC(C)C</chem>	1126.00 ¹⁶¹
14i	 <chem>CC(=O)N1CCN(C1)C2=CN=C(C=O)N2C(=O)CC(=O)O</chem>	317.30 ¹⁶¹
14j	 <chem>CC(=O)N1CCN(C1)C2=CN=C(C=O)N2C(=O)C[C@H](N)C(=O)O</chem>	34.65 ¹⁶¹
14k	 <chem>CC(=O)N1CCN(C1)C2=CN=C(C=O)N2C(=O)C[C@@H](N)C(=O)O</chem>	8.35 ¹⁶¹

1. Introduction

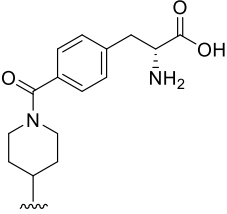
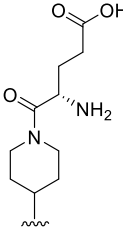
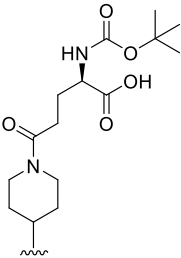
14l		ND ¹⁶¹
14m		ND ¹⁶¹
14n		ND ¹⁶¹

Table 1.10.1-1 : Pimavanserin ring A analogues 14a-n. No detectable binding (ND).

The *N*1-methyl-piperidin-4-yl ring moiety is crucial for binding in pimavanserin analogues.^{151,161} Under physiological conditions, it binds at the 5-HT_{2A}R as an *N*1-methyl-piperidinium ring via an essential ammonium ion. This structural motif is also utilized in analogues and other drugs that interact with the 5-HT_{2A}R, such as **4** and **10**.

Several ring A analogues have been reported **Table 1.10.1-1** are compared in context to **13**. Modification of the *N*-methyl piperidin-4-yl to a dimethylamino-ethyl amine **14a** and an *N*-dimethylacetamide **14b**, respectively, led to a decrease in antagonism at the receptor. Removing

1. Introduction

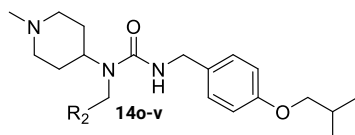
the basic nitrogen from the ring system by replacing the piperidin-4-yl ring with either a cyclobutene **14c**, cyclopentane **14d**, and cyclohexane ring **14e** with a 3-position dimethylamine significantly also decreased activity.¹⁵¹

Substituting the *N*-methyl group to either *N*-acetyl **14f**, *N*-methylsulfonyl **14g**, or *N*-isopropyl thiourea **14h** moiety resulted in decreased antagonism. *N*-carboxylic acid derivatives **14i-14m** convert the piperidin-4-yl nitrogen into an amide. Thus, they may bind via primary amines present on the amino acid moiety-carbon backbone. This aligns with the absence of detectable binding of **14n**, the *N*-Boc variant of **14k**. Moreover, the amine moiety position on the amino-acid backbone appears to be critical ligand binding with respect to **14l** and **14m**.

Overall modification of the *N*-methylpiperidinyl ring and repositioning the amine moiety resulted in a decrease in antagonism at the receptor with all analogues except **14k**. Analogue **14k** demonstrated improved selectivity towards the 5-HT_{2A}R, achieving a 6-fold greater selectivity for the 5-HT_{2A}R over the 5-HT_{2C}R.¹⁶²

The available ring A SAR data indicate that the piperidinyl ring system is optimal for 5-HT_{2A}R binding. *N*-piperidinyl substitution and alterations in the positioning of the amine moiety have proven detrimental to ligand binding in all analogues reported except one, for which improved 5-HT_{2A}R selectivity was highlighted.

1.10.2 Ring B analogues



Compound	R ₂	IC ₅₀ (nM)
13		27.3 ¹⁵¹
14o		>500 ¹⁵¹
14p		>500 ¹⁵¹
14q		>500 ¹⁵¹
14r		>500 ¹⁵¹
14s		8.64 ¹⁵¹

1. Introduction

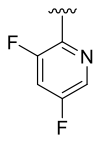
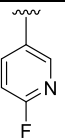
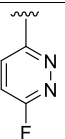
14t	 A pyridine ring with fluorine atoms at the 3 and 5 positions and a wavy line at the 2 position.	43.20 ¹⁵¹
14u	 A pyridine ring with a fluorine atom at the 3 position and a wavy line at the 2 position.	>500 ¹⁵¹
14v	 A pyridine ring with a fluorine atom at the 3 position and a wavy line at the 4 position.	14.70 ¹⁵¹

Table 1.10.2-1: Pimavanserin ring B analogues 14o-v. No detectable binding (ND).

The 4-fluorobenzyl ring appears to be a significant structural feature for ligand binding. During the binding of **13** it is predicted to occupy a hydrophobic cleft, which is also comparable to the binding conformation of **4** when bound to the 5-HT_{2A}R.¹⁷

In comparison to **13**, substituting the fluorobenzyl group with bulkier groups lacking a halogen atom, **Table 1.10.2-1**, such as benzothiophene **14o**, benzimidazole **14p**, pyrazole **14q** or 3,5-dimethyloxazole **14r**, leads to a reduction in antagonism. However the replacement of the 4-fluorobenzyl ring with a 3-fluoropyridyl ring **14s** significantly enhances antagonist potency.¹⁵¹

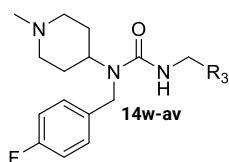
Introduction of an additional 3 position fluorine substitution to afford the disubstituted 3,3-difluoropyridyl ring **14t** lessens antagonist activity, and replacement of the pyridyl ring to a 2-fluoropyridyl ring **14u**

1. Introduction

abolishes binding affinity. Interestingly, replacement of the pyridyl ring to afford 3-fluoropyridazyl **14v** results in a complete loss of inverse agonism while still retaining binding affinity and antagonist activity.¹⁵¹ These findings highlight that ring B can be associated with modulating antagonism at the 5-HT_{2A}R. The reported modifications lead to reduction potency overall, except for the 3-fluoropyridyl analogue.

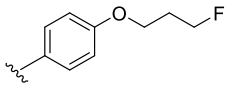
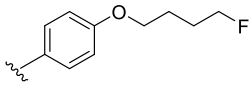
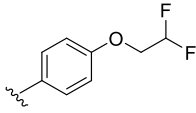
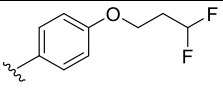
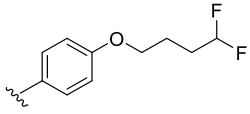
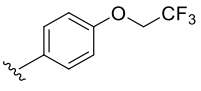
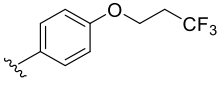
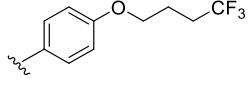
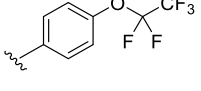
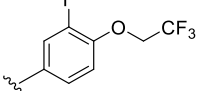
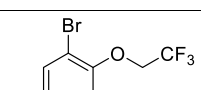
In contrast, many 5-HT_{2A}R agonists lack this type of structural feature which binds amongst the hydrophobic PIF motif residues in the 5-HT_{2A}R.¹⁵⁹ Thus, when agonist-bound the hydrophobic cleft is lessened or absent.^{41,69} These divergent binding modes and linked structural requirements between 5-HT_{2A}R antagonists and agonists highlight the complex nature of ligand-receptor interactions and association to functional selectivity.

1.10.3 Ring C analogues

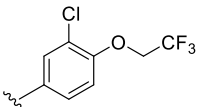
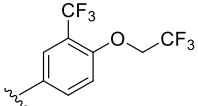
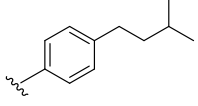
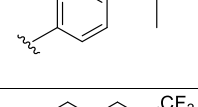
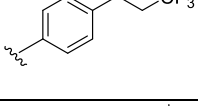
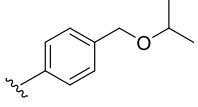
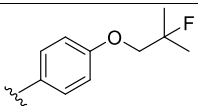
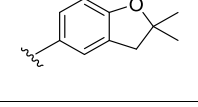
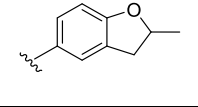
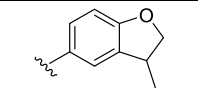
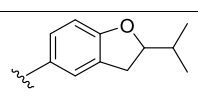


Compound	R ₃	IC ₅₀ (nM)
13		79.4, ¹⁵⁷ 27.3 ¹⁵¹
14w		2.11 ¹⁵¹

1. Introduction

14x		1.93 ¹⁵¹
14y		2.35 ¹⁵¹
14z		2.17 ¹⁵¹
14aa		4.64 ¹⁵¹
14ab		4.29 ¹⁵¹
14ac		0.54 ¹⁵¹
14ad		4.70 ¹⁵¹
14ae		3.78 ¹⁵¹
14af		33.40 ¹⁵¹
14ag		6.86 ¹⁵¹
14ah		12.00 ¹⁵¹

1. Introduction

14ai		27.30 ¹⁵¹
14aj		125.00 ¹⁵¹
14ak		67.20 ¹⁵¹
14al		26.40 ¹⁵¹
14am		18.30 ¹⁵¹
14an		2.05 ¹⁵¹
14ao		3.13 ¹⁵¹
14ap		3.49, ¹⁵¹ 0.0631 ¹⁵⁷
14aq		0.25 ¹⁵⁷
14ar		0.16 ¹⁵⁷
14as		9.98 ¹⁵¹

1. Introduction

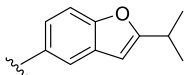
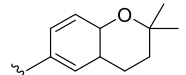
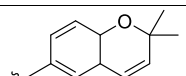
14at		20.90 ¹⁵¹
14au		21.25 ¹⁵¹
14av		17.27 ¹⁵¹

Table 1.10.3-1: Pimavanserin ring C analogues 14w-av.

The benzyl 4-isobutoxy moiety of **13** is an important structural feature associated to its 5-HT_{2A}R selectivity, which is reported to interact with the TM4-TM5 HP.¹⁷ In comparison to **13**, there are several analogues modified at the ring C position **Table 1.10.3-1** which exhibit significantly improved potency and selectivity.^{151,161,163}

Cell-based activation assays demonstrated substitutions of the 4-isobutoxy group with either mono- or di- fluorinated and tri- fluorinated alkyl chains, **14w-ae**, have led to analogues with 5 to 10-fold higher potency than that of **13**. A notable modification was replacement of the 4-isobutoxy moiety to a 2,2,2-trifluoroethoxy moiety, **14ac**. This resulted in a 54-fold increase in potency as compared to **13**. The affinity for the 5-HT_{2A}R ($K_i = 0.2$ nM) was 10-fold greater as compared to the 5-HT_{2C}R ($K_i = 2.0$ nM), and a 1000-fold greater over the 5HT_{2B}R ($K_i = 138.7$ nM).¹⁵¹ Docking was used to rationalize ligand binding, predicting the 4-trifluorobutoxy moiety to engage the TM4-TM5 HP.¹⁵¹ The modification of **14c** via introduction of a difluorinated methylene moiety on the alkyl

1. Introduction

chain back bone following resulted in **14af**, although this led to reduction in potency in comparison to **13**.¹⁵¹

The inclusion of electron withdrawing groups such as fluorine and bromine atoms at the 3 position on benzyl ring **14ag-ah**, improved the antagonist activity at the 5-HT_{2A}R 4-fold and 2-fold greater than **13** respectively. However, substitution to a chlorine atom **14ai** reduced the potency 5-fold. Substitution to a trifluoromethyl moiety **14aj** attained potency equal to **13**.¹⁵¹

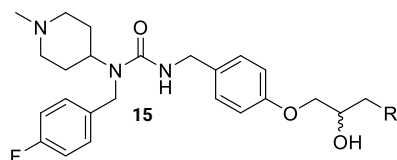
Replacement of the benzylic 4-isobutoxy moiety with an isopentyl moiety in **14ak** also reduced the potency in comparison to **13**. Contrary to this, a reduction of the alkyl chain backbone by a methylene unit to afford an isobutyl moiety **14al** regained potency similar to **13**. Substitution to a trifluoropropyl moiety **14am** increased potency further than that of **13**, but was over 2-fold weaker than that of its trifluoropropoxy analogue **14ad** indicating the oxygen atom at this position can be beneficial to ligand binding. This was further supported by the repositioning the oxygen atom one carbon away from the aromatic ring **14an** which also improved the potency 13-fold greater than **13**. Inclusion of a fluorine atom, **14ao**, substituting the isobutoxy moiety hydrogen atom on **13** also improved potency 9-fold.¹⁵¹

Restricted 4-O-alkoxy benzyl moiety isomers, featuring benzofuran moieties **14ap-ar** exhibited improved potency in comparison to **13**, but similar binding affinities in radioligand competition binding assays.¹⁵⁷

1. Introduction

However, benzopyran derivatives **14au-av** exhibited a decrease in potency, thus highlighting an association between the ring size and sterics of the *O*-benzyl substitution moiety.¹⁵¹ These ring C analogues demonstrate that sterics effects and bulk in this region can impact ligand binding affinity and potency.

1.10.3.1 Extension of ring C



Compound	R	IC ₅₀ (nM)
13	-	22 ¹⁶¹
15a		0.39 ¹⁶¹
15b		0.87 ¹⁶¹
15c		93.62 ¹⁶¹
15d		ND ¹⁶¹

Table 1.10.3.1-1: Pimavanserin (Ring C) amino alcohol analogues (15a-d). No detectable binding (ND).

1. Introduction

Extending the ring C further **Table 1.10.3.1-1** via substitution of 4-isobutoxy moiety with amino alcohol moieties **15a-d**, lead to increased ligand potency as compared to **13**

Two bulky bicyclic heterocyclic amino alcohol moieties reported: 6-fluoro-3-(piperidin-4-yl)benzo[*d*]-isoxazole **15a** and 3-(1-piperazinyl)-1,2-benzisothiazole **15b** analogues, exhibited the greatest improvement in antagonistic potency, 25-56-fold in comparison to **13**. The *N*-Boc-piperazine derivative **15c** also displayed a 10-fold increase in potency. Notably, *N*-Boc-deprotection to afford a piperazine ring to afford **15d**, resulted in no detectable binding.¹⁶¹ These findings demonstrate that extending **13** at the ring C region via amino alcohol amine moieties is an effective structural modification. Results display enhanced ligand potency appears to be correlated with the larger size, increased lipophilicity of the ligand, as well as additional hydrogen bond donor and acceptor atoms present associated to the amino alcohol moiety.

1.10.4 Pimavanserin scaffold core

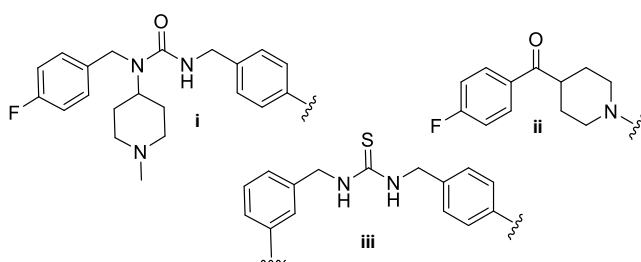


Figure 1.10.4-1: Structural cores of 5-HT_{2A}R selective ligands : (i) **13**, (ii) **10**, and (iii) general structure of 1,3-disubstituted thiourea ligands.

A urea moiety features as the central core of the **13** structure. It adopts a planar conformation, a characteristic shared by ligands with related similar skeletal structures, such as **10** which features a benzoylpiperidinyl core with a planar carbonyl group. Reducing the carbonyl group of **10** to an alcohol or replacement with a methyl moiety results in a decrease in binding affinity.^{162,164} Hence, preserving the planarity of the urea moiety may confer advantageous binding properties to analogues of **13**.

Biosteric replacement of the urea with a thiourea moiety **Figure 1.10.4-1** resulted in improved binding affinity, surpassing that of **10** *in vitro*. The incorporation of a substituted benzyl ring system on each ureic nitrogen atom resulted in ligands that maintained comparable antagonistic activity. Thus, demonstrating the ability of the receptor to accommodate diverse substitutions. For example, 3-trifluoropropyl, 3-nitro, and 4-chloro substituents on one ring, and halogen or alkoxy moieties at 3 and 4 positions on the opposite ring.¹⁶⁵ No subtype selective was demonstrated by the thiourea derivatives between the 5-HT_{2A}R and 5-HT_{2C}R.

1.11 Fluorescence-based methods to interrogate the 5-HT_{2A}R

In response to the plethora of molecules which bind to the 5-HT_{2A}R, two possible approaches to investigate their pharmacology are radioligand-based methods or fluorescent-based methods. One well-

1. Introduction

established fluorescent-based method is time-resolved Förster resonance energy transfer (TR-FRET) **Figure 1.11-1**.

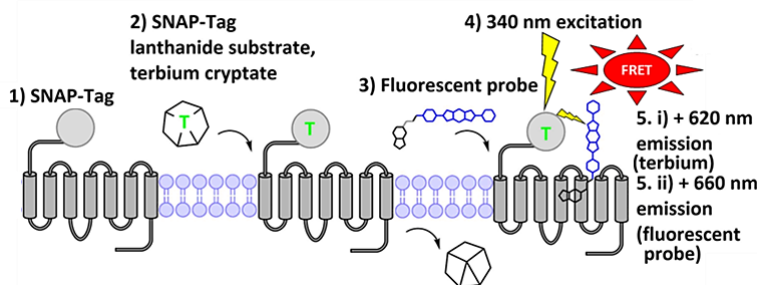


Figure 1.11-1: Labelling protocol of GPCR N-terminus and fluorescent probe binding during cell membrane-based fluorescent TR-FRET assay. (1) SNAP-Tag has been engineered onto the N terminus of a GPCR of interest, (2) a lanthanide donor using terbium cryptate is delivered to the receptor via a membrane impermeant lanthanide labelled SNAP-Tag substrate, (3) the fluorescent probe is added to the modified SNAP-Tag GPCR, (4) the lanthanide label is then excited using laser excitation (e.g. ~340 nm; yellow lightning arrow). If the lanthanide and fluorescent probe are within proximity to each other (typically <10 nm), the energy emitted following lanthanide excitation can be transferred to excite the fluorophore of the fluorescent probe (FRET). Fluorescence emissions from donor and acceptor can be recorded and to calculate FRET ratios. Source: Adapted from Sykes et al 2019 ^{166,167}

The cell membrane-based fluorescent TR-FRET assay enables the evaluation of ligand binding affinities, as well as the determination of binding kinetics over specified concentrations and time periods. Binding affinities are expressed as equilibrium dissociation constant (K_d). K_d represent the ligand concentration at which 50% binding sites are occupied. Kinetics may be expressed as the observed rate constant (K_{obs}). Both quantify ratio between the association rate (K_{on}), and the rate of dissociation (K_{off}) of drug binding to the molecular target.¹⁶⁶ However, K_{obs} quantifies the association and dissociation rate of drug binding to the molecular target at a specific ligand concentration. Unlike K_{obs} which

1. Introduction

is concentration-dependent, K_d is concentration-independent. Thus, making it a more universal measure of binding strength. Therefore, K_d values are often calculated from kinetic assays.

To obtain ligand binding affinities and kinetic rates, TR-FRET relies on the use of donor and acceptor fluorophores. These are fluorophores which have distinct emission peak maxima but are required to have spectral overlap within the emission spectrum to allow FRET to occur. Together they are considered a FRET pair which leverage the phenomenon of FRET.

Following laser excitation of the donor fluorophore FRET occurs between the acceptor fluorophore through non-radiative dipole-dipole interactions. This leads to changes in the fluorescence emission spectrum. Optimal distances between the donor and acceptor fluorophores range within 1–10 nm for efficient FRET.¹⁶⁶

Fundamental to TR-FRET, is the terbium donor fluorophore long emission lifetime and acceptor fluorophore short emission lifetime, which allows for a time gated/time resolved (tr) detection between excitation and fluorescence of the acceptor fluorophore. This time resolved feature is critical to the assay by allowing short-lived background fluorescence from the assay components to decay.^{166,167}

Labelling and probe requirements for TR-FRET assays are first target proteins are required to be modified by chemical labelling with lanthanides for example terbium, which acts as a donor fluorophore. This

1. Introduction

incorporates terbium into the protein structure. The next requirement is a high affinity fluorescent probe. These are based on high affinity ligands known to bind at the target receptor or protein which act as either antagonists or agonists. They have been strategically modified to feature a fluorophore as part of their molecular structure.¹⁶⁸ Therefore, attaching an acceptor fluorophore to a receptor-targeting moiety, a ligand that is known to target the 5-HT_{2A}R possessing donor fluorophore, TR-FRET-based probes may be developed.^{168,169} These fluorescent probes would assist the screening of unlabelled ligands at the 5-HT_{2A}R.

Several studies have documented the development of fluorescent probes with selective binding to the 5-HT subtypes, including 5-HT_{1A}R,¹⁷⁰ 5-HT_{2A}R,¹⁷¹ 5-HT_{2B}R,¹⁷² 5-HT_CR,¹⁷¹ 5-HT₃R,¹⁷³ 5-HT₄R,¹⁷⁴ and 5-HT₆R.¹⁷⁵ However, the current availability of a fully characterised fluorescent probe for the 5-HT_{2A}R is limited to CA201019,¹⁷⁶ a 5-HT_{2A}R and 5-HT_{2B}R-selective fluorescent probe. Its exact structure remains undisclosed, but it is based on 4-(4-fluorobenzoyl)-1-(4-phenylbutyl)piperidine (4F4PP) (16).

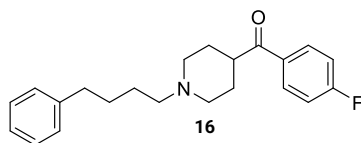


Figure 1.11-2: 4-(4-fluorobenzoyl)-1-(4-phenylbutyl)piperidine (4F4PP) (16).

One study has reported the utilization of this probe, CA201019, in conjunction with the TR-FRET technique to study the kinetics of

1. Introduction

antipsychotics binding to the 5-HT_{2A}R, but it demonstrated low specific binding across a concentration range used.¹⁷⁷ Therefore, there is a need to develop additional fluorescent probes targeting the 5-HT_{2A}R with improved binding profiles. For example, lower non-specific binding and assay ranges, which achieve binding at lower micromolar concentrations may allow better characterisation of the initial binding phase.

In comparison to the reported radioligands such as [¹²⁵I]-R-DOI,¹⁷⁸ [³H]-spiperone,¹²² or [³H]-ketanserin,¹³⁰ fluorescent probes offer several advantages; enhanced safety, cost-effectiveness, and faster experimental procedures.¹⁶⁷ As a result, they serve as attractive tools for researchers investigating GPCR function.

1.12 *In silico* tools for exploration of the 5-HT_{2A}R

Integration of experimental structural data, such as XRC, cryo-em, and NMR structures, with molecular modelling techniques into medicinal chemistry has made significant improvements in defining the molecular basis of drug interactions with the 5-HT_{2A}R, as well as providing insight into receptor structure and dynamics. Advancements in hardware and software have proved advantageous in permitting the visual analysis and juxtaposition of structural and physiochemical data, leading to structure-based drug design approach. This approach capitalizes on targeting distinct structural attributes of the receptor, particularly those not observed in closely related or structurally homologous receptors.

The structure-based drug design approach has proven successful in enhancing selectivity. For example, in A₂AR XRC structures, an uncharacterized pocket within the helices bundle not present in the A₁AR XRC structures was identified. The design of ligands targeting this novel pocket followed resulting in potent and selective 1,2,4-triazine A₂AR antagonists.¹⁷⁹

1.12.1 Homology modelling: building protein structure

Homology modelling is a technique for studying the structures of proteins that are not yet experimentally resolved. It relies on finding a suitable template structure that shares a high degree of similarity with the target protein sequence. A common criterion is for the template and target to share at least 30% sequence identity. Conserved residues and motifs act as anchors for sequence alignment, while another critical criterion is resolution.

In X-ray crystallography, structural resolution is a measure of detail in the diffraction pattern, providing insights into atomic arrangements within crystals.¹⁸⁰ Cryo-em utilizes high-energy electrons to illuminate specimens and generate diffraction patterns using a magnetic objective lens, enabling the study of non-crystalline structures.¹⁸¹ In contrast, NMR spectroscopy focuses on analysing nuclear magnetic resonance signals to study molecular structures and interactions,¹⁸² distinct from the diffraction patterns seen in XRC and cryo-em.

1. Introduction

The ideal electron density map calculated that is used must be below 3.0 Å. This allows for the identification of most or all atoms in the protein, as well as their interactions with ligands and solvent molecules. Lower resolution structures, above 3.0 Å, only reveal the general shape of the protein backbone, and the atomic details must be inferred from other sources.¹⁸³ The choice of software also affects quality and accuracy of the resulting homology model, and there are many options available for this purpose, from free web servers to expensive software packages that include tools for model refinement and evaluation.

In this work the web-based tool, the automated SWISS-MODEL server was the homology model builder.¹⁸⁴ It works by first searching for suitable XRC, cryo-em, or NMR structure in the Protein Data Bank (PDB)¹⁸⁵ that share significant sequence similarity with the target protein to be used as a template. Sequence alignment is then performed with the target sequence and template structure, transferring the coordinates of the conserved regions to the target. Finally, it uses various methods to refine the model and estimate its quality and reliability.

The XRC structures often necessitate modifications to aid in the formation of crystals that diffract to an acceptable resolution,¹⁸⁰ despite the potential disruption of their native conformation. These essential modifications significantly enhance the quality of crystal structures obtained through X-ray crystallography. These modifications encompass the insertion of polar proteins and antibodies, truncation of terminal regions, introduction of multiple point mutations of residues, and

crystallization under non-physiological conditions. Consequently, when modelling proteins and their ligands, it is important to consider reverse engineering mutations and conduct structural refinements to accurately represent canonical sequences in the natural environment.

The use of homology models based on early XRC structures of bovine rhodopsin (PDB: 1U19)¹⁸⁶ and β_2 AR (PDB: 2RH1)¹⁸⁷ enabled the identification of key structural features of 5-HT_{2A}R.¹⁸⁸ However, different receptor types can have low sequence homology or unique structural features. The availability of XRC structures of 5-HT_{2A}R with higher sequence identity to the canonical sequence offers an opportunity to significantly improve the accuracy and reliability of the 5-HT_{2A}R homology models.

1.12.2 Homology model assessment

One of the challenges of computational protein structure prediction is to ensure that the generated models reflect physiological conditions. Therefore, it is essential to evaluate the quality and reliability of the models using various assessment methods.

SWISS-MODEL¹⁸⁴ filters templates and alignments. 50 top-ranked templates are then selected from the full list according to a score which combines sequence coverage and similarity. The top-ranked templates and alignments are further assessed and ordered according to the expected quality of homology model, as estimated by a global model

1. Introduction

quality estimate (GMQE). This is set from 0-1, where nearing 1 indicates a higher expected quality of homology model.

SWISS-MODEL¹⁸⁴ employs a QMEAN score,¹⁸⁹ a scoring function that evaluates the quality of protein structure models based on their geometrical features. It can provide both global (for the whole structure) and local (for each residue) quality scores. It compares a single model with statistical potentials and distance constraints derived from homologous structures. The quality scores are normalized to match with high-resolution XRC structures. A QMEAN closer to 0 indicates a better agreement, while score below -4.0 indicate models of low quality.¹⁹⁰

Ramachandran plots are employed, which visualize regions for the backbone dihedral angles Phi (φ) and Psi (ψ) of amino acid residues from energetically favoured, to generously allowed, additionally allowed, and disallowed regions. Such categorisation is based on the stereochemical quality and statistical significance of the observed angles.¹⁹¹ The regions are determined by analysing the distribution of φ and ψ angles based from a large data set of high-quality experimental structures. SWISS-MODEL uses 12,521 non-redundant experimental structures with a pairwise sequence identity cut-off at 30% and an X-ray resolution cut-off at 2.5 Å, gathered from the protein sequence culling server (PISCES) database, used to cull sets of protein sequences from the PDB with the aim of generating non-redundant datasets.¹⁹²

MolProbity¹⁹³ a web service can also be used to validate the quality of protein structures at both global and local scales. It calculates the MolProbity score, which is a measure of how well the structure matches the expected quality at a given resolution. Evaluations include the clash score, the amount of overlap between van der Waals radii of atoms and the rotamer outliers, which are amino acids with unlikely side chain conformations. Additionally, MolProbity also calculates the Ramachandran plot. It then combines these evaluations into a single score, normalized at an equivalent scaling to X-ray resolution.¹⁹³

Herein, the SWISS-MODEL assessment protocol and MolProbity was used for 5-HT_{2A}R homology model validation to evaluate the quality and reliability before being employed *in silico* interrogation.

1.12.3 Modelling ligand binding: molecular docking

Molecular docking is a computational method that simulates the interaction between a ligand and a protein target. It aims to find the optimal orientation and conformation of the ligand that minimizes the free energy of the complex. It can be used in structure-based design approaches to develop various ligands and study ligand-protein interactions.

One of the molecular docking programs that has been widely validated is Glide, developed by Schrödinger.^{194,195} Glide can dock various molecules into molecular structure such as proteins and enzymes to varying degrees of rigor and accuracy at the expense of computational

1. Introduction

efficiency by either rigid or flexible docking methods. The poses are scored using an empirical function called ChemScore that consists of several energy components that aim to represent key properties of ligand-protein binding,¹⁹⁶ and then refined using a proprietary function called GlideScore (Gscore).^{194,195} Glide can incorporate constraints, conditions that must be satisfied by the predicted poses. For example, specific interactions or distances between atoms. Glide can reject any poses that do not meet the constraints during the docking process. Results, docked poses of the ligand, are then ranked in order of decreasing Gscore.^{194,195} The lower Gscore indicates a more energetically favoured and stable complex. A molecular docking workflow in Glide is represented by **Figure 1.12.3-1**.

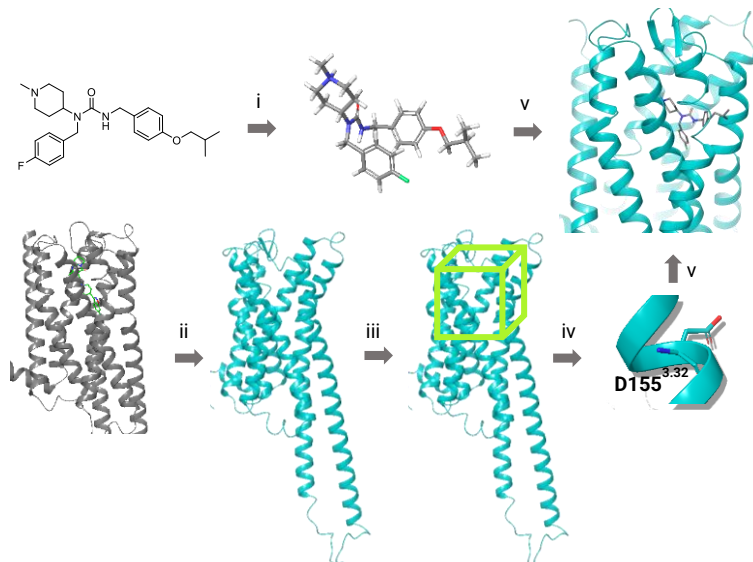


Figure 1.12.3-1: Molecular docking workflow schematic, (i) ligand preparation, (ii) protein preparation of XRC structure or homology model (iii) grid-box generation, (iv) setting docking constraints and protocol, (v) docking of prepared ligands using docking protocol. Predicted binding poses ranking docked ligands by Gscore.

1.12.3.1 Glide docking process summary

Glide employs a hierarchical series of filters to explore potential ligand locations within the receptor's active-site region. The receptor's shape and properties are represented on a grid through various fields, which provide an increasingly accurate scoring of ligand poses. Glide is most effective when generating ligand conformations within the software, as opposed to other methods such as the RDKit cheminformatics open source software experimental-torsion-knowledge distance geometry (ETKDG) and deep molecular conformation generative method (DMCG)¹⁹⁷ which dock the ligand core plus all possible rotamer-group conformations as a single object, or using pre-computed conformations respectively.

For each ligand, a search of potential locations and orientations is conducted across the defined grid-box.¹⁷⁴ The Glide process involves several stages is described below:

- 1) **Site point selection:** The search begins by identifying "site points" on a 2Å grid covering the grid-box. These points are selected based on distances from grid-box surfaces, with Glide positioning the ligand centre at a site point.
- 2) **Hierarchical filtering:** The filtering proceeds through a series of processes: A) *Orientation Examination:* Atoms within a specified distance of the ligand diameter are examined for possible orientations. If steric clashes are encountered, orientations are skipped. B) *Rotation Consideration:* Rotation about the ligand diameter is then explored,

1. Introduction

scoring interactions of atoms capable of forming hydrogen bonds or ligand-metal interactions with the receptor. C) *Greedy Scoring*: Interactions with the receptor are scored next using Schrödinger's discretized version of the ChemScore empirical scoring function, considering hydrophobic, hydrogen-bonding, and metal-ligand interactions, while penalizing steric clashes. D) *Refinement*: The top-scoring poses then undergo refinement, allowing rigid movements in Cartesian directions to improve accuracy. E) *Energy Minimization*: Energy minimization is then performed on pre-computed grids for van der Waals and electrostatic interactions, followed by optimization of torsional motion for internally generated conformations. F) *Rescoring*: Lastly, after minimizing the poses, Schrödinger's proprietary GlideScore scoring function is applied to rescore them. This hierarchical approach and optimizing rotamer groups individually enables Glide to predict ligand binding modes while significantly reducing computational resource as compared to exhaustive searches.

The GlideScore **Equation: 12.3.1-A**, originating from ChemScore, incorporates additional factors such as steric-clash and buried polar terms, introduced by Schrödinger to penalize electrostatic mismatches, along with hydrophobic enclosure terms, as well as amide twist, and excluded volume penalties.¹⁹⁴

Equation: 12.3.-A

$$\text{Gscore} = 0.05\text{vdW} + 0.15\text{Coul} + \text{Lipo} + \text{Hbond} + \text{Metal} + \text{Rewards} + \text{RotB} + \text{Site}$$

1. Introduction

Each component in the Gscore formula represents distinct energetic contributions. Van der Waals energy (vDW) accounts for interactions with groups possessing formal charges, such as metals, carboxylates, and guanidiniums, while Coulomb energy (Coul) considers reduced net ionic charges on such groups. The Lipophilic term (Lipo) is derived from the hydrophobic grid potential, and Hydrogen-bonding interactions (HBond) involve weighted components based on the charge state of donor and acceptor atoms. Metal-binding interactions (Metal) include considerations of anionic or highly polar acceptor atom interactions. Rewards encompass various features such as buried polar groups, hydrophobic enclosure, correlated hydrogen bonds, and amide twists, offering both rewards and penalties. Penalties for freezing rotatable bonds is represented as (RotB), and polar interactions in the active site is expressed as (Site) reward polar but non-hydrogen-bonding atoms in a hydrophobic region. For Glide Standard Precision (SP) Gscores of -10 or lower are generally considered to represent good binding. In Glide Extra Precision (XP), results tend to achieve Gscores -12 or lower.¹⁹⁴

3) **Scoring and selection:** The best-docked structure for each ligand is determined by a model energy score (Emodel score) that combines energy grid score, binding free energy predicted by GlideScore, and internal strain energy. Additionally, a specially formulated Coulomb-van der Waals interaction-energy score is computed for comparing binding affinities.¹⁹⁴

4) **Constraints:** These are conditions that must be satisfied by the predicted poses. For example, these may be known or required ligand-protein interactions. Constraints play part as integral functions to docking in Glide. These dictate specific ligand-receptor interaction criteria, guiding ligand placement relative to critical receptor features during docking. They ensure ligand poses adhere to predefined requirements.¹⁹⁴

During the Glide process, first ligand atoms are evaluated, and ligands lacking the necessary atom types for interactions are skipped. Subsequent filters ensure matching distances between partner atoms and receptor atoms, while also orienting ligand rotations appropriately. Additionally, a restraining potential maintains constraint-satisfying distances, preventing ligand atom displacement. The grid-optimized poses are rejected if they do not satisfy all selected constraints. Core constraints place matching core atoms to the same coordinates as the reference ligand and rebuilding non-core atoms. These non-core atoms undergo refinement via grid minimization and torsional sampling to improve poses. Finally, post-docking minimization adjusts core atom positions as needed.¹⁹⁴

Glide has been successfully applied to study ligand binding at the 5-HT_{2A}R and predicted accurate binding poses and interactions of ligands compared to their associated bound complex.^{17,68,93,151}

1.12.4 *In silico* calculations of binding free energy

Molecular modelling in drug design primarily involves visualizing structures and calculating forces between ligands and receptors or within biological systems. The binding free energy $\Delta G_{\text{binding}}$ value is commonly used to estimate binding strength of ligand-protein interactions in various computational methods.

In silico approaches to calculate free energies include techniques like linear interaction energy analysis¹⁹⁸ or molecular mechanics-Poisson Boltzmann surface area / generalized born and surface area (MM-PBSA/GBSA) calculations.¹⁹⁹ MM-PBSA/GBSA calculations have been employed in drug discovery for its ability to efficiently compute relative binding free energies with acceptable accuracy over a short time scale, as compared to other established techniques.²⁰⁰

Other established techniques such as free energy perturbation (FEP),^{201,202} umbrella sampling²⁰³, and thermodynamic integration²⁰⁴ may provide more accurate calculations. These methods analyse trajectories from molecular dynamics (MD) or Monte Carlo (MC) simulations to compute free energies. However, these methods are more resource demanding and calculations take longer timescales.

1.12.4.1 MM-PBSA/GBSA methodology

The MM-PBSA/GBSA method, introduced in 1998,²⁰⁵ combines molecular mechanic energies and continuum solvent models²⁰⁶ to calculate the ligand-receptor binding free energy between solvated

1. Introduction

molecules' bound and unbound states.²⁰⁷ However the accuracy of results are dependent of the accuracy of force field and partial charge models, ²⁰⁸ as well as difficulties in sampling within a large conformational space.²⁰⁹ Additionally, extended simulation durations can result in the system becoming trapped in local energy minima, which are stable configurations necessitating the overcoming of energy barriers for transitions between structural conformations. This confinement can restrict the exploration of the complete conformational space, potentially impacting result accuracy. ²¹⁰ However, with prolonged simulations, there is also the increased probability of the system breaking free from these local minima and expanding its exploration into a broader conformational space. This expanded exploration facilitates transitions between diverse structural conformations, enabling a more comprehensive sampling process.²¹¹

These are stable configurations of atoms or molecules on the potential energy surface where the system has reached a relatively low energy state compared to its immediate surroundings and require overcoming energy barriers to transition between structure conformations. Thereby, potentially affecting the accuracy of the MM-PBSA/GBSA results.²¹²

MM-PBSA/GBSA calculation of the receptor-ligand complex can be performed using multiple or single trajectory approaches. In the multiple trajectory approach, MD simulations are conducted independently for the

1. Introduction

unbound receptor, unbound ligands, and the complex. Energy terms are then calculated from snapshots of these individual trajectories.²⁰⁸

In the single trajectory approach, MD simulations are carried out only for the complex system. Snapshots from this single trajectory are used to generate conformations of the receptor and ligand, and their free energies are calculated.^{213,214} The single trajectory approach is more commonly used due to its lower computational expense and provides relatively accurate results for investigating protein-ligand interactions.²⁰⁹ However, compared to the multiple trajectory approach, the single trajectory neglects the explicit structural relaxation of the protein and ligand before binding.²¹⁵ Both approaches require a crystal or minimized structure. The conformation ensembles are compared to the reference structure to calculate the energy of the conformers and average them. Thus, conformational changes in the system components contribute to the final energy.²¹⁶

MM-PBSA/GBSA process depicted by **Figure 1.12.4.1-1**, calculates the binding free energy ($\Delta G_{\text{binding}}$) of molecular systems summing their gas-phase energy (E_{mm}), polar and nonpolar contributions of the solvation free energy, (G_{solv}), and the configurational entropy of the solute ($-T\Delta S$). Solvation effects are approximated by solving the Generalized Born ($G_{\text{PB/GB}}$) model for polar solvation. Polar contributions are dependent on the transfer of charged molecules between a gas-phase medium (with a dielectric constant of 1) and a solvent medium (with a dielectric constant of 78-80), estimated by implicit solvent

1. Introduction

models.²¹⁷ An empirical term for non-polar solvation based on the solvent-accessible surface area (SA) is also added. Currently, the GB theory is preferred over the PB equation due to its computational efficiency.^{216,218}

Notably, Schrödinger Maestro employs a variable dielectric constant in the Generalized Born solvation model and better accounts for the electrostatic interactions between the solute and the solvent, leading to more accurate predictions.

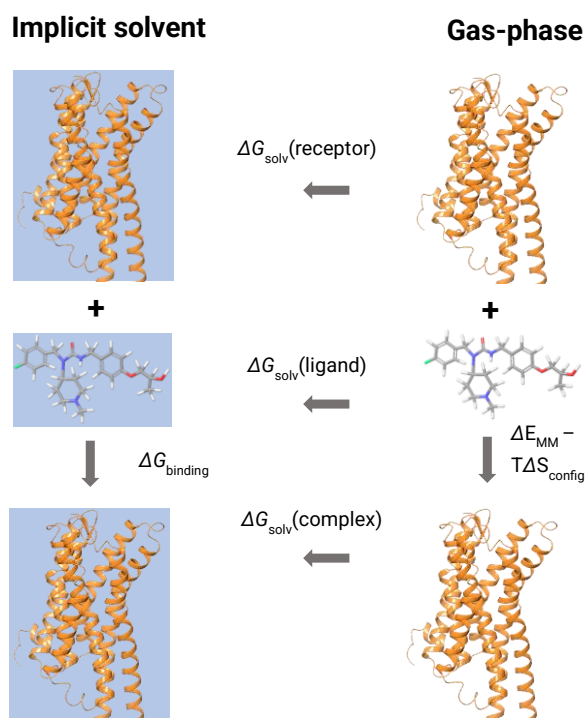


Figure 1.12.4.1-1: Diagram representing MM-PBSA/GBSA receptor-ligand binding free energy calculation method. Source: Adapted from Gohlke 2012²¹⁶

1. Introduction

Equation: 1.12.4.1-A represents the calculation of binding free energy of a protein-ligand complex using the MM-PBSA/GBSA methods:

Equation: 1.12.4.1-A

$$\Delta G_{\text{binding}} = G_{\text{complex}} - G_{\text{receptor}} - G_{\text{ligand}}$$

Where $\Delta G_{\text{binding}}$ is the binding free energy of the protein-ligand complex, G_{complex} is the complex energy, G_{receptor} is the receptor energy, and G_{ligand} is the ligand energy.²¹⁹²²⁰

The free energy of each component in **Equation: 1.12.4.1-A** is predicted by **Equation: 1.12.4.1-B**

Equation: 1.2.4.1-B

$$G = H - TS$$

Where H denotes enthalpy, T is the absolute temperature, and S is the entropy of the molecule. **Equation: 1.12.4.1-C** defines H:

Equation: 1.12.4.1-C

$$H = E_{\text{mm}} + G_{\text{solv}}$$

Where E_{mm} represents the molecular mechanical energy of the molecule and G_{solv} is the free energy of solvation in the MM-PBSA method. **Equation: 1.12.4.1-D** and **Equation: 1.12.4.1-E** define E_{mm} and G_{solv} :

Equation: 1.12.4.1-D

$$E_{\text{mm}} = E_{\text{internal}} + E_{\text{electrostatic}} + E_{\text{vdW}}$$

1. Introduction

Where E_{internal} is the summation of all internal energies, bond angles, angle, and dihedral energies. $E_{\text{electrostatic}}$ and E_{vdW} are used respectively to define the electrostatic and van der Waals interaction energies.²¹⁹

Equation: 1.12.4.1-E

$$G_{\text{solv}} = G_{\text{PB/GB}} + G_{\text{SA}}$$

Where G_{solv} is the summation of the polar ($G_{\text{PB/GB}}$, $E_{\text{electrostatic}}$) and nonpolar (G_{SA} , non-electrostatic) constituents. $G_{\text{PB/GB}}$ is the polar contribution of solvation energy of the molecule, and G_{SA} is the nonpolar solvation free energy. Poisson-Boltzmann (PB) and Generalized Born (GB) models are implicit solvation models used to compute the polar contribution of solvation.²⁰⁸

The MM-PBSA/GBSA methodology **Figure 1.12.4.1-1**, calculates the $\Delta G_{\text{binding}}$ of molecular systems by summing their gas-phase energy, G_{solv} , and the configurational entropy of the solute ($-T\Delta S$). The gas-phase energy, represented by the molecular mechanical (MM) energy of the molecules (E_{mm}), is a key component.²²¹ G_{solv} comprises the polar and nonpolar contributions of the solvation free energy, with the polar contribution ($G_{\text{PB/GB}}$) dependent on the transfer of charged molecules between a gas-phase medium (with a dielectric constant of 1) and a solvent medium (with a dielectric constant of 78-80), estimated by implicit solvent models.²¹⁷ Currently, the GB theory is preferred over the PB equation due to its computational efficiency.^{216,218}

1. Introduction

The nonpolar solvation free energy (GSA) reflects the energy needed to create a cavity for the solute by the solvent, proportional to the solvent-accessible surface area (SASA) of the solute. The configurational entropy (S) of solvation in the gas-phase is determined using either quasi-harmonic²²² or normal model analysis.²²³

Equation: 1.12.4.1-F

$$\Delta G_{\text{binding}} = E_{\text{MM}} + (G_{\text{solvComplex}} - G_{\text{solvreceptor}} - G_{\text{solvligand}}) - T\Delta S$$

Finally, the $\Delta G_{\text{binding}}$, **Equation: 1.12.4.1-F**, in the implicit solvent is the sum of the E_{mm} in the gas-phase, the difference in G_{solv} between the complex and non-bound molecules, and the configurational entropy related to complex formation in the gas-phase at specific temperature ($T\Delta S$).

MMPBSA/GBSA has been widely used in drug discovery for its ability to efficiently compute relative binding free energies with acceptable accuracy.²⁰⁰

1.12.4.2 Entropy and Enthalpy

A combination of favourable enthalpy and entropy leads to high affinity compounds.²²⁴ The Gibbs free energy of the molecule (G) is the difference of enthalpy (H) and sum of entropy (S) at a constant temperature (T). Thus, $\Delta G_{\text{binding}}$, **Equation: 1.12.4.2-G**, determining the binding free energy between receptor and ligand, depends on changes in enthalpy (ΔH) and entropy (ΔS).²²⁵

Equation: 1.12.4.2-G

$$\Delta G_{\text{binding}} = \Delta H - T\Delta S$$

Structural modification of a molecule to enhance binding interactions with the target receptor is a regular strategy that can increase enthalpy. Although, extensive modifications often fails to improve ligand potency due to unfavourable entropy resulting from conformational entropy loss and inhibiting desolvation.²²⁶

Moreover, data from broad off-target assay profiling and associated thermodynamics measurements indicate compounds binding at their primary targets with high entropy contributions are less selective, hitting more off-targets compared with those ligands that demonstrated enthalpy-driven binding.²²⁷

1.12.5 Alternative *in silico* approaches to develop 5-HT_{2A}R ligands

Alternative computational methods used in ligand design targeting the 5-HT_{2A}R have identified and assessed molecular interactions associated to binding affinity and selectivity.

Ligand-based drug discovery which use 3D-QSAR methods, such as comparative molecular field analysis (CoMFA). CoMFA models can predict the binding affinity of potential ligands based on their electrostatic and steric properties. Unlike traditional quantitative structure-activity relationship (QSAR) models, CoMFA models can

1. Introduction

include structurally diverse analogues that are usually excluded from QSAR analyses.²²⁸ For example, a training set of experimental data has been used to build CoMFA models that can estimate the 5-HT_{2A}R activity of new ligands. A 3D-QSAR model for 3-(1,2,5,6-tetrahydropyridin-4-yl)indole derivative was able to predict the binding affinity of six new ligands from a training set of 45 compounds.²²⁸

Virtual screening is another method that has increased in use, supported by improvements in computing hardware and software. It can explore a much larger chemical space than experimental high throughput screening (HTS) and predict the binding modes of the compounds. Virtual screening has been successfully applied to discover novel ligands for 5-HT_{2A}R.^{68,229} The ability to discover novel 5-HT_{2A}R ligands can be advanced by free ultra-large ligand libraries, including the ZINC database,²³⁰ a growing library of over a billion compounds. Virtual HTS and ultra-large library docking have identified potent 5-HT_{2A}R modulators.⁶⁸

Molecular dynamic (MD) simulations are another *in silico* technique that can reveal the dynamic and temporal aspects of protein function. MD simulations have been used to demonstrate agonist or antagonist binding at the 5-HT_{2A}R which stabilized distinct receptor states.²³¹ MD simulations of the 5-HT_{2A}R bound to psychedelic or non-psychedelic 5-HT_{2A}R agonists associated different conformations of the ICL2 to 5-HT_{2A}R biased agonism,²³² and was supported experimentally.²³³

1. Introduction

The available computational-based methodologies have been employed in the design and investigating the binding of ligands targeting the 5-HT_{2A}R. These approaches have facilitated elucidating interactions associate to both agonist and antagonist binding. The integration of techniques such as virtual screening,⁶⁸ molecular docking,^{70,234} and molecular dynamics⁸³ have rationalized the pharmacological effects associated to their binding mode

2. In silico docking of pimavanserin analogues at the human 5-HT_{2A}R

1.13 Research aims and objectives

The research project aims to investigate 5-HT_{2A}R subtype selectivity by targeting the 5-HT_{2A}R TM4-TM5 HP. This involves structure-based design, synthesis, and evaluation of novel 5-HT_{2A}R ligands, employing a multidisciplinary approach integrating *in silico*, organic chemistry, and pharmacology methods. The objectives are as follows:

- 1) Use **13**, as a model ligand and predict its binding conformation when bound to 5-HT_{2A}R. Identify the optimal structural position for modifications targeting the TM4-TM5 HP.
- 2) Develop a matched molecular pair analogue series through structure-based design by performing structural modifications to **13** at the identified position for targeting the TM4-TM5 HP.
- 3) Use and optimize *in silico* screening methods, including docking and free energy calculations, to predict and evaluate binding poses, interactions, and binding free energy (ΔG) values of the structure-based analogue series.
- 4) Synthesize the analogue series using synthetic chemistry methods and prepare for cell-based fluorescence assays.
- 5) Develop fluorescent probes for the 5-HT_{2A}R through a structure-based design process for use in a cell-based fluorescence assay.
- 6) Evaluate the binding affinity of the analogue series at the 5-HT_{2A}R via cell-based fluorescence assay.

2. *In silico* docking of pimavanserin analogues at the human 5-HT_{2A}R

2. *In silico* exploration of pimavanserin analogues at the human 5-HT_{2A}R

2.1 Introduction

This chapter investigates the binding interactions of pimavanserin analogues with the 5-HT_{2A}R using *in silico* methods. Homology modelling and molecular docking provide a way to explore predicted binding interactions within the TM4-TM5 HP of the 5-HT_{2A}R. This approach allows for the visualization of the receptor's structure, to support the design of ligands to specifically interact with distinct binding sites

2.2 Aims

The aims of this section were to; 1) Utilize a structure-based approach to design a series of pimavanserin analogues targeting the TM4-TM5 HP of the 5-HT_{2A}R. 2) Investigate the binding interactions between the designed pimavanserin analogues and the 5-HT_{2A}R using *in silico* methods, including molecular modelling and molecular docking. 3) Rationalize the binding modes, associated interactions, and binding scores of the pimavanserin analogues. 4) Provide theoretical support for the synthesis of the pimavanserin analogue series based on *in silico* results.

2.3 Designing the pimavanserin analogue series

The discovery of a unique structural feature in the 5-HT_{2A}R resolved XRC structures in the 5-HT_{2A}R, the TM4-TM5 HP, sets it apart from other

2. In silico docking of pimavanserin analogues at the human 5-HT_{2A}R

5-HT₂ receptor subtypes. Experimental evidence, such as mutagenic studies combined with molecular docking,^{17,93} provide strong support that, **13**, a selective 5-HT_{2A/2C}R ligand, binds into the 5-HT_{2A}R TM4-TM5 HP using the 4-isobutoxy moiety positioned on ring C. Notably, this results in higher binding affinity for the 5-HT_{2A}R compared to the 5-HT_{2C}R, and minimal binding to the 5-HT_{2B}R. Consequently this presents **13** as a model ligand for selectively targeting the 5-HT_{2A}R sub-type via the TM4-TM5 HP on account of the modelled binding pose.^{17,88}

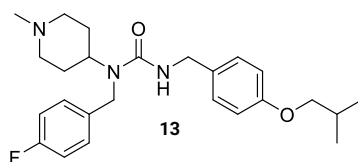


Figure 2.3-1: Pimavanserin (13).

Reported, pimavanserin amino alcohol analogues, **Figure 1.10.3.1-1** have exhibited significantly increased potency upon modifying the 4-isobutyl moiety to an amino alcohol moiety. Thus, demonstrating a relationship between the size and type of substituent at this position on the ring C.

It was hypothesized that modifications from an isobutyl moiety to the amino alcohol moiety would enable deeper ligand binding into the 5-HT_{2A}R TM4-TM5 HP and increase binding interactions more than **13**, which lead to the enhanced 5-HT_{2A}R binding in comparison to the other 5-HT₂ receptor subtypes.

2. In silico docking of pimavanserin analogues at the human 5-HT_{2A}R

To begin investigating this hypothesis, a pimavanserin amino alcohol matched molecular pair series featuring different O-benzyl substitutions was designed, **Figure 2.3-2**. Initially a series of pimavanserin analogues **17a-c** were chosen that incorporate different 4-alkyloxy moieties on ring C. This would permit a comparison between the performance of an unfunctionalized carbon backbone, and subsequent variants containing hetero-atoms and chiral centres in the amino alcohol moiety.

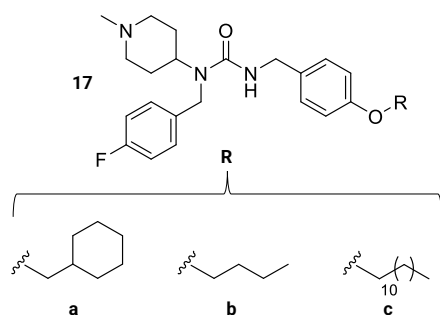


Figure 2.3-2: Structure-based designed pimavanserin ring C analogues (17a-c).

Next, the design of the 4-amino alcohol series **R/S-18a-j** was initiated from the ring C oxygen atom in place of the 4-isobutyl moiety, **Figure 2.3-3**. The first amino alcohol group would feature a primary amine. This would then be followed by matched pairs between each amino alcohol amine moiety, thus ranging from the primary amine to larger substituted tertiary amines.

2. In silico docking of pimavanserin analogues at the human 5-HT_{2A}R

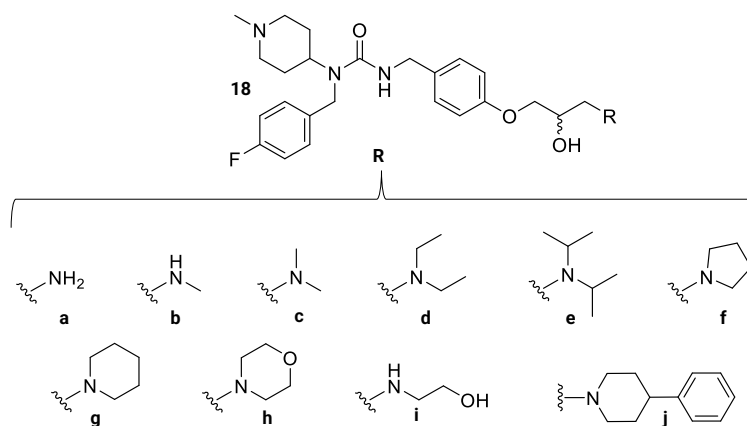


Figure 2.3-3: Structure-based designed pimavanserin ring C amino alcohol analogues (18a-j).

Incorporating matched molecular pairs provides a comparative approach to evaluate the SAR associated with the amino alcohol moiety, relating to size, introduction of ring constraints, or changes in elemental content. Systematically exploring these modifications may improve understanding and rationalise how different structural features influence ligand binding and selectivity via the 5-HT_{2A}R TM4-TM5 HP.

Increasing the length of the ligands or introducing ring constraint, provides a method to explore the optimal size and shape of the amino alcohol moiety required for effective binding within the 5-HT_{2A}R TM4-TM5 HP. This can highlight information about the spatial requirements and interactions necessary for ligand-receptor recognition and stabilization. Modulating electrostatics through the introduction of heteroatoms such as oxygen or and nitrogen atoms, as well as associated functional groups offers insights into the role of electronic

2. In silico docking of pimavanserin analogues at the human 5-HT_{2A}R

properties in ligand binding. It can help elucidate how charge distribution and polarity influence the interaction between the ligand and the receptor, potentially enhancing binding affinity and selectivity.

Overall, this approach provides a comprehensive way to predict the structural and electronic factors that govern ligand binding to the 5-HT_{2A}R. This can rationalise the design of novel ligands thus subsequently facilitating their synthesis.

2.4 5-HT_{2A}R homology model

The available XRC structures of the 5-HT_{2A}R include point mutations and loop insertions to improve the receptor crystallisation process,^{17,69} as such they do not represent the true human wild-type sequence, thus, a homology model process was carried out to remediate this.

In this study, the human 5-HT_{2A}R sequence obtained from UniProt a protein sequence database was utilized²³⁵ to construct the homology model for molecular docking using SWISS-MODEL, a fully automated protein structure homology-modelling server.¹⁸⁴

2.4.1 Template search

For the construction of the homology model, SWISS-MODEL¹⁸⁴ utilized BLAST²³⁶ and HHblits²³⁷ algorithms to search the SWISS-MODEL template library (version 2022-05-18) for templates (protein

2. In silico docking of pimavanserin analogues at the human 5-HT_{2A}R

structures in the PDB) that aligned with the canonical human 5-HT_{2A}R target protein sequence.

This search resulted in the identification of 487 potential templates. Subsequently, an HHblits profile was generated.²³⁸ This profile was then subjected to one iteration of HHblits against Uniclust30.²³⁹ The resulting profile was used to search against all profiles available in the SWISS-MODEL template library, affording an additional 937 templates.

The alignment process identified the lumateperone-5HT_{2A}R XRC structure (PDB: 7WC8) as a potentially optimal template, with a resolution of 2.45 Å, a sequence similarity of 85.71%, and a global model quality estimate (GMQE) score of 0.54. The GMQE score is set between 0-1,²⁴⁰ with 1 indicating better quality of homology model and suggests a favourable alignment. Thereby indicating the lumateperone-5HT_{2A}R XRC structure is a suitable template for building a homology model of the canonical human 5-HT_{2A}R.

2.4.2 Model Building

Homology models were built based on the target-template alignment using ProMod3 (**ProMod 3: Release 3.2.1**. 2021) as part of SWISS-MODEL homology model builder pipeline.²⁴¹ Conserved coordinates between the target and the template were copied from the template to the model. Insertions and deletions were reengineered using a fragment library. Side chains were then reconstructed. Finally, the

2. In silico docking of pimavanserin analogues at the human 5-HT_{2A}R

geometry of the resulting model was regularized by using a force field-based approach.

SWISS-MODEL automatically omitted N-terminus residues 1-70 and C-terminus residues 400-471. The TM1 region was truncated at the extracellular end of the helices not part of the binding site by 4 residues: L69^{1.27}, H70^{1.28}, L71^{1.29}, and Q72^{1.30}. The wt human ICL3 (intracellular loop 3) region was automatically constructed between T266^{5.70} and M312^{6.24} to represent the complete structure, improve docking accuracy, and could be advanced into molecular dynamic simulations.

Commented [LD1]: I have reexamined the template and found these mutations had not been carried out. This was referring to an earlier piece of work I had carried out using an older template PDB: 6A93

2.4.3 Ligand Modelling

In SWISS-MODEL, ligands present in the template structure are transferred by homology to the model when the following criteria are met: (i) The ligands are annotated as biologically relevant in the template library, (ii) the ligand is in contact with the model, (iii) the ligand is not clashing with the protein, (iv) the residues in contact with the ligand are conserved between the target and the template. If any of these four criteria is not satisfied, the ligand will be excluded from the model. SWISS-MODEL retained lumateperone, cholesterol (x4), and (2R)-2,3-dihydroxypropyl (9Z)-octadec-9-enoate (x9).

2.4.4 Model quality assessment

Using the lumateperone-5-HT_{2A}R XRC structure (PDB: 7WC8) as a template structure SWISS-MODEL was able to construct a 5-HT_{2A}R

2. In silico docking of pimavanserin analogues at the human 5-HT_{2A}R

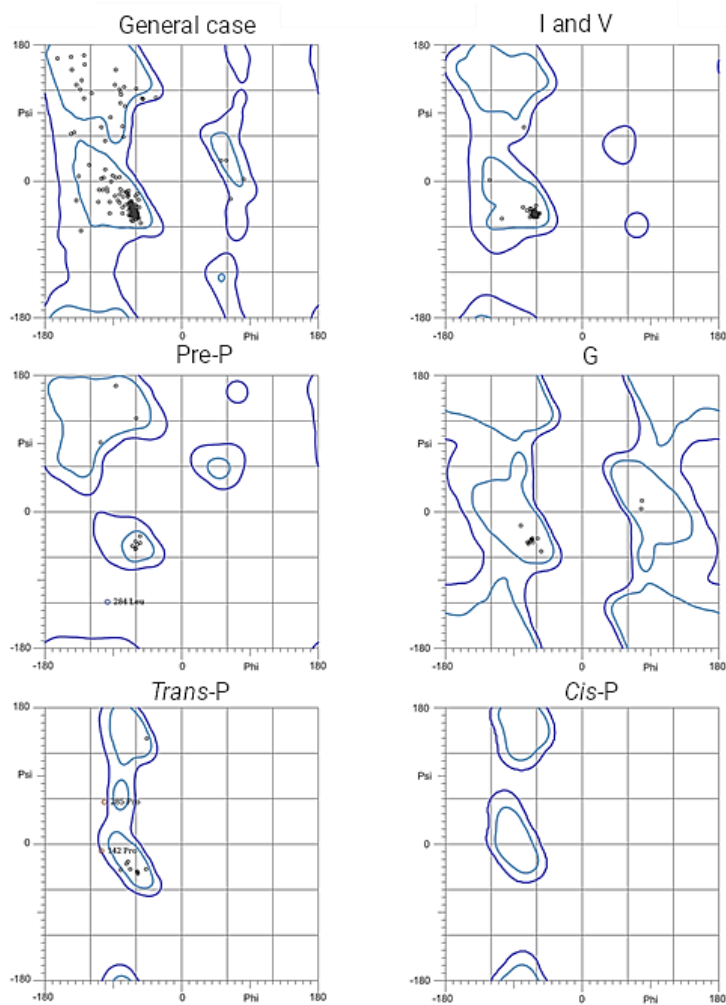
homology model with a low RMSD (0.09 Å³) by 3-point manual superimposition of identical α-carbons between the homology model and template backbone. The low RMSD value indicates a high degree of structural similarity between the homology model and the template structure. This was attributed to the large degree of sequence conservation between the template and target.

The quality assessment of the homology model was performed using various scoring methods. First assessed was the QMEANisCO score, 0.74 ± 0.05 , that suggested good agreement between the homology model accuracy and the lumateperone-5-HT_{2A}R XRC structure at a global and local scale. A QMEANisCo ranges between 0-1, with nearer 1 indicating better agreement between the homology model and template.¹⁹⁰

Ramachandran plot analysis **Graph 2.4.4-1**, was used to assess the conformational quality of the model.¹⁹¹ This revealed that 95% of the residues in the model exhibited favoured backbone dihedral angles. Several, there were some outliers observed were reported, specifically P142^{ECL1}, L284^{ICL3}, and P285^{ICL3}, approximately 1% of the residues. However, from visual inspection these outliers were found to be spatially distant from the central binding pocket and TM4-TM5 HP, suggesting that further refinement of these regions might not be necessary at this stage. It is worth noting that no crystal structure for the canonical ICL3 sequence is available. The homology model, assessed with MolProbity 4.4, achieved a score of 1.47 within the range of 0 to 100,

2. In silico docking of pimavanserin analogues at the human 5-HT_{2A}R

lower than the XRC structure resolution of the homology model template. Lower indicate better quality and structural accuracy, thus supporting the reliability of the constructed homology model.¹⁹³



Graph 2.4.4-1: Ramachandran plot analysis of SWISS-MODEL 5-HT_{2A}R homology mode displaying 94.8% (310/327) of all residues were in favoured (98%) regions.

Considered together, results of the validation scoring methods and the high level of conservation observed between the template it was

2. In silico docking of pimavanserin analogues at the human 5-HT_{2A}R

concluded the SWISS-MODEL automated homology model building server provided a dependable and accurate homology model suitable for predicting the pimavanserin analogue binding modes at the 5-HT_{2A}R.

2.5 Molecular docking protocol

2.5.1 Ligand preparation

The structures of **13**, **15a-d**, **17a-c**, and **18a-j** were drawn using the 2D sketcher in Maestro. These structures were then converted to 3D and prepared for docking using LigPrep (**Schrödinger Release 2021-1**: LigPrep, Schrödinger, LLC, New York, NY, 2021).

During the preparation process, where ligands featured a chiral centre models for both *R* and *S* enantiomers were generated. Thus, labelled as individual enantiomers e.g **R-18** or **S-18** within **Chapter 2**. Protonation state(s) relevant to physiological pH were predicted using EPIK ^{242,243}. The optimized potentials for liquid simulations 4 (OPLS4) force field (**Schrödinger Release 2021-1**: Schrödinger, LLC, New York, NY, 2021) ²⁴⁴ was utilized for the geometry optimisation of the ligands.

2.5.2 Protein preparation

The 5-HT_{2A}R homology model obtained from SWISS-MODEL was imported into Maestro (**Schrödinger Release 2021-2**: Maestro, Schrödinger, LLC, New York, NY, 2021). To prepare the structure for docking, the Protein Preparation Wizard (**Schrödinger Release 2021-1**: Protein Preparation Wizard, Schrödinger, LLC, New York, NY, 2021) was

2. In silico docking of pimavanserin analogues at the human 5-HT_{2A}R

employed. In the preparation process, non-standard heteroatoms and ligands were removed from the model. Hydrogen bond assignments were optimized using simplified rules, and the pH was set to neutral to simulate physiological conditions. The OPLS4²⁴⁴ force field was utilized for the energy minimization of the model.

The OPLS4 force field minimization protocol consists of several key steps: 1) Initial structure preparation, ensuring proper atom types and connectivity. 2) Application of OPLS4 force field parameters to the system. 3) Restrained energy minimization, where heavy atoms are constrained to maintain overall structure. 4) Gradual relaxation of constraints through multiple minimization cycles. 5) Final unconstrained minimization allowing all atoms to move freely. 6) Convergence, of heavy atoms, set at 0.30 Å RMSD, 7) Validation of the minimized structure for geometric and energetic consistency. This process optimizes molecular geometry while preserving essential structural features.

2.5.3 Receptor grid generation method

2.5.3.1 Receptor grid generation for pimavanserin

To establish an accurate docking space for the binding of pimavanserin analogues **15a-d**, **17a-c**, and **18a-j** into the 5-HT_{2A}R homology model, the predicted complex of pimavanserin-5HT_{2A}R^{17,88} previously reported was considered best suited. However, due to the unavailability of a freely accessible pimavanserin-5-HT_{2A}R complex, it was necessary to remodel the binding pose. This involved generating a

2. In silico docking of pimavanserin analogues at the human 5-HT_{2A}R

receptor grid using the co-crystalised ligand lumateperone to define the centroid of the grid (37 Å³) for the docking of **13**. One core constraint was applied. The grid constraint requiring H-bond formation with D155^{3,32}. This was successful in regenerating the pimavanserin-5-HT_{2A}R complex previously predicted ^{17,93} and provided a suitable model for defining a reliable receptor grid to dock **15a-d**, **17a-c**, and **18a-j**.

2.5.3.2 Receptor grid generation for pimavanserin analogues

The hypothesised pimavanserin-5-HT_{2A}R complex previously reported ^{17,88} was used to define the centroid of a grid (30 Å³) for self-docking of **13** and docking of **15a-d**, **17a-c**, and **18a-j**. The grid constraint requiring H-bond formation with D155^{3,32} was carried over. Additionally, a core constraint was introduced requiring that the ligands dock within a 2 Å distance from the heavy atoms of **13** to better refine the sampling to a specific binding pose of interest. This constraint had been successfully employed in previous docking studies and has proven effective in generating meaningful results that could rationalize experimental binding affinities.²⁴⁵ Together, the defined grid and 2 constraints guide the docking process to generate predicted binding poses of the pimavanserin analogues. Glide was able to redock **13**, **Figure 2.5.3.2-1** with a low RMSD (0.32 Å) in the self-docking process after manual superimposition, demonstrating the suitability of the modified receptor grid and applied constraints.

2. In silico docking of pimavanserin analogues at the human 5-HT_{2A}R

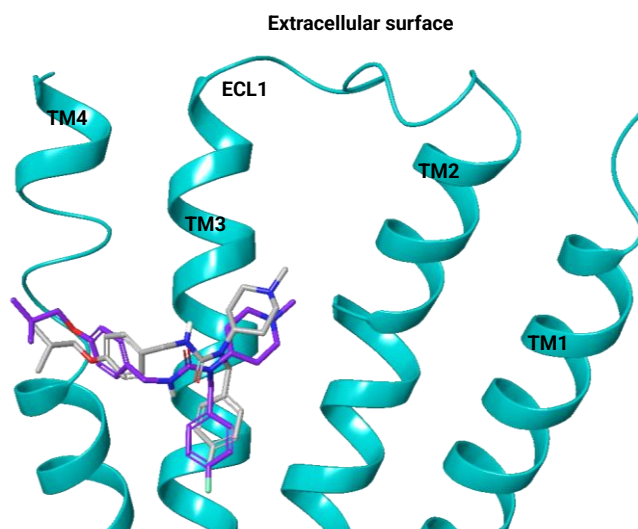


Figure 2.5.3.2-1: Superimposition of 13 self-docking pose (purple) via pimavanserin analogue receptor grid generation protocol and the docked pose of 13 (grey) via the receptor grid generation protocol for 13.

2.5.4 Docking protocol

Analogues **15a-d** and **18a-j** were docked as individual enantiomers *R/S*-**15a-d** and *R/S*-**18a-j**. Standard precession (SP) sampling was enabled for the docking protocol, which involved minimizing 50 poses for each ligand after docking. A maximum of 20 poses were then selected as the output. Default settings were utilized unless specifically mentioned. Gscores of -10 or lower are considered to represent good binding within Glide SP.

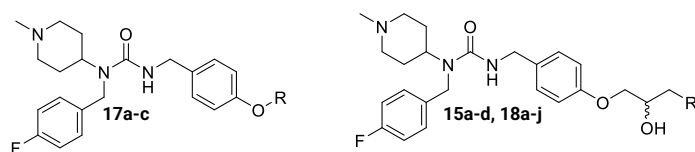
2. In silico docking of pimavanserin analogues at the human 5-HT_{2A}R

2.6 Molecular docking results and discussion

2.6.1 Glide results

The top ranked docking pose is reported for each analogue of **13** in

Table 2.6.1-1.



Compound	R group	R/S	Gscore (kcal.mol ⁻¹)	IC ₅₀ (nM)
13	-	-	-10.30	22 ¹⁶¹
17a		-	-8.73	-
17b		-	-8.16	-
17c		-	-9.34	-
15a		R	-10.53	0.39 ¹⁶¹ *
		S	-12.14	
15b		R	-9.12	0.87 ¹⁶¹ *
		S	-11.47	
15c		R	-11.78	1.93 ¹⁶¹ *
		S	-10.35	
15d		R	-10.66	ND ¹⁶¹ *
		S	-10.12	
18a		R	-9.40	-
		S	-9.20	
18b		R	-10.90	-

2. In silico docking of pimavanserin analogues at the human 5-HT_{2A}R

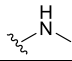
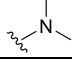
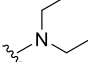
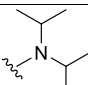
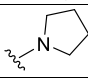
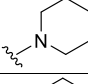
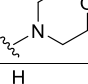
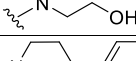
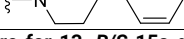
		S	-10.30	-
18c		R	-10.90	-
		S	-7.79 [†]	-
18d		R	-11.00	-
		S	-9.80	-
18e		R	-9.40	-
		S	-9.10	-
18f		R	-11.30	-
		S	-10.65	-
18g		R	-10.80	-
		S	-10.80	-
18h		R	-11.10	-
		S	-9.30	-
18i		R	-7.59 [†]	-
		S	-9.30	-
18j		R	-10.90	-
		S	-12.30	-

Table 2.6.1-1: Gscore for 13, R/S-15a-d, and R/S-18a-j. Reversed pose ([†]), Gscore lower (green) or higher (red) than pimavanserin. Top Gscore (blue highlight). (*) denotes compounds were tested as racemic mixtures. No detectable binding (ND). Compounds not tested experimentally (-).

All analogues docked demonstrate good Glide scores (Gscores) (< -9 kcal.mol⁻¹), except **17a**, **17b**, **S-18c** and **R-18i**. Lower Gscores were achieved by known analogues **R/S-15a**, **R/S-15c**, and **S-15b** in comparison to **13**. Of these, **R/S-15a** demonstrated the lowest Gscores. In contrast, **R-15b** scored highest, including **13**. As the racemic mixture, analogue **15d** showed no detectable binding experimentally; however, a docking pose is predicted for both **R/S-15d** with an improved Gscore respectively in comparison to **13**.

The structure-based design of novel pimavanserin analogues **17a-c** resulted in lower Gscores than **13**. However, analogues **R/S-18f**, **R/S-**

2. In silico docking of pimavanserin analogues at the human 5-HT_{2A}R

18g, R/S-18j, R-18b, R-18c, R-18d, and R-18h achieve improved Gscores in comparison to **13**, **Table 2.6.1-1**. This also suggests the inclusion of the chiral centre at position of the amino alcohol moiety may be associated to the improved Gscores. Analogue **S-18j** is predicted as the most stable complex with the lowest Gscore compared to **R/S-18a-j**. Whereas **S-18c** and **R-18i** appeared to be the least stable complexes with the highest Gscores. Overall, Glide has predicted that several novel analogues could exhibit binding affinities or potencies equal to or greater than **13**.

2.6.2 Glide binding pose assessment

Glide docked analogues all structure-based design pimavanserin analogues **17a-c, R/S-15a-d, and R/S-18a-j**, docked into the SWISS-MODEL 5-HT_{2A}R homology model. Several of these were predicted with a binding pose and interactions like **13**, exemplified by **Figure 2.6.2-1 (i-ii)** and **Figure 2.6.2-2 (i)** Contrary to this **S-18c** and **R-18i** are predicted to favour a different binding pose exemplified by **Figure 2.6.2-2 (ii)**.

The amino alcohol moiety of **R/S-15a-d** occupied the TM4-TM5 HP, with the ammonium ion of their respective *N*-methyl- piperidinium ring positioned near to D155^{3,32}, allowing for the formation of a H-bond and salt bridge, or salt-bridge alone. This interaction is highly conserved across aminergic GPCR and plays a crucial role in the binding of most amine-containing ligands⁸⁰

2. *In silico* docking of pimavanserin analogues at the human 5-HT_{2A}R

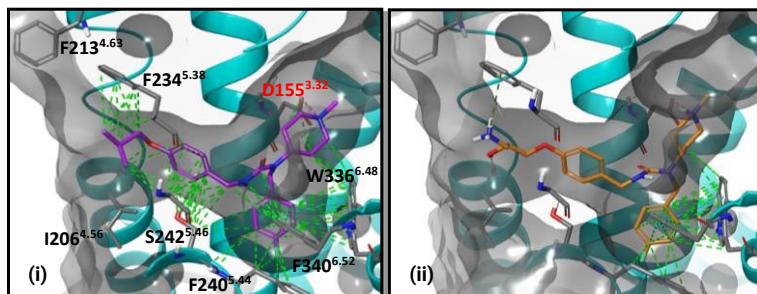


Figure 2.6.2-1: (i) **13** and (ii) **S-18a** docked into 5-HT_{2A}R homology model. Reduced hydrophobic interactions with the TM4-TM5 HP by the amino alcohol moiety of the latter, which features a primary amine, is associated to weaker Gscore in comparison to **13**. Interactions displayed as dashed lines; hydrophobic (lime green), H-bond (yellow), salt bridge (purple), π -cation (green), π -CH (blue).

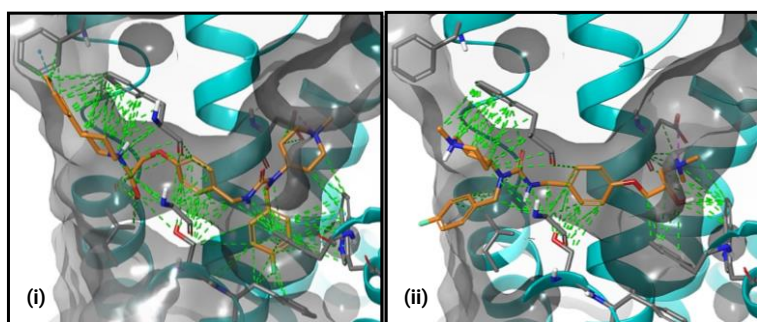


Figure 2.6.2-2: (i) **S-18j** docked into 5-HT_{2A}R homology model, showing the amino alcohol moiety within the TM4-TM5 HP. Compared to pimavanserin, increased hydrophobic interactions by the amino alcohol moiety's 4-phenyl-piperdiny ring is associated to a better Gscore. (ii) **S-18c** docked into 5-HT_{2A} SWISS-MODEL homology model, illustrating a "reversed" pose. Interactions displayed as dashed lines; hydrophobic (lime green), H-bond (yellow), salt bridge (purple), π -cation (green), π -CH (blue).

The predicted binding poses of **13** and analogues **R/S-15a-d**, **R/S-18a-b**, **17a**, **R-18c**, **R/S-18d-h**, **S-18i**, and **R/S-18j** support previous observations. The fluorobenzyl ring can reside deep in the hydrophobic cleft of the central binding pocket. In this orientation, the 4-fluorobenzyl ring can interact directly with I163^{3.40} and F332^{6.44} of the conserved P246^{5.50}-I163^{3.40}-F322^{6.44} motif, which are amino acid residues

2. In silico docking of pimavanserin analogues at the human 5-HT_{2A}R

associated with the activation mechanism of 5-HT₂-type GPCR. Aromatic edge-to-face interactions are predicted between the 4-fluorobenzyl ring and the side chain of W336^{6,48}, known as a 'toggle switch' and suggested to play a critical role in mediating the activation or deactivation of class A GPCR. Aromatic edge-to-face interactions with the side chains of F340^{6,52} were also predicted, and the urea core appears to be able to adopt different orientations within the central binding pocket. These aromatic interactions were comparable with previous docking studies^{17,88,93,151} and align with mutagenic studies reporting that mutations W336^{6,48} and F340^{6,52} to either alanine or leucine significantly impacted the binding of agonists²⁴⁶ and antagonists.⁹³

In comparison to **13**, the highest scoring docked poses of **17b** and **17c** adopted similar binding pose and interactions, engaging and protruding through the TM4-TM5 HP respectfully, with the ring C 4-position alkoxy substituents. However, in these complexes the fluorophenyl ring is orientated in an opposite pose away from the hydrophobic cleft towards the extracellular. The highest scoring docked poses **S-18c** and **R-18i** exhibit a "reversed" orientation when compared to **13**, **Figure 2.6.2-2 (ii)**. In this conformation, the amino alcohol moiety amine extended through the TM4-TM5 HP and established a salt bridge with D155^{3,32} in **S-18c**. Notably, no interactions with the residues forming the hydrophobic cleft were predicted, as both the piperidin-4-yl ring and 4-fluorobenzyl ring were predicted outside of the receptor parallel to the

2. In silico docking of pimavanserin analogues at the human 5-HT_{2A}R

TM4-TM5 helices. Therefore, is not clear if the reversed orientation of **S-18c** is an alternative binding pose.

Consistent with previous docking studies,^{17,88} the 4-isobutoxy moiety of **13** is predicted to occupy the TM4-TM5 HP formed by conserved and non-conserved amphipathic and hydrophobic side chains between TM4-TM5 of the 5-HT_{2A}R. This observation, further supports mutagenesis studies,¹⁷ which provides a structural rationale for the subtype selectivity of **13** towards the 5-HT_{2A}R.

A similar binding pose is also predicted for analogues **R/S-15a-d**, **R/S-18a-b**, **17a**, **R-18c**, **R/S-18d-h**, **S-18i**, and **R/S-18j** where the amino alcohol moiety is occupying the TM4-TM5 HP, suggesting the potential to interact via hydrophobic, polar, and charged interactions, leading to improved ligand binding. The amino alcohol moiety is not obstructed by the α -hydrogen of G238^{5,42}, a conserved residue in 5-HT₂ receptor subtypes,²⁴⁷ and the rotamer conformation of F234^{5,38}, as revealed by 5-HT_{2A}R XRC structures.^{17,41,69} Side chain conformations of F213^{4,63} and F234^{5,38} increases the volume and length of the TM4-TM5 HP. This may permit the amino alcohol moiety to protrude or extend outside of the TM4-TM5 HP and receptor should the size of the amino alcohol moiety be long enough to do so. Increased hydrophobic interactions with F213^{4,63} and F234^{5,38} appear to significantly contribute to the binding strength of **S-18j** in comparison to **13** and **R/S-18a**, including edge-to-face CH- π interactions. Moreover, the hydroxyl moiety is predicted to participate as an H-bond donor to the carbonyl backbone oxygen atom

2. In silico docking of pimavanserin analogues at the human 5-HT_{2A}R

of I206^{4,56}. In a comparable manner the docked pose of known pimavanserin analogue **S-15a** also shows increased hydrophobic interactions with F234^{5,38} and new cation- π interactions compared to **13** itself. Ligand interaction diagram showing these interactions are provided, **Figure 2.6-2-3**. Seemingly, the involvement of the amino alcohol moiety in binding in certain cases is associated with lower G scores in comparison to **13**.

2. *In silico* docking of pimavanserin analogues at the human 5-HT_{2A}R

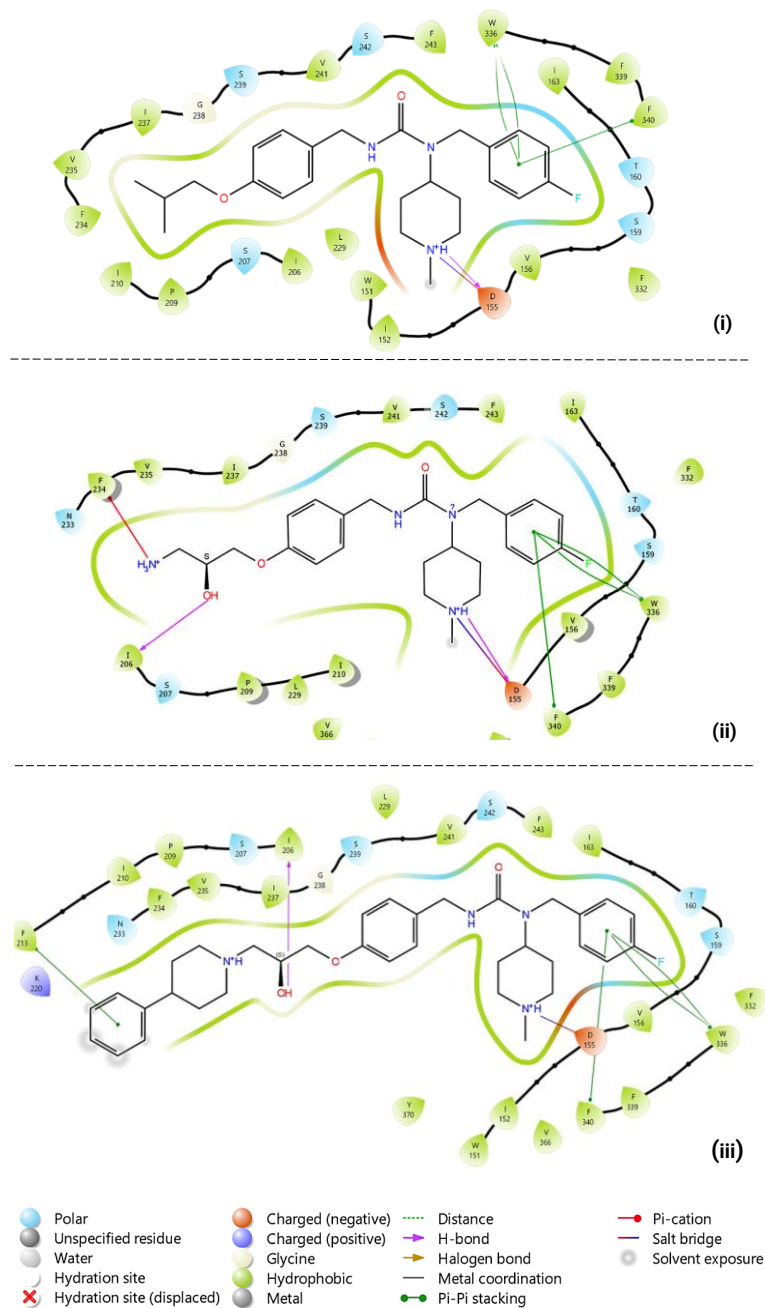


Figure 2.6.2-3: Ligand interaction diagram (i) 13, (ii) S-18a, and (iii) S-18j.

2. In silico docking of pimavanserin analogues at the human 5-HT_{2A}R

2.6.3 Glide discussion

From comparison with **13**, the modification of an amino alcohol moiety from the 4-position oxygen atom on the ring C region appears to improve Gscores. Comparison of Gscores between the smallest analogue (**R/S-18a**), and the largest (**R/S-18j**), suggest the larger hydrophobic amino alcohol substitutions at this position will be most favoured.

This also aligns with previously reported experimental potency of **R/S-15a-c**, although these were tested as racemic mixtures.¹⁶¹ Notably docking of individual enantiomers results in a comparable trend of Gscore to IC₅₀, predicting increase binding strength and demonstrating increased potency respectively, compared to **13**, **Table 2.6.3-1**.

Compound	IC ₅₀ (nM)	R/S	Gscore (kcal.mol ⁻¹)
13	22 ¹⁶¹	-	-10.30
15a	0.39 ¹⁶¹	R	-10.53
		S	-12.14
15b	0.87 ¹⁶¹	R	-9.12
		S	-11.47
15c	1.93 ¹⁶¹	R	-11.78
		S	-10.35
15d	ND ¹⁶¹	R	-10.66
		S	-10.12

Table 2.6.3-1: Experimental potency of 13 and 15a-d compared to their individual enantiomer Gscores, shows an increasing trend between both. No detectable binding (ND).

Gscores suggest, stereospecificity does not appear to be significant across the analogue series. However, it does result in differences in predicted ligand-protein interactions. Any predicted

2. In silico docking of pimavanserin analogues at the human 5-HT_{2A}R

differences in *R/S* enantiomer Gscores may be attributed partially to the static nature of the receptor in this Glide docking technique,^{194,248} which may not fully optimize the interactions between residue side chains and the ligand. Therefore, the weaker binding scores may be obtained due to suboptimal ligand-receptor interactions. These differences may be lessened by further accounting for receptor flexibility in alternative *in silico* techniques that may refine the docked complexes.

Docking of *R/S-15a-c* resulted in predicted complexes which rationalize the reported increased experimental potency in comparison to pimavanserin.¹⁶¹ Interactions modelled with the amino alcohol moiety occupying the TM4-TM5 HP provide a structural basis for the observed increase in binding potency, the amino alcohol moiety, 3-(1-piperazinyl)-1,2-benzisothiazole and 6-fluoro-3-(piperidin-4-yl)benzo[d]isoxazole, permit increased interactions with TM4-TM5 HP residues.

This trend is also apparent for larger lipophilic substituted amino alcohol moieties of *R/S-18f*, *R/S-18g*, *R/S-18j*, and *R-18d* in comparison to *R/S-18a* and *S-18i* which feature an amino alcohol moiety with a primary amine or hydroxyl moiety respectively. Cation- π interactions were predicted between the amino alcohol primary amine and F234^{5,38}, and H-bond donation between the hydroxy moiety and I206^{4,56}. It predicted the lack of steric bulk and charged, or polar nature of several amino alcohol moieties present in certain analogues limits their overall binding interactions with the hydrophobic TM4-TM5 HP thus making them less favoured. However, this does not account for the higher

2. In silico docking of pimavanserin analogues at the human 5-HT_{2A}R

Gscore award to **R/S-18e** and **R/S-18a**, compared to **13**. The amino alcohol diisopropyl amine group, respectively, exhibits good steric bulk; however, its size might be constrained by the steric tolerance in this specific region of the receptor or the rigid receptor docking method employed. Additionally, the cationic amine faces electrostatic unfavorability among hydrophobic residues.

Overall, from visual assessment of predicted binding poses and Gscores it appears the predicted improvements in ligand binding correlate to the size, sterics and lipophilicity of the amino alcohol moiety as this impacts on hydrophobic and electrostatic interactions between the amino alcohol moiety and TM4-TM5 HP residues.

2.6.4 MM-GBSA assessment

The Molecular Mechanics-Generalized Born and Surface Area (MM-GBSA) method is a computational technique used to estimate the free energy of binding between a ligand and its target protein. By calculating the binding free energy (ΔG), the MM-GBSA approach allows us to estimate the potential binding affinity of **13** and **R/S-18a-j** at the 5-HT_{2A}R, and further highlight specific chemical features or trends that ligand improve binding.

The MM-GBSA method can provide refinements to docking results obtained from Glide. However, it is essential to be cautious of the accuracy of the predicted complexes used, that are obtained from the docking method and the limitations of the MM-GBSA method. For

2. In silico docking of pimavanserin analogues at the human 5-HT_{2A}R

example, one major limitation is the neglect of conformational contributions and the influence of binding-site water molecules in the estimation of entropy. As entropy plays a critical role in ligand binding, the absence of this information could lead to potential inaccuracies in the free energy calculations.²²¹

In the MM-GBSA calculation, the binding free energy (ΔG) is a fundamental term that quantifies the stability of the ligand-protein complex. A lower (more negative) ΔG indicates a more stable complex and suggests a higher predicted affinity or potency for the ligand, potentially more effective as selective ligands.

2.6.4.1 Ligand-5-HT_{2A}R complex refinement

The variable dielectric generalised born (VSGB) solvation model²⁴⁹ and OPLS4²⁴⁴ force field were employed. The ligand-5HT_{2A}R complexes were refined using Prime (**Schrödinger Release 2023-2**: Prime, Schrödinger, LLC, New York, NY, 2021)²⁵⁰ by considering atoms within a 5.0Å distance from the ligand. Default settings were used for all other parameters.

MM-GBSA calculation results **Table 2.6.4-1** lists the predicted ΔG MM-GBSA calculations of docked complexes **13**, **R/S-15a-d**, and **R/S-18a-j**.

R group	R/S	Gscore (kcal. mol ⁻¹)	MM-GBSA ΔG Bind (kcal. mol ⁻¹)	HAC	cLog P
13		-10.30	-95.27	31	5.1

2. In silico docking of pimavanserin analogues at the human 5-HT_{2A}R

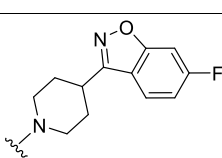
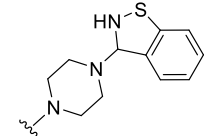
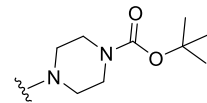
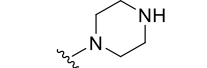
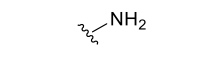
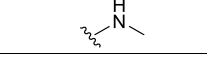
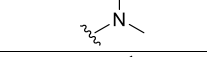
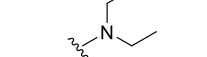
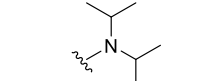
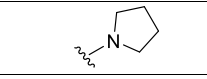
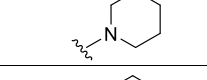
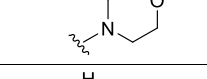
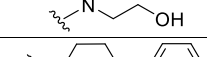
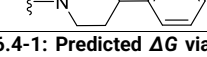
15a		<i>R</i>	10.53 ⁻	-106.33	47	5.3
		<i>S</i>	-12.14	-116.17	47	5.67
15b		<i>R</i>	-9.12	-90.12	46	6.34
		<i>S</i>	-11.47	-122.52	46	5.84
15c		<i>R</i>	-11.78	-119.30	37	1.85
		<i>S</i>	-10.35	-114.40	37	2.35
15d		<i>R</i>	-10.66	-103.28	44	5.18
		<i>S</i>	-10.12	-85.36	44	5.2
18a		<i>R</i>	-9.40	-94.66	32	2.71
		<i>S</i>	-9.20	-88.83	32	2.72
18b		<i>R</i>	-10.90	-110.27	33	3.51
		<i>S</i>	-10.30	-99.50	33	3.54
18c		<i>R</i>	-10.90	-112.70	34	3.91
		<i>S</i>	-7.79 ⁺	-82.09 ⁺	34	3.93
18d		<i>R</i>	-11.00	-115.22	36	4.49
		<i>S</i>	-9.80	-89.37	36	4.64
18e		<i>R</i>	-9.40	-112.58	38	5.19
		<i>S</i>	-9.10	-115.85	38	5.18
18f		<i>R</i>	-11.30	-117.25	36	4.44
		<i>S</i>	-10.65	-110.20	36	4.39
18g		<i>R</i>	-10.80	-110.84	37	4.64
		<i>S</i>	-10.80	-104.51	37	4.62
18h		<i>R</i>	-11.10	-110.18	37	3.45
		<i>S</i>	-9.30- 11.10	-100.37	37	3.44
18i		<i>R</i>	-7.59 ⁺	-81.05 ⁺	35	2.85
		<i>S</i>	-9.30	-86.68	35	2.86
18j		<i>R</i>	-10.90	-119.34	43	6.4
		<i>S</i>	-12.30	-117.63	43	6.3

Table 2.6.4-1: Predicted ΔG via MM/GBSA, cLogP, and heavy atom count (HAC) of docked complexes 13, *R/S*-15a-d, and *R/S*-18a-j, reversed pose (*), MM-GBSA ΔG lower (green) or higher (red) than 13. Highest Gscore pimavanserin amino alcohol analogue (blue shaded).

2. In silico docking of pimavanserin analogues at the human 5-HT_{2A}R

A lower ΔG is calculated for known analogues **R/S-15a**, **S-15b**, **R/S-15c**, and **S-15d** featuring substituted amino alcohol substituents, in comparison to **13** and **R/S-18a**. Contrary to this **R-15b** displayed a ΔG higher than its S enantiomer and **13**. Although **R/S-15d** is determined to be non-binding experimentally, a MM-GBSA ΔG is comparable to other ligands. In general, the ranking of calculated ΔG did not follow Gscore ranking.

R/S-18j were again predicted to have strongest binding strength, thus lowest ΔG MM-GBSA value, amongst the proposed analogues **R/S-18a-j**. Moreover, a lower MM-GBSA ΔG is also calculated for **R/S-18b**, **R-18c**, and **R/S-18f-h** in comparison to **13** and **R/S-18a**. Notably, **R/S-18e** were also predicted to achieve ΔG lower than **13**, now contrary to their Gscore rank, as did **R-18d**. Overall, the ΔG of these predicted complexes demonstrate improved MM-GBSA ΔG calculations over **13**, and stronger experimental binding affinity is predicted.

In contrast to this, an increase in ΔG MM-GBSA value, thus a decrease in binding affinity is predicted for analogues with either charge and polar amino alcohol moieties such as, **R/S-15a** and **R/S-18m**. Moreover, the ΔG of reverse binding poses **S-18c** and **R-18i** were calculated to be the highest amongst analogues, thus predicting them to form the least stable complexes.

Further analysis of the amino alcohol moieties ΔG obtained from MM/GBSA in association to the predicted binding affinity was carried

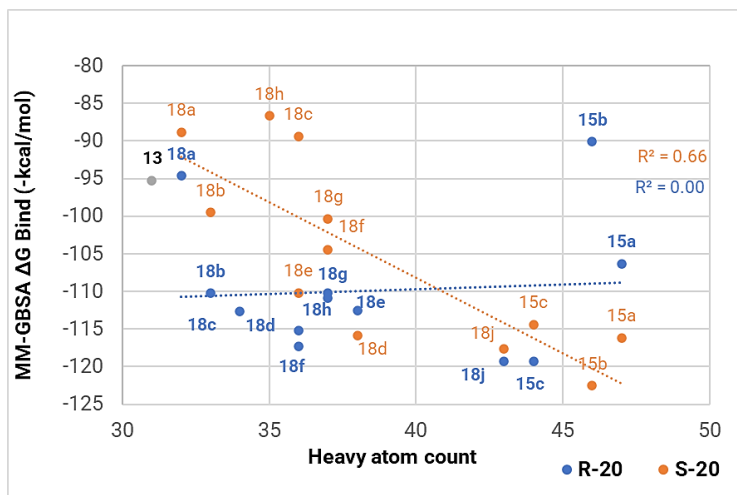
2. In silico docking of pimavanserin analogues at the human 5-HT_{2A}R

out. **Graph 2.6.4-1** depicts relationship between ΔG of the pimavanserin analogues obtained from MM/GBSA and increase in the heavy atom count. The change in heavy atom count reflects the change of the amino alcohol moiety size since this is the only part of the molecular structure to change in the analogue series. However, it is important to highlight that because analogues **R/S-15c** were determined to be non-binding experimentally, ¹⁶¹ and **S-18c** and **R-18i** adopted "reversed" binding poses in comparison to **13** in molecular docking, data for these analogues has not been included.

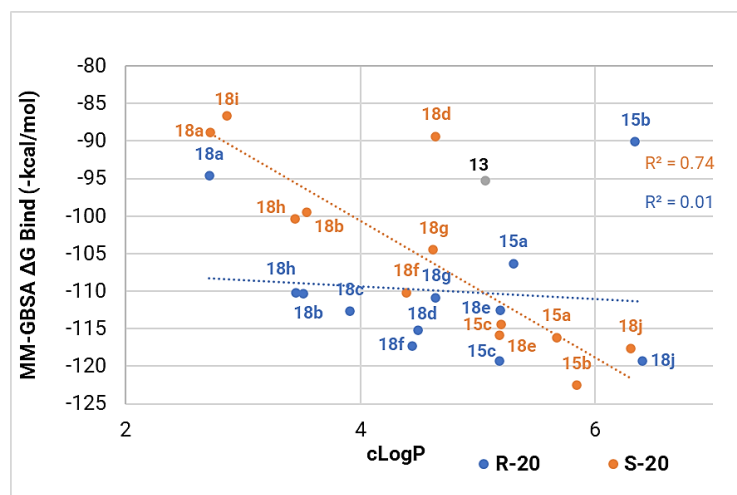
It was predicted that the relationship between the predicted ΔG of the pimavanserin analogues obtained from MM/GBSA calculations, and heavy atom count differed significantly between the *R* and *S* enantiomers ($R^2 = 0.00$ / $R^2 = 0.66$). For the *S* enantiomers, a relatively strong correlation was predicted, suggesting the amino alcohol moiety size could modulate the binding affinity. However, this result may be associated with the rigid receptor docking method used initially. In contrast, no correlation for the *R* enantiomers is demonstrated. Notably, **R-15a** and **R-15b** appear to be outliers from the remaining *R* enantiomer amino alcohol analogues. A relatively strong correlation ($R^2 = 0.74$) was also found between lipophilicity, represented as the computational estimate of the logarithm of the partition coefficient (cLogP) calculated via QikProp in Maestro, and the ΔG MM-GBSA values for *S* enantiomers, **Graph 2.6.4-2**. Thus demonstrating lipophilicity of the amino alcohol moiety contributes to modulating the ΔG of the ligand also. Taken

2. In silico docking of pimavanserin analogues at the human 5-HT_{2A}R

together both correlations predicted the size and lipophilicity of the amino alcohol moiety have an important effect on ligand binding which could be optimized to increase binding affinity towards the 5-HT_{2A}R.



Graph 2.6.4-1: MM-GBSA ΔG plotted against the HAC of R/S-15a-d, R/S-18a-e, R-18c, R/S-18e-h, S-18i, and R/S-18j.



Graph 2.6.4-2: MM-GBSA ΔG plotted against the cLogP for R/S-15a-d, R/S-18a-e, R-18c, R/S-18e-h, S-18i, and R/S-18j.

2. In silico docking of pimavanserin analogues at the human 5-HT_{2A}R

2.6.5 MM-GBSA calculation discussion

MM-GBSA calculations suggest, if the predicted binding pose of the structure-based designed analogues **R/S-18a-b**, **R-18c**, **R/S-18d-h**, **S-18i**, and **R/S-18j** from Glide are accurate, they may bind to the 5-HT_{2A}R receptor with good affinity. By considering residue flexibility within a 5.0 Å radius around the ligand during MM-GBSA calculations, it has permitted optimisation of the ligand-receptor interactions. In many cases, these analogues could demonstrate greater binding affinity than **13**, as indicated by their lower ΔG MM-GBSA values. This aligns with known analogues **R/S-15a-c** demonstrating lower binding affinities than **13** experimentally. The ranking of ΔG MM-GBSA values did not match the ranking of experimental binding affinity ¹⁶¹ **Table 2.6.5-1**.

Compound	IC ₅₀ (nM)	R/S	ΔG MM-GBSA (kcal.mol ⁻¹)
13	22 ¹⁶¹		-95.27
15a	0.39 ¹⁶¹	R	-106.3
		S	-116.2
15b	0.87 ¹⁶¹	R	-90.12
		S	-122.5
15c	1.93 ¹⁶¹	R	-119.3
		S	-114.4
15d	ND ¹⁶¹	R	-103.3
		S	-85.36

Table 2.6.5-1: Experimental potency of 13 and 15a-d compared to their individual enantiomer MM-GBSA ΔG values showing no ranking order correlation between binding strength.

The lower ΔG MM-GBSA values were associated to larger amino alcohol moieties, such as diisopropylamine, pyrrole, piperidine, morpholine, and 4-phenyl-piperidine. These moieties were shown to

2. In silico docking of pimavanserin analogues at the human 5-HT_{2A}R

afford deeper binding into the TM4-TM5 HP and create further interactions with residue side chains such as hydrophobic interactions, particular with compared to those limited by the smaller amino alcohol moieties. Consequently, the ligand-receptor complex becomes more stable than that of **13** or **R/S-18a**, **R-18d**, and **S-18i**.

It appears either polar or charged groups are not well-tolerated in the TM4-TM5 HP either, potentially affecting the binding affinity of ligands to the receptor. Both charged or polar groups such as the amine or hydroxyl group featured on **R/S-18a** and **R/S-18i** have higher ΔG MM-GBSA values compared to **13** or larger lipophilic amine groups featured on **R/S-18e** or **R/S-18j**. Conversely, lipophilic groups show to have better compatibility with the TM4-TM5 HP, as they exhibit lower ΔG MM-GBSA values, suggesting stronger binding interactions within the pocket. Thus, highlighting the hydrophobic characteristic of the pocket or passage.

Moreover, differences in ΔG MM-GBSA values appears to be modulated by the lipophilicity of the amino alcohol moiety binding into the TM4-TM5 HP, potentially leading to higher binding affinities. This aligns with recent finds where substituted phenylethylamines were predicted to bind into the side extend pocket. The change in lipophilicity of the phenylethylamines resulting from the substitution at the position bound into the TM4-TM5 HP was correlated experimentally with miniGq protein activation.¹⁰⁴

2. In silico docking of pimavanserin analogues at the human 5-HT_{2A}R

Though the size and lipophilicity of the amino alcohol moiety appears to impact the ΔG MM-GBSA of the pimavanserin amino alcohol analogues, particularly in the context of the S enantiomers, it is crucial to consider the limitations of docking and refinement alone.^{251,252} Thus, modelled poses between R/S enantiomers are influenced by the lack of flexibility in the receptor model during docking and time given to complex refinement.

Overall predicted MM-GBSA calculations have built upon the Glide docking, which indicated that larger and lipophilic amino alcohol moieties are associated with lower ΔG MM-GBSA values. Thus, they show a modulating effect that might confer to enhanced binding affinity, potency, and selectivity at the 5-HT_{2A}R. Further experimental validation is now necessary to confirm the binding activity of the new structure-based analogues **R/S-18a-j** at the 5-HT_{2A}R before selectivity at alternative receptor subtypes can be compared.

2.7 Conclusion of pimavanserin analogue docking

In docking the 5-HT_{2A}R TM4-TM5 HP has been targeted and the predicted binding mode of the structure-based designed analogues **17a-c** and **R/S-18a-j** and resulting complexes interrogated. Modification to an amino alcohol moiety at the position of the ring c 4-isobutyl moiety of **13**, appears to be an effective strategy for increasing the pimavanserin scaffold length and size. The amino alcohol moiety extension was predicted to enable deeper binding within the TM4-TM5 HP towards the

2. In silico docking of pimavanserin analogues at the human 5-HT_{2A}R

transmembrane space. This resulted in a range of Gscores and calculated MM-GBSA ΔG demonstrated by analogues **R/S-15a-d** and **R/S-18a-j**. Notably improved *in silico* scoring and calculations were achieved by several analogues compared to **13**. MM-GBSA predicted a potential of stereochemical preference of the amino alcohol moiety highlighted by ΔG MM-GBSA calculations, and potentially ligand binding. Therefore, consideration to stereospecific synthesis to afford a specific enantiomer could be warranted, as it could potentially enhance ligand binding and selectivity.

However, caution must be exercised when interpreting *in silico* results, as several factors may influence accuracy and lead to confounding outcomes due to the chosen methodology. For instance, employing a rigid receptor docking method resulted in a false positive result for **R/S-15d**, which was experimentally determined to be non-binding, despite achieving G-scores comparable to **13**.

In a similar manner to their Gscores, analogues **S-18c** and **R-18i** achieved higher ΔG MM-GBSA values than **13** and were predicted to bind in opposite directions across the binding sites. However, this is based upon the complexes from the initial docking method, which predicted **S-18c** and **R-18i** to bind in reversed orientation across the binding sites in comparison to **13**.

2. In silico docking of pimavanserin analogues at the human 5-HT_{2A}R

Moreover, it is crucial to note that these predictions do not fully consider the binding of the analogue series to other receptor subtypes, such as the 5-HT_{2C}R, for which **13** exhibits binding affinity. This suggests steric tolerance in this region of the 5-HT_{2C}R that may also accommodate the analogue series.

Overall, the results obtained from molecular docking provide important structural insights into the putative binding modes of structure-based designed pimavanserin analogues **17a-c** and **R/S-18a-j**, with some predicted to demonstrate enhanced binding at the 5-HT_{2A}R in comparison to **13**. Although, these *in silico* results do not assess 5-HT_{2A}R subtype selectivity. Further *in silico* techniques maybe employed to investigate this, such as molecular dynamics or induced fit docking at other the 5-HT₂ receptor subtypes or D₂R, and experimental validation is required.

In conclusion, while *in silico* results provide initial insights for the structure-based designed pimavanserin analogue series **17a-c** and **R/S-18a-j**, these predictions must be interpreted cautiously. The study revealed limitations in the rigid receptor docking method, exemplified by the false positive result for **R/S-15d**. Moreover, the current predictions do not fully account for binding to other receptor subtypes or assess 5-HT_{2A}R subtype selectivity. Although docking results showed some correlation between **R/S-15a-c** G-scores and experimental trends, the potential inaccuracy of predicted poses, particularly for **R/S-15d**, highlights the need for refined methodologies. The MM-GBSA

2. In silico docking of pimavanserin analogues at the human 5-HT_{2A}R

calculations, while indicating enhanced binding for **R/S-15a-c** as compared to **13**, no correlation between experimental or ΔG MM-GBSA values was demonstrated and are based on potentially incorrect initial complexes. To improve the accuracy of the docking protocol, future work should focus on expanding the training set to include additional experimentally validated analogues of **13**. Ultimately, experimental validation remains crucial to confirm *in silico* predictions and assess the actual binding properties and selectivity of these analogues, underscoring the complementary nature of *in silico* and experimental approaches in drug design. Thus, the synthesis of the pimavanserin analogues **17a-c** and **R/S-18a-j** becomes evident.

3. Design, synthesis, characterisation of 5-HT_{2A}R fluorescent probes

3. Design, synthesis, characterisation of 5-HT_{2A}R fluorescent probes

3.1 Introduction

The human 5-HT_{2A}R is an important therapeutic target for many neuropsychiatric conditions.^{113,153,253–255} As such, new 5-HT_{2A}R-targeting drugs and ligands require pharmacological interrogation at the receptor. Fluorescence-based pharmacological techniques, such as bioluminescence resonance energy transfer (BRET) assays and Förster resonance energy transfer (FRET) assays, prove effective for interrogating ligand-GPCR binding.¹⁶⁹

Crucial to this is utilizing high-affinity fluorescent probes – biologically active compounds such as 1-(2,5-dimethoxy-4-iodophenyl)propan-2-amine (DOI) and ketanserin (**10**), linked to fluorophores, resulting in fluorescent ligand conjugates/probes.²⁵⁶

High-affinity fluorescent antagonist conjugates such as probes can effectively target the GPCR,^{170,257,258} as can fluorescent agonist conjugates.^{170,172} These may also enable the monitoring of dynamic processes like receptor internalization and trafficking.²⁵⁹ A fluorescent probe can be substituted in place of a radiolabelled ligand in a competition-based binding assay, which gives them a considerable advantage.^{166,260–262}

Utilizing FRET offers the advantage of evaluating specific binding in a homogeneous format. This obviates the need to separate bound

3. Design, synthesis, characterisation of 5-HT_{2A}R fluorescent probes

from free tracers, or ligands, enabling continuous real-time monitoring²⁶³ and at high-throughput if required.²⁶¹ Thus, reducing operator process steps and mitigating inherent safety risks, legal concerns, and disposal costs associated with conventional radioligand binding assays^{130,166} that can employ agonist and antagonists based radioligands such as [¹²⁵I]-R-DOI,^{264,265} [³H]-spiperone,¹²² and [³H]-ketanserin.¹³⁰

The approach of the competition-based binding assays remain consistent whether a ligand possesses a radioisotope or a fluorophore. The primary goal being the estimation of bound ligand. Radioligands commonly employ scintillation counting to measure bound ligand concentration, although this requires the separation of bound and free ligands. The methods to measure the concentration of bound fluorescent probes include fluorescence spectroscopy, fluorescence plate readers, flow cytometry, confocal microscopy, and FRET techniques.^{168,169}

Fluorescent probes can be developed from antagonists and agonist ligands for the molecular target. Unless bound to an internalized receptor the probe should remain extracellular, exhibit minimal non-specific binding to the cell membrane, undergo quenching when not bound to either receptor or cell membrane, and be displaceable using higher concentrations of a known unlabelled chemical probe targeting the same receptor. Following the synthesis of a fluorescent probe, thorough pharmacological characterization of its affinity and efficacy profile is necessary. Fluorescent probes are unique chemical entities with

3. Design, synthesis, characterisation of 5-HT_{2A}R fluorescent probes

modifications to the parent pharmacophore, leading to significant differences in properties compared to the selected pharmacophore.¹⁶⁸

3.1.1 5-HT₂ receptor fluorescent probes

Several studies have reported the development and use of fluorescent probes targeting the 5-HT₂ subtypes.^{171,172,177} Fluorescent probes previously designed for the 5-HT_{2B}R are conjugates of the known 5-HT₂ receptor type agonist DOI. The receptor targeting moiety, **Figure 3.1.1-1**.

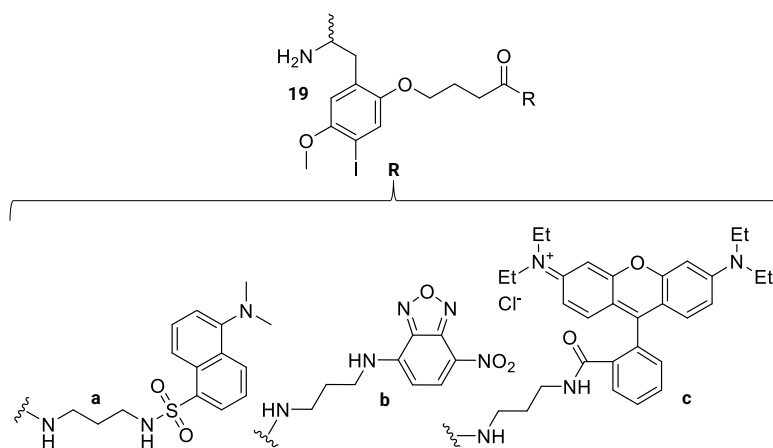


Figure 3.1.1-1: DOI based fluorescent probes featuring acid functionalised propoxy linker tethered to; dansyl (19a), NBD (19b), or rhodamine-based (19c) fluorophores.

Position 2 of the DOI phenyl ring was known to increase binding affinity and selectivity towards the receptor.^{172,266} Thus, the integration of an acid-functionalized ether linker tethered to a dansyl fluorophore, **19a** at this position was chosen in the fluorescent probe design strategy. In radioligand binding competition binding assays used to characterise the fluorescent probe, a propyl chain was identified as the optimal linker

3. Design, synthesis, characterisation of 5-HT_{2A}R fluorescent probes

length. Although selectivity was improved for the 5-HT_{2B}R, this resulted in a reduction of binding affinity ($K_i = 111.79$ nM). Binding affinity was diminished at the 5-HT_{2A}R ($K_i = 1709$ nM) and 5-HT_{2C}R ($K_i = 273.25$ nM), in comparison to DOI ($K_i = 48.19$ nM, $K_i = 61.15$ nM, $K_i = 18.24$ nM) also.¹⁷²

Different fluorophores were then tethered to the linker to explore their effect on photochemical and pharmacological profile of the fluorescent probe. Substituting the dansyl fluorophore **19a** with a 7-nitrobenz-2-oxa-1,3-diazole (NBD) based fluorophore via classical amide coupling reaction conditions²⁶⁷ was notable **19b**, as this retained potency and improved selectivity at 5-HT_{2B}R ($K_i = 90.99$ nM) compared to 5-HT_{2A}R ($K_i = 3307$ nM) and 5-HT_{2C}R ($K_i = 1806$ nM). Subsequently, tethering of a rhodamine-based fluorophore to afford **19c** resulted in reduced binding affinity across all 5-HT₂ receptor subtypes as compared to DOI. However, selectivity was maintained for the 5-HT_{2B}R ($K_i = 261.60$ nM) over the 5-HT_{2A}R ($K_i = 1217$ nM) and 5-HT_{2C}R ($K_i = 994.32$ nM).

Moreover, in fluorescence microscopy studies the favourable photochemical properties of the rhodamine-based fluorophore in **19c** in comparison to the NBD-based fluorophore in **19b**, such as longer excitation and emission wavelength $\sim 555/580$ nm and $\sim 461/530$ nm respectively, permitted specific labelling of the 5-HT_{2B}R stably expressed in Chinese hamster ovary (CHO) cells in a concentration-dependent manner. However, such labelling was not observed in CHO cells stably expressing 5-HT_{2A}R, highlighting the structural differences between receptor subtype binding pockets.¹⁷²

3. Design, synthesis, characterisation of 5-HT_{2A}R fluorescent probes

Attempts have also been made to develop 5-HT_{2C}R, agonist-based fluorescent probes **Figure 3.1.1-2** as tools for cell-based fluorescent polarization assays.

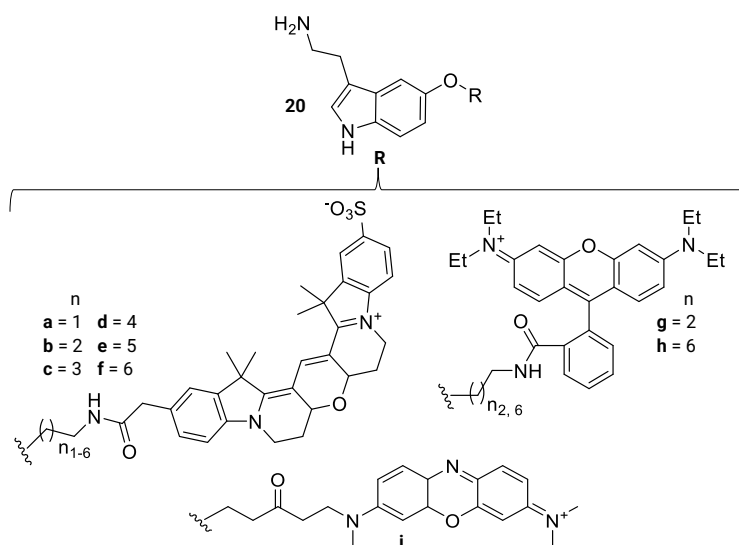


Figure 3.1.1-2: 5-HT-based fluorescent probes tethered to fluorophores; Cyannie3B (Cy3B) (20a-f), tetramethylrhodamine (TMR) (20g-h), and EVOBlue™ (20i).

5-HT was used as receptor targeting moiety. The 5-position hydroxy moiety was identified as a potential linker attachment site, thus several different amino ether linker with carbon chains ranging from 2-7 carbons, were installed, and tethered to Cyannie3B (Cy3B) **20a-f**, a yellow-emitting cyanine dye, under amide coupling conditions. In addition, tetramethylrhodamine (TMR), **20g** and **20h**, an orange emitting dye with a 3 and 7 carbon linkers, and EVOBlue™, **20i**, a red emitting dye with a 2-carbon linker were also tethered.¹⁷¹ Interestingly, modelling not shown by the authors suggested the fluorophore was oriented perpendicular

3. Design, synthesis, characterisation of 5-HT_{2A}R fluorescent probes

towards the TM5 region in the 5-HT_{2C}R,¹⁷¹ also the position of the HP in the 5-HT_{2A}R.¹⁷

To characterize the designed serotonin-based fluorescent probes radioligand binding assays were employed. The binding affinities of serotonin at the 5-HT_{2A}R ($K_i = 7.8$ nM), 5-HT_{2B}R ($K_i = 128$ nM), and 5-HT_{2C}R ($K_i = 7.5$ nM) was determined. The addition of Cy3B-based fluorophore with 2-carbon linker from the 5-position phenol oxygen atom next improved binding affinity of the fluorescent probe at the 5-HT_{2C}R ($K_i = 1.9$ nM) and the 5-HT_{2A}R ($K_i = 6.09$ nM), and selectivity over 5-HT_{2B}R ($K_i = 552$ nM) in comparison to serotonin. Increasing the linker length to 3 carbons appeared to reduce potency of the fluorescent probe at the 5-HT_{2C}R ($K_i = 3.4$ nM), but improved selectivity over the 5-HT_{2A}R ($K_i = 32.18$ nM), and 5-HT_{2B}R ($K_i = 6713$ nM), in comparison to the 2-carbon linker.¹⁷¹

Conversely, increasing linker length to 4 carbons was associated to an increase in 5-HT_{2A}R binding affinity and selectivity ($K_i = 4.57$) over the 5-HT_{2C}R ($K_i = 10$ nM), and 5-HT_{2B}R ($K_i = 2657$ nM). Extending the linker length longer than 4 carbons binding activity was diminished at the 5-HT_{2A}R but maintained at the 5-HT_{2C}R. Overall a decreasing trend in potency was observed at the 5-HT_{2C}R with all Cy3B, TMR, and EVO based fluorescent probes as linker length increased between 1-6 carbons. Notably, only the Cy3B based serotonin probes demonstrated 5-HT_{2A}R affinity.¹⁷¹

3. Design, synthesis, characterisation of 5-HT_{2A}R fluorescent probes

The favourable binding profile of the **20b**, featuring the 2-carbon linker prompted its selection for evaluation in a fluorescent polarization competition binding assay for the 5-HT_{2C}R. The kinetically derived K_d for the fluorescent probe at the 5-HT_{2C}R receptor ($K_d = 0.23 \pm 0.04$ nM) closely matched saturation experiments ($K_d = 0.20 \pm 0.04$ nM). Moreover, **20b** was employed in a fluorescence polarization competition binding assay, affording binding affinities of known therapeutics which closely mirrored those determined by radioligand binding assays. The favourable binding profile of **20b** for 5-HT_{2A}R also prompted attempts at further characterization via a fluorescent polarization competition binding assay. However, these efforts were impeded by low 5-HT_{2A}R expression.¹⁷¹

An advantage of fluorescence anisotropy (FA) and fluorescence polarization (FP) assays is their ability to distinguish between bound and unbound ligands without requiring a wash or filtration step, allowing for homogenous assays, and typically employ cell membranes. However, high receptor concentrations and low ligand concentrations necessary to observe a substantial change in FA/FP upon ligand binding often lead to significant ligand depletion. Consequently, there is the potential for notable alterations in the free concentrations of both labelled and unlabelled ligands during kinetic and competition binding experiments using this method.¹⁶⁹

One commercially available fluorescent probe from Hello Bio developed to bind at the 5-HT_{2A}R, as well as the 5-HT_{2B}R is CA201019

3. Design, synthesis, characterisation of 5-HT_{2A}R fluorescent probes

CellAura fluorescent 5-HT_{2A/2B}R antagonist [4F4PP].¹⁷⁶ The complete structure and fluorophore details remain undisclosed, but the molecular weight is provided (987 g mol⁻¹). It is based on the molecular structure of (4-fluorophenyl)(1-(4-phenylbutyl)piperidin-4-yl)methanone (4F4PP), **16**, and has a red emitting dye according to its excitation and emission wavelength (633/650 nm).

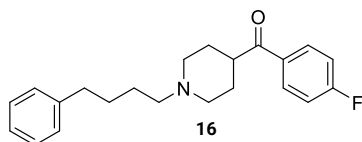


Figure 3.1.1-3: Molecular structure of 5-HT_{2A}R and 5-HT_{2C}R antagonist 4F4PP (**16**).

One study has characterised the fluorescent probe CA201019 in a human 5-HT_{2A}R cell-membrane-based fluorescent TR-FRET competition binding assay.¹⁷⁷ This assay employed CHO-K1 cell lines transiently transfected with cDNA encoding a SNAP-tagged human 5-HT_{2A}R, aiming to explore the binding affinity and kinetics of antipsychotics binding to the receptor. When characterising the binding affinity, or equilibrium dissociation constant (K_d) of CA201019 ($K_d = 3.98 \pm 0.65$ nM) at the receptor via this assay, its specific binding appeared not to be significantly higher than the background signal from non-specific binding, which represented over 50% total binding. This could be result of the CLogP (4.69) of receptor targeting moiety and type of fluorophore CA201019 features at physiological pH.¹⁷⁷

3. Design, synthesis, characterisation of 5-HT_{2A}R fluorescent probes

In evaluating the binding affinity of pimavanserin analogues **R/S-18a-j** at the human 5-HT_{2A}R through fluorescence-based techniques like a cell-membrane based fluorescent assay employing TR-FRET, the selection of an appropriate fluorescent probe becomes crucial. A promising starting point is provided by the fluorescent probe CA201019 from Hello Bio highlighted above.¹⁷⁶ This ligand offers the starting molecular scaffold of **16** which has been reported as an antagonist with high affinity for the 5-HT_{2A}R ($K_i = 5.3$ nM) but low affinity for the 5-HT_{2C}R ($K_i = 620$ nM),¹⁶⁴ and may also be useful in the attempt to develop subtype-selective fluorescent probes.

3.2 Aims

The primary goals of this study were twofold: 1) develop a 5-HT_{2A}R fluorescent probe for the human 5-HT_{2A}R; 2) Evaluate the probes binding at the receptor by cell-membrane based fluorescent TR-FRET saturation assays. These probes could serve as the pharmacological tools for assessing the binding affinity of the pimavanserin analogues **R/S-18a-j** at the 5-HT_{2A}R in TR-FRET competition binding assays.

3.3 5-HT_{2A}R fluorescent probe design

The fluorescent probe incorporates three key elements: the pharmacophore as the receptor targeting moiety, a linker region, and fluorophore. This follows the functionalized congener approach **Figure 3.3-1**, originating in the 1980s,^{268,269} that was used to design adenosine

3. Design, synthesis, characterisation of 5-HT_{2A}R fluorescent probes

receptor congeners and catecholamine conjugates, and has now been extensively applied to a range of ligands targeting GPCRs.^{172,175,263,270}

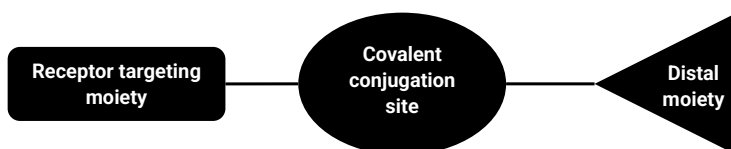


Figure 3.3-1: Functionalised congener schematic.

The design strategy of the functionalised congener approach enables the modulation of a nonpeptide drug's affinity or selectivity for its target receptor. This modulation was achieved through the strategic introduction of chemical motifs and functional groups at the terminus of an attached chain, positioned at a permissive site on the ligand. Implicit in this approach is the assumption that the steric constraints within the target binding site diminish at the distal region of this appended chain.²⁷¹ This approach offered the added advantage of enabling tethering to a distal moiety with additional chemical functionality to the receptor targeting moiety. Thereby making it feasible to design spectroscopic ligands with high receptor affinity.²⁷¹

The design process initiates by identifying a suitable model ligand or therapeutic as the receptor targeting moiety, followed by an examination of its molecular structure to identify optimal sites for linker attachment. Subsequently, the selection of an appropriate linker is determined, and the final step involves choosing a fluorophore that is well-suited for covalent tethering, based on its intended application.²⁷² SAR and protein structural and modelling data where available should be

3. Design, synthesis, characterisation of 5-HT_{2A}R fluorescent probes

employed to rationally identify linker position on the pharmacophore tolerant to chemical modification, or is predicted by the later approach.¹⁶⁸

3.3.1 The receptor targeting moiety

The receptor targeting moiety is the section of the molecule binding at the target site of the protein. This may be an orthosteric binding pocket²⁷⁰ or allosteric binding pocket.²⁶³ It is crucial in the fluorescent probe design strategy as it must interact with the target binding pocket ideally with high affinity. Therefore, **16** was chosen as a model ligand because of its high affinity for the 5-HT_{2A}R where it acts as an antagonist. The structure of **16** incorporates binding motifs that are recognised by the 5-HT_{2A}R. A 4-(4-fluorobenzoyl)piperidine moiety introduces an essential amine group, a prerequisite for effective ligand binding to the aminergic receptors via a hydrogen bond/ionic interaction with D155^{3,32,80}.

Additionally, the significance of the 4-fluorophenyl ring binding at inactive conformations within the hydrophobic cleft of the 5-HT_{2A}R has been elucidated.^{124,162} Respectively the 4-fluorophenyl ring in **4** and **13** has been observed and predicated to interact with the residues of the PIF motif and W336^{6,48}, indicating its role in ligand binding, and its association to a ligand's antagonism.

To ascertain the binding conformation of **16** and identify potential linker attachment sites, molecular docking was conducted employing the 5-HT_{2A}R homology model and docking protocol in **Chapter 2**.

3. Design, synthesis, characterisation of 5-HT_{2A}R fluorescent probes

Compound **16** was docked into the central binding pocket within the helices bundle **Figure 3.3.1-1**. The favourable Gscore calculated < -9 kcal.mol⁻¹ (-9.29 kcal.mol⁻¹) aligns with the high affinity reported for **16** at 5-HT_{2A}R ($K_i = 5.3$ nM).¹⁶⁴ Predicted interactions offer a structural basis for the demonstrated antagonism at the receptor.²² The binding of **16** was predicted to involve a salt bridge/hydrogen bond interaction between the piperidinium ring ammonium ion and D155^{3,32}, including edge-to-face π -CH interactions between F340^{6,52} and W366^{6,48}, and the fluorophenyl ring inserted into the hydrophobic cleft.

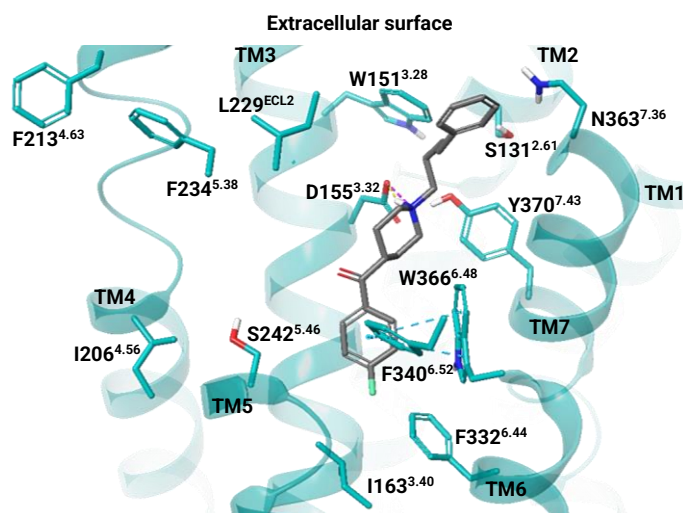


Figure 3.3.1-1: Compound **16** docked into the human 5-HT_{2A}R. Residues surrounding central pocket and TM4-TM5 HP displayed. Key binding interactions; H-bond (purple), salt bridge (yellow), and π -CH (blue).

This may be supported by superimposing the docked pose of **16** with the antagonist **4**,²⁴ in the risperidone-5HT_{2A}R XRC structure (PDB: 6A93), **Figure 3.3.1-2**.

3. Design, synthesis, characterisation of 5-HT_{2A}R fluorescent probes

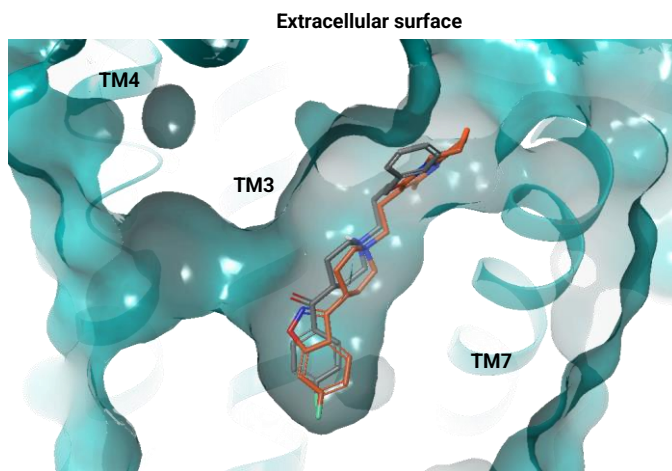


Figure 3.3.1-2: Superimposition sideview of **16** (grey) docked and **4** (red-orange) co-crystallised ligand in the human 5-HT_{2A}R. Molecular surface displayed. No TM4-TM5 HP binding predicted by **16** or **4**.

Crucially, the orientation of the phenyl butyl moiety was bound through the vestibule connecting the central binding pocket to the extracellular loop region, a more solvent-exposed region of the receptor, forming hydrophobic interactions (not displayed for clarity) with the alkyl chain and phenyl ring. Therefore, its adoption as receptor targeting moiety in the fluorescent probe design appeared reasonable.

The structural analysis of the predicted binding conformation of **16** in the 5-HT_{2A}R central binding pocket justified constructing the linker from the phenyl butyl moiety, thus minimizing the chance of unfavourable interactions with the receptor or modifications at this part of the molecule. However, the absence of suitable attachment points for further linker extension from the phenyl moiety was noted. Consequently, it was envisioned substitution to a phenol moiety proposed by **21**, in place of the aryl moiety on the butyl chain present in **16**, could be a suitable

3. Design, synthesis, characterisation of 5-HT_{2A}R fluorescent probes

strategy to enable linker extension, **Figure 3.3.1-3**. The substitution would afford a viable attachment site to start the linker with amino ether linkers, as exemplified in analogous fluorescent probe design strategies.^{171, 268, 271}

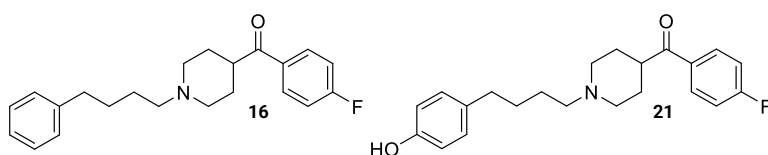


Figure 3.3.1-3: Proposed phenol substitution on 4F4PP molecular structure

3.3.2 Linker region

A linker forms the region between the pharmacophore and tethered a fluorophore outside the central binding pocket at an optimal distance from the receptor. A well-designed linker region is vital for preserving the pharmacophore's binding properties as the nature and length of the spacer, type of linker, and the fluorophore itself significantly influencing the final pharmacological profile of the fluorescent conjugate.²⁶ For example short linker chains have proved useful in the design of potent A₁AR fluorescent probes.²⁷ Strategic structural modifications at specific positions are essential to ensure easy tolerance without causing a significant impact on pharmacological activity of the pharmacophore.²⁷⁶

One approach to the linker region construction in the fluorescent probe design has been the incorporation of amino ether linkers and spacers.^{263,274,276,277} Therefore it was hypothesized, based on the predicted binding pose of the proposed 4F4PP-based receptor targeting

3. Design, synthesis, characterisation of 5-HT_{2A}R fluorescent probes

moiety, an amino ether linker could be initiated from the oxygen atom of phenol ring. However, due to the unknown optimal linker and spacer distance between the pharmacophore and fluorophore, a viable solution involved commencing the linker region from the phenol oxygen atom with a short linker such as an ethanamine linker featuring 2 carbons as previously used **Figure 3.3.2.-1, (i)**.¹⁷¹ To interrogate this, a proposed 4F4PP-based *N*-Boc protected congener, **22**, featuring the aminoethoxy linker was then docked into the 5-HT_{2A}R homology model.

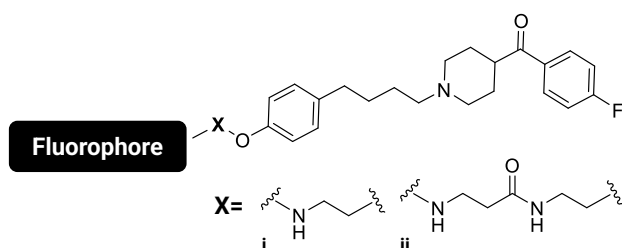


Figure 3.3.2-1: Proposed linker regions for the modified 4F4PP-based fluorescent probes. (i) ethanamine linker (ii) amino propanamide linker.

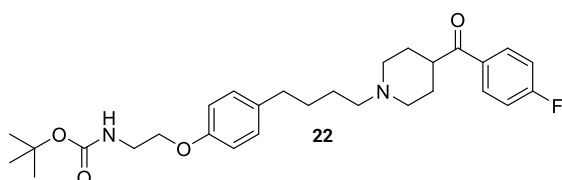


Figure 3.3.2-2: Proposed *N*-Boc protected 4F4PP-based congener (22**) with 2 carbon amino-alkyl linker.**

The predicted docking model **Figure 3.3.2-3** resulted in **22** maintaining a similar binding pose to **4** and **16** bound and docked to the 5-HT_{2A}R respectively. The Gscore calculated (-9.67 kcal.mol⁻¹) predicted favourable binding would be maintained. The binding of the receptor

3. Design, synthesis, characterisation of 5-HT_{2A}R fluorescent probes

target moiety was still predicted to involve the same interactions as previous. Additional interactions were predicted with the G359^{7.32} backbone oxygen atom and the sidechain carbonyl oxygen atom of N363^{7.36}. Crucially, the ethanamine linker was predicted directed towards the solvent exposed extracellular loop region, extending the ligand further from the phenol ring oxygen atom. However, the *N*-Boc group was predicted to bind within a hydrophobic pocket between TM6-TM7.

To increase the length linker region in a methodical approach *N*-Boc- β -alanine can be coupled via an amide bond. This would introduce an additional linker length incorporating an amide group, an additional of 2 carbon spacer, and a terminal amine, **Figure 3.3.2-2, (ii)**, for fluorophore conjugation following *N*-Boc deprotection.

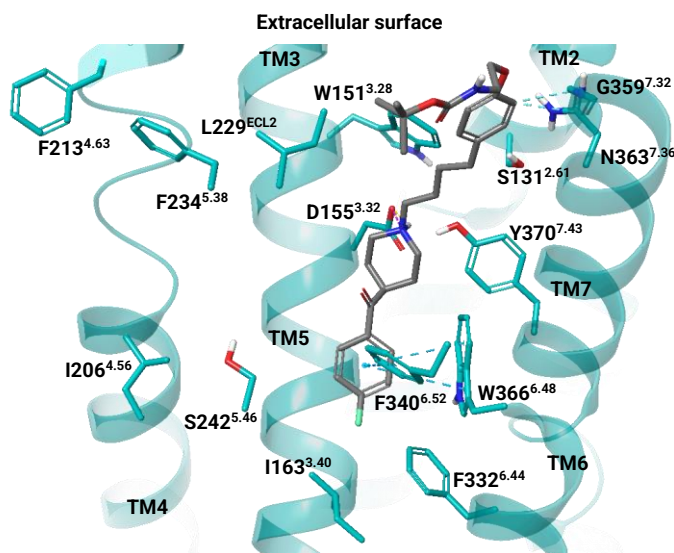


Figure 3.3.2-3: *N*-Boc protected congener (22) docked into the human 5-HT_{2A}R. Residues surrounding central pocket and TM4-TM5 HP displayed. Key binding interactions; H-bond (purple), salt bridge (yellow), and π -CH (blue).

3. Design, synthesis, characterisation of 5-HT_{2A}R fluorescent probes

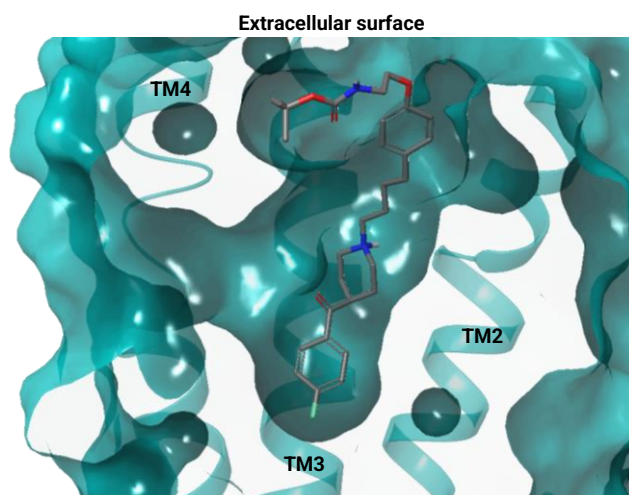


Figure 3.3.2-4: *N*-Boc protected congener (22) docked the human 5-HT_{2A}R. Molecular surface displayed. No TM4-TM5 HP binding predicted by 22.

3.3.3 Fluorophore

A variety of fluorophores can be tethered to the fluorescent ligand congener tailored to individual applications. It is the crucial component in a cell-membrane based fluorescent TR-FRET assay operating as the acceptor molecule in the FRET process. Fluorophores can vary significantly in size and impact upon the pharmacological activity. Thus, the choice of an appropriate fluorophore is critical to ensure efficient energy transfer and accurate detection. When selecting the appropriate fluorophore for attaching to a ligand of a target receptor, essential considerations include the absorption and emission profile of the fluorophore, its lipophilicity, which can influence its distribution in a biological system, and identifying the particular environments the fluorophore undergoes quenching.¹⁶⁸

3. Design, synthesis, characterisation of 5-HT_{2A}R fluorescent probes

The 4,4-difluoro-4-bora-3a,4a-diaza-s-indacene (BODIPY) fluorophore has been successfully applied in the design of fluorescent probes targeting various Class A GPCRs.^{263,270,275} However they have not been reported in fluorescent probes targeting the 5-HT_{2A}R, thus their effectiveness as a molecular tool in a fluorescent 5-HT_{2A}R cell-based assay is unknown. BODIPY dyes are favoured in high-throughput fluorescence-based assays due to their extended fluorescence lifetimes (>5 nanoseconds), visible wavelength emission, favourable anisotropy, high molar absorptivity, and minimal pH sensitivity.²⁷⁸

One BODIPY fluorophore variant, BODIPY 630/650, offers advantageous spectral characteristics, with excitation and emission occurring at longer wavelength, approximately 630/650 nm, respectively. Its emission profile is particularly beneficial for cell-based TR-FRET assays due to its red-shifted emission in comparison to those at a shorter wavelength **Table 3.3.3.-1**.

The longer wavelength helps reduce background interference and minimizes autofluorescence from biological samples, thereby enhancing the sensitivity and specificity of the TR-FRET assay. Quenching of BODIPY 630/650 has also been observed in aqueous solutions which is favourable. This suggests that an optimal environment for this fluorophore would be within a lipid environment, as it effectively diminishes background fluorescence stemming from non-bound ligands.²⁷⁴ Therefore, ideally suited to study GPCRs in cell membranes. This may be advantageous over more hydrophilic fluorophores such as

3. Design, synthesis, characterisation of 5-HT_{2A}R fluorescent probes

cyanine-5 (Cy5), or cyanine 3 (Cy3). However, consideration should also be given to potential interactions with the cell membrane due to the fluorophores lipophilicity.^{274,276}

Fluorophore	Absorbance nm	Emission nm	Emitting colour
Fluorescein	498	517	Green
BODIPY FL	505	513	Green
Cy3	550	570	Green yellow
Alexa Fluor Cy3	555	565	Orange
BODIPY TMR	542	574	Orange
BODIPY 630/650	630	650	Red
Sulf-Cy5	647	663	Red
Alexa Fluor Cy5	650	665	Red
Cy5	651	670	Red
Sulf-Cy5	647	663	Red

Table 3.3.3-1: List of fluorophore excitation and emission wavelengths.

Among the BODIPY 630/650 fluorophores, options include the commercially available BODIPY 630/650 carboxylic acid (**23**) and the BODIPY 630/650 X succinimidyl ester (NHS) activated form (**24**). Incorporation of either a carboxylic acid or NHS moieties into the structure was tailored for the acylation of amino-containing molecules. Moreover, BODIPY 630/650 X features an integrated aminohexanoyl linker denoted as "X," contributing to a linker region that should also be taken into consideration in fluorescent probe and linker region design.

3. Design, synthesis, characterisation of 5-HT_{2A}R fluorescent probes

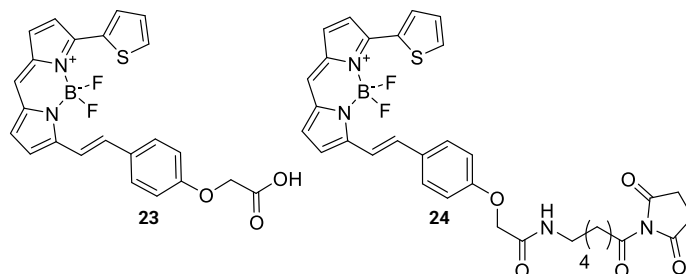


Figure 3.3.3-1: BODIPY 630/650 carboxylic acid (23) and 630/650 X NHS variants (24).

3.4 Proposed 5-HT_{2A}R fluorescent probes

From the evaluation of the fluorescent probe design strategy the fluorescent probes **25** and **26**, **Figure 3.4-1**, were proposed and a retrosynthetic analysis undertaken **Scheme 3.4.-1** and **Scheme 3.4.-2**.

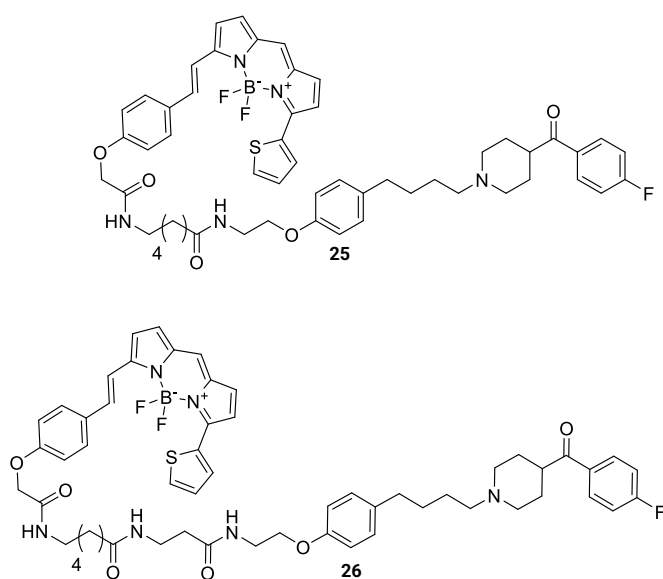
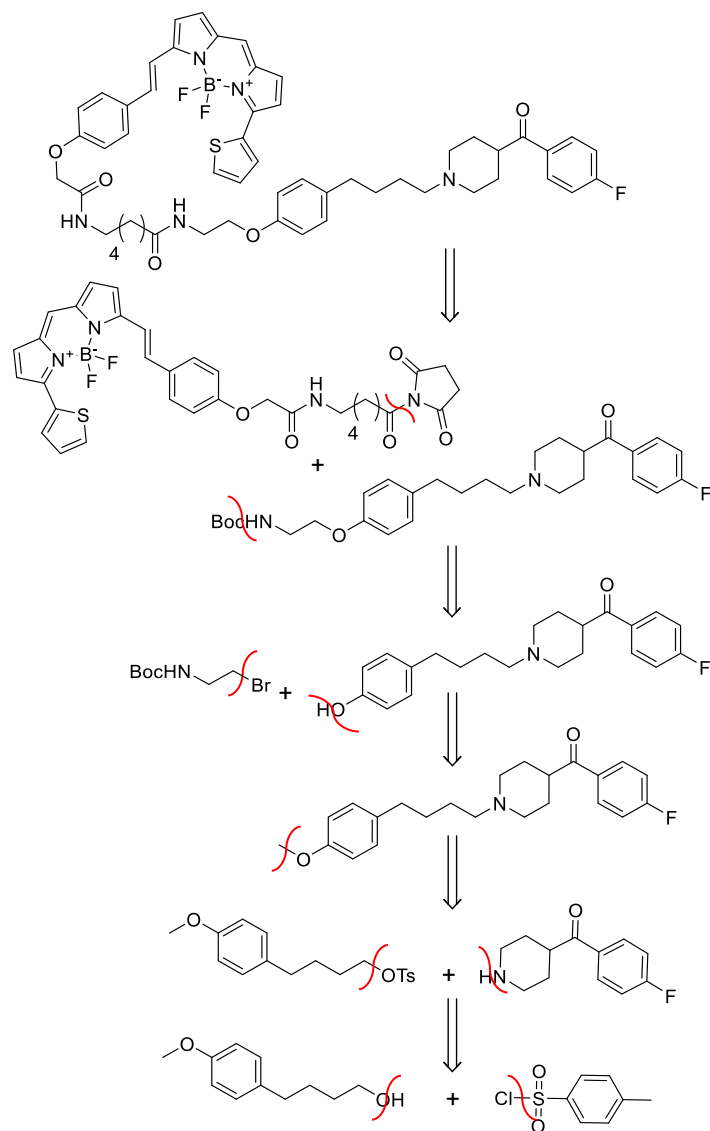


Figure 3.4-1: Proposed 5-HT_{2A}R fluorescent probes (25) and (26).

3. Design, synthesis, characterisation of 5-HT_{2A}R fluorescent probes

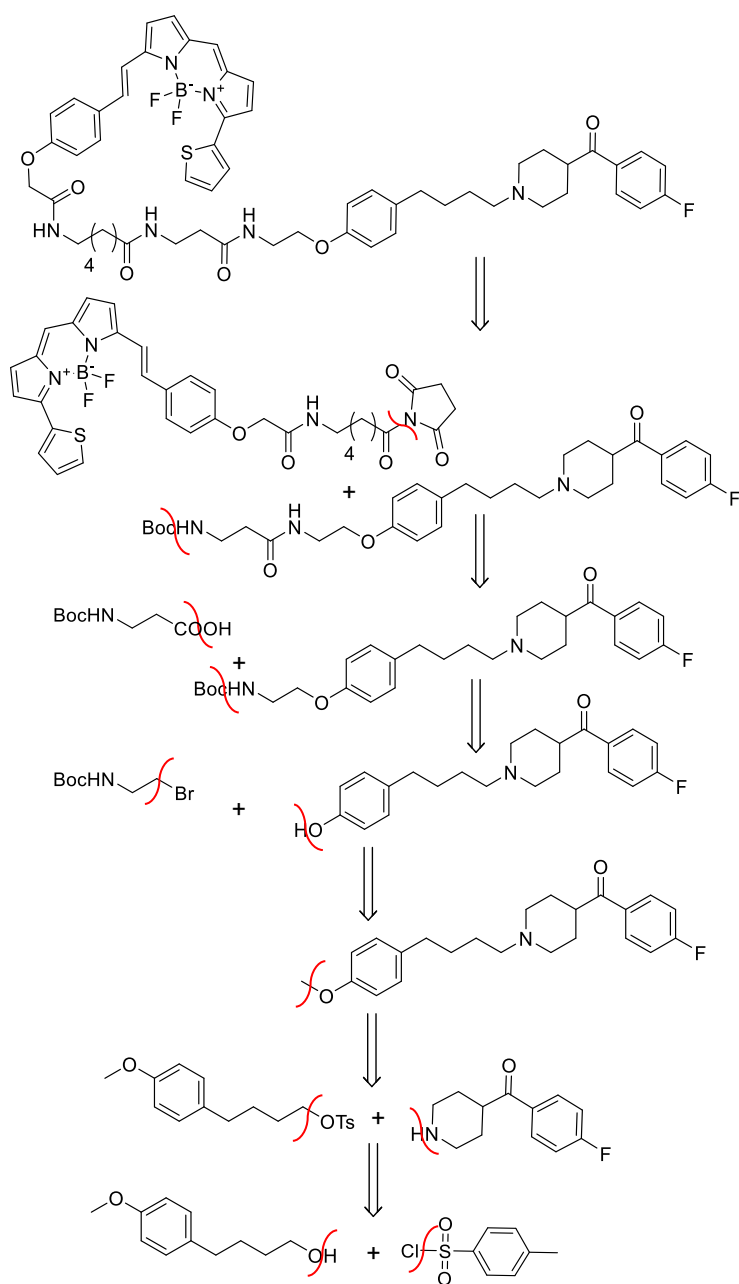
3.4.1 Retrosynthetic analysis of proposed 5-HT_{2A}R

fluorescent probes



Scheme 3.4.1-1: Retrosynthesis of 25.

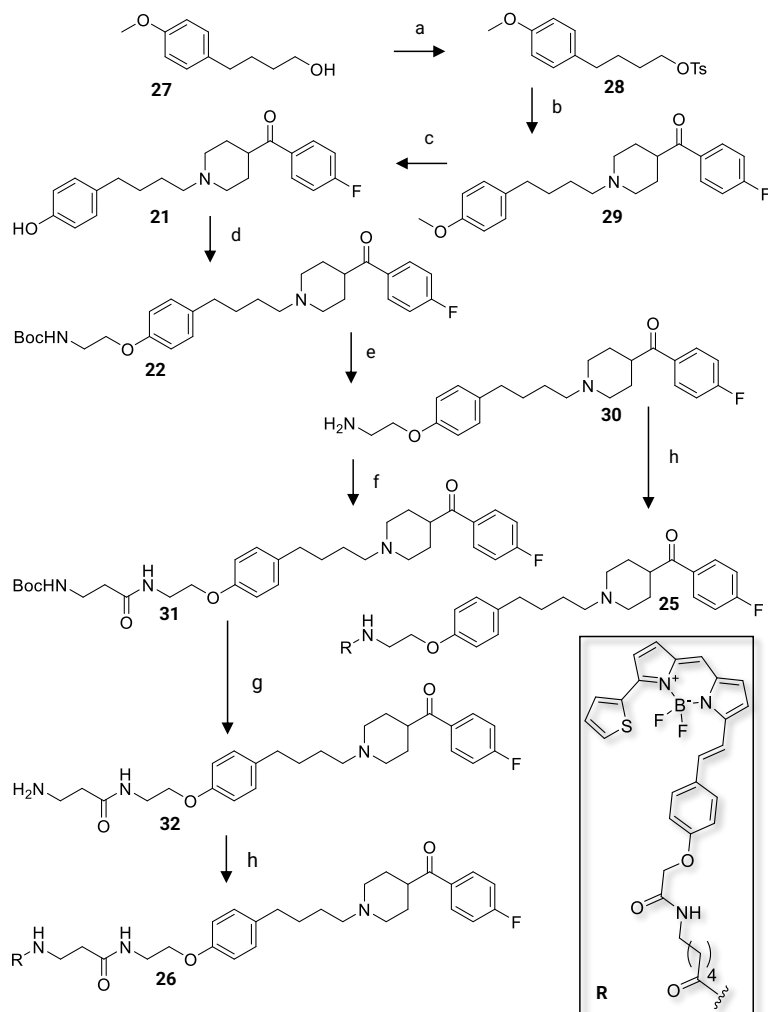
3. Design, synthesis, characterisation of 5-HT_{2A}R fluorescent probes



Scheme 3.4.1-2: Retrosynthesis of 26.

3. Design, synthesis, characterisation of 5-HT_{2A}R fluorescent probes

3.5 Synthetic route to 5-HT_{2A}R fluorescent probes



Scheme 3.5-1: Synthesis pathway for 25 and 26.

Reagents and conditions: (a) triethylamine (TEA) 3 eq, DMAP 0.2 eq, p-tosyl chloride 1.1 eq, r.t, 96%; (b) 4-fluorobenzoylpiperidine.HCl 0.9 eq, K₂CO₃ 4 eq, r.t, 72%; (c) pyridine.HCl 7 eq, MW 160°C, 66%; (d) 60% NaH/mineral oil 1.1 eq, tert-butyl-2-bromoethyl)carbamate 1.5 eq, dimethylformamide (DMF) 0°C-r.t, 30%; (e) 4M HCl/1,4-dioxane excess, r.t, 94%; (f) N-Boc-β-alanine 1.1 eq, (1-cyano-2-ethoxy-2-oxoethylideneaminoxy)dimethylamino-morpholino-carbenium hexafluorophosphate (COMU) 1.1 eq, N,N-diisopropylethylamine (DIPEA) 4 eq, 0°C, 17%; (g) 4M HCl/1,4-dioxane, excess, r.t, 94%; (h) BODIPY 630/650-X-NHS ester, 1 eq, DIPEA, 2.1 eq, darkness, r.t. 70-79%.

3. Design, synthesis, characterisation of 5-HT_{2A}R fluorescent probes

Retrosynthetic analysis above of both **25** and **26** allowed the design of tractable synthetic route **Scheme 3.5-1**. Starting with 4-(4-methoxyphenyl)butanol, **27**, the hydroxyl group was converted to the corresponding tosylate ester **28**. Displacement of the tosylate moiety by the amine of 4-(4-fluorobenzoyl)piperidine was carried out under alkylating conditions using MeCN and K₂CO₃ with warming at 70°C to afford **29**, the receptor targeting moiety, and to provide a point of further attachment to the linker from phenol moiety oxygen atom after demethylation of the arylmethoxy group.

To find a suitable *O*-demethylation method, three distinct conditions: pyridine HCl,²⁷⁹ aqueous HBr, and BBr₃ in DCM²⁸⁰ were trialled. Initially, the pyridine HCl method (**method A**) was employed. This method offered an advantage of short reaction times and being solventless but relied on a substantial excess of demethylating agent and combined with high temperatures. Therefore, the reaction was monitored at 5-minute intervals. After a total of 25 minutes of microwave irradiation (215W) at 160°C, no starting material was detected by LCMS. However, workup and purification led to a 66% yield, suggesting either mechanical loss, or degradation of the product and starting material during the reaction. Ensuring anhydrous pyridine HCl is used may help improve yield, as wet pyridine HCl can lead to water competing with the intended nucleophile, the chloride ion.

Despite achieving fair yields with the pyridine HCl demethylation method, the desire for increased yield prompted experimentation with

3. Design, synthesis, characterisation of 5-HT_{2A}R fluorescent probes

the established BBr₃ method²⁸⁰ (**method B**). This 24-hour procedure, conducted at a lower temperature range (0°C to room temperature), required a substantial molar excess of the demethylating agent due to boron forming complexes with non-target lone pair electrons. Purification yielded 53%, but no starting material was recovered. The decrease in yield is likely attributed to the formation of unhydrolyzed boron complexes during workup and the degradation of the starting material and mechanical loss.

Next the classical method employing aqueous 48% HBr (**method C**), a Brønsted-Lowry acid, was considered as an alternative to a Lewis acid BBr₃. However, this process involved reflux under strong acidic conditions. LCMS revealed no detectable starting material after 24 hours of reflux however work-up and purification proceed to afford a 56% yield.

Overall, none of the investigated methods afforded high yields of the desired phenol product, thus sub-optimal and demonstrated the requirement for substrate specific optimization of each reaction type. Demethylation via pyridine HCl was selected as the preferred approach to afford **22**. This would serve as a suitable point for the subsequent attachment of the linker region.

A bimolecular nucleophilic substitution (S_N2) reaction, displacing the bromide ion from *tert*-butyl-(2-bromoethyl)carbamate under alkylation conditions, using DMF and 60% NaH/mineral oil at 0°C to r.t, led to the formation of **22** the *N*-Boc protected congener, although in poor yield. Low yield may be attributed to competition between an elimination

3. Design, synthesis, characterisation of 5-HT_{2A}R fluorescent probes

reaction mechanism pathway occurring with *N*-Boc-2-bromoethane before nucleophilic attack by the phenolate occurs. *N*-Boc deprotection was carried out using 4M HCl/1,4-dioxane to afford **30** featuring the terminal amine for fluorophore conjugation.

Acylation between **30** and BODIPY 630/650 X (NHS) ester was carried out using in-house developed methodology at milligram scale previously reported.^{263,270} This step allowed the conjugation of the BODIPY 630/650 fluorophore via an attached aminohexanoyl linker to afford **25**.

Concurrently, **30** was coupled to *N*-Boc β-alanine under amide coupling conditions employing COMU as the coupling reagent to extend the linker, resulting in **31**. However, during preparative HPLC (HPLC-method E), **31** exhibited *N*-Boc deprotection, leading to decreased yield, which is attributed to exposure to the acidic eluent environment containing formic acid.²⁸¹ *N*-Boc deprotection of **31** was carried out using 4M HCL in 1, 4 dioxane to afford **32** featuring the terminal amine for fluorophore conjugation.

Finally, as before the congener and BODIPY 630/650 X NHS ester was coupled using the same methodology as above, affording **26**. Both fluorescent probes were isolated and purified via preparative reverse phase high performance liquid chromatography (prep HPLC).

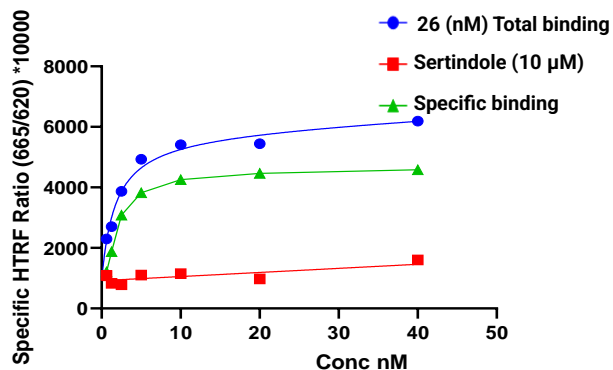
3.6 Pharmacological characterisation of fluorescent probes binding to the human 5-HT_{2A}R

The cell-membrane based fluorescent TR-FRET assay used in this study to evaluate the probe-receptor interactions in a cellular context by monitoring real-time ligand binding. Thus, making it suitable for studying compounds targeting specific receptors like the human 5-HT_{2A}R expressed in CHO membranes.

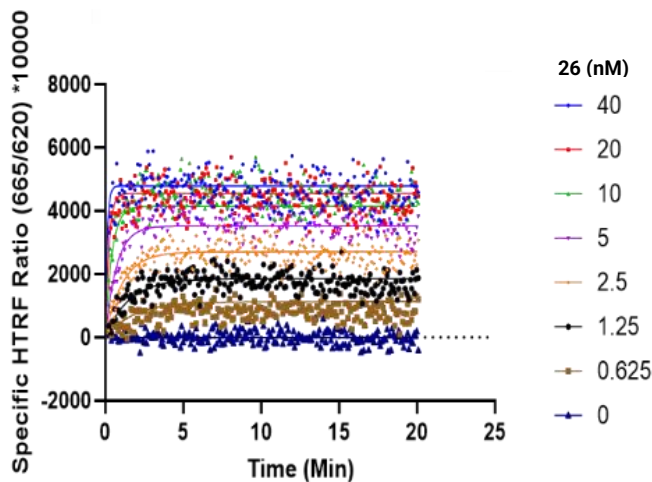
In this assay, 5-HT_{2A}R is labelled with a donor fluorophore, terbium, emitting light at a specific wavelength. When this lanthanide interacts with the BODIPY 630/650 acceptor fluorophore, FRET occurs, producing a longer lasting measurable emission that is recorded after a short time delay allowing the background fluorescence to diminish.

The binding of **25** and **26** was tested in a cell-membrane based fluorescent TR-FRET assay with human 5-HT_{2A}R expressed in CHO membranes. Fluorescent probe **26** showed saturable binding and low non-specific binding (NSB) **Graph 3.6-1**, determined by the competition of a high concentration of unlabelled ligand, sertindole (10 µM), for a single population of inactive receptor conformation binding sites forced by guanylyl-imidodiphosphate (GppNHp), a non-hydrolysable analogue of guanosine triphosphate (GTP), thereby preventing an active receptor conformation.

Design, synthesis, characterisation of 5-HT_{2A}R fluorescent probes



Graph 3.6-1: Saturation binding experiment employing endpoint analysis for derivation of 26 affinity to the human 5-HT_{2A}R expressed in CHO-cell membranes (4 µg per well) were incubated for 30 min with gentle agitation, with increasing concentrations of 26. Assay was performed in the presence of GppNHp (0.1mM) with non-specific binding levels determined by the inclusion of sertindole (10 µM). Data presented is a single representative from *n*=3 performed in singlet.



Graph 3.6-2: Saturation time course binding experiment employing kinetic analysis for derivation of 26 affinity to the human 5-HT_{2A}R expressed in CHO-cell membranes (4 µg per well) were incubated for 30 min with gentle agitation with increasing concentrations of 26. Assay was performed in the presence of GppNHp (0.1mM) with non-specific binding levels determined by the inclusion of sertindole (10 µM). Data presented is a single representative from *n*=3 performed in singlet.

Design, synthesis, characterisation of 5-HT_{2A}R fluorescent probes

Compound	Saturation end point	Kinetic rate parameters from global fit concentration range		
	K_d (nM)	K_d (nM)	K_{on} (M ⁻¹ min ⁻¹)	K_{off} (min ⁻¹)
25	ND	ND	ND	ND
26	1.74 ± 0.46	2.16 ± 0.22	1.96 ± 0.13 × 10 ⁸	0.42 ± 0.02
CA201019 ¹⁷⁷	3.98 ± 0.65	2.82 ± 0.47	4.21 ± 0.47 × 10 ⁷	0.09 ± 0.01

Table 3.6-1 Binding affinities and kinetic rate parameters of **25** and **26** in 5-HT_{2A}R membranes determined by saturation binding assays. All values represent mean ± SEM of $n=3$, not determined (ND).

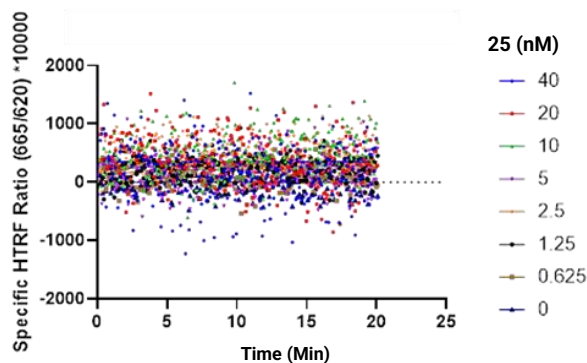
This technique allowed the real-time tracking of specific ligand binding to the receptor by observing changes in the FRET ratio, which represents the relationship between the energy emitted by the acceptor and donor fluorophores. From these studies, the saturation endpoint-derived equilibrium dissociation constant (K_d) of **26** was calculated to be (K_d 1.74 ± 0.46 nM, $n = 3$), based on three independent experiments performed in singlets **Table 3.6-1**. Furthermore, the binding kinetics of **26** were also examined by monitoring the observed association rates across six different ligand concentrations, **Graph 3.6-2**, which displayed a logarithmic saturation curve, extending up to 40 nM, (> 20x K_d).

To determine the kinetic rate parameters of **25** and **26**, **Table 3.6-1**, the association curves were globally fitted across a concentration range of 0-40 nM. Probe **26** resulted in a single best-fit estimate for the association rate constant (K_{on}), K_{on} (1.96 ± 0.13 × 10⁸ M⁻¹ min⁻¹), the dissociation rate constant (K_{off}), K_{off} (0.42 ± 0.02 min⁻¹), and a kinetically derived binding affinity (K_d), K_d (2.16 ± 0.22 nM, $n = 3$). Notably, this K_d value aligned closely with the binding affinity determined through

Design, synthesis, characterisation of 5-HT_{2A}R fluorescent probes

saturation endpoint analysis, thereby supporting the accuracy of the kinetic assessment.

Binding at the receptor was not determined (ND) for **25** as represented by **Graph 3.6-3**, which appears to be associated to the in difference in linker region length of **25** and **26**. By comparison it appears the shorter linker length of **25** is less well tolerated and appears to have an adverse impact on fluorescent probe binding.



Graph 3.6-3: Saturation time course binding experiment employing kinetic analysis for derivation of **25** affinity to the human 5-HT_{2A}R expressed in CHO-cell membranes (4 µg per well) incubated for 30 min with gentle agitation with increasing concentrations of **25**. Assay was performed in the presence of GppNHp (0.1mM) with non-specific binding levels determined by the inclusion of sertindole (10 µM). Data presented is a single representative from *n*=3 performed in singlet.

3.7 5-HT_{2A}R fluorescent probe pharmacology

discussion

The cell-membrane based fluorescent TR-FRET assay described here in has provided a means to accurately measure the binding affinity

Design, synthesis, characterisation of 5-HT_{2A}R fluorescent probes

of the novel molecular entity, **26**. This fluorescent probe successfully bound to the human 5-HT_{2A}R expressed in CHO cell membranes.

Probe **26** demonstrated an enhanced specific binding window in comparison to CA201019, as indicated by analogous cell-membrane based fluorescent TR-FRET saturation endpoint experiments. The favourable combination of a high B_{\max} value (4512) and low background (970) from minimal non-specific binding of **26** provided a large separation between the specific and non-specific binding curves. Consequently, the specific binding signal could be reliably measured above the non-specific levels across the full concentration range of the fluorescent probe. Notably, the binding affinity of **26** at the receptor determined via TR-FRET saturation endpoint experiments was greater than that reported for CA201019. demonstrated by is lower K_d value.¹⁷⁷ However, in kinetic studies, probe **26** exhibited a similar binding affinity to CA201019, but significantly different kinetic rates via TR-FRET kinetic rate experiments. Probe **26** exhibited a faster K_{on} and K_{off} indicating faster binding and dissociation in comparison, **Table 3.6-1**.

This builds on previous attempts of fluorescent probe development at the receptor¹⁷¹ and as no synthetic or structural data is available for CA201019, **26** offers an accessible alternative for researchers in need of high affinity fluorescent probe targeting the 5-HT_{2A}R.

The kinetic parameters of **26** may enhance sensitivity in a cell-based TR-FRET assay, particularly towards low unlabelled ligand

Design, synthesis, characterisation of 5-HT_{2A}R fluorescent probes

concentrations and low-affinity binding interactions. This improved sensitivity results in more accurate measurements and more precise determination of a ligands binding affinity. The use of lower probe ligand concentrations can also minimize non-specific binding and reduces background signals, simplifying the identification of specific binding events.¹⁶⁹ Lower probe and ligand concentrations also help prevent aggregation or precipitation issues during solvation which can occur with high ligand concentrations, as well as maintaining a linear response range through lower ligand concentrations improves the overall fit of the assay.²⁸² Thus, enhancing its accuracy and reliability. Moreover, the quantification of **26** kinetic rates also facilitate kinetic studies investigating the on- and off-rates of unlabelled ligands or therapeutics.¹⁷⁷

In comparison, the successful characterisation of **25** affinity and kinetic rates at the 5-HT_{2A}R may have been perturbed by the probes shorter linker region, potentially disrupting ligand binding and FRET. However, this should not deter interrogating the binding of **25** at the other 5-HT₂R subtypes.

3.8 Conclusion of pharmacological characterisation of fluorescent probes binding to the human 5-HT_{2A}R

The primary objective of this study was the development of high affinity 5-HT_{2A}R fluorescent probes as tools for assessing unlabelled ligand binding at the 5-HT_{2A}R. The fluorescent probes design strategy involved the selection of the receptor targeting moiety, linker region, and appropriate fluorophore optimized for a cell membrane-based fluorescent TR-FRET assay. This was achieved by the design, synthesis, and characterisation of **26**. Docking of **16** and **22** in the 5-HT_{2A}R could be used to rationalize the binding conformation of **26**, as the fluorophore must be in 1-10 nm proximity to the terbium labelled SNAP-tag engineered on to the receptor N-terminus of the receptor.

Pharmacological characterization of **26** resulted in good 5-HT_{2A}R binding, demonstrating a high binding affinity ($K_d = 1.74 \pm 0.46$ nM), fast kinetics, ($K_{on} 1.96 \pm 0.13 \times 10^8$ M⁻¹ min⁻¹), and ($K_{off} 0.42 \pm 0.02$ min⁻¹), good receptor saturation, and weak non-specific binding, thus affirming its suitability for advancement as a competitor ligand in fluorescence-based 5-HT_{2A}R competition binding assays.

The fluorescent probe (**26**) can be employed as molecular tool in facilitating the evaluation of binding affinity and kinetics of unlabelled ligands at the human 5-HT_{2A}R,¹⁷⁷ such as the structure-based designed

Design, synthesis, characterisation of 5-HT_{2A}R fluorescent probes

pimavanserin analogues **17a-c** and **R/S-18a-j** via cell membrane-based fluorescent TR-FRET 5-HT_{2A}R competition binding assays. Moreover, it is a new addition to the available 5-HT_{2A}R targeting fluorescent probes.

4. Synthesis and pharmacological evaluation of pimavanserin analogues

4. Synthesis and pharmacological evaluation of pimavanserin analogues

4.1 Introduction

The availability of the human 5-HT_{2A}R XRC structures discussed in **Chapter 1**, makes it possible to develop more accurate structure-based designed ligands, which could potentially enhance therapeutic efficacy. These XRC structures have facilitated the comparison of co-crystallized ligands, such as risperidone,¹⁷ zotepine,¹⁷ and lumateperone,⁶⁹ none of which bind in the TM4-TM5 HP. Furthermore, these structures facilitate *in silico* techniques such as modeling and docking on unknown ligand-receptor complexes, predicting binding poses and interactions correlated to residue point mutations within the receptor, exemplified by pimavanserin.^{17,88,93}

Pimavanserin, also discussed in **Chapter 1**, demonstrates selectivity for the 5-HT_{2A}R and 5-HT_{2C}R subtypes.¹⁴³ Consequently, it emerges as a promising scaffold for modification to target the TM4-TM5 HP.

In silico results, **Chapter 2**, indicate, the pimavanserin analogues are predicted to adopt a binding conformation like **13** within the binding pocket. These are associated with lower ΔG MM-GBSA values as compared to **13**, except for **S-18c** and **R-18i**, which are predicted to bind in an opposite orientation. These are associated to higher ΔG MM-GBSA values.

4. Synthesis and pharmacological evaluation of pimavanserin analogues

The range in ΔG of the pimavanserin analogues appears to be associated to analogues with larger and lipophilic amino alcohol moieties, which may establish more favorable interactions within the TM4-TM5 HP. Whereas analogues with smaller, polar, or charged amino alcohol amine moieties appear less favored.

Synthesis of the structure-based designed pimavanserin analogues **R/S-18a-j** will enable the assessment of SARs associated with their experimental binding affinity at the 5-HT_{2A}R, resulting from modifications to the amino alcohol moiety. This data can be further correlated with the *in silico* results obtained from modeling, docking, and simulation to evaluate their accuracy.

Fluorescent cell-based assays provide a suitable approach for experimentally assessing binding affinity. TR-FRET assays are particularly attractive due to their ability to quantitatively measure ligand-receptor binding and circumvent the use of hazardous radioactive probes.¹³⁰ Therefore fluorescent probe **26** reported in **Chapter 3** could be utilized.

Investigation into the 5-HT_{2A}R binding affinity of pimavanserin analogues with ring C modifications longer than an isobutyl moiety has remained largely unexplored. Only four analogues that extend the pimavanserin model at the ring C position through alkanol amino moieties have been previously reported.¹⁶¹ Thus, the need for a well-structured exploration of the SARs associated to the extension of the

4. Synthesis and pharmacological evaluation of pimavanserin analogues

pimavanserin scaffold via ring C, in combination with suitable cell-based binding assays, becomes evident.

4.2 Aims

The main aim of the study was twofold:

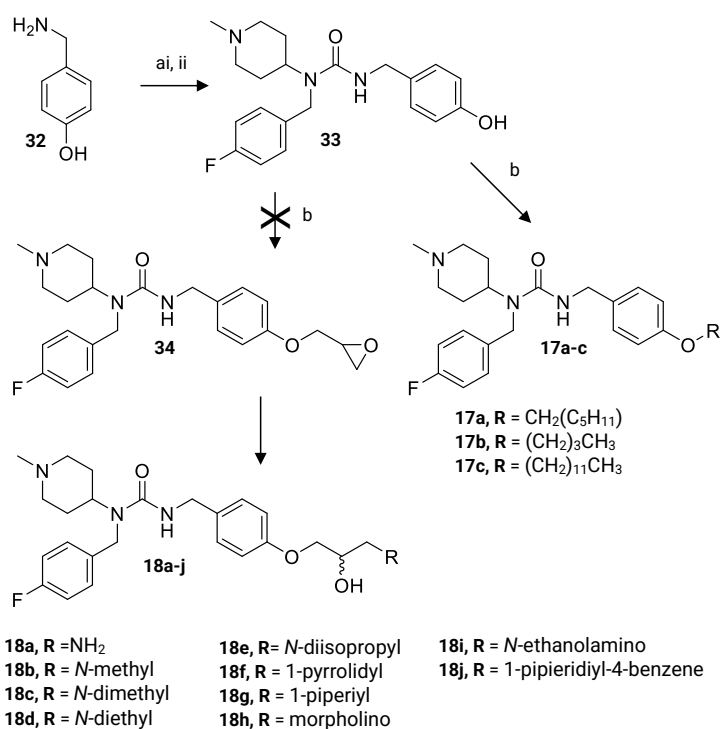
1) Synthetic route design for synthesizing the structure-based designed pimavanserin analogues **17a-c** and **R/S-18a-j**, which were evaluated via docking in **Chapter 2** as their *R/S* enantiomers. Although the *S* enantiomer was predicted to exhibit improved binding over *R* enantiomers after MM-GBSA calculations, the analogue series would be synthesized as racemic mixtures, **18a-j**. The static receptor in the initial docking method via Glide SP does not account for receptor flexibility, thus potentially compromising the accuracy of the method. Additionally, one enantiomer could be rendered inactive and offers a means to explore the SAR of racemic mixtures of **18a-j**. Furthermore, the enantioselective synthesis of enantiomers can be strategically planned or achieved through chiral column resolution using chromatography at a later stage.

2) Evaluate the binding affinity of the analogue series at the 5-HT_{2A}R using a fluorescence cell membrane-based fluorescent TR-FRET competition binding assay with employing the fluorescent probe **26** at the 5-HT_{2A}R (with a K_d of 1.74 ± 0.46) following the successful characterisation within the cell membrane-based fluorescent TR-FRET saturation assay in **Chapter 3**.

4. Synthesis and pharmacological evaluation of pimavanserin analogues

4.3 Synthesis of structure-based pimavanserin analogues

4.3.1 Pimavanserin analogues synthesis route 1



Scheme 4.3.1-1: 17a-c and 18a-j synthesis route 1.

Reagents and conditions: (a) (i) 1,1-Carbonyldiimidazole (CDI) 1 eq, dimethylformamide (DMF), (ii) *N*-(4-fluorobenzyl)-1-methylpiperidin-4-amine 1 eq - 1.1 eq, r.t., 53%; (b) bromobutane, 1.1 eq, (bromomethyl)cyclohexane 1.1 eq, bromododecane 1.1 eq, or epichlorohydrin 1.1 eq, 60% NaH/mineral oil 1.1 eq, DMF, 0°C-rt; 0-53%.

To begin the synthesis a linear synthetic pathway was designed

Scheme 4.3.1-1. Starting with 4-hydroxybenzylamine (**32**), the primary amine was reacted as the first nucleophile with 1,1-carbonyldiimidazole (CDI) to form a mono-imidazole-carboxamide intermediate *in situ*. *N*-(4-

4. Synthesis and pharmacological evaluation of pimavanserin analogues

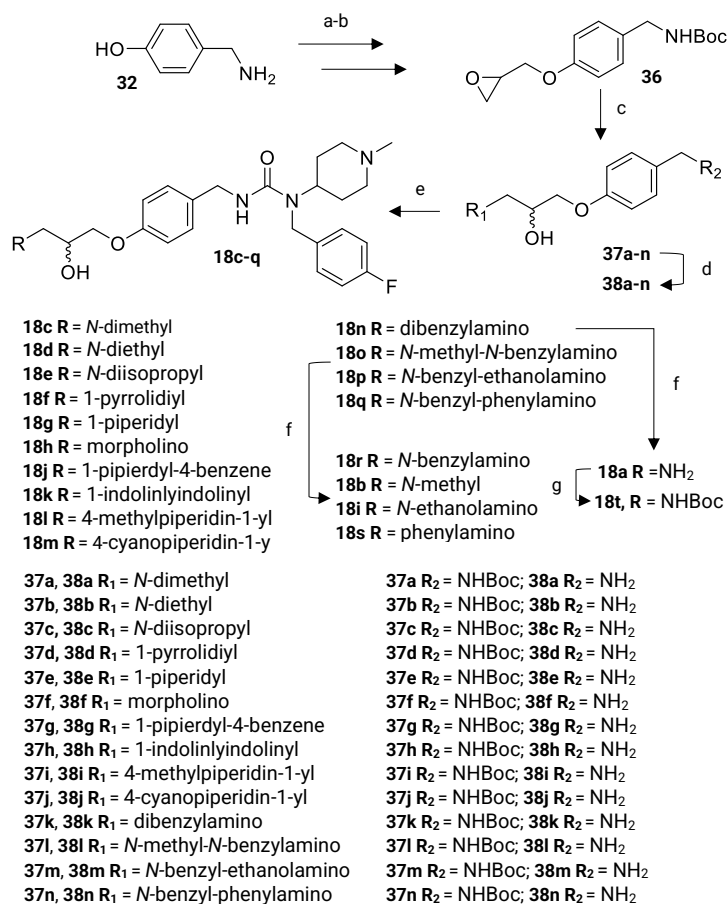
Fluorobenzyl)-1-methylpiperidin-4-amine would then be added as the second nucleophile to afford **33**, a phenol analogue of **13**. Compound (**33**) was a key intermediate featuring a phenol moiety at the ring C. This gave access to compounds **17a-c** via S_N2 halide displacement of the respective alkyl halide in moderate yields.

Attempts were then made to react **33** with epichlorohydrin under the same alkylating conditions used before to afford **34** featuring an epoxide handle. This would have had acted as second key intermediate to the pimavanserin amino alcohol analogues via ring opening of the epoxide handle with the respective the amines. However, attempts to purify and isolate **34** via normal phase and reverse phase chromatography were not successful at that time. No product or by products were recovered in collected fractions. Attempts to afford **18a-j** via this synthetic route were ceased.

4.3.2 Pimavanserin analogues synthesis route 2

The following convergent synthetic route was then adopted **Scheme 4.3.2-1**,¹⁶¹ as this synthetic pathway had been proven to work for the previously reported analogues **15a-d**.

4. Synthesis and pharmacological evaluation of pimavanserin analogues



Scheme 4.3 2-1: 18a-t synthesis route 2.

Reagents and conditions: (a) Di-*tert*-butyl-dicarbonate 2 eq, NaHCO₃ 1 eq, MeOH, H₂O, r.t, 95%; (b) 60% NaH/mineral oil 1.15 eq, epichlorohydrin 1.5 eq, DMF, 0°C-r.t; 63%; (c) HNR₁a-n 1 eq - 1.5 eq, IPA, 60°C, 21-99%; (d) 4M HCl/1,4-dioxane excess, EtOAc, r.t; 95-96% (e) (i) TEA 2 eq, CDI 1 eq, (ii) *N*-(4-fluorobenzyl)-1-methylpiperidin-4-amine 1 eq - 1.2eq, DCM, r.t, 3-46%; (f) Pd/C 5% 0.1 eq, EtOH, H₂O, AcOH, H₂, r.t 6-47%, (g) di-*tert*-butyl-dicarbonate 2 eq, NaHCO₃ 1 eq, MeOH, H₂O, r.t, 27%.

Use of this synthetic route afforded all pimavanserin analogues featuring an amino alcohol moiety with a tertiary amine, **18c-h** and **18j**. To afford the pimavanserin amino alcohol analogues **18a**, **18b**, and **18i** featuring primary and secondary amines, a second amine protection

4. Synthesis and pharmacological evaluation of pimavanserin analogues

strategy was required to avoid chemo selectivity issues during the final step when reacting the benzylic primary amine with CDI. Thus, their *N*-benzyl protected amine derivatives were synthesised first, **18n-q**.

To begin the second synthetic pathway **32** was treated with di-*tert*-butyl-dicarbonate to afford *N*-Boc protection of the primary amine moiety to afford, **33**. Alkylating conditions were then used employing 60% NaH in mineral oil in DMF to react the phenol moiety with epichlorohydrin via S_N2, thereby affording the epoxide intermediate **36** in good yield. This provided access the amino alcohols featuring tertiary amines **37a-n** via epoxide ring opening under facile conditions with the respective secondary amines.

N-Boc deprotection of amino alcohols via HCl in 1,4-dioxane was then carried out to afford the amino alcohols **38a-n** as either their HCl salts, or free amines after purification. Following neutralisation with triethylamine were the HCl salts were used or as their free amine, the deprotected amino alcohols were then reacted as the first nucleophiles with CDI to afford the mono-imidazole-carboxamide *in situ*. Commercially available *N*-(4-fluorobenzyl)-1-methylpiperidin-4-amine was then added as the second nucleophile. This afforded pimavanserin amino alcohol analogues featuring the tertiary amines, **18c-h** and **18j**, and pimavanserin amino alcohol analogues featuring a tertiary amine with *N*-benzyl protection group **18n-q**.

4. Synthesis and pharmacological evaluation of pimavanserin analogues

N-Benzyl deprotection **18n-q** successfully proceeded via H₂ in the presence of 5% Pd/C under optimised solvent conditions doped with the addition of acetic acid. The addition of acetic acid for the Pd/C-catalysed hydrogenative deprotection of the *N*-benzyl protecting group reduces the poisoning rate of Pd/C by the formation of amine salts²⁸³ to facilitate the deprotection to afford **18a**, **18b**, **18i**, **18r**, and **18s**. Overall the pimavanserin amino alcohol analogues were obtained in low to moderate yields as either their acid salt forms or free amines.

It was recognised that the epoxide **41** was a key intermediate within the synthetic route having facilitated convenient access to pimavanserin amino alcohol intermediates one step prior to forming the pimavanserin analogue. Consequentially the synthesis of **18k-m** was carried out and *N*-Boc protection of the primary amine analogue **18a** afforded **18t**, although these had not been explored *in silico*.

4.4 Pharmacological characterisation of pimavanserin analogues binding to the human 5- HT_{2A}R

The unlabelled ligand binding of **17a-c** and **18a-t** was evaluated in a cell membrane-based TR-FRET assay with human 5-HT_{2A}R expressed in CHO membranes. While compound **26** showed promising binding in fluorescent probe characterization, data could not confirm ligand binding events in the TR-FRET competition binding assay when both probe and

4. Synthesis and pharmacological evaluation of pimavanserin analogues

analogue series were used together. Overall, the structure-based analogues **17a-c** and **18a-t** demonstrated either no detectable binding or low confidence in the affinity recorded during the binding assays. This includes commercially bought **13** used in the assay. The inconsistency in the data across the three assay replicates does not provide insights into the SAR associated with amino alcohol modifications. This inconsistency may be due to an increased impact of mechanical errors from performing the assay in singlet. Therefore, conducting a competition binding assay for each ligand in multiples would be a more suitable approach.

4.5 Conclusions of pimavanserin analogues binding to the human 5-HT_{2A}R

The attempt to synthesize structure-based pimavanserin analogues **17a-c** via the proposed synthetic route 1 was achieved in moderate yields. However, attempts to synthesis pimavanserin amino alcohols **18a-j** was hindered by challenges in isolating compound **34**. Adaption of the previously reported synthetic pathway¹⁶¹ for **15a-d** led to the development of synthetic route 2, yielding **18a-j**, as well as **18k-t**, but in low to moderate yield. Thus, there is scope to optimise these reactions or explore alternative routes. For example, the *N*-benzyl deprotection step to afford the primary and secondary amino alcohol moieties. The attempt to develop a cell membrane-based fluorescent TR-FRET competition binding assay to evaluate the series at the human 5-

4. Synthesis and pharmacological evaluation of pimavanserin analogues

HT_{2A}R expressed in CHO membranes following did not result in obtaining affinity data. This prevents SAR analysis, but also prevents correlating with the results from modelling and docking in **Chapter 2**. Therefore, future work is required.

5. Future work

5.1.1 Binding affinity evaluation of the pimavanserin analogue series at the 5-HT₂ receptor subtypes

The further development of a cell membrane-based fluorescent TR-FRET competition binding assay is outstanding and required to evaluate the affinity of **17a-c** and **18a-t**, as this remains unknown. Thus, it is not possible to determine if modifying pimavanserin 4-isobutyl moiety to an amino alcohol moiety enhances binding affinity for the 5-HT_{2A}R compared **13**, or to assess the accuracy of the model and docking results in **Chapter 2**.

A further limitation arises due to the absence of binding affinity data against the 5-HT_{2B}R and 5-HT_{2C}R, hindering the determination of the analogue's selectivity profiles. Therefore, evaluation of the analogue series at the 5-HT_{2C}R and 5-HT_{2B}R via an analogous cell membrane-based fluorescent TR-FRET competition assay could be considered. However, this requires the use of a high-binding affinity 5-HT_{2B}R and 5-HT_{2C}R fluorescent probe.

The development of a BRET-based method, NanoBRET, could be explored employing **26**. NanoBRET utilizes the NanoLuc (Nluc) luciferase as the energy donor, which exhibits ~150 times greater luminescence than the Renilla luciferase used in previous BRET methods. This increased luminescence allows for more sensitive detection binding events. Additionally, Nluc's emission spectrum is slightly blue-shifted

5. Future work

compared to Renilla luciferase, providing better spectral separation from the fluorescent acceptor proteins. Nluc is also more physically stable under various conditions, improving the robustness of the assay also.²⁸⁴

NanoBRET permits independent quantification of donor and acceptor levels and unlike FRET, BRET does not require excitation illumination. This renders it better suited for *in vivo* imaging and advantageous for light-sensitive cells and avoiding issues like photobleaching.²⁸⁵ However, compared to FRET signals which can be amplified, BRET signals may be too dim without specialized equipment. For example, luminometers or plate readers equipped with BRET detection capabilities, modified microscopy systems, specialized BRET biosensors.²⁸⁴ Recently, a NanoBRET cell-based assay has successfully evaluated the affinity of BODIPY 630/650 X fluorescent probes targeting the CXCR2 chemokine receptor 2 (CXCR2) and demonstrated its use for *in vivo* imaging.²⁶³

5.1.2 Characterize fluorescent probes at 5-HT_{2c}R and 5-

HT_{2b}R

To determine binding affinity of unlabelled ligands at the 5-HT_{2b}R and 5-HT_{2c}R, high-affinity fluorescent probes becomes essential. The structural similarities among the 5-HT₂ receptor subtypes, characterized by conserved residues, binding sites, and sequence homogeneity, necessitate further investigation into probes **25** and **26** as potential fluorescent probes at the 5-HT_{2c}R and 5-HT_{2b}R. This may involve the

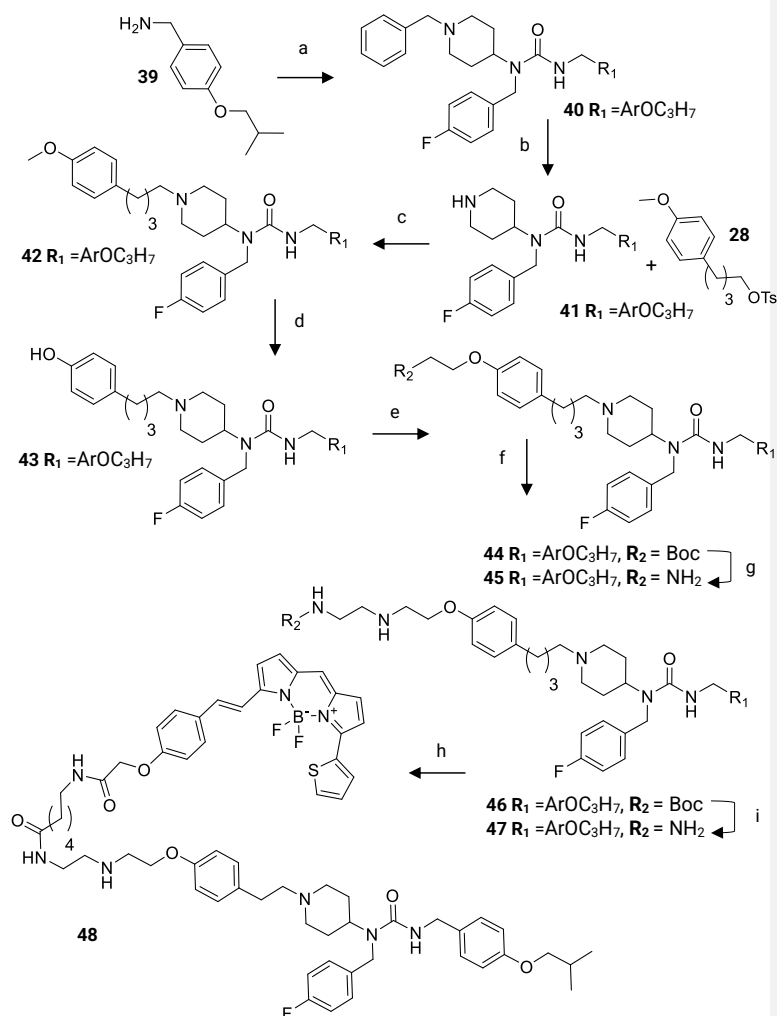
development of a cell membrane-based fluorescent TR-FRET saturation endpoint and kinetic assay to elucidate their binding affinity. Fluorescent probes successfully characterized as binding at each 5-HT₂ receptor subtype could be advanced into cell membrane-based fluorescent TR-FRET competing binding assays with the pimavanserin analogue series. This approach would allow for the assessment of ligand binding affinity across all three 5-HT₂ receptor subtypes.

5.1.3 Pimavanserin-based 5-HT_{2A}R fluorescent probe

The ongoing exploration into structural modifications of pimavanserin presents a promising avenue for the development of putative 5-HT_{2A}R subtype selective fluorescent probes. Similarities are predicted between the docked poses **13, Chapter 2** and **16, Chapter 3**. The piperidyl ring nitrogen atom of **13** provides a potential site for the linker region attachment. Thus, a strategic synthetic approach may involve integrating the linker and fluorophore selection strategies employed in the 5-HT_{2A}R fluorescent probe design **Chapter 3**. A plausible synthetic route is proposed **Scheme 5.1.3-1**.

To start, 4-isobutoxybenzylamine (**32**) can be reacted with CDI, followed by the addition of 1-benzyl-*N*-(4-fluorophenyl)piperidin-4-amine to afford an *N*-benzyl piperidinyl analogue of pimavanserin, (**40**). *N*-benzyl deprotection of the piperidine ring may proceed via H₂ and Pd/C to afford *N*-desmethylpimavanserin, (**41**), featuring a secondary amine as part of the piperidinyl ring.

5. Future work



Scheme 5.1.3-1: Synthetic route to pimavanserin-based fluorescent probe (48).

Reagents and conditions: (a) (i) 4-isobutoxybenzylamine, CDI, DMF, r.t.; (ii) 1-benzyl-*N*-(4-fluorophenyl)piperidin-4-amine, (b) Pd/C 5% EtOH, H₂O, AcOH, H₂, r.t., (c) K₂CO₃, MeCN, r.t-75°C, (d) pyridine.HCl, MW 160°C, (e) 60% NaH/mineral oil, tert-butyl-2-bromoethyl)carbamate, DMF, 0°C-r.t, (f) 4M HCl/1,4-dioxane, r.t, (g) *N*-Boc-β-alanine, COMU, DIPEA, 0°C, (h) 4M HCl/1,4-dioxane, r.t, (i) BODIPY 630/650-X-NHS ester, DIPEA, darkness, r.t.

Subsequently, this nitrogen can serve in displacement of the tosylate moiety of **28**, to afford **42**. Aryl-methoxy demethylation via pyridine.HCl and irradiation can then proceed to afford **43**, a phenol

5. Future work

intermediate suitable for further extension of the linker. Alkylation of the phenol via halide displacement of *N*-Boc ethyl bromide to afford **44** would initiate the linker with an aminoethoxy unit. *N*-Boc deprotection following via 4M HCl/1,4-dioxane would afford **45** featuring an amine handle. Coupling of *N*-Boc β -aniline to the terminal amine handle would lead to the congener **46**, increasing the linker length further. *N*-Boc deprotection of the congener leads to **47** with an amine handle. The amine handle then permits acylation with the BODIPY 630/650 X NHS fluorophore. Ultimately resulting in the pimavanserin-based fluorescent probe **48**.

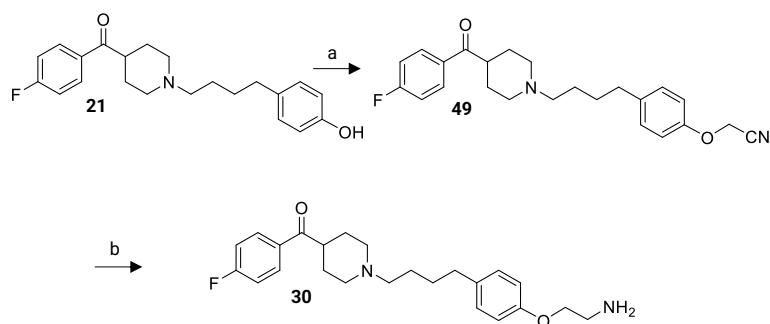
5.1.4 Optimize Synthetic Route

During the synthesis of fluorescent probes, challenges arose with low yields during the linker attachment in the S_N2 halide displacement involving *N*-Boc ethyl bromide and **21**, utilizing the alkylating conditions specified in **Scheme 3.5-1**.

To overcome this, a proposed alternative approach for linker attachment entails accessing the primary amine handle through its corresponding nitrile, **Scheme 5.1.4-1**. In this method, bromoacetonitrile (BrCH₂CN) replaces *N*-Boc ethyl bromide, with the methylene carbon serving as the site for nucleophilic attack. This strategy has shown success in similar fluorescent probe designs.¹⁷¹ Reduction of the nitrile using H₂ and Pd/C, Raney Ni, or LiAlH₄ would yield the primary amine. Moreover, the reaction could be modified to a Finkelstein reaction²⁸⁶ with

5. Future work

the addition of KI for Br to I halogen exchange, improving the ability of leaving group displacement using either choice of alkylating reagent.



Scheme 5.1.4-1: Proposed optimised synthetic route to fluorescent probe deprotected congeners via nitrile reduction.

Reagents and conditions: (a) 60% NaH/mineral oil, bromoacetonitrile, DMF, 0°C-r.t., (b) Pd/C 5% EtOH, H₂O, AcOH, H₂, r.t.

6. Experimental

6.1 Pharmacology methods

6.1.1 Materials

Tag-lite labelling medium (LABMED), SNAP-Lumi4-Tb was acquired from Hello Bio (Bristol, UK). 96-well polypropylene plates (Corning) were acquired from Fisher Scientific UK (Loughborough, UK) and 384-well Optiplate plates were sourced from Perkin Elmer (Beaconsfield, UK). 5'-Guanylyl imidodiphosphate (GppNHp) sertindole was obtained from Sigma-Aldrich (Poole, UK). Pimavanserin was sourced from Generon Ltd (Slough, UK). The host Chinese hamster ovary (CHO) K1 cell line was transiently transfected using Fugene (Fugene: DNA ratio 3:1) with the cDNA encoding a SNAP-tagged human serotonin 5-HT_{2A}R (Cis Bio, France). CHO-5HT_{2A}R cells were maintained in Dulbecco's modified Eagle's medium: Ham F12 (DMEM: F12) including 2mM glutamine (Sigma-Aldrich, Poole, UK) and supplemented with 10% fetal calf serum (Life Technologies, Paisley UK).

6.1.2 Terbium labelling of SNAP-tagged cells

***This section of work was carried out by PhD student Hannah Lockington
in the School of Life Sciences, University of Nottingham***

Cell culture medium was separated from the t175cm² flasks containing confluent adherent CHO-5HT_{2A}R 12 mL of Tag-lite labelling medium containing 100 nM of SNAP-Lumi4-Tb was added to the flask

6. Experimental

and incubated for 1 hour at 37 °C under 5% CO₂. Cells were washed 2x in PBS (GIBCO Carlsbad, CA) to remove excess SNAP-Lumi4-Tb then detached using 5 mL of GIBCO enzyme-free Hank's-based cell dissociation buffer (GIBCO, Carlsbad, CA) and collected in a vial containing 5mL of DMEM: F12 containing 2mM glutamine (Sigma-Aldrich) and supplemented with 10% fetal calf serum. Cells were pelleted by centrifugation (5 min at 1500 rpm) and the pellets were frozen to -80 °C. To prepare membranes homogenisation steps were performed at 4°C (to reduce receptor degradation). Specifically, 20 ml per t175-cm² flask of wash buffer (10 mM HEPES and 10 mM EDTA, pH 7.4) was added to the pellet, followed by homogenization via an electrical homogenizer Ultra-Turrax (Ika-Werk GmbH & Co. KG, Staufen, Germany) (position 6, 4 x 5-s bursts) and subsequently centrifuged at 48,000g at 4°C (Beckman Avanti J-251 Ultracentrifuge; Beckman Coulter, Fullerton, CA) for 30 min. The supernatant was discarded, and the pellet was re-homogenized and centrifuged as described above in wash buffer. The final pellet was suspended in ice-cold 10 mM HEPES and 0.1 mM EDTA, pH 7.4, at a concentration of 5 to 10 mg/ml. Protein concentration was determined using the bicinchoninic acid assay kit (Sigma-Aldrich), using BSA as a standard and aliquots maintained at -80°C until required. Prior to their use, the frozen membranes were thawed, and the membranes suspended in the assay buffer at a membrane concentration of 0.2mg/ml.

6.1.3 Fluorescent probe-binding assays

5-HT_{2A}R fluorescent binding experiments employed **25** and **26**. Experiments were conducted in white 384-well Optiplates, in assay binding buffer; Hanks' balanced salt solution (HBSS) containing 5 mM (4-(2-hydroxyethyl)-1-piperazineethanesulfonic acid (HEPES), 0.02% pluronic acid, 1% DMSO pH 7.4 and 100 μM GppNHp. GppNHp was included to remove the G-protein coupled population of receptors that can result in two distinct populations of binding sites in membrane preparations, since the Motulsky–Mahan model (1984)²⁸⁷ is only appropriate for ligands competing at a single site. In the case of the human 5-HT_{2A}R, nonspecific binding was determined in the presence of sertindole (10 μM).

6.1.4 Determination of fluorescent probe binding kinetics

To accurately determine **25** and **26** association rate (k_{on}) and dissociation rate (k_{off}) values, the observed rate of association (k_{obs}) was calculated using at least six different concentrations. The appropriate concentration of **25** and **26** was incubated with human 5-HT_{2A}R CHO cell membranes (4 μg per well) in assay binding buffer (final assay volume, 40μl). The degree of **25** and **26** bound to the receptor was assessed at multiple time points by HTRF detection to allow construction of association kinetic curves. The resulting data were fitted to a one phase exponential association model, equation (1) to derive an estimate of k_{on} and k_{off} from plotting tracer concentration versus observed association

(k_{obs}) as described under Data Analysis. As previously described by Sykes et al (2017).²⁸⁸

6.1.5 Unlabelled ligand-binding assays

5-HT_{2A}R unlabelled ligand binding experiments employed **17a-c** and **18a-t**. Experiments were conducted in white 384-well Optiplates, in assay binding buffer; HBSS containing 5 mM HEPES, 0.02% pluronic acid, 1% DMSO pH 7.4 and 100 μ M GppNHp, competing for the same population of binding sites against **26** (5 nM) added simultaneously. 5-HT_{2A}R, nonspecific binding was determined in the presence of sertindole (10 μ M).

6.1.6 Signal detection and data analysis

Signal detection was performed on a Pherastar FS (BMG Labtech, Offenburg, Germany) using standard HTRF settings. The terbium donor fluorophore was always excited with 3 laser flashes at a wavelength of 337 nm. A kinetic TR-FRET signal was collected at 20 seconds intervals both at 665 nm and 620 nm, when using red acceptor fluorophore. HTRF ratios were obtained by dividing the acceptor signal (665 nm) by the donor signal (620 nm) and multiplying this value by 10,000. Probe dissociation rates were analysed by displacement of the tracer with a large excess of an unlabelled ligand known to bind to the same site with similar or higher affinity. All experiments were analysed by non-regression using GraphPad Prism version 10.0.0 for Windows, GraphPad Software, Boston, Massachusetts USA, www.graphpad.com. **26**

6.Experimental

association data was analysed using nonlinear regression to fit the specific binding data to a one phase exponential association equation,

Equation: 6.1.6-A:

Equation: 6.1.6-A

$$Y = Y_{\max} [1 - \exp(-k_{\text{ob}} * X)]$$

Where X is time (min) and k_{ob} is the observed rate of association (min^{-1}). **26** followed a simple law of mass action model, with k_{ob} increasing in a logarithmic fashion as a function of fluorescent probe concentration up to a value of 40 nM. The slope of the line equates to the association rate (k_{on}), and extrapolation of the plot to $y = 0$ yields the dissociation rate (k_{off}).²⁸⁹ Competition displacement binding data were fitted to sigmoidal (variable slope) curves using a "four parameter logistic equation" **Equation: 6.1.6-B:**

Equation: 6.1.6-B

$$Y = \text{Bottom} + (\text{Top} - \text{Bottom}) / (1 + 10^{(\log EC_{50} - X) \cdot \text{Hillcoefficient}})$$

IC_{50} values obtained from the inhibition curves were converted to K_i values using the method of Cheng and Prusoff (1973).²⁹⁰

6.2 General chemistry

Chemicals and solvents (reagent and HPLC grade) were purchased from commercial suppliers used without further purification. BODIPY630/650-X-NHS was purchased from Molecular Probes (Thermo Fisher Scientific). Unless otherwise stated all reactions carried out at room temperature (r.t). All organic extracts after aqueous work-up procedures were dried over MgSO_4 or Na_2SO_4 before filtering and evaporation to dryness. Organic solvents were removed under vacuum at ≤ 40 °C (water bath temperature).

Thin layer chromatography employed precoated aluminium-backed plates (Merck Kieselgel 60 F²⁵⁴). Visualization was by examination under UV light (254 and 366 nm). General staining was carried out with ninhydrin (solution in ethanol), KMnO_4 , bromocresol green, or iodine. Column chromatography was carried out using technical grade silica gel 60 Å, 230–400 mesh particle size, 40–63 μm particle size. Preparative layer chromatography (PLC) was carried out using Analtech Uniplate silica gel GF UV254 2000 μm (200 mm x 200 mm) unless otherwise specified. Flash chromatography was performed using Biotage SP4 flash purification system and Interchim prepack PuriFlash columns, high performance spherical silica 50 μm (50SIHP) unless otherwise specified. Reverse phase (RP) flash chromatography was performed using Interchim PuriFlash 4100 system and Interchim prepack RP PuriFlash columns, high performance C18, 30 μm (30C18HP) unless otherwise specified.

6. Experimental

¹H NMR spectra were recorded on a Bruker-AV 400 at 400.13 MHz. ¹³C NMR spectra were recorded at 101.62 MHz and ¹⁹F NMR spectra were recorded at 377 MHz. Chemical shift (δ) are recorded in parts per million (ppm) with reference to the chemical shift of the deuterated solvent. Solvents used for NMR analysis were CDCl₃ (Cambridge Isotope Laboratories Inc.), ($\delta_{\text{H}} = 7.26$ ppm, $\delta_{\text{C}} = 77.16$ ppm) and DMSO-*d*₆ supplied by Sigma Aldrich ($\delta_{\text{H}} = 2.50$ ppm, $\delta_{\text{C}} = 39.52$ ppm). Coupling constants (*J*) are recorded in hertz and the significant multiplicities described by singlet (s), doublet (d), triplet (t), quadruplet (q), broad (br), multiplet (m) doublet of doublets (dd), and doublet of triplets (dt). The spectra were analysed using Mestrenova software (**Release 15.0.0 2024**).²⁹¹

LC-MS spectra were recorded on a Shimadzu UFLCXR system coupled to an Applied Biosystems API2000 and visualised at 254 nm (channel 1) and 220 nm (channel 2). LC-MS was carried out using a Phenomenex Gemini-NX C18 110A, column (50 mm × 2 mm × 3 μ m) at a flow rate 0.5 mL/min using a gradient of 10–95% solvent B in solvent A over 5 minutes (HPLC-method A, solvent A = 0.01% formic acid in H₂O, solvent B = 0.01% formic acid in MeCN). All high-resolution mass spectra (HRMS) were recorded on a Bruker microTOF mass spectrometer using MS electrospray ionization operating in positive ion mode.

Analytical RP-HPLC was performed using Shimadzu Nexera XR HPLC system and monitored using a Shimadzu SPD-M40 photodiode array detector at wavelengths 220 and 254 nm. Spectra were analysed

6. Experimental

using LabSolutions software. Phenomenex Luna C8 100 Å column (150 mm × 4.6 mm × 5 µm) at a flow rate of 1.0 mL/min. Final products were one single peak and >96% pure. The retention time of the final product is reported using a gradient of 10–100% solvent B in solvent A over 30 minutes (HPLC-method B, solvent A = 0.01% formic acid in H₂O, solvent B = 0.01% formic acid in MeCN), or gradient of 5–100% solvent B in solvent A over 30 minutes (HPLC-method C, solvent A = 0.01% formic acid in H₂O, solvent B = 0.01% formic acid in MeCN).

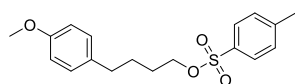
Preparative (prep) RP-HPLC was performed using Shimadzu Nexera preparative HPLC system and monitored using a Shimadzu SPD-40V at wavelengths 220 and 254 nm. Spectra were analysed using Lab Solutions software. Phenomenex Gemini NX-C18 110 Å column (250 mm × 21.2 mm × 5 µm) at a flow rate of 20.0 mL/min. Final products were automatically collected as one single peak using either, a gradient of 5–100% solvent B in solvent A over 25 minutes (HPLC-method D, solvent A = 0.01% formic acid in H₂O, solvent B = 0.01% formic acid in MeCN), a gradient of 10–100% solvent B in solvent A over 25 minutes (HPLC-method E, solvent A = 0.01% formic acid in H₂O, solvent B = 0.01% formic acid in MeCN), a gradient of 30–70% solvent B in solvent A over 25 minutes (HPLC-method F, solvent A = 0.01% formic acid in H₂O, solvent B = 0.01% formic acid in MeCN), or a gradient of 30–100% solvent B in solvent A over 25 minutes (HPLC-method G, solvent A = 0.06% TFA in H₂O, solvent B = 0.06% trifluoroacetic acid (TFA) in MeCN).

Fluorescent probes **25**, **26** and pimavanserin analogues **17a-c** and **18a-t** were synthesised at a purity > 95%.

6.3 Fluorescent probe synthesis methods

4-(4-Methoxyphenyl)butyl 4-methylbenzenesulfonate (**28**)

4-(4-Methoxyphenyl)butan-1-ol (**27**) (0.500 g, 2.774 mmol) and triethylamine (0.840 g, 1.15 mL, 8.301 mmol, 3 eq) were dissolved in DCM (10 mL) under an atmosphere of N₂. Next, *N,N*-dimethylaminopyridine (4-DMAP) (0.067 g, 0.558 mmol, 0.2 eq) was added, and the reaction mixture cooled to 0°C. *p*-Tosyl chloride (0.581 g, 3.047 mmol, 1.1 eq) was then added. The reaction progress was monitored by TLC (eluent EtOAc:cyclohexane, 2:8) until starting material had been consumed, and a ppt was noted to form as the reaction progressed. A saturated solution of NH₄Cl_(aq) (50 mL) was then added, resulting in a clear solution. The mixture was extracted with EtOAc (3 x 20 mL), and the organic layer was dried over Na₂SO₄, suction filtered, concentrated under vacuum, and purified by flash column chromatography (eluent EtOAc:cyclohexane 0-30%) to obtain the title compound as a clear colourless oil (0.866 g, 96%).



¹H NMR (CDCl₃) δ_H 7.78 (d, *J* = 8.7 Hz, 2H, tosyl Ar ring 2-H, 6-H), 7.33 (s, 2H, tosylate Ar ring 3-H, 5-H), 7.02 (d, *J* = 8.1 Hz, 2H, methoxy ring 2-H, 6-H), 6.80 (d, *J* = 7.8 Hz, 2H, methoxy ring 3-H, 5-H), 4.03 (t, *J* = 1.1 Hz, 2H, SO₂CH₂), 3.78 (s, 3H, methoxy ring 4-COCH₃), 2.50 (t, *J* = 7.1 Hz, 2H, methoxy ring 1-

6. Experimental

CCH₂), 2.44 (s, 3H, tosyl Ar ring 4-CCH₃), 1.63 (m, 4H, methoxy ring 1-CCH₂CH₂CH₂).

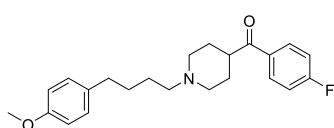
¹³C NMR (CDCl₃) δ_c 157.8 (methoxy ring 4-C), 144.6 (tosyl Ar ring 4-C), 133.6 (tosyl Ar ring 1-C), 133.2 (methoxy ring 1-C), 129.8 (methoxy ring 2-C, 6-C), 129.2 (tosyl Ar ring 2-C, 6-C), 127.8 (tosyl Ar ring -C, 5-C), 113.7, (methoxy ring 3-C, 5-C), 70.45 (CH₂SO₂), 55.2 (methoxy ring 4-COCH₃), 34.1 (methoxy ring 1-CCH₂), 28.2 (methoxy ring 1-CCH₂CH₂), 27.3 (tosyl Ar ring 4-CCH₃), 21.6 (methoxy ring 1-CCH₂CH₂CH₂).

((4-Fluorophenyl)(1-(4-(4-methoxyphenyl)butyl)piperidin-4-yl) methanone) (29)

4-(4-Methoxyphenyl)butyl-4-methylbenzenesulfonate (**28**) (0.374 g, 1.119 mmol) was dissolved in MeCN (5 mL), and 4-fluorobenzoylpiperidine.HCl (0.218 g, 0.897 mmol, 0.9 eq) added. Next, K₂CO₃ (0.496 g, 3.589 mmol, 4 eq) was added and the reaction mixture was warmed to 70°C with stirring. Upon completion, as indicated by TLC (eluent MeOH[1M NH₃]:DCM, 12:82) H₂O was then added to the reaction mixture, and volatiles removed under vacuum. The remaining aqueous solution was extracted with EtOAc (3 x 20 mL). The organic layer was then dried over Na₂SO₄, suction filtered, concentrated under vacuum, and purified using flash chromatography (eluent MeOH[1M NH₃]:DCM, 0-1%) to give the title compound as a clear colourless oil (0.241 g, 72%).

LC-MS m/z calculated for C₂₃H₂₉FNO₂ [M+H]⁺: 370.2, found: 370.00, t_R = 2.32 mins (HPLC-method A).

6. Experimental



¹H NMR (CDCl₃) δ_H 7.96 (dd, *J* = 8.8, 5.5 Hz, 2H, 4-fluorophenyl ring 3-H, 5-H), 7.18 – 7.05 (m, 4H, methoxy ring 3-H, 5-H, 4-fluorophenyl ring 2-H, 6-H), 6.82 (d, *J* = 8.6 Hz, 2H, methoxy ring 2-H, 6-H), 3.78 (s, 3H, methoxy ring 4-CCO₃H), 3.18 (ddd, *J* = 15.0, 8.9, 7.0 Hz, 1H, piperidin-4-yl ring 4-H), 2.98 (dt, *J* = 11.5, 3.6 Hz, 2H, piperidin-4-yl ring 6-H), 2.57 (t, *J* = 7.3 Hz, 2H, methoxy ring 1-CCH₂), 2.41 – 2.32 (m, 2H, piperidin-4-yl ring NCH₂), 2.11 – 1.98 (m, 2H, piperidin-4-yl 2-H), 1.88 – 1.79 (m, 4H, piperidin-4-yl 5-H, piperidin-4-yl ring 3-H), 1.71 – 1.47 (m, 4H, methoxy ring 4-CCH₂CH₂CH₂).

¹³C NMR (CDCl₃) δ_C 201.1 (C=O), 165.7 (d, ¹*J*_{CF} = 254.5 Hz, 4-fluorophenyl ring 4-C), 157.8 (methoxy ring 4-C), 134.7 (methoxy ring 1-C), 132.6 (d, ⁴*J*_{CF} = 3.1 Hz, 4-fluorophenyl ring 1-C), 130.9 (d, ³*J*_{CF} = 9.2 Hz, 4-fluorophenyl ring 2-C, 6-C), 129.3 (methoxy ring 2-C, 6-C), 115.8 (d, ²*J*_{CF} = 21.7 Hz, 4-fluorophenyl ring 3-C, 5-C), 113.8 (methoxy ring 3-C, 5-C), 58.9 (piperidin-4-yl-NCH₂), 55.3 (methoxy ring 4-OCCH₃), 53.4, (piperidin-4-yl ring 2-C, 6-C), 43.9 (piperidin-4-yl ring 4-C), 35.0 (methoxy ring 1-CCH₂), 29.8 (methoxy ring 1-CCH₂CH₂CH₂CH₂), 28.8 (piperidin-4-yl ring 3-C, 5-C), 26.7 (methoxy ring 1-CCH₂CH₂CH₂CH₂).

**((4-Fluorophenyl)(1-(4-(4-hydroxyphenyl)butyl)piperidin-4-yl)
methanone) (21)**

Pyridine. HCl demethylation method A

In a microwave vial ((4-Fluorophenyl)(1-(4-(4-methoxyphenyl)butyl)piperidin-4-yl)methanone) (**29**) (200 mg, 0.542 mmol) was powdered and mixed with pyridine HCl (440 mg, 3.780 mmol, 7 eq), flushed with N₂, and irradiated in 5-minute intervals at 160°C at 215 W. After 15 minutes LCMS showed no starting material remained. H₂O (20 ml) was then added, and the reaction mixture sonicated until crude solid residue was suspended. The aqueous suspension reaction mixture was then transferred into H₂O (100 ml) and adjusted to pH 9 using sat bicarb solution. The basic aqueous reaction mixture was then extracted with EtOAc (50 ml x 3). The organic layers were combined, dried over MgSO₄, concentrated under vacuum, and purified via column chromatography (eluent DCM, 100; and MeOH[1M NH₃]:DCM, 3.5:6.5) to afford the title compound as a yellow foam (0.126 g, 66%).

BBr₃ demethylation method B

((4-Fluorophenyl)(1-(4-(4-methoxyphenyl)butyl)piperidin-4-yl) methanone) (**29**) (55 mg, 0.149 mmol) was dissolved in anhydrous DCM (2 mL), under N₂, and chilled to -78°C. A solution of BBr₃ [1M] in DCM (0.75 mL, 0.745 mmol, 5 eq) was added over 30 seconds. After 24 hours of stirring, a brown residue formed. MeOH (1 M NH₃) in DCM (0.5 mL) was added to the reaction mixture at -78°C, resulting in a yellow solution

6.Experimental

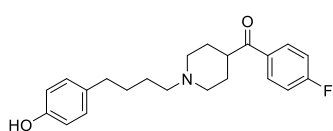
and a white precipitate. The reaction mixture was exposed to nitrogen for 5 minutes, and volatile components were removed to give a crude residue. DCM (10 mL) was added, and the reaction mixture was sonicated, and gravity filtered. MeOH[1M NH₃]:DCM,40:60 (10 ml) was added to the residue, sonicated, gravity filtered and combined with previous filtrate. Filtrate was concentrated under vacuum to give a crude residue upon which MeOH (10 mL) was added, followed by sonication, gravity filtering, concentrated under vacuum, followed by adsorption onto isolate, and purified via column chromatography (eluent MeOH [1M NH₃]:DCM, 0.1:9.9 and 0.4:9.6) to afford the title compound as a yellow residue (18 mg, 52%).

Aq 48% HBr demethylation method C

((4-Fluorophenyl)(1-(4-(4-methoxyphenyl)butyl)piperidin-4-yl) methanone) (**29**) (296 mg, 0.800 mmol) dissolved in aq.HBr 48% (5 mL, excess) and refluxed. Upon consumption of starting material determined by TLC (eluent MeOH[1M NH₃]:DCM, 3.5:6.5), N₂ was bubbled through reaction mixture for 10 mins, followed by removal of volatiles to give an orange solid. A saturated solution of NaHCO₃ (30 mL) was then added, and the mixture sonicate for 10 mins. The mixture was then extracted with EtOAc (3 x 30 mL). The organic layer was then washed with H₂O, dried over MgSO₄, concentrated under vacuum, and purified via column chromatography (eluent DCM, 100; and MeOH[1M NH₃]:DCM, 3.5:6.5) to afford the title compound as a clear yellow oil (0.190 g, 63%).

6. Experimental

LC-MS m/z calculated for $C_{22}H_{27}FNO_2$ $[M+H]^+$: 356.2, found: 356.50, t_R = 2.36 mins (HPLC-method A).



1H NMR ($CDCl_3$) δ_H 7.85 (dd, J = 8.9, 5.4 Hz, 2H, 4-fluorophenyl ring 3-H, 5-H), 7.01 (d, J = 8.6 Hz, 2H, 4-fluorophenyl ring 2-H, 6-H), 6.87 (d, J = 8.4 Hz, 2H, phenol 3-H, 5-H), 6.56 (d, J = 8.4 Hz, 2H, phenol 2-H, 6-H), 3.21 – 3.01 (m, 1H, piperidin-4-yl ring 4-H), 2.92 (d, J = 11.8 Hz, 2H, piperidin-4-yl 2-H), 2.44 (t, J = 6.8 Hz, 2H, phenol 4-CCH₂), 2.30 (t, J = 7.3 Hz, 2H, piperidin-4-yl ring NCH₂), 2.14 – 1.98 (m, 2H, piperidin-4-yl ring 6-H), 1.91 – 1.68 (m, 4H, piperidin-4-yl ring 3-H, 5-H), 1.62 – 1.32 (m, 4H, phenol 4-CCH₂CH₂CH₂).

^{13}C NMR ($CDCl_3$) δ_C 200.9 (C=O), 165.6 (d, $^1J_{CF}$ = 254.6 Hz, 4-fluorophenyl ring 4-C), 154.2 (phenol 1-C), 133.5 (phenol 4-C), 132.4 (d, $^4J_{CF}$ = 3.0 Hz, 4-fluorophenyl ring 1-C), 130.8 (d, $^3J_{CF}$ = 9.2 Hz, 4-fluorophenyl ring 2-C, 6-C), 129.3, (phenol 3-C, 5-C), 115.7 (d, $^2J_{CF}$ = 21.8 Hz, 4-fluorophenyl ring 3-C, 5-C), 115.2 (Ar ring 2-C, 6-C), 58.8 (piperidin-4-yl ring NCH₂), 53.1 (piperidin-4-yl ring 2-C, 6-C), 43.5 (piperidin-4-yl ring 4-C), 34.7 (phenol 4-CCH₂CH₂CH₂), 29.4 (phenol 4-CCH₂CH₂CH₂), 28.2 (piperidin-4-yl ring 3-C, 5-C), 26.0 (phenol 4-CCH₂CH₂CH₂).

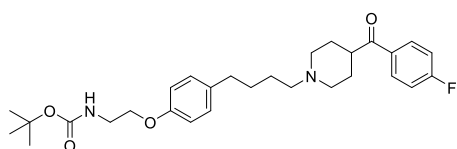
(tert-Butyl-(2-(4-(4-(4-(4-fluorobenzoyl)piperidin-1-yl)butyl)phenoxy)ethyl)carbamate) (22)

((4-Fluorophenyl)(1-(4-(4-hydroxyphenyl)butyl)piperidin-4-yl)methanone) (21) (0.255 mg, 0.718 mmol) was dissolved in DMF (3 mL), triethylamine

6. Experimental

(0.126 g, 0.180 mL, 1.245 mmol, 1.5 eq) and stirred for 10 mins at 0°C. NaH 60% in mineral oil (0.037 g, 0.910 mmol, 1.1 eq) was then added. Upon cessation of evanescence, *N*-Boc-ethylbromide (0.279 g, 1.250 mmol, 1.5 eq) was added. Upon completion as determined by LC-MS the solvent was removed under vacuum and H₂O (50 mL) added. The reaction vial was sonicated for 10 mins and then extracted with EtOAc (3 x 30 mL). The organic extracts were combined, dried over MgSO₄, suction filtered, concentrated under vacuum, and purified via column chromatography, (eluent DCM, 100; and MeOH[1M NH₃]:DCM, 2.5:7.5) to afford the title compound as a yellow residue (0.123 g, 30%)

LC-MS *m/z* calculated for C₂₉H₄₀FN₂O₄ [M+H]⁺: 499.3, found 498.80, *t_R* = 2.83 mins (HPLC-method A).



¹H NMR (CDCl₃) δ_H 7.96 (dd, *J* = 8.9, 5.4 Hz, 2H, 4-fluorophenyl ring 3-H, 5-H), 7.20 – 7.04 (m, 4H, Ar ring 2-H, 6-H), 4-fluorophenyl ring 2-H, 6-H), 6.80 (d, *J* = 8.6 Hz, 2H, Ar ring 3-H, 5-H), 5.00 (s, 1H, H_NCOCH₂CH₂O), 3.99 (t, *J* = 5.1 Hz, 2H, H_NCOCH₂CH₂O), 3.51 (d, *J* = 5.4 Hz, 2H, H_NCOCH₂CH₂O), 3.18 (p, *J* = 7.6 Hz, 1H, piperidin-4-yl ring 4-H), 2.98 (d, *J* = 11.5 Hz, 2H, piperidin-4-yl ring 2-H), 2.57 (t, *J* = 7.3 Hz, 2H, Ar ring 1-CCH₂), 2.46 – 2.29 (m, 2H, piperidin-4-yl ring NCH₂), 2.26 – 1.95 (m, 2H, piperidin-4-yl ring 6-H), 1.93 – 1.78 (m, 4H, piperidin-4-yl ring 3-H, 5-H), 1.71 – 1.50 (m, 4H, Ar ring 1-CCH₂CH₂CH₂), 1.45 (s, 9H, Boc OC(CH₃)₃).

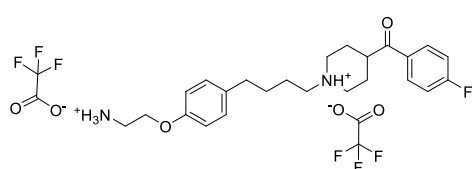
6. Experimental

¹³C NMR (CDCl₃) δ_C 201.1 (C=O), 165.7 (d, ¹J_{CF} = 254.5 Hz, 4-fluorophenyl ring 4-C), 156.8 (HNCOCH₂CH₂O), 156.0 (Ar ring 4-C), 135.1 (Ar 1-C), 132.6 (d, ⁴J_{CF} = 3.1 Hz, 4-fluorophenyl ring 1-C), 130.9 (d, ³J_{CF} = 9.2 Hz, 4-fluorophenyl ring 2-C, 6-C), 129.4 (Ar 2-C, 6-C), 115.8 (d, ²J_{CF} = 21.8 Hz, 4-fluorophenyl ring 3-C, 5-C), 114.4 (Ar ring 3-C, 5-C), 79.6 Boc C(CH₃)₃, 67.3 (HNCOCH₂CH₂O), 58.8 (piperidin-4-yl ring NCH₂), 53.4 (piperidin-4-yl ring 2-C, 6-C), 43.9 (piperidin-4-yl ring 4-C), 40.3 (HNCOCH₂CH₂O), 35.0 (Ar ring 1-CCH₂), 29.7 (Ar ring 1-CCH₂CH₂CH₂), 28.8 (piperidin-4-yl ring 3-C, 5-C), 28.5 (Boc OC(CH₃)₃), 26.6 (Ar ring 1-CCH₂CH₂CH₂)

(1-(4-(4-(2-Aminoethoxy)phenyl)butyl)piperidin-4-yl)(4-fluorophenyl) methanone. di-trifluoroacetate salt (30)

tert-Butyl-(2-(4-(4-(4-(4-fluorobenzoyl)piperidin-1-yl)butyl)phenoxy)ethyl) carbamate (23) (0.123 g, 0.250 mmol) was dissolved in 4M HCl in 1, 4 dioxane (2 mL, excess). After completion determined by LC-MS a precipitate had formed. Volatiles were removed under vacuum give an orange residue followed by purification via prep-HPLC (HPLC-method G). Collected fractions were concentrated under vacuum and lyophilised to afford the title compound as a clear residue (0.110 g, 94%)

LC-MS *m/z* calculated for C₂₄H₃₂FN₂O₂ [M+H]⁺: 400.2, found: 399.50, *t_R* = 2.13 mins (HPLC-method A).



¹H NMR (DMSO) δ_H 9.67

(s, 1H, piperidin-1-ium ring 1-H), 8.16 – 8.04 (m, 3H, 4-

6. Experimental

fluorophenyl ring 3-H, 5-H, $\text{H}_3^+\text{NCH}_2\text{CH}_2\text{O}$), 7.39 (t, $J = 8.8$ Hz, 2H, 4-fluorophenyl ring 2-H, 6-H), 7.15 (d, $J = 8.6$ Hz, 2H, Ar ring 2-H, 6-H), 6.90 (d, $J = 8.6$ Hz, 2H, Ar ring 3-H, 5-H), 4.13 (t, $J = 5.2$ Hz, 2H, $\text{H}_3^+\text{NCH}_2\text{CH}_2\text{O}$), 3.79 – 3.64 (m, 1H, piperdin-1-ium ring 4-H), 3.55 (d, $J = 12.1$ Hz, 2H, piperdin-1-ium ring 2-H), 3.21 (q, $J = 5.4$ Hz, 2H, piperdin-1-ium ring NH^+CH_2), 3.14 – 2.98 (m, 4H piperdin-1-ium ring 6-H), 2.56 (t, $J = 7.3$ Hz, 2H, Ar ring 1- CCH_2), 2.00 (d, $J = 14.1$ Hz, 2H, piperdin-1-ium ring 3-H), 1.87 – 1.76 (m, 2H, piperdin-1-ium ring 5-H), 1.78 – 1.51 (m, 4H, Ar ring 1- $\text{CCH}_2\text{CH}_2\text{CH}_2$).

^{13}C NMR (DMSO) δ_c 200.0 (C=O), 165.6 (d, $^1J_{\text{CF}} = 252.3$ Hz, 4-fluorophenyl ring 4-C), 158.8 (q, $^1J_{\text{CF}} = 33.3$ Hz, F_3COOH), 156.5 (Ar ring 4-C), 134.6 (Ar ring 1-C), 132.2 (d, $^4J_{\text{CF}} = 2.7$ Hz, 4-fluorophenyl ring 1-C), 131.8 (d, $^3J_{\text{CF}} = 9.5$ Hz, 4-fluorophenyl ring 2-C, 6-C), 129.7 (Ar ring 2-C, 6-C), 116.4 (d, $^2J_{\text{CF}} = 21.8$ Hz, 4-fluorophenyl ring 3-C, 5-C), 115.0 (Ar ring 3-C, 5-C), 64.7 ($\text{H}_3^+\text{NCH}_2\text{CH}_2\text{O}$), 56.3 (piperdin-1-ium ring NH^+CH_2), 51.5 (piperdin-1-ium ring 2-C, 6-C), 49.1 (piperdin-1-ium ring 4-H), 38.8 ($\text{H}_3^+\text{NCH}_2\text{CH}_2\text{O}$), 34.0 (Ar ring 1- CCH_2), 28.5 (Ar ring 1- $\text{CCH}_2\text{CH}_2\text{CH}_2$), 26.2 (piperdin-1-ium ring 3-C, 5-C), 23.2 (Ar ring 1- $\text{CCH}_2\text{CH}_2\text{CH}_2$).

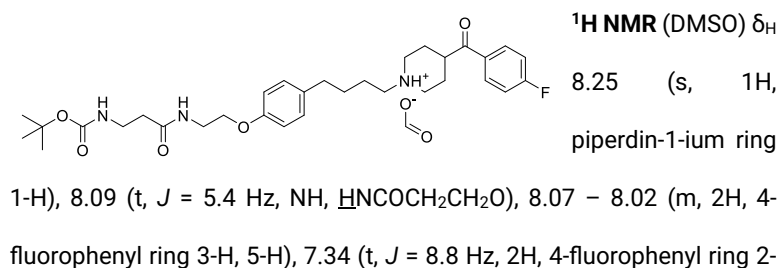
^{19}F NMR (377 MHz, DMSO) δ_f -74.1 (F_3COOH), -105.5 (4-fluorophenyl ring 4-F).

6. Experimental

tert-Butyl-(3-((2-(4-(4-(4-(4-fluorobenzoyl)piperidin-1-yl)butyl)phenoxy)ethyl)amino)-3-oxopropyl)carbamate. formate salt (31)

(1-(4-(4-(2-Aminoethoxy)phenyl)butyl)piperidin-4-yl)(4-fluorophenyl) methanone. di-trifluoroacetate salt (**30**) (0.092 g, 0.195 mmol) was dissolved in DMF (3 mL) under N₂ and transferred into a stirring solution of *N*-Boc-β-alanine (0.042 g, 0.222 mmol, 1.1 eq) and COMU® (0.094 g, 0.291 mmol, 1.1 eq) dissolved in DMF (2 mL). The reaction mixture was chilled to 0°C. DIPEA (0.094 g, mmol, 4 eq) was then added. The reaction mixture turned yellow. Upon completion as determined by LC-MS EtOAc (5 mL) was added and portioned against cold H₂O (100 mL). The aqueous was extracted further with EtOAc (3 x 10 mL). Organic extracts were combined, dried over MgSO₄, suction filtered, and concentrated under vacuum to give an orange residue, purified via column chromatography (eluent DCM, 100; and MeOH[1M NH₃]:DCM, 0.1:9.9, 0.2:9.8), and prep-HPLC (HPLC-method E) to afford the title compound as a clear residue (0.020 g, 17%).

LC-MS *m/z* calculated for C₃₂H₄₅FN₃O₅ [M+H]⁺: 570.3, found: 570.10, *t_R* = 2.71 mins (HPLC-method A).



6. Experimental

H, 6-H), 7.09 (d, $J = 8.8$ Hz, 2H, Ar ring 2-H, 6-H), 6.84 (d, $J = 8.6$ Hz, 2H, Ar ring 3-H, 5-H), 6.72 (t, 1H, HNBoc), 3.93 (t, $J = 4.0$ Hz, 2H, H $\text{NCOCH}_2\text{CH}_2\text{O}$), 3.47 – 3.32 (m, 3H, H $\text{NCOCH}_2\text{CH}_2\text{O}$, piperdin-1-ium ring 4-H), 3.14 – 3.07 (q, $J = 6.44$, 2H, HNBoc $\text{CH}_2\text{CH}_2\text{HNCO}$), 2.86 (d, $J = 11.2$ Hz, 2H, piperdin-1-ium ring 2-H), 2.52 (d, $J = 5.8$ Hz, 2H, piperdin-1-ium ring NH^+CH_2), 2.26 (m, 4H, Ar ring 1-C CH_2 , HNBoc $\text{CH}_2\text{CH}_2\text{HNCO}$), 2.11 – 1.96 (t, $J = 10.33$, 2H, piperdin-1-ium ring 6-H), 1.73 (d, $J = 12.9$ Hz, 2H, piperdin-1-ium ring 3-H), 1.68 – 1.47 (m, 4H, piperdin-1-ium ring 6-H, 5-H, Ar ring 1-C $\text{CH}_2\text{CH}_2\text{CH}_2$), 1.36 (m, 11H, Ar ring 1-C $\text{CH}_2\text{CH}_2\text{CH}_2$, Boc $\text{OC}(\text{CH}_3)_3$).

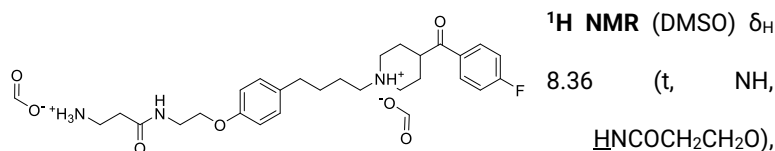
^{13}C NMR (DMSO) δ_c 170.6 (HOOCH), 157.9 (H $\text{NCOOC}(\text{CH}_3)$), 157.6 (Ar ring 1-C), 138.9 (Ar ring 4-C), 134.5 (d, $^3J_{\text{CF}} = 10.0$, 4-fluorophenyl ring 2-C, 6-C), 131.4 (d, $^4J_{\text{CF}} = 2.9$ Hz, 4-fluorophenyl ring 1-C), 129.2 (Ar ring 2-C, 6-C), 115.9 (d, $^2J_{\text{CF}} = 21.9$ Hz, 4-fluorophenyl ring 3-C, 5-C), 114.3 (Ar ring 3-C, 5-C), 70.3 H $\text{NCOCH}_2\text{CH}_2\text{O}$, 58.6 (piperdin-1-ium ring NH^+CH_2), 51.0 (piperdin-1-ium ring 3-C, 5-C), 42.0 (piperdin-1-ium ring 4-H), 38.5 (H $\text{NCOCH}_2\text{CH}_2\text{O}$), 36.9 (HNBoc $\text{CH}_2\text{CH}_2\text{HNCO}$), 35.2 (HNBoc $\text{CH}_2\text{CH}_2\text{HNCO}$), 33.5 (HNBoc $\text{CH}_2\text{CH}_2\text{HNCO}$), 31.9 (Ar ring 1-C $\text{CH}_2\text{CH}_2\text{CH}_2$), 28.2 (Boc $\text{OC}(\text{CH}_3)_3$), 28.0 (piperdin-1-ium ring 3-C, 5-C), 25.8 (Ar ring 1-C $\text{CH}_2\text{CH}_2\text{CH}_2$, Ar ring 1-C $\text{CH}_2\text{CH}_2\text{CH}_2$). Missing: (4-fluorophenyl ring 4-C).

6. Experimental

3-Amino-N-(2-(4-(4-(4-(4-fluorobenzoyl)piperidin-1-yl)butyl)phenoxy)ethyl)propenamide. di-formate salt (32)

tert-Butyl-(3-((2-(4-(4-(4-(4-fluorobenzoyl)piperidin-1-yl)butyl)phenoxy)ethyl)amino)-3-oxopropyl)carbamate. formate salt (31) (0.020 g, 0.035 mmol) was dissolved in 4M HCl in 1,4-dioxane (2 mL, excess). Upon completion determined by LC-MS volatiles were removed to give a crude residue, followed by purification via column chromatography (eluent DCM, 100; and MeOH[1M NH₃]:DCM 0.3:0.7) followed by prep-HPLC (HPLC-method E). Collected fractions were concentrated under vacuum and lyophilised to afford the title compound as a clear residue (0.010 g, 94%).

LC-MS *m/z* calculated for C₂₇H₃₇FN₃O₃ [M+H]⁺: 470.3, found: 470.40, *t_R* = 2.24 mins (HPLC-method A).



8.36 (t, NH, HNCOCH₂CH₂O),
8.24 (s, 2H, piperidin-1-ium ring 1-H, H₃⁺NCH₂CH₂NHCO), 8.05 (dd, *J* = 8.7, 5.7 Hz, 2H, 4-fluorophenyl ring 3-H, 5-H), 7.36 (t, *J* = 8.8 Hz, 2H, 4-fluorophenyl ring 2-H, 6-H), 7.11 (d, *J* = 8.5 Hz, 2H, Ar ring 2-H, 6-H), 6.85 (d, *J* = 8.5 Hz, 2H, Ar ring 3-H, 5-H), 3.97 (t, *J* = 5.6 Hz, 2H, HNCOCH₂CH₂O), 3.45 (dt, *J* = 5.5, 5.5 Hz, 2H, HNCOCH₂CH₂O), 3.38 (tt, *J* = 11.4, 4.0 Hz, 1H, piperidin-1-ium ring 4-H), 2.99 (t, *J* = 6.8 Hz, 2H, H₃⁺NCH₂CH₂OCNH), 2.89 (d, *J* = 11.4 Hz, 2H, piperidin-1-ium ring 2-C), 2.49 – 2.42 (m, 4H, piperidin-1-ium ring NH⁺CH₂, H₃⁺NCH₂CH₂OCNH), 2.34 (t, *J* = 7.3 Hz, 2H,

6. Experimental

Ar ring 1-CCH₂), 2.19 – 2.02 (m, 2H, piperdin-1-ium ring 6-C), 1.75 (d, $J = 14.9$ Hz, 2H, piperdin-1-ium ring 3-C), 1.69 – 1.50 (m, 4H, Ar ring 1-CCH₂CH₂CH₂, piperdin-1-ium ring 5-C), 1.47 – 1.31 (m, 2H, Ar ring 1-CCH₂CH₂CH₂).

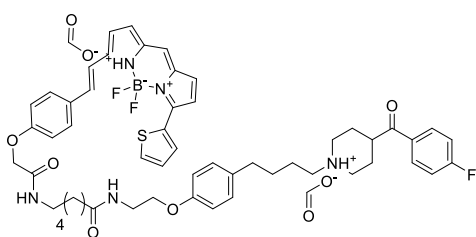
¹³C NMR (DMSO) δ_c : 201.1 (C=O), 169.7 (HNCOCH₂CH₂O), 164.9 (d, $^1J_{CF} = 251.4$ Hz, 4-fluorophenyl ring 4-C), 164.0 (HCOOH), 156.4 (Ar ring 4-C), 134.3 (Ar ring 1-C), 132.3 (d, $^4J_{CF} = 2.90$ Hz, 4-fluorophenyl ring 1-C), 129, 131.1 (d, $^3J_{CF} = 9.5$ Hz, 4-fluorophenyl ring 2-C, 6-C), 129.2 (Ar ring 2-C, 6-C), 115.8 (d, $^2J_{CF} = 21.7$ Hz, 4-fluorophenyl ring 3-C, 5-C), 114.2 Ar ring 3-C, 5-C), 66.1 (HNCOCH₂CH₂O), 57.7 (piperdin-1-ium ring NH⁺CH₂), 52.4 (piperdin-1-ium ring 2-C, 6-C), 42.5 (piperdin-1-ium ring 4-C), 38.3 (HNCOCH₂CH₂O), 35.3 (H₃⁺NCH₂CH₂), 34.0 (H₃⁺NCH₂CH₂), 32.2 (Ar 1-CCH₂CH₂CH₂), 29.0 (Ar CH₂CH₂CH₂), 27.4 (piperdin-1-ium ring 3-C, 5-C), 25.7 (Ar ring 1-CCH₂CH₂CH₂). Missing: (4-fluorophenyl ring 4-C).

6. Experimental

***E*-6-(2-(4-(2-(5,5-difluoro-7-(thiophen-2-yl)-5H-5 λ^4 ,6 λ^4 -dipyrrolo [1,2-*c*:2',1'-*f*][1,3,2]diazaborinin-3-yl)vinyl)phenoxy) acetamido)-*N*-(2-(4-(4-(4-(4-fluorobenzoyl)piperidin-1-yl)butyl)phenoxy)ethyl) hexanamide. di-formate salt (25)**

(1-(4-(4-(2-Aminoethoxy)phenyl)butyl)piperidin-4-yl)(4-fluorophenyl) methanone. di-trifluoroacetate salt (**30**) (9.000x10⁻⁴ g, 1.438x10⁻³ mmol) was dissolved in DMF (1 mL) and DIPEA (4.0x10⁻⁴ mL, 3.200x10⁻³ mmol, 2.1 eq) which was then combined with BODIPY 630/650 X NHS (9.000x10⁻⁴ g, 1.3636x10⁻³ mmol, 1 eq), covered to darkness and stored at r.t. Upon completion determined by LC-MS the solvent was removed under vacuum to give blue crude residue which was then purified prep-HPLC (HPLC-method E). Collected fractions were concentrated under vacuum and lyophilization, to afford the title compound as a clear residue (8.000x10⁻⁴ g, 70%).

HRMS *m/z* (ESI-TOF+) calculated for C₅₃H₅₈BF₃N₅O₅S: 943.4200, found: 944.4242 [M+H]⁺

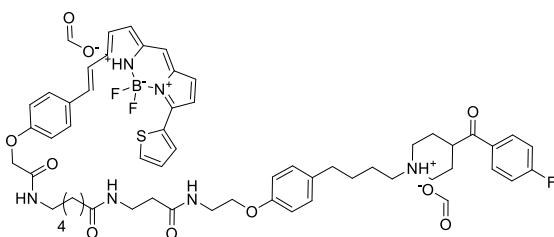


6. Experimental

(E)-6-(2-(4-(2-(5,5-difluoro-7-(thiophen-2-yl)-5H-5 λ^4 ,6 λ^4 -dipyrrolo[1,2-c:2',1'-f][1,3,2]diazaborinin-3-yl) vinyl)phenoxy)acetamido)-N-(3-((2-(4-(4-(4-(4-fluorobenzoyl)piperidin-1-yl)butyl)phenoxy)ethyl)amino)-3-oxopropyl)hexanamide. di-formate salt (26)

3-Amino-N-(2-(4-(4-(4-(4-fluorobenzoyl)piperidin-1-yl)butyl)phenoxy)ethyl)propenamide. di-formate salt (32) (8.000×10^{-4} g, 1.279×10^{-3} mmol) was dissolved in DMF (1 mL) and DIPEA (2.000×10^{-4} mL, 1.279×10^{-3} mmol, 1 eq) which was then combined with BODIPY 630/650 X NHS (8.000×10^{-4} g, 1.212×10^{-3} mmol, 0.95 eq). Covered to darkness and stored at r.t. Upon completion determined by LC-MS the solvent was removed under vacuum to give blue crude residue which was then purified prep-HPLC (HPLC-method E). Collected fractions were concentrated under vacuum and lyophilised to afford the title compound as a clear residue (1.000×10^{-3} g, 79%).

HRMS m/z (ESI-TOF+) calculated for $C_{56}H_{63}BF_3N_6O_6S$: 1014.46, found: 1015.4600 [M+H]⁺

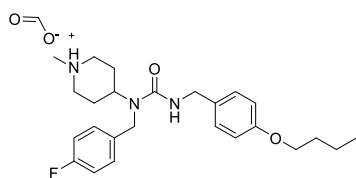


6.4 Pimavanserin analogues synthesis methods

4-(3-(4-Butoxybenzyl)-1-(4-fluorobenzyl)ureido)-1-methylpiperidin-1-ium (17a)

1-(4-Fluorobenzyl)-3-(4-hydroxybenzyl)-1-(1-methylpiperidin-4-yl)urea (**33**) (0.100 g, 0.270 mmol) was dissolved in anhydrous DMF (10 mL) under N₂, stirred, and cooled to 0°C. NaH 60% in mineral oil (0.041 g, 0.297 mmol, 1.1 eq) was added in one portion and stirred until effervescence ceased. The reaction mixture turned yellow. Bromobutane (32 µl, 0.297 mmol, 1.1 eq) was added dropwise over 1 minute and the reaction was allowed to come up to room temperature. Upon completion as determined by LCMS (HPLC-method A) the solvent was removed under vacuum and crude residue partitioned between H₂O (50 mL) and EtOAc (30 mL). The aqueous was extracted further with EtOAc (30 mL x 2), combined, dried over MgSO₄, suction filtered, concentrated under vacuum, purified via prep HPLC (HPLC-method E) and lyophilised to afford the title compound as clear colourless residue (50 mg, 43%).

HRMS *m/z* (ESI-TOF+) calculated for C₂₅H₃₅FN₃O₂ [M+H]⁺: 428.26, found: 428.2726 [M+H]⁺



¹H NMR (DMSO) δ_H 8.23 (s, 1H, piperidin-1-ium ring NH⁺), 7.24 (dd, *J* = 8.4, 5.6 Hz, 2H, 4-fluorophenyl ring 3-H, 5-H), 7.16 – 7.06 (m, 4H, 4-fluorophenyl ring 3-H, 5-H, phenol ring 3-H, 5-H), 6.88 (t, *J* = 5.7 Hz, 1H,

6. Experimental

NHCH₂), 6.83 (d, *J* = 8.6 Hz, 2H, phenol ring 2-H, 6-H), 4.41 (s, 2H, 4-fluorophenyl ring 4-CCH₂), 4.18 (d, *J* = 5.6 Hz, 2H, NHCH₂), 4.01 – 3.88 (m, 3H, piperdin-1-ium ring 4-CH, Ar ring 4-COCH₂CH₂CH₂CH₃), 2.81 (d, *J* = 11.2 Hz, 2H, piperdin-1-ium ring 2-H), 2.19 (s, 3H, piperdin-1-ium ring N1-CH₃), 2.11 – 2.01 (m, 2H, piperdin-1-ium ring 6-H), 1.73 – 1.54 (m, 4H, piperdin-1-ium ring 3-H, Ar ring 4-COCH₂CH₂CH₂CH₃), 1.50 – 1.35 (m, 4H, piperdin-1-ium ring 5-H, Ar ring 4-COCH₂CH₂CH₂CH₃), 0.92 (t, *J* = 7.4 Hz, 3H, Ar ring 4-COCH₂CH₂CH₂CH₃).

¹³C NMR (DMSO) δ_c 164.2 (HCOOH), 161.1 (d, ¹J_{CF} = 241.6 Hz, 4-fluorophenyl ring 4-C), 157.7 (C=O), 157.54 (butoxybenzyl ring 1-C), 137.2 (d, ⁴J_{CF} = 3.0 Hz, 4-fluorophenyl ring 1-C), 133.2 (butoxybenzyl ring 4-C), 128.5 (d, ³J_{CF} = 8.0 Hz, 4-fluorophenyl ring 2-C, 6-C), 128.3 (butoxybenzyl ring 2-C, 6-C), 115.0 (d, ²J_{CF} = 21.2 Hz, 4-fluorophenyl ring 3-C, 5-C), 114.2 (butoxy aryl 3-H, 5-H), 67.3 (Ar ring 1-CCH₂CH₂CH₂CH₃), 54.7 (piperdin-1-ium 2-C, 6-C), 52.1 (piperdin-1-ium ring 4-C), 45.3 (piperdin-1-ium ring 6-C), 44.2 (4-fluorophenyl ring 4-CH₂), 43.3 (Ar ring 1-CCH₂), 31.0 (Ar ring 1-CCH₂CH₂CH₂CH₃), 30.0 (piperdin-1-ium ring 3-C, 5-C), 19.0 (Ar ring 1-CCH₂CH₂CH₂CH₃), 14.0 (Ar ring 1-CCH₂CH₂CH₂CH₃).

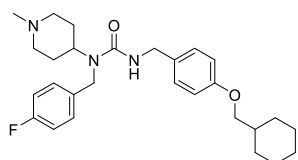
3-(4-(Cyclohexylmethoxy)benzyl)-1-(4-fluorobenzyl)-1-(1-methyl piperidin-4-yl)urea (17b)

1-(4-Fluorobenzyl)-3-(4-hydroxybenzyl)-1-(1-methylpiperidin-4-yl)urea (33) (0.100 g, 0.270 mmol) was dissolved in anhydrous DMF (10 mL), under N₂, stirred, and cooled to 0°C. NaH 60% in mineral oil (0.041 g,

6. Experimental

0.297 mmol, 1.1 eq) was added in one portion and stirred until effervescence ceased. The reaction mixture turned yellow. Bromomethylcyclohexane (42 μ l, 0.297 mmol, 1.1 eq) was added dropwise over 1 minute and the reaction was allowed to come up to room temperature. Upon completion as determined by LCMS (HPLC-method A) the solvent was removed under vacuum and crude residue partitioned between H₂O (50 mL) and EtOAc (30 mL). The aqueous was extracted further with EtOAc (30 mL x 2), combined, dried over MgSO₄, suction filtered, concentrated under vacuum, purified via prep HPLC (HPLC-method E), and lyophilised to afford the title compound as the yellow residue (40 mg, 53%).

HRMS m/z (ESI-TOF+) calculated for C₂₈H₃₈FN₃O₂ [M+H]⁺: 468.29, found: 468.3019 [M+H]⁺



¹H NMR (CDCl₃) δ _H 7.17 (dt, J = 8.4, 5.2 Hz, 2H, 4-fluorophenyl ring 3-H, 5-H), 7.04 – 6.93 (m, 4H, 4-fluorophenyl ring 2-H, 6-H, cyclohexylmethoxybenzyl ring 3-H, 5-H), 6.77 (d, J = 8.5 Hz, 2H, cyclohexylmethoxybenzyl ring 2-H, 6-H), 4.46 (t, J = 5.5 Hz, 1H, urea NH), 4.33 (s, 3H, piperidin-4-yl ring 4-CH, 4-fluorophenyl ring 4-CCH₂), 4.27 (d, J = 5.4 Hz, 2H, cyclohexylmethoxybenzyl ring 1-CHCH₂), 3.70 (d, J = 6.3 Hz, 2H, cyclohexyl ring 1-CHCH₂O), 2.86 (d, J = 11.1 Hz, 2H, piperidin-4-yl ring 2-H), 2.25 (s, 2H, piperidin-4-yl ring N1-CH₃), 2.07 (td, J = 11.7, 3.1 Hz, 2H, piperidin-4-yl ring 6-H), 1.85 (dd, J = 12.3, 3.6 Hz, 2H, piperidin-4-yl ring 3-H), 1.82 – 1.58 (m, 7H, piperidin-4-yl ring 5-H, cyclohexyl ring 1-H,

6. Experimental

cyclohexyl ring 2-H, 6-H), 1.36 – 1.13 (m, 4H, cyclohexyl ring 3-H, 5-H), 1.03 (qd, $J = 12.0, 3.4$ Hz, 2H, cyclohexyl ring 4-H).

^{13}C NMR (CDCl_3) δ_{C} 162.0 (d, $^1J_{\text{CF}} = 245.8$ Hz, 4-fluorophenyl ring 4-C), 158.5 (C=O), 158.1 (cyclohexylmethoxybenzyl ring 1-C), 134.1 (d, $^4J_{\text{CF}} = 3.1$ Hz, 4-fluorophenyl ring 1-C), 131.1 (cyclohexylmethoxybenzyl ring 4-C), 128.7 (cyclohexylmethoxybenzyl ring 3-C, 5-C), 127.7 (d, $^3J_{\text{CF}} = 8.0$ Hz, 4-fluorophenyl ring 2-C, 6-C), 115.7 (d, $^2J_{\text{CF}} = 21.6$ Hz, 4-fluorophenyl ring 3-C, 5-C), 114.5 (cyclohexylmethoxybenzyl ring C-2, C-6), 73.6 (cyclohexyl ring 1-CH $\underline{\text{C}}\text{H}_2\text{O}$), 55.3 (piperidin-4-yl ring C-2, C6), 52.2 (piperidin-4-yl ring 4-H), 46.1 (4-fluorophenyl ring 4-C $\underline{\text{C}}\text{H}_2$) 45.1 (piperidin-4-yl ring N1-CH $_3$), 44.5 (cyclohexylmethoxybenzyl ring 1-CH $\underline{\text{C}}\text{H}_2$), 37.7 (cyclohexyl ring 1-C), 30.1 cyclohexyl ring 2-C, 6-C), 29.9 (piperidin-4-yl ring 3-C, 5-C), 26.5 (cyclohexyl ring 4-C), 25.8 (cyclohexyl ring 3-C, 5-C).

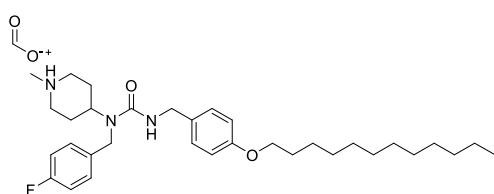
4-(3-(4-(Dodecyloxy)benzyl)-1-(4-fluorobenzyl)ureido)-1-methyl piperidin-1-ium (17c)

1-(4-Fluorobenzyl)-3-(4-hydroxybenzyl)-1-(1-methylpiperidin-4-yl)urea (**33**) (0.100 g, 0.270 mmol) was dissolved in anhydrous DMF (10 mL) with stirring and cooled to 0°C. NaH 60% in mineral oil (0.041 g, 0.297 mmol, 1.1 eq) was added in one portion and stirred until effervescence ceased. The reaction mixture turned yellow. Bromododecane (65 μl , 0.297 mmol, 1.1 eq) was added dropwise over 1 minute and the reaction mixture was allowed to come up to room temperature. Upon completion as determined by LCMS (HPLC-method A) the solvent was removed under

6. Experimental

vacuum and crude residue partitioned between H₂O (50 mL) and EtOAc (30 mL). The aqueous was extracted further with EtOAc (30 mL x 2), combined, dried over MgSO₄, suction filtered, concentrated under vacuum, purified via prep HPLC (HPLC-method E), and lyophilised to afford the title compound was a clear residue (2 mg, 1.4%).

HRMS *m/z* (ESI-TOF+) calculated for C₃₃H₅₁FN₃O₂ [M+H]⁺: 540.39, found: 540.3972 [M+H]⁺



¹H NMR (DMSO) δ_H

8.31 (s, 1H, piperidin-1-ium ring NH⁺), 7.24 (dd, *J* = 8.4, 5.5 Hz, 2H, 4-

fluorophenyl ring 3-H, 5-H), 7.10 (m, 4H, dodecyloxybenzy ring 3-H, 5-H, 4-fluorophenyl ring 2-H, 6-H), 6.91 – 6.78 (m, 3H, dodecyloxybenzy ring 2-H, 6-H, urea NH), 4.41 (s, 2H, 4-fluorophenyl ring 4-CCH₂), 4.18 (d, *J* = 5.6 Hz, 1H, dodecyloxybenzy ring 4-CCH₂), 4.01 – 3.84 (m, 3H, piperdin-1-ium ring 4-H, dodecyloxybenzy ring OCH₂), 2.71 (d, *J* = 11.3 Hz, 2H, piperdin-1-ium ring 2-H), 2.10 (s, 3H, piperdin-1-ium ring N1-CH₃), 1.89 (t, *J* = 11.4 Hz, 2H, piperdin-1-ium ring 6-H), 1.68 (p, *J* = 6.7 Hz, 2H, dodecyloxybenzy ring OCH₂CH₂), 1.61 – 1.48 (m, 2H, piperdin-1-ium ring 3-H), 1.46 – 1.36 (m, 2H, piperdin-1-ium ring 5-H), 1.25 (s, 18H, dodecyloxybenzy ring OCH₂CH₂(CH₂)₉CH₃), 0.86 (t, *J* = 6.6 Hz, 3H, O(CH₂)₁₁CH₃).

6. Experimental

¹³C NMR (DMSO) δ_c 160.9 (d, $^1J_{CF}$ = 241.4 Hz, 4-fluorophenyl ring 4-C), 157.5 (C=O), 157.3 (dodecyloxybenzy ring 1-C), 137.0 (d, $^4J_{CF}$ = 3.1 Hz, 4-fluorophenyl ring 1-C), 133.0 (dodecyloxybenzy ring 4-C), 128.3 (d, $^3J_{CF}$ = 8.1 Hz, 4-fluorophenyl ring 3-C, 5-C), 128.1 (dodecyloxybenzy ring 2-C, 6-C), 114.7 (d, $^2J_{CF}$ = 21.3 Hz, 4-fluorophenyl ring 2-C, 6-C), 114.0 (dodecyloxybenzy ring 3-C, 5-C), 67.3 (dodecyloxybenzy ring OCH₂), 54.7 (piperdin-1-ium ring 2-C, 6-C), 52.1 (piperdin-1-ium ring 4-C), 45.5 (4-fluorophenyl ring 4-CCH₂), 44.0 (dodecyloxybenzy ring 4-CCH₂), 43.1 (piperdin-1-ium ring N-CH₃), 31.3 (piperdin-1-ium ring 2-C, 6-C), 29.7 (dodecyloxybenzy ring OCH₂CH₂(CH₂)₄(CH₂)₅CH₃), 29.1 – 28.9 (m, dodecyloxybenzy ring OCH₂CH₂(CH₂)₇CH₂CH₂CH₃), 28.7 (dodecyloxybenzy ring O(CH₂)₇CH₂(CH₂)₃CH₃), 25.5 (dodecyloxybenzy ring O(CH₂)₂CH₂(CH₂)₇CH₃), 22.1 (dodecyloxybenzy ring O(CH₂)₁₀CH₂CH₃), 14.0 (dodecyloxybenzy ring O(CH₂)₁₁CH₃).

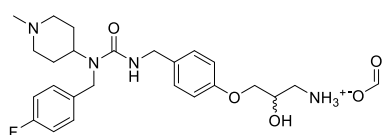
3-(4-((3-(4-Fluorobenzyl)-3-(1-methylpiperidin-4-yl)ureido)methyl)phenoxy)-2-hydroxypropan-1-aminium (18a)

4-(3-(4-(3-(Dibenzylammonio)-2-hydroxypropoxy)benzyl)-1-(4-fluorobenzyl)ureido)-1-methylpiperidin-1-ium (**18n**) (97 mg, 0.16 mmol) was dissolved in EtOH (4 mL) and sonicated for 10 minutes. AcOH (1.16 mL) was then added, and the mixture saturated with H₂. The mixture was then transferred to Pd/C 10% (41 mg, 0.02 mmol, 0.2 eq) suspended in H₂O (2.28 mL) and stirred. After completion as determined by LC-MS Reaction mixture was filtered through Celite® and filter cake washed with MeOH (20 mL x 3). Filtrate was concentrated under vacuum to give

6. Experimental

crude residue, purified by silica gel column chromatography (eluent DCM, 100; and MeOH[1M NH₃]:DCM, 0.2:9.8], 0.5:9.5, 0.7:9.3, 1:9, 1.5:8.5) and prep-HPLC (HPLC-method D). Collected fractions were concentrated under vacuum and lyophilised, to give the title compound as a clear residue (4 mg, 6%).

HRMS *m/z* (ESI-TOF+) calculated for C₂₅H₃₆FN₄O₃ [M+H]⁺: 459.2800, found: 445.2596 [M+H]⁺



¹H NMR (DMSO) δ_H 8.31 (s, 1H, ammonium NH₃⁺), 7.28 – 7.20 (m, 2H, 4-fluorophenyl ring 3-H, 5-H),

7.15 – 7.05 (m, 4H, 4-fluorophenyl 2-H, 6-H, Ar ring 2-H, 6-H), 6.89 (t, 1H, ureido NH), 6.86 (d, *J* = 8.6 Hz, 2H, Ar ring 3-H, 5-H), 4.43 – 4.38 (m, 2H, 4-fluorophenyl ring 1-CCH₂), 4.18 (d, *J* = 5.6 Hz, 2H, Ar ring 1-CCH₂), 3.98 (s, 1H, chiral HC), 3.95 – 3.78 (m, 3H, 1-methylpiperidin-1-ium ring 4-H, Ar ring 4-COCH₂), 2.97 (d, *J* = 12.4 Hz, 1H, H_aCNH₃⁺), 2.84 – 2.62 (m, 3H, H_bCNH₃⁺, 1-methylpiperidin-1-ium ring 2-H), 2.11 (s, 3H, 1-methylpiperidin-1-ium ring CH₃), 1.96 – 1.85 (m, 2H, 1-methylpiperidin-1-ium ring 6-H), 1.62 – 1.49 (m, 2H, 1-methylpiperidin-1-ium ring 3-H), 1.48 – 1.39 (m, 2H, 1-methylpiperidin-1-ium ring 5-H).

¹³C NMR (DMSO) δ_C 172.0 (HCOOH), 158.0 (Ar ring 4-C), 157.5 (C=O), 137.6 (d, ⁴*J*_{CF} = 2.7 Hz, 4-fluorophenyl ring 1-C), 134.0 (Ar ring 1-C), 128.9 (d, ³*J*_{CF} = 8.0 Hz, 4-fluorophenyl ring 2-C, 6-C), 128.6 (Ar ring 2-C, 6-C), 115.2 (d, ²*J*_{CF} = 21.43 Hz, 4-fluorophenyl ring 3-C, 5-C), 114.6 (Ar ring 3-C,

6. Experimental

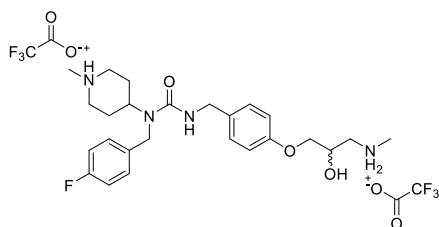
5-C), 70.3 (Ar ring 4-COCH₂), 67.0 (chiral C), 55.3 (1-methylpiperidin-1-ium ring 2-C, 6-C), 52.7 (1-methylpiperidin-1-ium ring 4-C), 46.2 (1-methylpiperidin-1-ium ring CH₃), 46.0 (4-fluorophenyl ring 1-CCH₂), 44.7 (Ar ring 1-CCH₂), 43.5 (H₂CNH₃⁺), 30.3 (1-methylpiperidin-1-ium ring 3-C, 5-C). Missing: (4-fluorophenyl ring 4-C).

4-(1-(4-Fluorobenzyl)-3-(4-(2-hydroxy-3-(methylammonio)propoxy)-benzyl)ureido)-1-methylpiperidin-1-ium (18b)

3-(4-(3-(Benzyl(methyl)amino)-2-hydroxypropoxy)benzyl)-1-(4-fluorobenzyl)-1-(1-methylpiperidin-4-yl)urea (**18o**) (111 mg, 0.20 mmol) was dissolved in EtOH (4 mL) and sonicated for 10 minutes. AcOH (1.16 mL) was then added, and the mixture saturated with H₂. The mixture was then transferred to Pd/C 10% (22 mg, 0.02 mmol, 0.1 eq) suspended in H₂O (2.28 mL) and stirred. After completion as determined by LC-MS Reaction mixture was filtered through Celite® and filter cake washed with MeOH (20 mL x 3). Filtrate was concentrated under vacuum to give crude residue, purified by silica gel column chromatography (eluent MeOH[1M NH₃]:DCM, 18:82), and prep-HPLC (HPLC-method G). Collected fractions were concentrated under vacuum and lyophilised, to afford the title compound as a clear residue (10 mg, 9%).

HRMS *m/z* (ESI-TOF+) calculated for C₂₅H₃₆FN₄O₃ [M+H]⁺: 459.2800, found: 459.2765 [M+H]⁺

6. Experimental



¹H NMR (DMSO) δ_{H} 9.59 (s, 1H, 1-methylpiperidin-1-ium ring NH⁺), 8.56 (s, 2H, methylammonium NH₂⁺), 7.24 (ddt, $J = 8.9, 5.6, 2.0$ Hz, 2H, 4-fluorophenyl ring 3-H, 5-H), 7.14 (t, $J = 8.4$ Hz, 4H, Ar ring 2-H, 6-H, 4-fluorophenyl ring 2-H, 6-H), 7.01 (t, $J = 6.0$ Hz, 1H, ureido NH), 6.90 – 6.82 (m, 2H, Ar ring 3-H, 5-H), 4.41 (s, 2H, 4-fluorophenyl ring 1-CCH₂), 4.20 (d, $J = 5.5$ Hz, 3H, 4-fluorophenyl ring 1-CCH₂, 1-methylpiperidin-1-ium ring 4-H), 4.12 (dtd, $J = 9.2, 4.7, 2.0$ Hz, 1H, chiral HC), 4.00 – 3.79 (m, 2H, Ar ring 4-COCH₂), 3.43 – 3.33 (m, 2H, 1-methylpiperidin-1-ium ring 2-H), 3.12 (ddd, $J = 8.1, 6.3, 4.0$ Hz, 1H, H_aCNH₂⁺), 3.07 – 2.93 (m, 3H, H_bCNH₂⁺, 1-methylpiperidin-1-ium ring 6-H), 2.71 (d, $J = 4.0$ Hz, 3H, 1-methylpiperidin-1-ium ring CH₃), 2.61 (t, $J = 5.3$ Hz, 3H, NH₂⁺CH₃), 1.92 – 1.77 (m, 2H, 1-methylpiperidin-1-ium ring 3-H), 1.71 – 1.64 (m, 2H, 1-methylpiperidin-1-ium ring 5-H).

¹³C NMR (DMSO) δ_{C} 161.5 (d, $^1J_{\text{CF}} = 241.9$ Hz, 4-fluorophenyl ring 4-C), 158.8 (COCF₃), 158.5 (COCF₃), 157.8 (C=O), 157.4 (Ar ring 4-C), 136.7 (d, $^4J_{\text{CF}} = 2.93$ Hz, 4-fluorophenyl ring 1-C), 133.9 (Ar ring 1-C), 128.8 (d, $^3J_{\text{CF}} = 8.1$ Hz, 4-fluorophenyl ring 2-C, 6-C), 128.7 (Ar ring 2-C, 6-C), 119.8 (CF₃), 118.8 (CF₃), 115.4 (d, $^2J_{\text{CF}} = 21.3$ Hz, 4-fluorophenyl ring 3-C, 5-C), 114.6 (Ar ring 3-C, 5-C), 70.2 (Ar ring 4-COCH₂), 65.3 (chiral C), 53.7 (1-methylpiperidin-1-ium ring 2-C, 6-C), 51.4 (H₂CNH₂⁺) 50.2 (Ar ring 1-CCH₂), 44.9 (4-fluorophenyl ring 1-CCH₂), 43.5 (1-methylpiperidin-1-ium

6. Experimental

ring 4-C), 42.9 (1-methylpiperidin-1-ium ring CH₃), 33.5 (NH₂⁺CH₃), 27.7 (1-methylpiperidin-1-ium ring 3-C, 5-C).

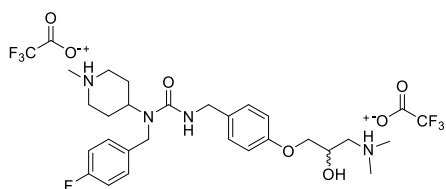
¹⁹F NMR (DMSO) δ_F -73.84 (HOOCF₃), -116.62, (4-fluorophenyl F).

4-(3-(4-(3-(Dimethylammonio)-2-hydroxypropoxy)benzyl)-1-(4-fluorobenzyl)ureido)-1-methylpiperidin-1-ium (18c)

3-(4-(Ammoniomethyl)phenoxy)-2-hydroxy-*N,N*-dimethylpropan-1-aminium (**38a**) (279 mg, 0.94 mmol) was dissolved in anhydrous DCM (6 mL) and triethylamine (327 μL, 2.36 mmol, 2.5 eq) under N₂ and stirred. CDI (239 mg, 2.36 mmol, 1.1 eq) was added after 5 minutes. After formation of a mono-substituted imidazole intermediate species as determined by LC-MS *N*-(4-fluorobenzyl)-1-methylpiperidin-4-amine (195 μL, 0.94 mmol, 1 eq) was added. Upon completion as determined by LC-MS volatiles were removed and crude residue portioned between H₂O (20 mL) and EtOAc (20 mL). Saturated bicarb solution was added to the aqueous until basic and extracted with EtOAc (20 mL x 2). Organics were then combined, dried over MgSO₄, suction filtered, concentrated under vacuum, and purified by silica gel column chromatography (eluent MeOH[1M NH₃]:DCM, 0.6:9.4 and 0.9:9.1), and prep-HPLC (HPLC-method G). Collected fractions were concentrated under vacuum and lyophilised to afford the title compound as a clear residue (67 mg, 10%).

HRMS *m/z* (ESI-TOF+) calculated for C₂₆H₃₈FN₄O₃ [M+H]⁺: 472.2900, found: 473.2912 [M+H]⁺

6. Experimental



¹H NMR (DMSO) δ_{H} 9.80 (s, 1H, 1-methylpiperidin-1-ium ring NH⁺), 9.50 (d, $J = 10.9$ Hz, 1H, dimethylammonio NH⁺), 7.31 – 7.19 (m, 2H, 4-fluorophenyl ring 3-H, 5-H), 7.19 – 7.08 (m, 4H, 4-fluorophenyl 2-H, 6-H, Ar ring 2-H, 6-H), 7.02 (t, $J = 5.9$ Hz, 1H, ureido NH), 6.87 (d, $J = 8.6$ Hz, 2H, Ar ring 3-H, 5-H), 4.41 (s, 2H, 4-fluorophenyl ring 1-CCH₂), 4.30 – 4.16 (m, 5H, 1-methylpiperidin-1-ium ring 4-H, Ar ring 1-CCH₂, chiral HC), 3.98 – 3.86 (m, 2H, Ar ring 4-COCH₂), 3.46 – 3.36 (m, 2H, 1-methylpiperidin-1-ium ring 2-H), 3.32 – 3.14 (m, 2H, H₂CNH⁺), 3.05 – 2.91 (m, 2H, 1-methylpiperidin-1-ium ring 6-H), 2.84 (dd, $J = 14.5, 4.5$ Hz, 6H, NH⁺(CH₃)₂), 2.71 (d, $J = 4.0$ Hz, 3H, 1-methylpiperidin-1-ium ring CH₃), 1.86 (qd, $J = 13.3, 3.9$ Hz, 2H, 1-methylpiperidin-1-ium ring 3-H), 1.73 – 1.65 (m, 2H, 1-methylpiperidin-1-ium ring 5-H).

¹³C NMR (DMSO) δ_{c} 161.5 (d, $^1J_{\text{CF}} = 242.0$ Hz, 4-fluorophenyl ring 4-C), 158.9 (q, $J = 35.0$ Hz, C=O), 157.8 (Ar ring 4-C), 157.4 (C=O), 136.7 (d, $^4J_{\text{CF}} = 2.9$ Hz, (4-fluorophenyl ring 1-C), 133.9 (Ar ring 1-C), 128.8 (d, $^3J_{\text{CF}} = 8.0$ Hz, 4-fluorophenyl ring 2-C, 6-C), 128.7 (Ar ring 2-C, 6-C), 121.0 (CF₃), 118.0 (CF₃), 115.4 (d, $^2J_{\text{CF}} = 21.2$ Hz, 4-fluorophenyl ring 3-C, 5-C), 114.6 (Ar ring 3-C, 5-C), 70.4 (Ar ring 4-COCH₂), 64.1 (chiral C), 59.4 (H₂CNH⁺), 53.7 (1-methylpiperidin-1-ium ring 2-C, 6-C), 50.2 (1-methylpiperidin-1-ium ring 4-C), 44.8 (4-fluorophenyl ring 1-CCH₂), 43.5 (Ar ring 1-CCH₂), 42.9 (1-methylpiperidin-1-ium ring CH₃), 42.0 (NH⁺(CH₃)₂), 27.6 (1-methylpiperidin-1-ium ring 3-C, 5-C).

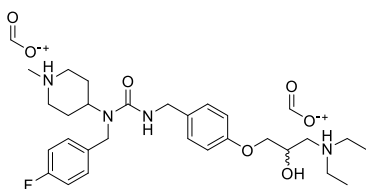
6. Experimental

^{19}F NMR δ_{F} (DMSO) δ_{F} -74.5 (HOOCF₃), -116.7 (1F, 4-fluorophenyl F).

4-(3-(4-(3-(Diethylammonio)-2-hydroxypropoxy)benzyl)-1-(4-fluorobenzyl)ureido)-1-methylpiperidin-1-ium (18d)

3-(4-(Ammoniomethyl)phenoxy)-*N,N*-diethyl-2-hydroxypropan-1-aminium (**38b**) (289 mg, 1.10 mmol) was dissolved in anhydrous DMF (5 mL) under N₂ and stirred. CDI (194 mg, 1.20 mmol, 1.1 eq) was added stirred. After formation of a mono-substituted imidazole intermediate species as determined by LC-MS *N*-(4-fluorobenzyl)-1-methylpiperidin-4-amine (170 μl , 0.82 mmol, 1 eq) was added. Upon completion as determined by LC-MS volatiles were removed and crude residue portioned between H₂O (20 mL) and EtOAc (20 mL). Aqueous was further extracted with EtOAc (15 mL x 3). Organics were combined, dried over MgSO₄, concentrated under vacuum, and purified by silica gel column chromatography (eluent MeOH[1M NH₃]:DCM, 18:82) and prep-HPLC (HPLC-method E). Collected fractions were concentrated under vacuum and lyophilised to afford the title compound as a clear residue (17 mg, 28%).

HRMS m/z (ESI-TOF+) calculated for C₂₈H₄₂FN₄O₃ [M+H]⁺: 501.3200, found: 501.3244 [M+H]⁺



^1H NMR (CDCl₃) δ_{H} 8.43 (s, 2H, 1-methylpiperidin-1-ium ring NH⁺, diethylammonio NH⁺), 7.19 – 7.13 (m, 2H, 4-fluorophenyl ring 3-H, 5-H),

6. Experimental

7.08 – 6.90 (m, 4H, 4-fluorophenyl 2-H, 6-H, Ar ring 2-H, 6-H), 6.76 (d, $J = 8.6$ Hz, 2H, Ar ring 3-H, 5-H), 4.63 (tt, $J = 12.2, 4.2$ Hz, 1H, 1-methylpiperidin-1-ium ring 4-H), 4.58 (t, $J = 5.4$ Hz, 1H, ureido NH), 4.51 – 4.37 (m, 1H, chiral HC), 4.35 (s, 2H, 4-fluorophenyl ring 1-CCH₂), 4.25 (d, $J = 5.4$ Hz, 2H, Ar ring 1-CCH₂), 4.11 (dd, $J = 9.4, 4.5$ Hz, 1H, Ar ring 4-COCH_a), 3.84 (dd, $J = 9.4, 8.2$ Hz, 1H, Ar ring 4-COCH_b), 3.46 – 3.33 (m, 2H, 1-methylpiperidin-1-ium ring 2-H), 3.18 (qd, $J = 7.1, 3.1$ Hz, 5H, $\underline{H}_b\text{CNH}^+$, $\text{NH}^+(\underline{\text{C}}\underline{\text{H}}_2)_2$), 3.07 (dd, $J = 13.3, 9.9$ Hz, 1H, $\underline{H}_a\text{CNH}^+$), 2.68 – 2.56 (m, 5H, 1-methylpiperidin-1-ium ring CH₃, 1-methylpiperidin-1-ium ring 2-H), 2.12 (qd, $J = 13.2, 3.9$ Hz, 2H, 1-methylpiperidin-1-ium ring 3-H), 1.94 – 1.75 (m, 2H, 1-methylpiperidin-1-ium ring 5-H), 1.35 (t, $J = 7.3$ Hz, 6H, $\text{NH}^+(\text{CH}_2)_2(\underline{\text{C}}\underline{\text{H}}_3)_2$).

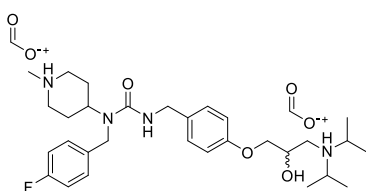
¹³C NMR (CDCl₃) δ_{C} 168.3 (HCOOH), 162.3 (d, $^1J_{\text{CF}} = 246.1$ Hz, 4-fluorophenyl ring 4-C), 158.1 (C=O), 157.5 (Ar ring 4-C), 133.4 (d, $^4J_{\text{CF}} = 2.57$ Hz, 4-fluorophenyl ring 1-C), 132.1 (Ar ring 1-C), 128.8 (Ar ring 2-C, 6-C), 127.7 (d, $^3J_{\text{CF}} = 8.0$ Hz, 4-fluorophenyl ring 2-C, 6-C), 116.1 (d, $^2J_{\text{CF}} = 21.6$ Hz, 4-fluorophenyl ring 3-C, 5-C), 114.6 (Ar ring 3-C, 5-C), 69.9 (Ar ring 4-COCH₂), 64.5 (chiral C), 57.3 (H₂CNH⁺), 54.2 (1-methylpiperidin-1-ium ring 2-C, 6-C), 50.3 (1-methylpiperidin-1-ium ring 4-C), 48.6 (NH⁺(CH₂)₂), 45.4 (4-fluorophenyl ring 1-CCH₂), 44.4 (Ar ring 1-CCH₂), 43.8 (1-methylpiperidin-1-ium ring CH₃), 27.6 (1-methylpiperidin-1-ium ring 3-C, 5-C), 8.9 (NH⁺(CH₂)₂(CH₃)₂).

6. Experimental

4-(3-(4-(3-(Diisopropylammonio)-2-hydroxypropoxy)benzyl)-1-(4-fluorobenzyl)ureido)-1-methylpiperidin-1-ium (18e)

3-(4-(Ammoniomethyl)phenoxy)-2-hydroxy-*N,N*-diisopropylpropan-1-aminium (**38c**) (286 mg, 0.81 mmol) was dissolved in anhydrous DCM (5 mL) and triethylamine (277 μ l, 0.2 mmol, 2.5 eq) under N_2 and stirred. CDI (146 mg, 0.90 mmol, 1.1 eq) was added after 5 minutes. After formation of a mono-substituted imidazole intermediate species as determined by LC-MS *N*-(4-fluorobenzyl)-1-methylpiperidin-4-amine (187 μ l, 0.80 mmol, 1 eq) was added. Upon completion as determined by LC-MS volatiles were removed and crude residue portioned between H_2O (50 mL) and EtOAc (30 mL). The aqueous was further extracted with EtOAc (30 mL x 2). Organics were combined, dried over $MgSO_4$, suction filtered, concentrated under vacuum, and purified by silica gel column chromatography (eluent MeOH[1M NH_3]:DCM, 0.8:9.2) and prep-HPLC (HPLC-method D). Collected fractions were concentrated under vacuum and lyophilised to afford the title compound as a clear residue (13 mg, 33%).

HRMS m/z (ESI-TOF+) calculated for $C_{30}H_{46}FN_4O_3$ $[M+H]^+$: 529.3500, found: 529.3568 $[M+H]^+$



1H NMR ($CDCl_3$) δ_H 8.47 (d, J = 0.9 Hz, 2H, diisopropylammonio NH^+ , 1-methylpiperidin-1-ium ring NH^+), 7.17 (dd, J = 8.5, 5.2 Hz, 2H, 4-

6. Experimental

fluorophenyl ring 3-H, 5-H), 7.00 (t, $J = 7.8$ Hz, 4H, Ar ring 2-H, 6-H, 4-fluorophenyl ring 2-H, 6-H), 6.83 – 6.68 (m, 2H, Ar ring 3-H, 5-H), 4.63 – 4.52 (m, 2H, ureido NH, 1-methylpiperidin-1-ium ring 4-H), 4.44 (td, $J = 9.2, 4.4$ Hz, 1H, chiral HC), 4.35 (s, 2H, 4-fluorophenyl ring 1-CCH₂), 4.26 (d, $J = 5.4$ Hz, 2H, Ar ring 1-CCH₂), 4.13 (dd, $J = 9.4, 4.4$ Hz, 1H, Ar ring 4-COCH_a), 3.80 (t, $J = 9.1$ Hz, 1H, 4-COCH_b), 3.53 (hept, $J = 6.7$ Hz, 2H, NH⁺(CH₂)₂), 3.35 – 3.27 (m, 2H, 1-methylpiperidin-1-ium ring 6-H), 3.21 (d, $J = 13.9$ Hz, 1H, H_aCNH⁺), 2.93 (dd, $J = 14.0, 9.7$ Hz, 1H, H_bCNH⁺), 2.53 (s, 3H, 1-methylpiperidin-1-ium ring 6-H, 1-methylpiperidin-1-ium ring CH₃), 2.05 (qd, $J = 12.3, 3.6$ Hz, 2H, 1-methylpiperidin-1-ium ring 3-H), 1.87 – 1.76 (m, 2H, 1-methylpiperidin-1-ium ring 5-H), 1.39 (dd, $J = 11.1, 6.5$ Hz, 12H, NH⁺(CH₂)₂(CH₃)₄).

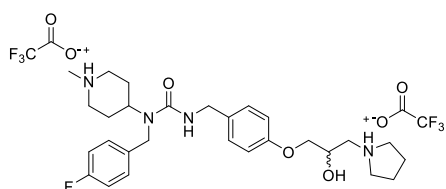
¹³C NMR (CDCl₃) δ_C 168.2 (HCOOH), 158.0 (C=O), 161.0 (4-fluorophenyl ring 4-C), 157.4 (Ar ring 4-C), 133.3 (d, ⁴J_{CF} = 3.01 Hz, 4-fluorophenyl ring 1-C), 131.9 (Ar ring 1-C), 128.7 (Ar ring 2-C, 6-C), 127.6 (d, ³J_{CF} = 8.0 Hz, 4-fluorophenyl ring 2-C, 6-C), 116.0 (d, ²J_{CF} = 21.6 Hz, 4-fluorophenyl ring 3-C, 5-C), 114.4 (Ar ring 3-C, 5-C), 70.0 (Ar ring 4-COCH₂), 65.3 (chiral C), 55.0 (NH⁺(CH₂)₂), 54.1 (1-methylpiperidin-1-ium ring 2-C, 6-C), 52.5 (H₂CNH⁺), 50.4 (1-methylpiperidin-1-ium ring 4-C), 45.2 (4-fluorophenyl ring 1-CCH₂), 44.3 (Ar ring 1-CCH₂), 43.9 (1-methylpiperidin-1-ium ring CH₃), 27.8 (1-methylpiperidin-1-ium ring 3-C, 5-C), 18.5 (NH⁺(CH₂)₂(CH₃)₂), 17.8 (NH⁺(CH₂)₂(CH₃)₂).

6. Experimental

4-(1-(4-Fluorobenzyl)-3-(4-(2-hydroxy-3-(pyrrolidin-1-ium-1-yl)propoxy)benzyl)ureido)-1-methylpiperidin-1-ium (18f)

(4-(2-Hydroxy-3-(pyrrolidin-1-yl)propoxy)phenyl)methanaminium (38d) (252 mg, 0.82 mmol) was dissolved in anhydrous DCM (10 mL) and triethylamine (350 μ l, 4.6 mmol, 5.6 eq) under N₂ and stirred. CDI (139 mg, 0.86 mmol, 1.05 eq) was added after 5 minutes. After formation of a mono-substituted imidazole intermediate species as determined by LC-MS *N*-(4-fluorobenzyl)-1-methylpiperidin-4-amine (170 μ l, 0.82 mmol, 1 eq) was added. Upon completion as determined by LC-MS volatiles were removed and crude residue portioned between H₂O (50 mL) and EtOAc (30 mL) and set. The aqueous was further extracted with EtOAc (30 mL x 2). Organics were combined, dried over MgSO₄, concentrated under vacuum, and purified by RP flash chromatography (H₂O:MeCN, 0.1% formic acid, 100-10%) and prep-HPLC (HPLC-method G). Collected fractions were concentrated under vacuum and lyophilised, to afford the title compound as a clear residue (20 mg, 3%).

HRMS *m/z* (ESI-TOF+) calculated for C₂₈H₄₀FN₄O₃ [M+H]⁺: 499.3100, found: 499.3077 [M+H]⁺



¹H NMR (DMSO) δ _H 9.68 (s, 2H, pyrrolidin-1-ium-1-yl ring NH⁺), 7.24 (dd, *J* =

8.5, 5.6 Hz, 2H, 4-fluorophenyl ring 3-H, 5-H), 7.13 (dt, *J* = 8.9, 4.6 Hz, 2H,

6. Experimental

4-fluorophenyl ring 2-H, 6-H), 7.02 (t, $J = 5.7$ Hz, 3H, ureido NH, Ar ring 2-H, 6-H), 6.94 – 6.83 (m, 1H Ar ring 3-H, 5-H), 4.41 (s, 2H, 4-fluorophenyl ring 1-CCH₂), 4.27 – 4.14 (m, 3H, 1-methylpiperidin-1-ium ring 4-H, Ar ring 1-CCH₂, chiral HC), 3.98 – 3.86 (m, 2H, Ar ring 4-COCH₂), 3.63 – 3.53 (m, 2H, H₂CNH), 3.46 – 3.35 (m, 2H, 1-methylpiperidin-1-ium ring 2-H), 3.29 (dtd, $J = 12.9, 8.1, 4.3$ Hz, 2H, pyrrolidin-1-ium-1-yl ring 2-H, 3.10 (dt, $J = 10.9, 7.4$ Hz, 2H, pyrrolidin-1-ium-1-yl ring 5-H), 3.03 – 2.90 (m, 2H, 1-methylpiperidin-1-ium ring 6-H), 2.71 (d, $J = 4.1$ Hz, 3H, 1-methylpiperidin-1-ium ring CH₃), 2.09 – 1.96 (m, 2H, pyrrolidin-1-ium-1-yl ring 3-H), 1.92 – 1.79 (m, 4H, 1-methylpiperidin-1-ium ring 3-H, pyrrolidin-1-ium-1-yl ring 4-H), 1.72 – 1.62 (m, 2H, 1-methylpiperidin-1-ium ring 5-H).

¹³C NMR (DMSO) δ_c 161.0 (d, $^1J_{CF} = 242.0$ Hz, 4-fluorophenyl ring 4-C), 158.5 (HOOCF₃), 158.2 (HOOCF₃), 157.4 (C=O), 157.0 (Ar ring 4-C), 136.3 (4-fluorophenyl ring 1-C), 133.4 (Ar ring 1-C), 128.3 (d, $^3J_{CF} = 8.1$ Hz, 4-fluorophenyl ring 2-C, 6-C), 128.2 (Ar ring 2-C, 6-C), 118.7 (4-fluorophenyl ring 4-C), 114.9 (d, $^2J_{CF} = 21.3$ Hz, 4-fluorophenyl ring 3-C, 5-C), 114.1 (Ar ring 2-C, 6-C), 70.0 (Ar ring 4-COCH₂), 64.9 (chiral C), 56.6 (pyrrolidin-1-ium-1-yl ring 2-C), 54.9 (pyrrolidin-1-ium-1-yl ring 5-C), 53.2 (H₂CNH⁺), 52.7 (1-methylpiperidin-1-ium ring 2-C, 6-C), 49.7 (1-methylpiperidin-1-ium ring 4-C), 44.3 (4-fluorophenyl ring 1-CCH₂), 43.1 (Ar ring 1-CCH₂), 42.5 (1-methylpiperidin-1-ium ring CH₃), 27.2 (pyrrolidin-1-ium-1-yl ring 3-C, 4-C), 22.5 (1-methylpiperidin-1-ium ring 3-C, 5-C).

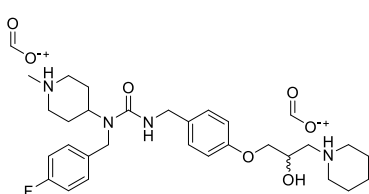
¹⁹F NMR (DMSO) δ_F -73.6 (6F, HOOCF₃), -116.7 (1F, 4-fluorophenyl F).

6. Experimental

4-(1-(4-Fluorobenzyl)-3-(4-(2-hydroxy-3-(piperidin-1-ium-1-yl)propoxy)benzyl)ureido)-1-methylpiperidin-1-ium (18g)

1-(3-(4-(Ammoniomethyl)phenoxy)-2-hydroxypropyl)piperidin-1-ium (38e) (252 mg, 0.82 mmol) was dissolved in anhydrous DCM (10 mL), triethylamine (350 μ l, 4.6 mmol, 5.6 eq) under N₂ and stirred. CDI (139 mg, 0.86 mmol, 1.05 eq) was added after 5 minutes. After formation of a mono-substituted imidazole intermediate species as determined by LC-MS *N*-(4-fluorobenzyl)-1-methylpiperidin-4-amine (170 μ l, 0.82 mmol, 1 eq) was added. Upon completion as determined by LC-MS volatiles were removed and crude residue portioned between H₂O (50 mL) and EtOAc (30 mL) and set. The aqueous was further extracted with EtOAc (30 mL x 2). Organics were combined, dried over MgSO₄, concentrated under vacuum, and purified by silica gel column chromatography (eluent DCM, 100; and MeOH[1M NH₃]:DCM, 0.4:9.6, 0.65:9.35) and prep-HPLC (HPLC-method D). Collected fractions were concentrated under vacuum and lyophilised, to afford the title compound as a clear residue (30 mg, 9%).

HRMS *m/z* (ESI-TOF+) calculated for C₂₉H₄₂FN₄O₃ [M+H]⁺: 513.3200, found: 513.3242 [M+H]⁺



¹H NMR (DMSO) δ _H 8.29 (s, 2H, 1-methylpiperidin-1-ium ring NH⁺, piperidin-1-ium-1-yl ring NH⁺), 7.41 – 7.17 (m, 2H, 4-fluorophenyl ring 3-

6. Experimental

H, 5-H), 7.16 – 7.06 (m, 4H, 4-fluorophenyl 2-H, 6-H, Ar ring 2-H, 6-H), 6.92 (t, $J = 5.8$ Hz, 1H, ureido NH), 6.85 (d, $J = 8.6$ Hz, 2H, Ar ring 3-H, 5-H), 4.41 (s, 2H, 4-fluorophenyl ring 1-CCH₂), 4.19 (d, $J = 5.5$ Hz, 2H, Ar ring 1-CCH₂), 4.13 – 3.97 (m, 2H, 1-methylpiperidin-1-ium ring 4-H, chiral HC), 3.96 – 3.82 (m, 2H, 4-COCH₂), 2.93 (d, $J = 3.0$ Hz, 2H, 1-methylpiperidin-1-ium ring 2-H), 2.78 – 2.69 (m, 5H, H_aCNH⁺, piperidin-1-ium-1-yl ring 2-H, 6-H), 2.64 (dd, $J = 12.9, 7.9$ Hz, 1H, H_bCNH⁺), 2.43 – 2.15 (m, 5H, 1-methylpiperidin-1-ium ring CH₃, 1-methylpiperidin-1-ium ring 6-H), 1.77 – 1.38 (m, 10H, 1-methylpiperidin-1-ium ring 3-H, 5-H, piperidin-1-ium-1-yl ring 3-H, 4-H, 5-H).

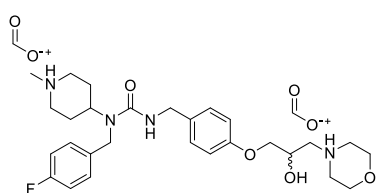
¹³C NMR (DMSO) δ_c 164.8 (HCOOH), 160.9 (d, $^1J_{CF} = 241.7$ Hz, 4-fluorophenyl ring 4-C), 157.5 (C=O), 157.2 (Ar ring 4-C), 136.8 (d, $^4J_{CF} = 2.9$ Hz, 4-fluorophenyl ring 1-C), 133.3 (Ar ring 1-C), 128.3 (d, $^3J_{CF} = 8.2$ Hz, 4-fluorophenyl ring 2-C, 6-C), 128.2 (Ar ring 3-C, 5-C), 114.8 (d, $^2J_{CF} = 21.3$ Hz, 4-fluorophenyl ring 3-C, 5-C), 114.1 (Ar ring 3-C, 5-C), 70.8 (Ar ring 4-COCH₂), 65.3 (chiral C), 60.6 (H₂CNH⁺), 54.0 (1-methylpiperidin-1-ium ring 2-C, 6-C, piperidin-1-ium-1-yl ring 2-H, 6-H), 51.4 (4-fluorophenyl ring 1-CCH₂), 44.2 (1-methylpiperidin-1-ium ring CH₃), 44.1 (4-fluorophenyl ring 1-CCH₂), 43.1 (Ar ring 1-CCH₂), 28.7 (1-methylpiperidin-1-ium ring 3-C, 5-C), 24.2 (piperidin-1-ium-1-yl ring 3-C, 5-C), 22.9 (piperidin-1-ium-1-yl ring 4-C).

6. Experimental

4-(3-(4-((3-(4-Fluorobenzyl)-3-(1-methylpiperidin-1-ium-4-yl)ureido)methyl)phenoxy)-2-hydroxypropyl)morpholin-4-ium (18h)

4-(3-(4-(Ammoniomethyl)phenoxy)-2-hydroxypropyl)morpholin-4-ium (38f) (292 mg, 0.87 mmol) was dissolved in anhydrous DCM (5 mL) and triethylamine (420 μ l, 1.90 mmol, 2.5 eq) under N₂ and stirred. CDI (156 mg, 0.96 mmol, 1.1 eq) was added after 5 minutes. After formation of a mono-substituted imidazole intermediate species as determined by LC-MS *N*-(4-fluorobenzyl)-1-methylpiperidin-4-amine (180 μ l, 0.87 mmol, 1 eq) was added. Upon completion as determined by LC-MS volatiles were removed and crude residue portioned between H₂O (50 mL) and EtOAc (30 mL) and setted. The aqueous was further extracted with EtOAc (30 mL x 2). Organics were combined, dried over MgSO₄, concentrated under vacuum, and purified by silica gel column chromatography (eluent MeOH[1M NH₃]:DCM) [12:88] and prep-HPLC (HPLC-method D). Collected fractions were concentrated under vacuum and lyophilised, to afford the title compound as a clear residue (28 mg, 8%).

HRMS *m/z* (ESI-TOF+) calculated for C₂₈H₄₀N₄O₄ [M+H]⁺: 515.3000, found: 515.3044 [M+H]⁺



¹H NMR (CDCl₃) δ _H 8.30 (s, 2H, morpholin-4-ium ring NH⁺, 1-methylpiperidin-1-ium ring NH⁺), 7.21 – 7.12 (m, 2H, 4-fluorophenyl

ring 3-H, 5-H), 7.05 – 6.93 (m, 4H, 4-fluorophenyl 2-H, 6-H, Ar ring 2-H, 6-

6. Experimental

H), 6.82 – 6.73 (m, 2H, Ar ring 3-H, 5-H), 4.68 (tt, $J = 12.3, 3.9$ Hz, 1H, 1-methylpiperidin-1-ium ring 4-H), 4.60 (t, $J = 5.5$ Hz, 1H, ureido NH), 4.35 (s, 1H, 4-fluorophenyl ring 1-CCH₂), 4.34 – 4.25 (m, 1H, chiral HC), 4.25 (d, $J = 5.5$ Hz, 2H, Ar ring 1-CCH₂), 4.00 (dd, $J = 9.6, 5.0$ Hz, 1H, Ar ring 4-COCH_a), 3.91 (dd, $J = 9.5, 5.8$ Hz, 1H, Ar ring 4-COCH_b), 3.85 (dt, $J = 6.6, 3.3$ Hz, 4H, morpholin-4-ium ring 3-H, 5-H), 3.50 (d, $J = 12.4$ Hz, 1H, (1-methylpiperidin-1-ium ring 2-C), 2.97 – 2.69 (m, 8H, H₂CNH⁺, morpholin-4-ium ring 2-H, 6-H, 1-methylpiperidin-1-ium ring 6-H), 2.68 (s, 3H, 1-methylpiperidin-1-ium ring CH₃), 2.20 (qd, $J = 12.9, 3.8$ Hz, 2H, 1-methylpiperidin-1-ium ring 3-H), 1.86 (d, $J = 14.0$ Hz, 2H, 1-methylpiperidin-1-ium ring 5-H).

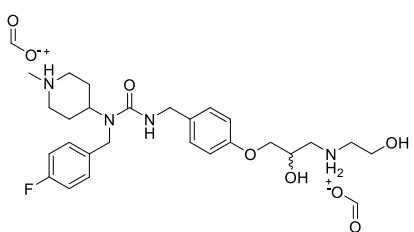
¹³C NMR (CDCl₃) δ_C 166.8 (HCOOH), 163.6 (4-fluorophenyl ring 4-C), 158.2 (C=O), 157.8 (Ar ring 4-C), 133.1 (d, $^4J_{CF} = 3.0$ Hz, 4-fluorophenyl ring 1-C), 131.7 (Ar ring 1-C), 128.8 (Ar ring 2-C, 6-C), 127.7 (d, $^3J_{CF} = 8.0$ Hz, 4-fluorophenyl ring 2-C, 6-C), 116.2 (d, $^2J_{CF} = 21.6$ Hz, 4-fluorophenyl ring 3-C, 5-C), 114.7 (Ar ring 3-C, 5-C), 70.2 (Ar ring 4-COCH₂), 65.7 (morpholin-4-ium ring 3-C, 5-C), 65.0 (chiral C), 61.4 (H₂CNH⁺), 54.2 (1-methylpiperidin-1-ium ring 2-C, 6-C), 53.7 (1-methylpiperidin-1-ium ring 2-C, 6-C), 49.8 (1-methylpiperidin-1-ium ring 4-C), 45.3 (4-fluorophenyl ring 1-CCH₂), 44.5 (Ar ring 1-CCH₂), 43.5 (1-methylpiperidin-1-ium ring CH₃), 27.1 (1-methylpiperidin-1-ium ring 3-C, 5-C).

6. Experimental

4-(1-(4-Fluorobenzyl)-3-(4-(2-hydroxy-3-((2-hydroxyethyl)ammonio)propoxy)benzyl)-1-(4-fluorobenzyl)ureido)-1-methylpiperidin-1-ium (18i)

4-(3-(4-(3-(Benzyl(2-hydroxyethyl)ammonio)-2-hydroxypropoxy)benzyl)-1-(4-fluorobenzyl)ureido)-1-methylpiperidin-1-ium (**18p**) (92 mg, 0.16 mmol) was dissolved in EtOH (8 mL) and sonicated for 10 minutes. AcOH (2.72 mL) was then added, and the mixture saturated with H₂. The mixture was then transferred to Pd/C 10% (15 mg, 0.03 mmol, 0.15 eq) suspended in H₂O (4.60 mL) and stirred. After completion as determined by LC-MS Reaction mixture was filtered through Celite® and filter cake washed with MeOH (30 mL x 4). The reaction mixture was adjusted to basic, pH 9, with saturated bicarbonate solution and volatiles removed under vacuum. The remaining aqueous reaction mixture was extracted with EtOAc (30 mL x 3). Organics were dried over MgSO₄ and concentrated under vacuum to give crude residue purified by prep-HPLC (HPLC-method D). Collected fractions were concentrated under vacuum and lyophilised, to afford the title compound as a clear residue (10 mg, 11%).

HRMS *m/z* (ESI-TOF+) calculated for C₂₆H₃₈N₄O₃ [M+H]⁺: 489.2900
found: 489.2887 [M+H]⁺



¹H NMR (DMSO) δ_H 8.35 – 8.25 (m, 2H, 1-methylpiperidin-1-ium ring NH⁺), 7.29 – 7.20 (m, 2H, 4-fluorophenyl ring 3-H, 5-H), 7.16

6. Experimental

– 7.05 (m, 4H, 4-fluorophenyl ring 2-H, 6-H, Ar ring 2-H, 6-H), 6.92 – 6.81 (m, 3H, ureido NH, Ar ring 3-H, 5-H), 4.41 (s, 2H, 4-fluorophenyl ring 1-CCH₂), 4.18 (d, $J = 5.6$ Hz, 2H, Ar ring 1-CCH₂), 4.00 – 3.80 (m, 4H, 1-methylpiperidin-1-ium ring 4-H, chiral HC, Ar ring 4-COCH₂), 3.75 – 3.43 (m, 2H, CH₂OH), 2.96 – 2.80 (m, 1H, 1-methylpiperidin-1-ium ring 3-H_a), 2.73 (dd, $J = 11.1, 6.4$ Hz, 2H, H₂CNH⁺, 1-methylpiperidin-1-ium ring 3-H_b), 2.11 (s, 2H, 7), 1.92 (t, $J = 11.6$ Hz, 2H, 1-methylpiperidin-1-ium ring 6-H), 1.62 – 1.49 (m, 2H, 1-methylpiperidin-1-ium ring 3-H), 1.47 – 1.39 (m, 2H, 1-methylpiperidin-1-ium ring 5-H). Missing: (2H CH₂CH₂OH).

¹³C NMR (DMSO) δ_c 160.1 (4-fluorophenyl ring 4-C), 158.0 (C=O), 157.7 (Ar ring 4-C), 133.8 (Ar ring 1-C), 128.8 (d, $^3J_{CF} = 7.7$ Hz, 4-fluorophenyl ring 2-C, 6-C), 128.6 (Ar ring 2-C, 6-C), 115.1 (d, $^2J_{CF} = 21.2$ Hz, 4-fluorophenyl ring 3-C, 5-C), 114.6 (Ar ring 3-C, 5-C), 71.0 (Ar ring 4-COCH₂), 70.8 (chiral C), 67.6 (1-methylpiperidin-1-ium ring 4-C), 59.6 (CH₂OH) 52.7 (4-fluorophenyl ring 1-CCH₂), 46.2 (1-methylpiperidin-1-ium ring CH₃), 44.4 (Ar ring 1-CCH₂), 43.6 (H₂CN), 40.9 (CH₂CH₂OH), 30.3 (1-methylpiperidin-4-yl ring 3-C, 5-C). Missing: (HCOOH, 4-fluorophenyl ring 1-C)

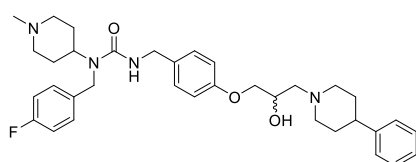
1-(4-Fluorobenzyl)-3-(4-(2-hydroxy-3-(4-phenylpiperidin-1-yl)propoxy)benzyl)-1-(1-methylpiperidin-4-yl)urea (18j)

1-(3-(4-(Ammoniomethyl)phenoxy)-2-hydroxypropyl)-4-phenylpiperidin-1-ium (**38g**) (269 mg, 0.65 mmol) was dissolved in anhydrous DCM (6 mL) and triethylamine (226 ul, 1.63 mmol, 2.5 eq) under N₂ and stirred.

6. Experimental

CDI (117 mg, 0.72 mmol, 1.1 eq) was added after 5 minutes. After formation of a mono-substituted imidazole intermediate species as determined by LC-MS *N*-(4-fluorobenzyl)-1-methylpiperidin-4-amine (144 μ l, 0.65 mmol, 1 eq) was added. Upon completion as determined by LC-MS volatiles were removed and crude residue portioned between H₂O (30 mL) and EtOAc (20 mL) and set. The aqueous was further extracted with EtOAc (20 mL x 2). Organics were combined, dried over MgSO₄, concentrated under vacuum, and purified by silica gel column chromatography (eluent MeOH[1M NH₃]:DCM, 0.9:9.1). Collected fractions were concentrated under vacuum, to afford the title compound as an off-white foam (131 mg, 34%).

HRMS *m/z* (ESI-TOF+) calculated for C₃₅H₄₆N₄O₃ [M+H]⁺: 589.3500
found: 589.3553 [M+H]⁺



¹H NMR (CDCl₃) δ _H 7.42 – 7.10

(m, 7H, 4-fluorophenyl ring 3-H,

5-H, 4-phenylpiperidin-1-yl

phenyl ring 2-H-6-H), 7.00 (m, 4H, 4-fluorophenyl 2-H, 6-H, Ar ring 2-H, 6-

H), 6.82 (d, *J* = 8.6 Hz, 2H, Ar ring 3-H, 5-H), 4.47 (t, *J* = 5.4 Hz, 1H, urea

NH), 4.38 – 4.30 (m, 3H, 1-methylpiperidin-4-yl ring 4-H, 4-fluorophenyl

ring 1-CCH₂), 4.28 (d, *J* = 5.4 Hz, 2H, Ar ring 1-CCH₂), 4.10 (dq, *J* = 9.4, 4.8

Hz, 1H, chiral HC), 3.97 (d, *J* = 4.9 Hz, 2H, Ar ring 4-COCH₂), 3.14 (d, *J* =

11.3 Hz, 1H, piperidin-1-yl ring 2-H_a), 2.98 (d, *J* = 11.3 Hz, 1H, piperidin-1-

yl ring 6-H_a), 2.86 (d, *J* = 11.5 Hz, 2H, 1-methylpiperidin-4-yl ring 2-H), 2.70

– 2.49 (m, 3H, H₂CNH, piperidin-1-yl ring 4-H), 2.43 (td, *J* = 11.2, 3.5 Hz,

6. Experimental

1H, piperidin-1-yl ring 6-H_b), 2.26 (s, 3H, 1-methylpiperidin-4-yl ring CH₃), 2.20 – 2.01 (m, 0H, 1-methylpiperidin-4-yl ring 6-H piperidin-1-yl ring 2-H_b), 1.93 – 1.82 (m, 2H, piperidin-1-yl ring 3-H), 1.82 – 1.59 (m, 6H, 1-methylpiperidin-4-yl ring 3-H, 5-H, piperidin-1-yl ring 5-H).

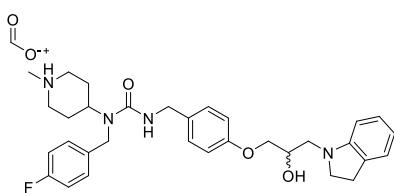
¹³C NMR (CDCl₃) δ_C 162.0 (d, ¹J_{CF} = 245.8 Hz, 4-fluorophenyl ring 4-C), 158.1 (C=O), 158.0 (Ar ring 4-C), 146.1 (4-phenylpiperidin-1-yl phenyl ring 1-C), 134.1 (d, ⁴J_{CF} = 2.9 Hz, 4-fluorophenyl ring 1-C), 131.8 (Ar ring 1-C), 128.7 (4-phenylpiperidin-1-yl phenyl ring 2-C, 6-C), 128.5 (4-phenylpiperidin-1-yl phenyl ring 3-C, 5-C), 127.7 (d, ³J_{CF} = 7.9 Hz, 4-fluorophenyl ring 2-C, 6-C), 126.8 (Ar ring 2-C, 6-C), 126.2 (4-phenylpiperidin-1-yl phenyl ring 4-C), 115.8 (d, ²J_{CF} = 21.6 Hz, 4-fluorophenyl ring 3-C, 5-C), 114.6 (Ar ring 3-C, 5-C), 70.5 (Ar ring 4-COCH₂), 65.6 (chiral C), 60.8 (H₂CNH⁺), 56.1 (phenylpiperidin-1-yl ring 2-C), 55.3 (1-methylpiperidin-4-yl ring 2-C, 6-C) 53.0 (phenylpiperidin-1-yl ring 6-C), 52.2 (1-methylpiperidin-4-yl ring 4-C), 46.1 (1-methylpiperidin-4-yl ring CH₃), 45.2 (4-fluorophenyl ring 1-CCH₂), 44.4 (Ar ring 1-CCH₂), 42.4 (piperidin-1-yl ring 4-C), 33.7 (piperidin-1-yl ring 3-C), 33.4 (piperidin-1-yl ring 5-C), 30.1 (1-methylpiperidin-4-yl ring 3-C, 5-C).

6. Experimental

4-(3-(4-(3-(7-Azabicyclo[4.2.0]octa-1(6),2,4-trien-7-yl)-2-hydroxypropoxy)benzyl)-1-(4-fluorobenzyl)ureido)-1-methylpiperidin-1-ium (18k)

1-(3-(4-(Ammoniomethyl)phenoxy)-2-hydroxypropyl)indolin-1-ium (38h) (374 mg, 1.01 mmol) was dissolved in anhydrous DCM (10 mL) and triethylamine (350 μ l, 2.50 mmol, 2.5 eq) under N₂ and stirred. CDI (178 mg, 1.11 mmol, 1.1 eq) was added after 5 minutes. After formation of a mono-substituted imidazole intermediate species as determined by LC-MS *N*-(4-fluorobenzyl)-1-methylpiperidin-4-amine (210 μ l, 1.01 mmol, 1 eq) was added. Upon completion as determined by LC-MS volatiles were removed and crude residue portioned between H₂O (50 mL) and EtOAc (50 mL) and set. The aqueous was further extracted with EtOAc (50 mL x 3). Organics were combined, dried over MgSO₄, concentrated under vacuum, and purified RP flash chromatography (H₂O:MeCN, 0.1% formic acid, 100-10%) and prep-HPLC (HPLC-method D). Collected fractions were concentrated under vacuum and lyophilised, to afford the title compound as a white residue (38 mg, 8%).

HRMS *m/z* (ESI-TOF+) calculated for C₃₂H₄₀N₄O₃ [M+H]⁺: 547.3100
found: 547.3109 [M+H]⁺



¹H NMR (DMSO) δ_{H} 8.23 (d, *J* = 1.5 Hz, 1H, 1-methylpiperidin-1-ium ring NH⁺), 7.25 (dd, *J* = 8.5, 5.7 Hz, 2H, 4-fluorophenyl ring 3-

6. Experimental

H, 5-H), 7.16 – 7.04 (m, 4H, 4-fluorophenyl 2-H, 6-H, Ar ring 2-H, 6-H), 7.00 (d, $J = 7.2$ Hz, 1H, indoline ring 7-H), 6.95 (t, $J = 7.7$ Hz, 1H, indoline ring 3-H), 6.91 – 6.83 (m, 3H, ureido NH, Ar ring 3-H, 5-H), 6.59 – 6.44 (m, 2H, indoline ring 3-H, 4-H), 4.42 (s, 2H, 4-fluorophenyl ring 1-CCH₂), 4.20 (d, $J = 5.6$ Hz, 2H, Ar ring 1-CCH₂), 4.06 (p, $J = 5.5$ Hz, 1H, chiral HC), 3.95 (h, $J = 4.6$ Hz, 3H, 1-methylpiperidin-1-ium ring 4-H, Ar ring 4-COCH₂), 3.53 – 3.36 (m, 2H, indoline ring 2-H), 3.29 – 3.15 (m, 1H, H_aCNH⁺), 3.11 (dd, $J = 13.9, 6.1$ Hz, 1H, H_bCNH⁺), 2.89 (t, $J = 8.4$ Hz, 2H, indoline ring 3-H), 2.81 (d, $J = 11.2$ Hz, 2H, 1-methylpiperidin-1-ium ring 2-H), 2.19 (d, $J = 1.8$ Hz, 3H, 1-methylpiperidin-1-ium ring CH₃), 2.05 (t, $J = 11.7$ Hz, 2H, 1-methylpiperidin-1-ium ring 6-H), 1.60 (tt, $J = 12.4, 6.8$ Hz, 2H, 1-methylpiperidin-1-ium ring 3-H), 1.46 (d, $J = 13.1$ Hz, 2H, 1-methylpiperidin-1-ium ring 5-H).

¹³C NMR (DMSO) δ_c 164.0 (HCOOH), 160.9 (d, $^1J_{CF} = 241.6$ Hz, 4-fluorophenyl ring 4-C), 157.5 (C=O), 157.3 (Ar ring 4-C), 152.7 (indoline ring 7_a-C), 137.0 (d, $^4J_{CF} = 2.9$ Hz, 4-fluorophenyl ring 1-C), 133.2 (Ar ring 1-C), 129.1 (indoline ring 5_a-C), 128.3 (d, $^3J_{CF} = 7.9$ Hz, 4-fluorophenyl ring 2-C, 6-C), 128.2 (Ar ring 3-C, 5-C), 127.1 (indoline ring 3-C), 124.1 (indoline ring 3-C), 116.8 (indoline ring 3_a-C), 114.8 (d, $^2J_{CF} = 21.2$ Hz, 4-fluorophenyl ring 3-C, 5-C), 114.1 (Ar ring 3-C, 5-C), 106.3 (indoline ring 4-C), 70.2 (Ar ring 4-COCH₂), 67.6 (chiral C), 54.5 (indoline ring 3-C), 54.1 (indoline ring 2-C), 52.6 (H₂CNH⁺), 52.0 (1-methylpiperidin-1-ium ring 4-C), 45.2 (1-methylpiperidin-1-ium ring CH₃), 44.0 (4-fluorophenyl ring 1-

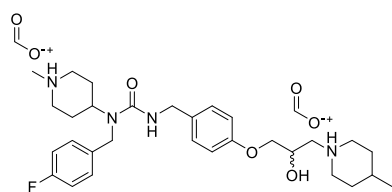
6. Experimental

CCH₂), 43.1 (Ar ring 1-C_qH₂), 29.4 (1-methylpiperidin-1-ium ring 2-C, 6-C), 28.2 (1-methylpiperidin-1-ium ring 3-C, 5-C).

1-(3-(4-((3-(4-Fluorobenzyl)-3-(1-methylpiperidin-1-ium-4-yl)ureido)methyl)phenoxy)-2-hydroxypropyl)-4-methylpiperidin-1-ium (18I)

1-(4-(Aminomethyl)phenoxy)-3-(4-methylpiperidin-1-yl)propan-2-ol (**38i**) (64 mg, 0.15 mmol) was dissolved in anhydrous DCM (5 mL) under N₂ and stirred. CDI (27 mg, 0.17 mmol, 1.1 eq) was added after 5 minutes. After formation of a mono-substituted imidazole intermediate species as determined by LC-MS *N*-(4-fluorobenzyl)-1-methylpiperidin-4-amine (31 μ l, 0.15 mmol, 1 eq) was added. Upon completion as determined by LC-MS volatiles were removed and crude residue portioned between H₂O (50 mL) and EtOAc (30 mL) and set. The aqueous was further extracted with EtOAc (30 mL x 3). Organics were combined, dried over MgSO₄, concentrated under vacuum, and purified by prep-HPLC (HPLC-method D). Collected fractions were concentrated under vacuum and lyophilised to afford the title compound as a clear residue (13 mg, 14%).

HRMS *m/z* (ESI-TOF+) calculated for C₃₀H₄₄N₄O₃ [M+H]⁺: 527.3400
found: 527.3400 [M+H]⁺



¹H NMR (DMSO) δ _H 8.25 (s, 2H, 1-methylpiperidin-1-ium-4-yl ring NH⁺, 1-methylpiperidin-1-ium ring NH⁺), 7.24 (dd, *J* = 8.4, 5.6 Hz, 2H, 4-fluorophenyl ring 3-H, 5-H), 7.11 (dt, *J* = 8.6, 4.6 Hz, 4H, 4-fluorophenyl

6. Experimental

2-H, 6-H, Ar ring 2-H, 6-H), 6.90 (t, $J = 5.7$ Hz, 1H, ureido NH), 6.85 (d, $J = 8.3$ Hz, 2H, Ar ring 3-H, 5-H), 4.41 (s, 2H, 4-fluorophenyl ring 1-CCH₂), 4.19 (d, $J = 5.5$ Hz, 2H, Ar ring 1-CCH₂), 4.12 – 3.96 (m, 2H, chiral HC, 1-methylpiperidin-1-ium ring 4-H), 3.92 (dd, $J = 10.1, 4.1$ Hz, 1H, Ar ring 4-COCH_a), 3.85 (dd, $J = 10.0, 5.7$ Hz, 1H, Ar ring 4-COCH_b), 3.06 (t, $J = 13.0$ Hz, 2H, 1-methylpiperidin-1-ium-4-yl ring 2-H), 2.91 (d, $J = 11.4$ Hz, 2H, 1-methylpiperidin-1-ium ring 2-H), 2.77 – 2.57 (m, 2H, H₂CNH), 2.38 – 2.19 (m, 7H, 1-methylpiperidin-1-ium-4-yl ring 6-H, 1-methylpiperidin-1-ium ring 6-H, 1-methylpiperidin-1-ium ring CH₃), 1.75 – 1.58 (m, 4H, 1-methylpiperidin-1-ium-4-yl ring 3-H, 1-methylpiperidin-1-ium ring 3-H), 1.49 (d, $J = 12.2$ Hz, 2H, 1-methylpiperidin-1-ium ring 5-H), 1.47 – 1.32 (m, 1H, 1-methylpiperidin-1-ium-4-yl 4-H), 1.24 (td, $J = 12.2, 3.7$ Hz, 2H, 1-methylpiperidin-1-ium-4-yl ring 5-H), 0.89 (d, $J = 6.4$ Hz, 3H, 1-methylpiperidin-1-ium-4-yl ring 4-CHCH₃).

¹³C NMR (DMSO) δ_c 164.3 (HCOOH), 160.9 (d, $^1J_{CF} = 241.5$ Hz, 4-fluorophenyl ring 4-C), 157.5 (C=O), 157.3 (Ar ring 4-C), 136.8 (d, $^4J_{CF} = 3.1$ Hz, 4-fluorophenyl ring 1-C), 133.2 (Ar ring 1-C), 128.3 (d, $^3J_{CF} = 8.0$ Hz, 4-fluorophenyl ring 2-C, 6-C), 128.2 (Ar ring 2-C, 6-C), 114.8 (d, $^2J_{CF} = 21.2$ Hz, 4-fluorophenyl ring 3-C, 5-C), 114.1 (Ar ring 3-C, 5-C), 70.8 (Ar ring 4-COCH₂), 65.5 (chiral C), 60.4 (H₂CNH⁺), 54.1 (1-methylpiperidin-1-ium ring 2-C, 6-C), 53.7 (1-methylpiperidin-1-ium-4-yl ring 2-C), 53.19 (1-methylpiperidin-1-ium-4-yl ring 6-C), 51.5 (1-methylpiperidin-1-ium ring 4-C), 44.4 (1-methylpiperidin-1-ium ring CH₃), 44.1 (4-fluorophenyl ring 1-CCH₂), 43.1 (Ar ring 1-CCH₂), 32.7 (1-methylpiperidin-1-ium-4-yl ring 5-C),

6. Experimental

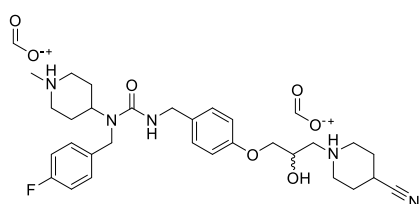
32.6 (1-methylpiperidin-1-ium-4-yl ring 3-C), 29.4 (1-methylpiperidin-1-ium-4-yl ring 4-C), 28.1 (1-methylpiperidin-1-ium ring 3-C, 5-C), 21.5 (1-methylpiperidin-1-ium-4-yl ring 4-CH₂CH₃).

4-Cyano-1-(3-(4-((3-(4-fluorobenzyl)-3-(1-methylpiperidin-1-ium-4-yl)ureido)methyl)phenoxy)-2-hydroxypropyl)piperidin-1-ium (18m)

1-(3-(4-(Ammoniomethyl)phenoxy)-2-hydroxypropyl)-4-cyanopiperidin-1-ium (**38j**) (200 mg, 0.55 mmol) was dissolved in anhydrous DCM (10 mL) and triethylamine (200 μ l, 1.38 mmol, 2.5 eq) under N₂ and stirred. CDI (98 mg, 0.61 mmol, 1.1 eq) was added after 5 minutes. After formation of a mono-substituted imidazole intermediate species as determined by LC-MS *N*-(4-fluorobenzyl)-1-methylpiperidin-4-amine (122 μ l, 0.55 mmol, 1 eq) was added. Upon completion as determined by LC-MS volatiles were removed and crude residue portioned between H₂O (50 mL) and EtOAc (30 mL) and separated. The aqueous was further extracted with EtOAc (30 mL x 3). Organics were combined, dried over MgSO₄, concentrated under vacuum, and purified by prep-HPLC (HPLC-method D). Collected fractions were concentrated under vacuum and lyophilised to afford the title compound as a clear residue (30 mg, 14%).

HRMS *m/z* (ESI-TOF+) calculated for C₃₀H₄₅N₄O₃ [M+H]⁺: 539.7000
found: 539.7000 [M+H]⁺

6. Experimental



¹H NMR (DMSO) δ_{H} 8.24 (s, 2H, 1-methylpiperidin-1-ium ring NH⁺, 4-cyanomethylpiperidin-1-ium-

4-yl ring NH⁺), 7.24 (dd, $J = 8.4, 5.5$ Hz, 2H, 4-fluorophenyl ring 3-H, 5-H), 7.15 – 7.07 (m, 4H, 4-fluorophenyl ring 2-H, 6-H, Ar ring 2-H, 6-H), 6.90 (t, $J = 5.8$ Hz, 1H, ureido NH), 6.84 (d, $J = 8.3$ Hz, 2H, Ar ring 3-H, 5-H), 4.41 (s, 2H, 4-fluorophenyl ring 4-CCH₂), 4.18 (d, $J = 5.5$ Hz, 2H, Ar ring 1-CCH₂), 4.06 – 3.96 (m, 1H, 1-methylpiperidin-1-ium ring 4-H), 3.94 – 3.87 (m, 2H, Ar ring 4-COCH₂), 3.86 – 3.77 (m, 1H, chiral HC), 2.92 (d, $J = 11.3$ Hz, 2H, 1-methylpiperidin-1-ium ring 2-H), 2.88 – 2.80 (m, 1H, 4-cyanomethylpiperidin-1-ium-4-yl ring 4-H), 2.64 – 2.59 (m, 2H, 4-cyanomethylpiperidin-1-ium-4-yl ring 2-H), 2.49 – 2.17 (m, 9H, 1-methylpiperidin-1-ium ring CH₃, 1-methylpiperidin-1-ium ring 6-H, H₂CNH⁺, 4-cyanomethylpiperidin-1-ium-4-yl ring 6-H), 1.89 – 1.79 (m, 2H, 4-cyanomethylpiperidin-1-ium-4-yl ring 3-H), 1.76 – 1.60 (m, 4H, 1-methylpiperidin-1-ium ring 3-H, 4-cyanomethylpiperidin-1-ium-4-yl ring 5-H), 1.50 (d, $J = 11.3$ Hz, 2H, 1-methylpiperidin-1-ium ring 5-H).

¹³C NMR (DMSO) δ_{C} 164.6 (HCOOH), 161.4 (d, $^1J_{\text{CF}} = 241.7$ Hz, -4-fluorophenyl ring 4-C), 158.0 (C=O), 157.9 (Ar ring 4-C), 137.3 (d, $^4J_{\text{CF}} = 3.23$ Hz, 4-fluorophenyl ring 1-C), 133.6 (Ar ring 1-C), 128.8 (d, $^3J_{\text{CF}} = 8.0$ Hz, 4-fluorophenyl ring 2-C, 6-C), 128.6 (Ar ring 2-C, 6-C), 122.9 (nitrile CN), 115.3 (d, $^2J_{\text{CF}} = 21.1$ Hz, 4-fluorophenyl ring 3-C, 5-C), 114.6 (Ar ring 3-C, 5-C), 71.4 (Ar ring 4-COCH₂), 67.0 (chiral C), 61.6 (1-methylpiperidin-1-ium

6. Experimental

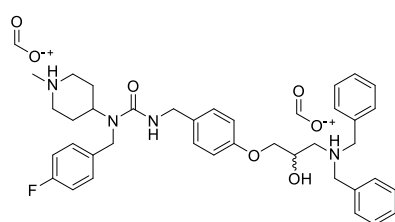
ring 4-C), 54.6 (4-fluorophenyl ring 1-C \underline{C} H₂), 52.2 (1-methylpiperidin-1-ium ring 2-C, 6-C), 51.9 (4-cyanomethylpiperidin-1-ium-4-yl ring 2-C, 6-C), 44.9 (1-methylpiperidin-1-ium ring CH₃), 44.5 (Ar ring 1-C \underline{C} H₂), 43.6 (H₂CNH⁺), 29.3 (1-methylpiperidin-4-yl ring 3-C, 5-C), 28.7 (4-cyanomethylpiperidin-1-ium-4-yl ring 3-C, 5-C), 25.5 (4-cyanomethylpiperidin-1-ium-4-yl ring 4-C).

4-(3-(4-(3-(Dibenzylammonio)-2-hydroxypropoxy)benzyl)-1-(4-fluorobenzyl)ureido)-1-methylpiperidin-1-ium (18n)

3-(4-(Ammoniomethyl)phenoxy)-*N,N*-dibenzyl-2-hydroxypropan-1-aminium (**38k**) (397 mg, 0.55 mmol) was dissolved in anhydrous DCM (10 mL) and triethylamine (200 μ l, 1.38 mmol, 2.5 eq) under N₂ and stirred. CDI (98 mg, 0.61 mmol, 1.1 eq) was added after 5 minutes. After formation of a mono-substituted imidazole intermediate species as determined by LC-MS *N*-(4-fluorobenzyl)-1-methylpiperidin-4-amine (122 μ l, 0.55 mmol, 1 eq) was added. Upon completion as determined by LC-MS volatiles were removed and crude residue portioned between H₂O (50 mL) and EtOAc (30 mL) and separated. The aqueous was further extracted with EtOAc (30 mL x 3). Organics were combined, dried over MgSO₄, concentrated under vacuum, and purified by silica gel column chromatography (eluent EtOAc, 100; and MeOH[1M NH₃]:DCM 0.5:99.5, 1:99, 2:98, 4:96) and prep-HPLC (HPLC-method D). Collected fractions were concentrated under vacuum and lyophilised to afford the title compound as a clear residue (21 mg, 5%).

6. Experimental

HRMS m/z (ESI-TOF+) calculated for $C_{36}H_{46}N_4O_3$ $[M+H]^+$: 625.3500
found: 625.3563 $[M+H]^+$



1H NMR (DMSO) δ_H 8.18 (d, $J = 1.0$ Hz, 4H, 1-methylpiperidin-1-ium ring NH⁺, 1-dibenzylammonio NH⁺), 7.43 – 7.19 (m, 12H, 4-fluorophenyl ring 3-H, 5-H, *N*-benzyl ring (2-H-6H)₂), 7.17 – 7.06 (m, 4H, 4-fluorophenyl 2-H, 6-H, Ar ring 2-H, 6-H), 6.91 (t, 1H, ureido NH), 6.73 (ddt, 2H, Ar ring 3-H, 5-H), 4.47 – 4.39 (m, 2H, 4-fluorophenyl ring 1-CCH₂), 4.24 – 4.14 (m, 2H, Ar ring 1-CCH₂), 4.03 (s, 1H, 1-methylpiperidin-1-ium ring 4-H), 3.96 (q, $J = 5.3$ Hz, 1H, chiral HC), 3.75 – 3.60 (m, 2H, *N*-benzyl (CH_a)₂), 3.58 – 3.47 (m, 2H, *N*-benzyl (CH_b)₂), 2.97 (d, 2H, 1-methylpiperidin-1-ium ring 2-H), 2.65 – 2.55 (m, 1H, H_aCNH⁺), 2.49 – 2.40 (m, 1H, H_bCNH⁺), 2.40 – 2.27 (m, 5H, 1-methylpiperidin-1-ium ring 6-H, 1-methylpiperidin-1-ium CH₃), 1.79 – 1.58 (m, 2H, 1-methylpiperidin-1-ium 3-H), 1.59 – 1.44 (m, 2H, 1-methylpiperidin-1-ium 5-H).

^{13}C NMR (DMSO) δ_C 163.6 (HCOOH) 163.5 (HCOOH), 160.9 (d, $^1J_{CF} = 241.8$ Hz, 4-fluorophenyl ring 4-C), 157.5 (C=O), 157.3 (Ar ring 4-C), 139.3 (*N*-benzyl ring 1-C), 136.7 (d, $^4J_{CF} = 2.02$ Hz, 4-fluorophenyl ring 1-C) 133.0 (Ar ring 1-C), 128.7 (*N*-benzyl ring (2-C, 6-C)₂), 128.3 (d, $^3J_{CF} = 8.1$ Hz, 4-fluorophenyl ring 2-C, 6-C), 128.7 (Ar ring 2-C, 6-C), 126.8 (*N*-benzyl ring (4-C)₂), 114.8 (d, $^2J_{CF} = 21.1$ Hz, 4-fluorophenyl ring 3-C, 5-C), 114.1 (Ar ring 3-C, 5-C), 114.0 (*N*-benzyl ring (3-C, 5-C)₂), 70.9, (Ar ring 4-COCH₂),

6. Experimental

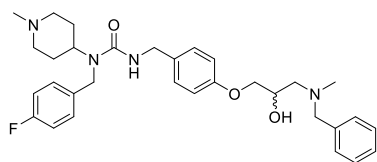
67.1 (chiral C), 58.4 (N-benzyl CH₂), 56.3 (H₂CNH⁺), 54.0 (1-methylpiperidin-1-ium 2-C, 6-C), 51.3 (1-methylpiperidin-1-ium ring 4-C), 44.2 (4-fluorophenyl ring 1-CCH₂, 1-methylpiperidin-4-yl ring CH₃), 43.1 (Ar ring 1-CCH₂), 28.6 (1-methylpiperidin-4-yl ring 3-C, 5-C).

3-(4-(3-(Benzyl(methyl)amino)-2-hydroxypropoxy)benzyl)-1-(4-fluorobenzyl)-1-(1-methylpiperidin-4-yl)urea (18o)

3-(4-(Ammoniomethyl)phenoxy)-N-benzyl-2-hydroxy-N-methylpropan-1-aminium (**38i**) (462 mg, 1.24 mmol) was dissolved in anhydrous DCM (10 mL) and triethylamine (420 µl, 2.50 mmol, 2.5 eq) under N₂ and stirred. CDI (220 mg, 1.36 mmol, 1.1 eq) was added after 5 minutes. After formation of a mono-substituted imidazole intermediate species as determined by LC-MS N-(4-fluorobenzyl)-1-methylpiperidin-4-amine (260 µl, 1.24 mmol, 1 eq) was added. Upon completion as determined by LC-MS volatiles were removed and crude residue partitioned between H₂O (30 mL) and EtOAc (20 mL) and separated. The aqueous was further extracted with EtOAc (20 mL x 3). Organics were combined, dried over MgSO₄, concentrated under vacuum, and purified by silica gel column chromatography (eluent EtOAc, 100; MeOH[1M NH₃]:DCM, 0.9:9.1, 0.3:9.7, and 0.4:9.6). Collected fractions were concentrated under vacuum to afford the title compound as a clear colourless oil (107 mg, 46%).

HRMS *m/z* (ESI-TOF+) calculated for C₃₂H₄₂N₄O₃ [M+H]⁺: 549.3200
found: 549.3235 [M+H]⁺

6. Experimental



¹H NMR (CDCl₃) δ_H 7.38 – 7.23 (m, 5H, *N*-benzyl ring 2-H-6H), 7.22 – 7.12 (m, 2H, 4-fluorophenyl ring 3-H, 5-H), 7.05 – 6.93 (m, 4H, Ar ring 2-H, 6-H, 4-fluorophenyl 2-H, 6-H), 6.83 – 6.74 (m, 2H, Ar ring 3-H, 5-H), 4.47 (t, *J* = 5.5 Hz, 1H, urea NH), 4.34 (s, 3H, 1-methylpiperidin-4-yl ring 4-H, 4-fluorophenyl ring 1-CCH₂), 4.27 (d, *J* = 5.4 Hz, 2H, Ar ring 1-CCH₂), 4.09 (dq, *J* = 9.4, 4.7 Hz, 1H, chiral HC), 3.92 (d, *J* = 4.9 Hz, 2H, Ar ring 4-COCH₂), 3.68 (d, *J* = 13.1 Hz, 1H, *N*-benzyl CH_a), 3.53 (d, *J* = 13.1 Hz, 1H, *N*-benzyl CH_b), 2.90 – 2.81 (m, 2H, 1-methylpiperidin-4-yl ring 2-H), 2.64 (dd, *J* = 12.4, 9.6 Hz, 1H, H_aCNH), 2.53 (dd, *J* = 12.4, 4.1 Hz, 1H, H_bCNH), 2.28 (s, 3H, *N*-methyl CH₃), 2.25 (s, 3H, 1-methylpiperidin-4-yl ring CH₃), 2.06 (td, *J* = 11.7, 3.0 Hz, 2H, 1-methylpiperidin-4-yl ring 6-H), 1.76 – 1.59 (m, 4H, 1-methylpiperidin-4-yl ring 3-H, 5-H).

¹³C NMR (CDCl₃) δ_C 162.1 (d, ¹*J*_{CF} = 245.8 Hz, 4-fluorophenyl ring 4-C), 158.17 (C=O), 158.0 (Ar ring 4-C), 138.4 (*N*-benzyl ring 1-C), 134.2 (d, ⁴*J*_{CF} = 3.1 Hz, 4-fluorophenyl ring 1-C), 131.8 (Ar ring 1-C), 129.1 (*N*-benzyl ring 2-C, 6-C), 128.7 (Ar ring 2-C, 6-C), 128.5 (*N*-benzyl ring 3-C, 5-C), 127.8 (d, ³*J*_{CF} = 8.0 Hz, 4-fluorophenyl ring 2-C, 6-C), 127.4 (*N*-benzyl ring 4-C), 115.8 (d, ²*J*_{CF} = 21.6 Hz, 4-fluorophenyl ring 3-C, 5-C), 114.6 (Ar ring 3-C, 5-C), 70.5 (Ar ring 4-COCH₂), 66.3 (chiral C), 62.7 (*N*-benzyl CH₂), 59.7 (H₂CNH), 55.3 (1-methylpiperidin-4-yl ring 2-H, 6-H), 52.3 (1-methylpiperidin-4-yl ring 4-C), 46.1 (1-methylpiperidin-4-yl ring CH₃), 45.2 (4-fluorophenyl ring

6. Experimental

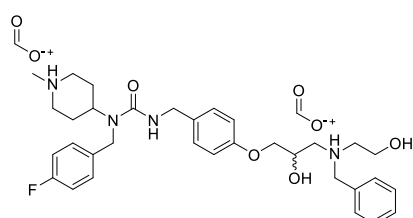
1-CCH₂), 44.5 (1-methylpiperidin-4-yl ring 4-C), 42.3 (*N*-methyl CH₃), 30.2 (1-methylpiperidin-4-yl ring 3-H, 5-H).

4-(3-(4-(3-(Benzyl(2-hydroxyethyl)ammonio)-2-hydroxypropoxy)benzyl)-1-(4-fluorobenzyl)ureido)-1-methylpiperidin-1-ium (18p)

3-(4-(Ammoniomethyl)phenoxy)-*N*-benzyl-2-hydroxy-*N*-(2-hydroxyethyl)propan-1-aminium (**38m**) (402 mg, 1.01 mmol) was dissolved in anhydrous DCM (10 mL) and triethylamine (350 μ L, 2.54 mmol, 2.5 eq) under N₂ and stirred. CDI (181 mg, 1.12 mmol, 1.1 eq) was added after 5 minutes. After formation of a mono-substituted imidazole intermediate species as determined by LC-MS *N*-(4-fluorobenzyl)-1-methylpiperidin-4-amine (210 μ L, 1.01 mmol, 1 eq) was added. Upon completion as determined by LC-MS volatiles were removed and crude residue partitioned between H₂O (50 mL) and EtOAc (30 mL) and set. The aqueous was further extracted with EtOAc (30 mL x 3). Organics were combined, dried over MgSO₄, concentrated under vacuum, and purified by silica gel column chromatography (eluent EtOAc, 100; and MeOH[1M NH₃]:DCM; 0.5:99.5, 1:99, 1.5:98.5, 4:96, and 6:94), and prep-HPLC (HPLC-method D). Collected fractions were concentrated under vacuum and lyophilised to afford the title compound as a clear residue (27 mg%).

HRMS *m/z* (ESI-TOF+) calculated for C₃₃H₄₄N₄O₄ [M+H]⁺: 579.3300
found: 579.3332 [M+H]⁺

6. Experimental



¹H NMR (CDCl₃) δ_H 8.36 (s, 2H, ammonio NH⁺, 1-methylpiperidin-1-ium ring NH⁺), 7.47 – 7.27 (m, 5H, *N*-benzyl ring 2-H-6H), 7.17 (dd, *J* = 8.5, 5.2 Hz, 2H, 4-fluorophenyl 3-H, 5-H), 7.08 – 6.87 (m, 4H, Ar ring 2-H, 6-H, 4-fluorophenyl 2-H, 6-H), 6.80 – 6.67 (m, 2H, Ar ring 3-H, 5-H), 4.63 (dt, *J* = 10.8, 4.7 Hz, 1H, ureido NH, 1-methylpiperidin-1-ium ring 4-H), 4.35 (s, 2H, 4-fluorophenyl ring 1-CCH₂), 4.24 (d, *J* = 5.5 Hz, 3H, 7, chiral HC), 4.03 (q, *J* = 13.5 Hz, 2H, CH₂OH), 3.93 (dd, *J* = 9.5, 5.3 Hz, 1H, Ar ring 4-COCH_a), 3.84 (dd, *J* = 9.5, 5.7 Hz, 1H, Ar ring 4-COCH_b), 3.79 (t, *J* = 5.1 Hz, 2H, *N*-benzyl CH₂), 3.46 (d, *J* = 11.8 Hz, 2H, 1-methylpiperidin-1-ium ring 2-H), 3.21 – 2.87 (m, 4H, H₂CNH⁺, CH₂CH₂OH), 2.69 (td, *J* = 12.6, 2.9 Hz, 2H, 1-methylpiperidin-1-ium ring 6-H), 2.64 (s, 1H, 1-methylpiperidin-4-yl ring CH₃), 2.15 (qd, *J* = 13.0, 4.1 Hz, 2H, 1-methylpiperidin-1-ium ring 3-H), 1.84 (d, *J* = 13.4 Hz, 2H, 1-methylpiperidin-1-ium ring 6-H).

¹³C NMR (CDCl₃) δ_C 167.3 (HCOOH), 162.3 (d, ¹*J*_{CF} = 246.6 Hz, 4-fluorophenyl ring 4-C), 158.2 (C=O), 157.7 (Ar ring 4-C), 134.4 (*N*-benzyl ring 1-C), 133.2 (d, ⁴*J*_{CF} = 3.03 Hz, 4-fluorophenyl ring 1-C), 131.8 (Ar ring 1-C), 130.3 (Ar ring 2-C, 6-C), 129.0 (*N*-benzyl ring 2-C, 6-C), 128.8 (*N*-benzyl ring 3-C, 5-C), 128.7 (*N*-benzyl ring 4-C), 127.7 (d, ³*J*_{CF} = 8.1 Hz, 4-fluorophenyl ring 2-C, 6-C), 116.1 (d, ²*J*_{CF} = 21.5 Hz, 4-fluorophenyl ring 3-C, 5-C), 114.6 (Ar ring 3-C, 5-C), 70.1 (Ar ring 4-COCH₂), 66.5 (chiral C), 59.8 (CH₂OH), 59.7 (*N*-benzyl CH₂), 57.6 (H₂CNH⁺), 57.1 (CH₂CH₂OH)

6. Experimental

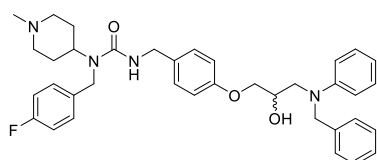
54.1 (1-methylpiperidin-1-ium ring 2-C, 6-C), 50.0 (11-methylpiperidin-1-ium ring 4-C), 45.3 (4-fluorophenyl ring 1-CCH₂), 44.5 (Ar ring 1-CCH₂), 43.6 (1-methylpiperidin-1-ium ring CH₃), 27.2 (1-methylpiperidin-1-ium ring 3-C, 5-C).

3-(4-(3-(Benzyl(phenyl)amino)-2-hydroxypropoxy)benzyl)-1-(4-fluorobenzyl)-1-(1-methylpiperidin-4-yl)urea (18q)

(4-(3-(Benzyl(phenyl)amino)-2-hydroxypropoxy)phenyl)methanaminium (**38n**) (545 mg, 1.25 mmol) was dissolved in anhydrous DCM (10 mL) and triethylamine (420 μ l, 3.14 mmol, 2.5 eq) under N₂ and stirred. CDI (224 mg, 1.38 mmol, 1.1 eq) was added after 5 minutes. After formation of a mono-substituted imidazole intermediate species as determined by LC-MS *N*-(4-fluorobenzyl)-1-methylpiperidin-4-amine (260 μ l, 1.25 mmol, 1 eq) was added. Upon completion as determined by LC-MS volatiles were removed and crude residue portioned between H₂O (50 mL) and EtOAc (30 mL) and set. The aqueous was further extracted with EtOAc (30 mL x 3). Organics were combined, dried over MgSO₄, concentrated under vacuum, and purified by NP flash chromatography (eluent MeOH[1M NH₃]:DCM, 0.5:99.5, 1:99, and 2:98). Collected fractions were concentrated under vacuum to afford the title compound as a clear residue (106 mg, 14%).

HRMS *m/z* (ESI-TOF+) calculated for C₃₇H₄₄N₄O₃ [M+H]⁺: 611.3300
found: 611.3365 [M+H]⁺

6. Experimental



¹H NMR (CDCl₃) δ_H 7.34 – 7.25 (m, 2H, *N*-benzyl ring 3-H, 5-H), 7.25 – 7.14 (m, 5H, *N*-benzyl ring 6-H, *N*-benzyl ring 4-H, *N*-benzyl ring 2-H, aniline ring 2-H, 6-H), 7.05 – 6.93 (m, 4H, Ar ring 2-H, 6-H, 4-fluorophenyl 2-H, 6-H), 6.81 – 6.68 (m, 5H, Ar ring 3-H, 5-H, aniline ring 3-H, 4-H, 5-H), 4.68 (d, *J* = 17.1 Hz, 1H, *N*-benzyl CH_a), 4.61 (d, *J* = 17.1 Hz, 1H, *N*-benzyl CH_b), 4.49 (t, *J* = 5.5 Hz, 1H, urea NH), 4.34 (m, 4H, 1-methylpiperidin-4-yl ring 4-H, 4-fluorophenyl ring 1-CCH₂, chiral HC), 4.28 (d, *J* = 5.4 Hz, 2H, Ar ring 1-CCH₂), 4.00 (dd, *J* = 9.5, 4.0 Hz, 1H, Ar ring 4-COCH_a), 3.93 (dd, *J* = 9.5, 5.5 Hz, 1H, Ar ring 4-COCH_b), 3.69 (dd, *J* = 15.0, 5.6 Hz, 1H, H_aCNH), 3.60 (dd, *J* = 15.0, 7.1 Hz, 1H, H_bCNH), 2.92 – 2.82 (m, 2H, 1-methylpiperidin-4-yl ring 2-H), 2.27 (s, 3H, 1-methylpiperidin-4-yl ring CH₃), 2.09 (td, *J* = 11.5, 3.5 Hz, 2H, 1-methylpiperidin-4-yl ring 6-H), 1.77 – 1.60 (m, 4H, 1-methylpiperidin-4-yl ring 3-H, 5-H).

¹³C NMR (CDCl₃) δ_C 162.0 (d, ¹*J*_{CF} = 246.0 Hz, 4-fluorophenyl ring 4-C), 158.1 (C=O), 157.6 (Ar ring 4-C), 148.6 (aniline ring 1-C), 138.4 (*N*-benzyl ring 1-C), 134.0 (d, ⁴*J*_{CF} = 3.1 Hz, 4-fluorophenyl ring 1-C), 132.1 (Ar ring 1-C), 129.3 (*N*-benzyl ring 2-C, 6-C), 128.7 (*N*-benzyl ring 3-C), 128.7 (*N*-benzyl ring 5-C), 127.7 (d, ³*J*_{CF} = 8.0 Hz, 4-fluorophenyl ring 2-C, 6-C), 126.9 (*N*-benzyl ring 4-C), 126.7 (Ar ring 2-C, 6-C), 117.3 (aniline ring 4-C), 115.8 (d, ²*J*_{CF} = 21.6 Hz, 4-fluorophenyl ring 3-C, 5-C), 114.6 (Ar ring 3-C, 5-C), 113.1 (aniline ring 2-C, 6-C), 69.7 (Ar ring 4-COCH₂), 68.3 (chiral C), 55.4 (*N*-benzyl CH₂), 55.2 (1-methylpiperidin-4-yl ring 2-C, 6-C), 54.2

6. Experimental

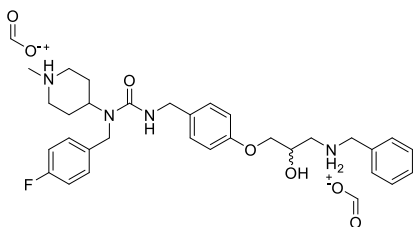
(H₂CNH), 52.1 (1-methylpiperidin-4-yl ring 4-C), 46.0 (1-methylpiperidin-4-yl ring CH₃), 45.7 (4-fluorophenyl ring 1-CCH₂), 44.3 (Ar ring 1-CCH₂), 30.0 (1-methylpiperidin-4-yl ring 3-C, 5-C).

4-(3-(4-(3-(Benzylammonio)-2-hydroxypropoxy)benzyl)-1-(4-fluorobenzyl)ureido)-1-methylpiperidin-1-ium (18r)

4-(3-(4-(3-(Dibenzylammonio)-2-hydroxypropoxy)benzyl)-1-(4-fluorobenzyl)ureido)-1-methylpiperidin-1-ium (**18n**) (264 mg, 0.42 mmol) was dissolved in EtOH (4 mL) and sonicated for 10 minutes. AcOH (1.16 mL) was then added, and the mixture saturated with H₂. The mixture was then transferred to Pd/C 10% (7 mg, 0.06 mmol, 0.1 eq) suspended in H₂O (2.28 mL) and stirred. After completion as determined by LC-MS Reaction mixture was filtered through Celite® and filter cake washed with MeOH (20 mL x 3). The reaction mixture was adjusted to basic, pH 9, with saturated bicarbonate solution and volatiles removed under vacuum. The remaining aqueous reaction mixture was extracted with EtOAc (30 mL x 3). Organics were dried over MgSO₄ and concentrated under vacuum to give crude residue purified by prep-HPLC (HPLC-method D). Collected fractions were concentrated under vacuum and lyophilised, to afford the title compound as a clear residue (60 mg, 27%).

HRMS *m/z* (ESI-TOF+) calculated for C₃₁H₄₀N₄O₃ [M+H]⁺: 535.3100, found: 535.3094 [M+H]⁺

6. Experimental



¹H NMR (DMSO) δ_{H} 8.24 (s, 2H, 1-methylpiperidin-1-ium ring NH⁺, benzylammonio NH⁺), 7.43 – 7.18 (m, 7H, 4-fluorophenyl ring 3-H, 5-H, *N*-

benzyl 2-H-6-H), 7.16 – 7.04 (m, 4H, Ar ring 2-H, 6-H, 4-fluorophenyl 2-H, 6-H), 6.94 – 6.86 (m, 1H, ureido NH), 6.83 (dt, $J = 8.7, 1.8$ Hz, 2H, Ar ring 3-H, 5-H), 4.41 (s, 2H, 4-fluorophenyl ring 1-CCH₂), 4.18 (m, 2H, Ar ring 1-CCH₂), 4.04 – 3.76 (m, 5H, 1-methylpiperidin-1-ium ring 4-H, chiral HC, Ar ring 4-COCH₂, *N*-benzyl CH₂), 2.91 – 2.74 (m, 3H, $\text{H}_{\text{a}}\text{CNH}^+$, 1-methylpiperidin-1-ium ring 2-H), 2.73 – 2.64 (m, 1H, $\text{H}_{\text{b}}\text{CNH}^+$), 2.19 (s, 3H, 1-methylpiperidin-1-ium ring CH₃), 2.07 (td, $J = 11.9, 2.1$ Hz, 2H, 1-methylpiperidin-1-ium ring 6-H), 1.61 (qd, $J = 12.5, 3.9$ Hz, 2H, 1-methylpiperidin-1-ium ring 3-H), 1.52 – 1.38 (m, 2H, 1-methylpiperidin-1-ium ring 5-H).

¹³C NMR (DMSO) δ_{C} 164.7 (HCOOH), 164.1 (HCOOH), 161.4 (d, $^1J_{\text{CF}} = 241.7$ Hz, 4-fluorophenyl ring 4-C), 158.0 (C=O), 157.7 (Ar ring 4-C), 137.4 (4-fluorophenyl ring 1-C), 133.7 (Ar ring 1-C), 129.1 (*N*-benzyl ring 2-C, 5-C), 128.8 (d, $^3J_{\text{CF}} = 9.0$ Hz, 4-fluorophenyl ring 2-C, 6-C), 128.6 (Ar ring 2-C, 6-C), 127.8 (*N*-benzyl ring 4-C), 115.2 (d, $^2J_{\text{CF}} = 21.1$ Hz, 4-fluorophenyl ring 3-C, 5-C), 114.6 (Ar ring 3-C, 5-C), 70.9 (Ar ring 4-COCH₂), 67.5 (chiral C), 54.9 (1-methylpiperidin-1-ium ring 2-C, 6-C), 52.5 (*N*-benzyl CH₂), 52.3 (1-methylpiperidin-1-ium ring 4-C), 51.3 (H_2CNH^+), 45.5 (1-

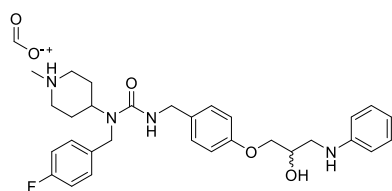
6. Experimental

methylpiperidin-1-ium ring CH₃), 44.5 (4-fluorophenyl ring 1-CCH₂), 43.5 (Ar ring 1-CCH₂), 78.0 (1-methylpiperidin-4-yl ring 3-C, 5-C).

4-(1-(4-Fluorobenzyl)-3-(4-(2-hydroxy-3-(phenylamino) propoxy) benzyl)ureido)-1-methylpiperidin-1-ium (18s)

3-(4-(3-(Benzyl(phenyl)amino)-2-hydroxypropoxy)benzyl)-1-(4-fluorobenzyl)-1-(1-methylpiperidin-4-yl)urea (**18q**) (84 mg, 0.16 mmol) was dissolved in EtOH (4 mL) and sonicated for 10 minutes. AcOH (1.16 mL) was then added, and the mixture saturated with H₂. The mixture was then transferred to Pd/C 10% (15 mg, 0.014 mmol, 0.1 eq) suspended in H₂O (2.28 mL) and stirred. After completion as determined by LC-MS Reaction mixture was filtered through Celite® and filter cake washed with MeOH (20 mL x 3). Filtrate was concentrated under vacuum to give crude residue, purified by silica gel column chromatography (eluent MeOH[1M NH₃]:DCM, 5.5:95.5), and prep-HPLC (HPLC-method D). Collected fractions were concentrated under vacuum and lyophilised, to afford the title compound as a clear residue (34 mg, 47%).

HRMS *m/z* (ESI-TOF+) calculated for C₃₀H₃₈N₄O₃ [M+H]⁺: 521.2900, found: 521.2915 [M+H]⁺



¹H NMR (CDCl₃) δ_H 8.38 (s, 1H, 1-methylpiperidin-1-ium ring NH⁺), 7.17 (dt, *J* = 8.3, 6.2 Hz, 4H, 4-fluorophenyl ring 3-H, 5-H, aniline ring 2-H, 6-H), 7.06 – 6.91 (m, 4H, 4-fluorophenyl ring 2-H, 6-H, Ar ring 2-

6. Experimental

H, 6-H), 6.79 (d, $J = 8.6$ Hz, 2H, Ar ring 3-H, 5-H), 6.73 (t, $J = 7.3$ Hz, 1H, aniline ring 4-H), 6.70 – 6.59 (m, 2H, aniline ring 3-H, 5-H), 4.67 – 4.56 (m, 2H, 1-methylpiperidin-1-ium ring 4-H, ureido NH), 4.34 (s, 2H, 4-fluorophenyl ring 1-CCH₂), 4.25 (d, $J = 5.4$ Hz, 2H, Ar ring 1-CCH₂), 4.22 (dd, $J = 7.6, 3.6$ Hz, 1H, chiral HC), 4.01 (dd, $J = 5.1, 3.8$ Hz, 2H, Ar ring 4-COCH₂), 3.48 – 3.33 (m, 3H, 1-methylpiperidin-1-ium ring 2-H, H_aCNH), 3.27 (dd, $J = 12.9, 7.1$ Hz, 1H, H_bCNH), 2.80 – 2.48 (m, 6H, 1-methylpiperidin-1-ium ring 6-H, 1-methylpiperidin-1-ium ring CH₃), 2.12 (qd, $J = 13.0, 4.1$ Hz, 2H, 1-methylpiperidin-1-ium ring 3-H), 1.86 – 1.76 (m, 2H, 1-methylpiperidin-1-ium ring 5-H).

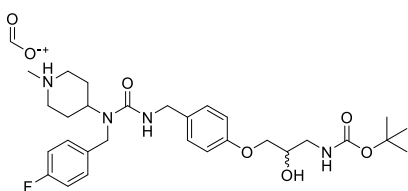
¹³C NMR (CDCl₃) δ_C 167.3 (HCOOH), 162.2 (d, $^1J_{CF} = 246.5$ Hz, 4-fluorophenyl ring 4-C), 158.0 (C=O), 157.7 (Ar ring 4-C), 148.1 (aniline ring 1-C), 133.2 (d, $^4J_{CF} = 3.2$ Hz, 4-fluorophenyl ring 1-C), 131.8 (Ar ring 1-C), 129.4 (aniline ring 3-C, 5-C), 128.7 (Ar ring 2-C, 6-C), 127.6 (d, $^3J_{CF} = 8.1$ Hz, 4-fluorophenyl ring 2-C, 6-C), 118.0 (aniline ring 4-C), 116.0 (d, $^2J_{CF} = 21.6$ Hz, 4-fluorophenyl ring 3-C, 5-C), 114.6 (Ar ring 3-C, 5-C), 113.3 (aniline ring 2-C, 6-C), 70.2 (Ar ring 4-COCH₂), 68.7 (chiral C), 54.0 (1-methylpiperidin-1-ium ring 4-C), 50.0 (4-fluorophenyl ring 1-CCH₂), 46.7 (1-methylpiperidin-1-ium ring 2-C, 6-C), 45.2 (H₂CN), 44.3 (Ar ring 1-CCH₂), 43.5 (1-methylpiperidin-1-ium ring CH₃), 27.3 (1-methylpiperidin-4-yl ring 3-C, 5-C).

6. Experimental

4-(3-(4-(3-((*tert*-Butoxycarbonyl)amino)-2-hydroxypropoxy)benzyl)-1-(4-fluorobenzyl)ureido)-1-methylpiperidin-1-ium (18t)

3-(4-((3-(4-Fluorobenzyl)-3-(1-methylpiperidin-4-yl)ureido)methyl)phenoxy)-2-hydroxypropan-1-aminium (**18a**) (120 mg, 0.27 mmol) was dissolved in MeOH (1.5 mL) and H₂O (1.5 mL). Boc₂O (70 mg, 0.32 mmol, 1.2 eq) was added, followed by NaHCO₃ (60 mg, 0.71 mmol, 2.6 eq). Upon completion as determined by LC-MS volatile solvents were removed under vacuum and aqueous extracted with EtOAc (10 mL x 3). Organics were then dried over MgSO₄, concentrated under vacuum, and purified by prep-HPLC (HPLC-method D). Collected fractions were concentrated under vacuum and lyophilised, to afford the title compound as a clear residue (40 mg, 27%).

HRMS *m/z* (ESI-TOF+) calculated for C₂₉H₄₂N₄O₅ [M+H]⁺: 545.3100, found: 545.3152 [M+H]⁺



¹H NMR (DMSO) δ_H 8.21 (s, 3H, 1-methylpiperidin-1-ium ring NH⁺), 7.24 (dd, *J* = 8.4, 5.5 Hz, 2H, 15, 17), 7.16 – 7.05 (m, 4H,

4-fluorophenyl ring 3-H, 5-H, Ar ring 2-H, 6-H), 6.90 (t, *J* = 5.7 Hz, 1H, ureido NH), 6.86 – 6.74 (m, 3H, Ar ring 3-H, 5-H, *N*-Boc NH), 4.41 (s, 2H, 4-fluorophenyl ring 1-CCH₂), 4.18 (d, *J* = 5.5 Hz, 2H, Ar ring 1-CCH₂), 4.11 – 3.95 (m, 1H, 1-methylpiperidin-1-ium ring 4-H), 3.86 (dd, *J* = 8.1, 5.6 Hz, 1H, Ar ring 4-COCH₃), 3.79 (h, *J* = 5.9 Hz, 2H, chiral HC, Ar ring 4-COCH₃),

6. Experimental

3.10 (dt, $J = 11.8, 5.7$ Hz, 1H, H_a -*N*-Boc), 3.05 – 2.86 (m, 3H, H_b -*N*-Boc, 1-methylpiperidin-1-ium ring 2-H), 2.29 (d, $J = 11.5$ Hz, 5H, 1-methylpiperidin-1-ium ring CH₃), 1-methylpiperidin-1-ium ring 6-H), 1.67 (dq, 2H, 1-methylpiperidin-1-ium ring 3-H), 1.50 (d, $J = 12.1$ Hz, 2H, 1-methylpiperidin-1-ium ring 5-H), 1.37 (d, $J = 1.1$ Hz, 9H, *N*-Boc (CH₃)₃).

¹³C NMR (DMSO) δ_c 164.0 (HCOOH), 160.9 (d, $^1J_{CF} = 241.4$ Hz, 4-fluorophenyl ring 4-C), 157.5 (C=O), 157.3 (Ar ring 4-C), 155.8 (*N*-Boc C=O), 136.8 (d, $^4J_{CF} = 3.0$ Hz, 4-fluorophenyl ring 1-C), 133.1 (Ar ring 1-C), 128.4 (d, $^3J_{CF} = 7.9$ Hz, 4-fluorophenyl ring 2-C, 6-C), 128.2 (Ar ring 2-C, 6-C), 114.8 (d, $^2J_{CF} = 21.3$ Hz, 4-fluorophenyl ring 3-C, 5-C), 114.1 (Ar ring 3-C, 5-C), 77.7 (*N*-Boc C(CH₃)₃), 70.4 (Ar ring 4-COCH₂), 68.2 (chiral C), 54.1 (1-methylpiperidin-1-ium ring 2-C, 6-C), 51.4 (1-methylpiperidin-1-ium ring 4-C), 44.3 (1-methylpiperidin-1-ium ring CH₃), 44.1 (4-fluorophenyl ring 1-CCH₂), 43.5 (H₂CN), 43.1 (Ar ring 1-CCH₂), 28.7 (1-methylpiperidin-4-yl ring 3-C, 5-C), 28.2 (*N*-Boc (CH₃)₃).

1-(4-Fluorobenzyl)-3-(4-hydroxybenzyl)-1-(1-methylpiperidin-4-yl)

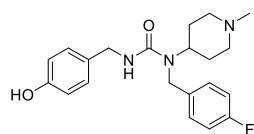
urea (33)

Under N₂ 4-hydroxybenzylamine (**32**) (0.67 g, 5.447 mmol) and CDI (1.06 g, 5.447 mmol, 1 eq) were dissolved in DMF (15 mL) and stirred. After visual disappearance of starting material and convergence to an intermediate determined by TLC (eluent MeOH[1M NH₃]:DCM, 10:90) *N*-(4-fluorobenzyl)-1-methylpiperidin-4-amine dissolved in DMF (10 mL) under N₂ was added. After visual disappearance of an intermediate determined by TLC (eluent MeOH[1M NH₃]:DCM, 10:90) H₂O was added

6. Experimental

(10 mL) and stirred for 1 hr. The reaction mixture was extracted with EtOAc (50mL x 3), dried over NaSO₄, suction filtered, and concentrated on vacuum, and purified by silica gel column chromatography (eluent (IMS:EtOAc, 1:3):cyclohexane, 95:5; NH₃.H₂O, 2%; and MeOH[1M NH₃]:DCM, 10:90) to afford the title compound as a clear semi-solid foam (1.05 g, 53%).

HRMS (TOF ES+) *m/z*: calculated for C₂₁H₂₈FN₃O₂ [M+H]⁺: 372.2000, found: 372.2400 [M+H]⁺



¹H NMR (CDCl₃) δ_H 7.09 – 7.00 (m, 2H, 4-fluorophenyl ring 3-H, 5-H), 6.92 – 6.83 (m, 2H, 4-fluorophenyl ring 2-H, 6-H), 6.82 – 6.73 (m, 2H, phenol ring 3-H, 5H), 6.60 – 6.52 (m, 2H, phenol ring 2-H, 6-H), 4.43 (t, *J* = 5.4 Hz, 1H, NHCH₂), 4.30 – 4.18 (m, 2H, 4-fluorophenyl ring 4-CH₂, piperidin-4-yl ring 4-CH), 4.15 (d, *J* = 5.4 Hz, 2H, NHCH₂), 2.85 – 2.76 (m, 2H, piperidin-4-yl ring 2-H), 2.18 (s, 3H, piperidin-4-yl ring N1-CH₃), 2.02 (m, 2H, piperidin-4-yl ring 6-H), 1.60 (m, 4H, piperidin-4-yl ring 3-H, 5-H).

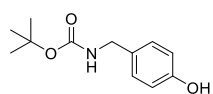
¹³C NMR (CDCl₃) δ_C 162.2 (d, ¹*J*_{CF} = 245.8 Hz, 4-fluorophenyl ring 4-C), 158.3 (C=O), 156.0 (phenol 4-C), 133.9 (d, ⁴*J*_{CF} = 3.17 Hz, 4-fluorophenyl ring 4-C), 130.47 (phenol 1-C), 128.8 (phenol 3-H, 5-H), 127.83 (d, ³*J*_{CF} = 8.06 Hz, 4-fluorophenyl ring 2-H, 6-H), 116.0 (4-fluorophenyl ring 3-H, 5-H), 115.8 (phenol 2-H, 6-H), 55.2 (piperidin-4-yl ring 2-C, 6-C), 52.2 (piperidin-4-yl ring 4-CH), 46.0 (4-fluorophenyl ring 4-CH₂), 45.4 (piperidin-4-yl ring N1-CH₃), 44.6 (NHCH₂), 29.8 (piperidin-4-yl ring 3-C, 5-C).

6. Experimental

tert-Butyl-(4-hydroxybenzyl)carbamate (35)

4-Hydroxybenzylamine (**32**) (2.700 g, 21.95 mmol) was dissolved in MeOH (30 mL) and H₂O (30 mL). Di-tert-butyl-dicarbonate (9.600 g, 43.99 mmol, 2 eq) was added and stirred for 5 minutes. NaHCO₃ (4.620 g, 90.58 mmol, 2.5 eq) was then added and stirred. After completion as determined by LC-MS (HPLC method A) the volatile solvent was removed under vacuum and aqueous extracted with EtOAc (50 mL x 3) to afford the title compound as a clear colourless oil (4.800 g, 98%) that was used without further purification.

LC-MS m/z calculated for C₁₂H₁₈NO₃ [M+H]⁺: 224.1, found: 224.10, t_R = 2.15 mins (HPLC-method A)



¹H NMR (CDCl₃) δ_H 7.07 (d, *J* = 8.0 Hz, 2H, Ar ring 2-H, 6-H), 6.77 (d, *J* = 8.5 Hz, 2H, Ar ring 3-H, 5-H), 4.97 (s, 1H, NH), 4.20 (d, *J* = 5.4 Hz, 2H, Ar ring 1-CCH₂), 1.46 (s, 9H, Boc (CH₃)₃).

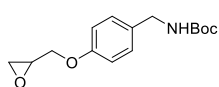
tert-Butyl-(4-(oxiran-2-ylmethoxy)benzyl)carbamate (36)

tert-Butyl-(4-hydroxybenzyl)carbamate (**35**) (4.600 g, 21.00 mmol) was dissolved in DMF (45 mL), sonicated for 10 minutes, flushed with N₂, stirred, and chilled to 0°C. NaH 60% in mineral oil (0.960 g, 24.15 mmol, 1.15 eq) was added. After cessation of effervescence epichlorohydrin (3.380 mL, 40.00 mmol, 2 eq) was added dropwise over 5 minutes. Upon completion as determined by LC-MS the volatile solvents were removed under vacuum and the crude residue portioned between H₂O (50 mL) and

6. Experimental

EtOAc (50 mL). The aqueous was then further extract with EtOAc (50 mL x 2), dried over MgSO₄, suction filtered, concentrated under vacuum, and purified via NP flash chromatography (eluent EtOAc: cyclohexane, 0-20%) to afford the title compound as a clear colourless oil (4.010 g, 68%).

LC-MS *m/z* calculated for C₁₅H₂₂NO₄ [M+H]⁺: 280.2, found: 280.20, t_R = 2.77 mins (HPLC-method A)



¹H NMR (CDCl₃) δ_H 7.19 (d, *J* = 8.2 Hz, 2H, oxiran-2-ylmethoxybenzyl ring 2-H, 6-H), 6.87 (d, *J* = 8.5 Hz, 2H, oxiran-2-ylmethoxybenzyl ring 3-H, 5-H), 4.80 (s, 1H, NH), 4.26 – 4.16 (m, 3H, oxirane ring 3-H_a, oxiran-2-ylmethoxybenzyl ring 4-CCH₂), 3.94 (dd, *J* = 11.0, 5.6 Hz, 1H, oxirane ring 3-H_b), 3.38 – 3.30 (m, 1H, oxirane ring OCH), 2.93 – 2.86 (m, 1H, oxirane ring 1-CCH_a), 2.74 (dd, *J* = 4.9, 2.6 Hz, 1H, oxirane ring 1-CCH_b), 1.45 (d, *J* = 1.0 Hz, 9H, Boc C(CH₃)₃).

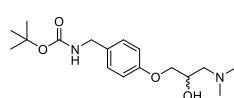
¹³C NMR (CDCl₃) δ_C 157.8 (oxiran-2-ylmethoxybenzyl ring 4-C), 155.9 (C=O), 131.7 (oxiran-2-ylmethoxybenzyl ring 1-C), 128.9 (oxiran-2-ylmethoxybenzyl ring 2-C, 6-C), 114.8 (oxiran-2-ylmethoxybenzyl ring 3-C, 5-C), 79.4 (Boc C(CH₃)₃), 68.8 (oxirane ring 1-CCH₂), 50.2 (oxirane ring 1-CCH₂), 44.7 (oxirane ring 3-C), 44.1 (oxiran-2-ylmethoxybenzyl ring 4-CCH₂), 28.4 (Boc C(CH₃)₃).

6. Experimental

tert-Butyl-(4-(3-(dimethylamino)-2-hydroxypropoxy)benzyl)carbamate (37a)

tert-Butyl-(4-(oxiran-2-ylmethoxy)benzyl)carbamate (**36**) (300 mg, 1.08 mmol) was dissolved in IPA (5 mL), stirred, and warmed to 70°C. Dimethylamine solution, 33 wt.% in EtOH (333 μ L, 1.62 mmol, 1.5 eq) was added. After completion as determined by LC-MS the solvent was removed under vacuum and remaining residue purified by silica gel column chromatography (eluent MeOH[1M NH₃]:DCM, 0.9:9.1) to afford the title compound as a clear colourless oil (296 mg, 85%).

LC-MS *m/z* calculated for C₁₇H₂₉N₂O₄ [M+H]⁺: 325.2, found: 325.20, *t_R* = 2.01 mins (HPLC-method A)



¹H NMR (CDCl₃) δ _H 7.10 (d, *J* = 8.5 Hz, 2H, Ar ring 3-H, 5-H), 6.82 – 6.74 (m, 2H, Ar ring 2-H, 6-H), 4.70 (s, 1H, NH), 4.14 (d, *J* = 5.8 Hz, 2H, Ar ring 1-CCH₂), 4.03 – 3.89 (m, 1H, chiral HC), 3.86 (d, *J* = 5.0 Hz, 2H, Ar ring 4-COCH₂), 2.45 (dd, *J* = 12.2, 9.8 Hz, 1H, H_aCN), 2.30 (dd, *J* = 12.2, 3.7 Hz, 1H, H_bCN), 2.23 (s, 5H, N(CH₃)₂), 1.36 (s, 9H, 19, Boc (CH₃)₃).

¹³C NMR (CDCl₃) δ _C 158.1 (Ar ring 6-C), 155.9 (C=O), 131.4 (Ar ring 4-C), 128.8 (Ar ring 3-C, 5-C), 114.7 (Ar ring 2-C, 6-C), 79.4 Boc C(CH₃)₃, 70.5 (Ar ring 4-COCH₂), 66.2 (chiral C), 61.8 (H₂CN), 45.6 (N(CH₃)₂), 44.2 (Ar ring 1-CCH₂), 28.4 Boc C(CH₃)₃. Missing: (Ar 1-C).

6. Experimental

tert-Butyl-(4-(3-(diethylamino)-2-hydroxypropoxy)benzyl)carbamate (37b)

tert-Butyl-(4-(oxiran-2-ylmethoxy)benzyl)carbamate (**36**) (300 mg, 1.08 mmol) was dissolved in IPA (3 mL), stirred, and warmed to 70°C. Diethylamine (170 μ L, 1.603 mmol, 1.5 eq) was added. After completion as determined by LC-MS the solvent was removed under vacuum and remaining residue purified by NP flash chromatography (eluent MeOH[1M NH₃]:DCM, 0-10%) to afford the title compound as a clear colourless oil (321 mg, 84%).

LC-MS *m/z* calculated for C₁₉H₃₃N₂O₄ [M+H]⁺: 353.2, found: 353.24, t_R = 2.05 mins (HPLC-method A)



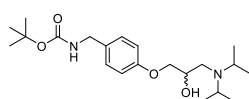
¹H NMR (CDCl₃) δ _H 7.19 (d, *J* = 8.4 Hz, 2H, Ar ring 3-H, 5-H), 6.92 – 6.84 (m, 2H, Ar ring 2-H, 6-H), 4.77 (s, 1H, NH), 4.23 (d, *J* = 5.8 Hz, 2H, Ar ring 1-CCH₂), 4.04 – 3.89 (m, 2H, Ar ring 4-COCH₂, chiral HC), 2.73 – 2.47 (m, 6H, CH₂N(CH₂)₂), 1.45 (s, 9H, Boc (CH₃)₃), 1.04 (t, *J* = 7.1 Hz, 3H, N(CH₂)₂(CH₃)₂).

¹³C NMR (CDCl₃) δ _C 158.2 (C=O), 155.9 (Ar ring 4-C), 131.2 (Ar ring 1-C), 128.8 (Ar ring 2-C, 6-C), 114.7 (Ar ring 3-C, 5-C), 79.4 (Boc C(CH₃)₃), 70.6 (chiral C), 65.8 (Ar ring 4-COCH₂), 55.9 (CH₂N(CH₂)₂), 47.3 (CH₂N(CH₂)₂), 44.2 (Ar ring 1-CCH₂), 28.4 (Boc (CH₃)₃), 12.0 (N(CH₂)₂(CH₃)₂).

**tert-Butyl-(4-(3-(diisopropylamino)-2-hydroxypropoxy)benzyl)-
carbamate (37c)**

tert-Butyl-(4-(oxiran-2-ylmethoxy)benzyl)carbamate (**36**) (500 mg, 1.43 mmol) was dissolved in IPA (5 mL), stirred, and warmed to 70°C. Diisopropylamine (300 μ l, 2.15 mmol, 1.5 eq) was added. After completion as determined by LC-MS the solvent was removed under vacuum and remaining residue purified by silica gel column chromatography (eluent MeOH[1M NH₃]:DCM, 0.5:9.5) to afford the title compound as a clear colourless oil (350 mg, 64%).

LC-MS m/z calculated for C₂₁H₃₇N₂O₄ [M+H]⁺: 381.3, found: 381.27, t_R = 2.18 mins (HPLC-method A)



¹H NMR (CDCl₃) δ _H 7.19 (d, *J* = 8.5 Hz, 2H, Ar ring 3-H, 5-H), 6.93 – 6.83 (m, 2H, Ar ring 2-H, 6-H), 4.77 (s, 1H, NH), 4.24 (d, *J* = 5.8 Hz, 2H, Ar ring 1-CCH₂), 4.03 – 3.85 (m, 3H, chiral HC, Ar ring 4-COCH₂), 3.07 (hept, *J* = 6.7 Hz, 2H, N(CH)₂), 2.71 (dd, 1H, H_aCN), 2.47 (dd, *J* = 13.3, 9.7 Hz, 1H, H_bCN), 1.45 (s, 9H, Boc (CH₃)₃), 1.11 – 1.00 (m, 12H, N(CH)₂(CH₃)₄).

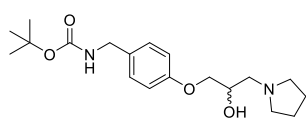
¹³C NMR (CDCl₃) δ _C 158.3 (Ar ring 4-C), 155.9 (C=O), 131.2 (Ar ring 1-C), 128.8 (Ar ring 2-C, 6-H), 114.7 (Ar ring 3-C, 5-C), 79.4 (Boc C(CH₃)₃), 70.9 (Ar ring 4-COCH₂), 65.5 (chiral C), 48.3 (N(CH)₂), 47.1 (H₂CN), 44.2 (Ar ring 1-CCH₂), 28.4 (Boc (CH₃)₃), 22.3 (NCH(CH₃)₂), 19.6 (NCH(CH₃)₂).

6. Experimental

tert-Butyl-(4-(2-hydroxy-3-(pyrrolidin-1-yl)propoxy)benzyl)carbamate (37d)

tert-Butyl-(4-(oxiran-2-ylmethoxy)benzyl)carbamate (**39**) (300 mg, 1.08 mmol) was dissolved in IPA (3 mL), stirred, and warmed to 70°C. Pyrrolidine (220 μ L, 1.605 mmol, 1.5 eq) was added. After completion as determined by LC-MS the solvent was removed under vacuum and remaining residue purified by silica gel column chromatography (eluent MeOH[1M NH₃]:DCM, 0.5:9.5) to afford the title compound as a clear colourless oil (296 mg, 78%).

LC-MS *m/z* calculated for C₁₉H₃₁N₂O₄ [M+H]⁺: 351.2, found: 351.20, *t_R* = 2.05 mins (HPLC-method A)



¹H NMR (CDCl₃) δ _H 7.09 (d, *J* = 8.3 Hz, 2H, Ar ring 3-H, 5-H), 6.82 – 6.74 (m, 2H, Ar ring 2-H, 6-H), 4.72 (s, 1H, NH), 4.14 (d, *J* = 5.7 Hz, 2H, Ar ring 1-CCH₂), 4.03 – 3.92 (m, 1H, chiral HC), 3.90 – 3.84 (m, 2H, Ar ring 4-COCH₂), 2.71 (dd, *J* = 12.1, 9.6 Hz, 1H, H_aCN), 2.65 – 2.55 (m, 2H, pyrrolidinyl ring 5-H), 2.43 (ddd, *J* = 12.1, 6.5, 2.7 Hz, 3H, H_bCN, pyrrolidinyl ring 2-H), 1.76 – 1.64 (m, 4H, pyrrolidinyl ring 3-H, 4-H), 1.36 (s, 9H, Boc (CH₃)₃).

¹³C NMR (CDCl₃) δ _C 158.3 (Ar ring 4-C), 156.0 (C=O), 131.4 (Ar ring 1-C), 128.9 (Ar ring 2-C, 6-C), 114.8 (Ar ring 3-C, 5-C), 79.5 (Boc C(CH₃)₃), 70.7 (Ar ring 4-COCH₂), 67.5 (chiral C), 58.6 (H₂CN), 54.3 (pyrrolidinyl ring 2-H,

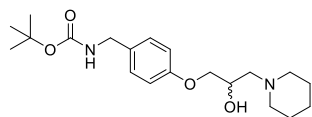
6. Experimental

5-H), 44.3 (Ar ring 1-C \underline{C} H $\underline{2}$), 28.5 (Boc (CH $\underline{3}$) $\underline{3}$), 23.8 (pyrrolidinyl ring 3-C, 4-C).

tert-Butyl-(4-(2-hydroxy-3-(piperidin-1-yl)propoxy)benzyl)carbamate (37e)

tert-Butyl-(4-(oxiran-2-ylmethoxy)benzyl)carbamate (**36**) (300 mg, 1.08 mmol) was dissolved in IPA (4 mL), stirred, and warmed to 70°C. Piperidine (160 μ L, 1.62 mmol, 1.5 eq) was added. After completion as determined by LC-MS the solvent was removed under vacuum and remaining residue purified by silica gel column chromatography (eluent MeOH[1M NH $\underline{3}$]:DCM, 0.9:9.1) to afford the title compound as a clear colourless oil (197 mg, 50%).

LC-MS m/z calculated for C $\underline{20}$ H $\underline{33}$ N $\underline{2}$ O $\underline{4}$ [M+H] $\underline{2}$ $\underline{+}$: 364.2, found: 366.20, t_R = 2.05 mins (HPLC-method A)



$^1\text{H NMR}$ (DMSO) δ_H 7.18 (d, J = 8.3 Hz, 2H, Ar 3-H, 5-H), 6.91 – 6.83 (m, 2H, Ar 2-H, 6-H), 4.78 (s, 1H, NH), 4.23 (d, J = 5.8 Hz, 2H, Ar ring 4-COCH $\underline{2}$), 4.08 (dq, J = 7.6, 5.2 Hz, 1H chiral HC), 4.01 – 3.89 (m, 2H, Ar ring 1-CCH $\underline{2}$), 2.67 – 2.58 (m, 2H, piperidinyl ring 2-H), 2.52 – 2.46 (m, 2H, H $\underline{2}$ CN), 2.40 (s, 2H, piperidinyl ring 6-H), 1.60 (dq, J = 9.6, 5.8 Hz, 4H, piperidinyl ring 3-H, 5-H), 1.46 – 1.43 (m, 11H, Boc (CH $\underline{3}$) $\underline{3}$, piperidinyl ring 4-H).

$^{13}\text{C NMR}$ (DMSO) δ_c 153.4 (Ar ring 4-C), 151.1 (C=O), 126.6 (Ar ring 1-C), 124.1 (Ar ring 2-C, 6-C), 110.0 (Ar ring 3-C, 5-C), 74.7 (Boc C(CH $\underline{3}$) $\underline{3}$), 65.8

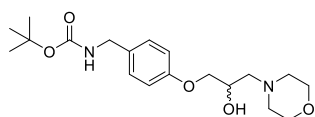
6. Experimental

(Ar ring 4-COCH₂), 60.5 (chiral C), 56.4 (CH₂CN), 50.0 (piperidiny ring 2-C, 6-C), 39.4 (Ar ring 1-CCH₂), 23.7 (Boc (CH₃)₃), 21.2 (piperidiny ring 3-C, 5-C), 19.4 (piperidiny ring 4-C).

tert-Butyl-(4-(2-hydroxy-3-morpholinopropoxy)benzyl)carbamate (37f)

tert-Butyl-(4-(oxiran-2-ylmethoxy)benzyl)carbamate (**39**) (300 mg, 1.08 mmol) was dissolved in IPA (4 mL), stirred, and warmed to 70°C. Morpholine (140 µl, 1.60 mmol, 1.5 eq) was added. After completion as determined by LC-MS the solvent was removed under vacuum and remaining residue purified by silica gel column chromatography (eluent MeOH[1M NH₃]:DCM, 0.6:9.4) to afford the title compound as a clear colourless oil (292 mg, 74%).

LC-MS *m/z* calculated for C₁₉H₃₁N₂O₅ [M+H]⁺: 367.2, found: 367.20, t_R = 2.13 mins (HPLC-method A)



¹H NMR (CDCl₃) δ_H 7.10 (d, *J* = 8.5 Hz, 2H, Ar ring 3-H, 5-H), 6.82 – 6.74 (m, 2H, Ar ring 2-H, 6-H), 4.69 (s, 1H, NH), 4.14 (d, *J* = 6.2 Hz, 2H, Ar ring 1-CCH₂), 4.01 (dq, *J* = 9.5, 4.9 Hz, 1H, chiral HC), 3.88 (d, *J* = 4.9 Hz, 2H, Ar ring 4-COCH₂), 3.70 – 3.57 (m, 4H, morpholino ring 2-H, 6-H), 2.57 (ddd, *J* = 11.6, 5.4, 3.8 Hz, 2H, morpholino ring 3-H), 2.52 – 2.32 (m, 2H, morpholino ring 5-H), 1.35 (s, 9H, Boc (CH₃)₃).

¹³C NMR (CDCl₃) δ_C 158.2 (Ar ring 1-C), 156.0 (C=O), 131.6 (Ar ring 4-C), 129.0 (Ar ring 2-C, 6-C), 114.8 (Ar ring 3-C, 5-C), 79.6 (Boc C(CH₃)₃), 70.4

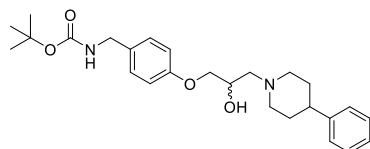
6. Experimental

(Ar ring 4-COCH₂), 67.1 (morpholino ring 2-C, 6-C), 65.5 (chiral C), 61.2 (CH₂N), 53.9 (morpholino ring 3-C, 5-C), 44.3 (Ar ring 1-CCH₂), 28.6 (Boc (CH₃)₃).

tert-Butyl-(4-(2-hydroxy-3-(4-phenylpiperidin-1-yl)propoxy)benzyl)- carbamate (37g)

tert-Butyl-(4-(oxiran-2-ylmethoxy)benzyl)carbamate (**36**) (300 mg, 1.08 mmol) was dissolved in IPA (4 mL), stirred, and warmed to 75°C. Phenyl-4-piperidine (260 mg, 1.88 mmol, 1.5 eq) was added. After completion as determined by LC-MS the solvent was removed under vacuum and remaining residue purified by (eluent MeOH[1M NH₃]:DCM, 1:9 and 2:8) to afford the title compound as an off-white semi solid (352 mg, 74%).

LC-MS m/z calculated for C₂₆H₃₇N₂O₄ [M+H]⁺: 441.3, found: 441.30, t_R = 2.46 mins (HPLC-method A)



¹H NMR (CDCl₃) δ_H 7.26 – 7.17 (m, 2H, phenyl ring 3-H, 5-H), 7.12 (ddd, J = 12.6, 7.7, 1.4 Hz, 5H, Ar ring 3-H, 5-H, phenyl ring 2-H, 4-H, 6-H), 6.84 – 6.75 (m, 2H, Ar ring 2-H, 6-H), 4.69 (s, 1H, NH), 4.15 (d, J = 5.9 Hz, 2H, Ar ring 1-CCH₂), 4.02 (dq, J = 9.4, 4.8 Hz, 1H, chiral HC), 3.89 (dd, J = 4.9, 0.9 Hz, 2H, Ar ring 4-COCH₂), 3.10 – 3.00 (m, 1H, H_aCN), 2.93 – 2.84 (m, 1H, H_bCN), 2.55 – 2.29 (m, 4H, phenylpiperidinyl ring 3-H, 5-H), 2.05 (td, J = 11.6, 2.6 Hz, 1H, phenylpiperidinyl 4-H), 1.81 – 1.58 (m, 4H, phenylpiperidinyl ring 2-H, 6-H), 1.36 (s, 9H, Boc (CH₃)₃).

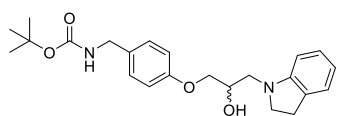
6. Experimental

¹³C NMR (CDCl₃) δ_c 158.2 (Ar ring 4-C), 155.9 (C=O), 146.1 (phenyl ring 1-C), 131.4 (Ar ring 1-C), 128.9 (Ar ring 2-C, 6-C), 128.5 (phenyl ring 3-C, 5-C), 126.8 (phenyl ring 2-C, 6-C), 126.3 (phenyl ring 4-C), 114.7 (Ar ring 3-C, 5-C), 79.4 (Boc C(CH₃)₃), 70.5 (Ar ring 4-COCH₂), 65.6 (chiral C), 60.8 (phenylpiperidiny ring 6-C), 56.1 (phenylpiperidiny ring 2-C), 53.0 (H₂CN), 44.2 (Ar ring 1-CCH₂), 42.4 (phenylpiperidiny ring 4-C), 33.7 (phenylpiperidiny ring 5-C), 33.4 (phenylpiperidiny ring 3-C), 28.4 (Boc (CH₃)₃).

tert-Butyl-(4-(2-hydroxy-3-(indolin-1-yl)propoxy)benzyl)carbamate (37h)

tert-Butyl-(4-(oxiran-2-ylmethoxy)benzyl)carbamate (**36**) (250 mg, 0.90 mmol) was dissolved in IPA (10 mL), stirred, and warmed to 75°C. Indoline (129 μl, 1.08 mmol, 1.2 eq) was added. After completion as determined by LC-MS the solvent was removed under vacuum and remaining residue purified by (eluent EtOAc:cyclohexane, 2:8) to the title compound as a purple oil (315 mg, 79%).

LC-MS m/z calculated for C₂₃H₃₁N₂O₄ [M+H]⁺: 399.2, found: 399.20, t_R = 2.33 mins (HPLC-method A)



¹H NMR (CDCl₃) δ_H 7.21 (d, J = 8.5 Hz, 2H, Ar ring 3-H, 5-H), 7.09 (ddd, J = 15.6, 7.7, 1.3 Hz, 2H, indoliny ring 6-H, 7-H), 6.90 (dt, J = 8.6 Hz, 2H, Ar ring 2-H, 6-H), 6.71 (td, J = 7.4, 0.9 Hz, 1H, indoliny ring 5-H), 6.56 (d, J = 7.8 Hz, 1H, indoliny ring 4-H), 4.81 (s, 1H,

6. Experimental

NH), 4.40 – 4.18 (m, 3H, Ar ring 1-CCH₂, chiral HC), 4.15 – 3.98 (m, 2H, Ar ring 4-COCH₂), 3.60 – 3.44 (m, 1H, indoliny ring 2-H_a), 3.43 – 3.29 (m, 2H, CH₂N, indoliny ring 2-H_b), 3.23 (dd, *J* = 13.8, 5.2 Hz, 1H, CH₂N), 3.01 (t, *J* = 8.3 Hz, 2H, indoliny ring 2-H), 2.73 (s, 1H, OH), 1.46 (s, 9H, Boc (CH₃)₃).

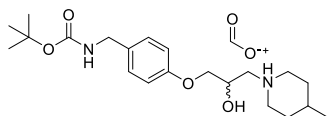
¹³C NMR (CDCl₃) δ_c 157.9 (Ar ring 4-C), 155.9 (C=O), 152.7 (indoliny ring 7_a-C), 131.6 (Ar ring 1-C), 129.8 (indoliny ring 3_a-C), 128.9 (indoliny ring 6-C), 127.4 (Ar ring 2-C, 6-C), 124.6 (indoliny ring 4-C), 118.4 (indoliny ring 5-C), 114.7 (Ar ring 3-C, 5-C), 107.2 (indoliny ring 7-C), 79.5 (Boc C(CH₃)₃), 70.0 (Ar ring 4-COCH₂), 68.4, (chiral C), 55.0 (CH₂N), 53.5 (indoliny ring 2-C), 44.2 (Ar ring 1-CCH₂), 28.8 (indoliny ring 3-C), 28.4 (Boc (CH₃)₃).

1-(3-(4-(((*tert*-Butoxycarbonyl)amino)methyl)phenoxy)-2-hydroxy propyl)-4-methylpiperidin-1-ium (37i)

tert-Butyl-(4-(oxiran-2-ylmethoxy)benzyl)carbamate (**36**) (200 mg, 0.73 mmol) was dissolved in IPA (5 mL), stirred, and warmed to 75°C. 4-methylpiperidine (75 μl, 0.78 mmol, 1.07 eq) was added. After completion as determined by LC-MS the solvent was removed under vacuum and remaining residue purified by RP flash chromatography (eluent H₂O:MeCN, 0.1% formic acid, 90-0%) and lyophilised afford the title compound as a clear residue (222 mg, 80%).

LC-MS *m/z* calculated for C₂₁H₃₅N₂O₄ [M+H]⁺: 379.3, found: 379.27, *t_R* = 2.35 mins (HPLC-method A)

6. Experimental



$^1\text{H NMR}$ (DMSO) δ_{H} 8.25 (s, 1H, NH^+), 7.30 (t, $J = 6.3$ Hz, 1H, NH), 7.14 (d, $J = 8.3$ Hz, 2H, Ar ring 3-H, 5-H), 6.87 (d, $J = 8.3$ Hz, 2H, Ar ring 2-H, 6-H), 4.04 (d, $J = 6.2$ Hz, 3H, chiral HC, Ar ring 1-C CH_2), 3.92 (dd, $J = 10.0, 4.1$ Hz, 1H, Ar ring 4-COCH $_a$), 3.85 (dd, $J = 10.0, 5.7$ Hz, 1H, Ar ring 4-COCH $_b$), 3.06 (t, $J = 13.3$ Hz, 2H, H_2CNH^+), 2.70 (dd, $J = 12.9, 4.8$ Hz, 1H, 1-methylpiperidin-1-ium ring 6-H $_a$), 2.60 (t, 1H, 1-methylpiperidin-1-ium ring 2-H $_a$), 2.33 (t, $J = 10.0$ Hz, 2H, 1-methylpiperidin-1-ium ring 6-H $_b$, 1-methylpiperidin-1-ium ring 2-H $_b$), 1.62 (d, $J = 15.2$ Hz, 2H, 1-methylpiperidin-1-ium ring 5-H), 1.51 – 1.13 (m, 13H, Boc (CH $_3$) $_3$, 1-methylpiperidin-1-ium ring 3-H, 4-H), 0.89 (d, $J = 6.4$ Hz, 3H, 1-methylpiperidin-1-ium ring 4-CHCH $_3$).

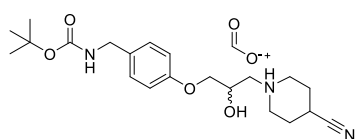
$^{13}\text{C NMR}$ (DMSO) δ_{C} 164.76 HCOOH, 157.9 (Ar ring 4-C), 156.2 (C=O), 132.8 (Ar ring 1-C), 128.7 (Ar ring 2-C, 6-C), 114.7 (Ar ring 3-C, 5-C), 78.1 (Boc C(CH $_3$) $_3$), 71.3 (Ar ring 4-COCH $_2$), 65.9 (chiral C), 60.8 (H_2CNH^+), 54.1 (1-methylpiperidin-1-ium ring 5-C), 53.6 (1-methylpiperidin-1-ium ring 2-C), 43.3 (Ar 1-CCH $_2$), 33.1 (1-methylpiperidin-1-ium ring 5-C), 33.1 (1-methylpiperidin-1-ium ring 3-C), 29.8 (1-methylpiperidin-1-ium ring 4-C), 28.7 (Boc (CH $_3$) $_3$), 22.0 (1-methylpiperidin-1-ium ring 4-CHCH $_3$)

6. Experimental

1-(3-(4-(((*tert*-Butoxycarbonyl)amino)methyl)phenoxy)-2-hydroxypropyl)-4-cyanopiperidin-1-ium (37j)

tert-Butyl-(4-(oxiran-2-ylmethoxy)benzyl)carbamate (**36**) (200 mg, 0.73 mmol) was dissolved in IPA (5 mL), stirred, and warmed to 75°C. Piperidine-4-nitrile (87 μ l, 0.78 mmol, 1.07 eq) was added. After completion as determined by LC-MS the solvent was removed under vacuum and remaining residue purified by RP flash chromatography (eluent H₂O:MeCN, 0.1% formic acid, 90-0%). Collected fractions were concentrated under vacuum and lyophilised to afford the title compound as a clear residue (281 mg, 99%).

LC-MS m/z calculated for C₂₁H₃₃N₃O₄ [M+H]⁺: 391.2, found: 391.25, t_R = 2.21 mins (HPLC-method A)



¹H NMR (DMSO) δ_H 8.15 (s, 1H, NH⁺),

7.24 – 7.15 (m, 1H, NH), 7.05 (d, J =

8.3 Hz, 2H, Ar ring 3-H, 5-H), 6.78 (d,

J = 8.2 Hz, 2H, Ar ring 2-H, 6-H), 6.71 – 6.66 (m, 1H, OH), 3.95 (d, J = 6.2 Hz, 3H, Ar ring 4-CCH₂, chiral HC), 3.83 (dd, J = 10.0, 4.1 Hz, 1H, Ar ring 4-COCH_a), 3.76 (dd, J = 10.0, 5.7 Hz, 1H, Ar ring 4-COCH_b), 3.06 – 2.94 (m, 2H, H₂CCHH⁺), 2.60 (dd, J = 13.0, 4.8 Hz, 1H, 4-cyanopropylpiperidin-1-ium ring 6-H_a), 2.50 (dd, J = 12.9, 7.5 Hz, 1H, 4-cyanopropylpiperidin-1-ium ring 6-H_b), 2.23 (t, J = 11.4 Hz, 2H, 4-cyanopropylpiperidin-1-ium ring 2-H), 2.05 (ddt, J = 10.9, 8.3, 4.1 Hz, 1H, 4-cyanopropylpiperidin-1-ium ring

6. Experimental

4-H), 1.68 – 1.48 (m, 4H, 4-cyanopropylpiperidin-1-ium ring 3-H, 5-H), 1.29 (s, 9H, Boc (CH₃)₃).

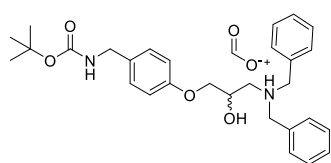
¹³C NMR (DMSO) δ_c 164.7 (HCOOH), 158.0 (C=O), 156.2 (Ar ring 4-C), 132.8, (Ar ring 1-C), 128.7 (Ar ring 2-C, 6-C), 114.7 (Ar ring 3-C, 5-C), 78.1 Boc C(CH₃)₃, 71.3 (Ar ring 4-COCH₂), 66.0 (chiral C), 60.8 (H₂CNH⁺), 53.6 (4-cyanopropylpiperidin-1-ium ring 6-C), 53.2 (4-cyanopropylpiperidin-1-ium ring 2-C), 43.3 (Ar ring 1-CCH₂), 41.0 (4-cyanopropylpiperidin-1-ium ring 4-C), 41.0 (4-cyanopropylpiperidin-1-ium ring 3-C, 5-C), 28.7 Boc (CH₃)₃. Not found (CN).

***N,N*-Dibenzyl-4-(4-(((*tert*-butoxycarbonyl)amino)methyl)phenoxy)-2-hydroxybutan-1-aminium (37k)**

tert-Butyl-(4-(oxiran-2-ylmethoxy)benzyl)carbamate (**36**) (350 mg, 1.13 mmol) was dissolved in IPA (10 mL), stirred, and warmed to 70°C. Dibenzylamine 97% (360 μl, 1.88 mmol, 1.5 eq) was added. After completion as determined by LC-MS the solvent was removed under vacuum and remaining residue purified by RP flash chromatography (H₂O:MeCN, 0.1% formic acid, 100-20%) to afford the title compound as clear colourless oil (250 mg, 48%).

LC-MS *m/z* calculated for C₂₉H₃₇N₂O₄ [M+H]⁺: 477.3, found: 477.30, t_R = 2.44 mins (HPLC-method A)

6. Experimental



¹H NMR (CDCl₃) δ_H 7.41 – 7.28 (m, 11H, NH⁺, *N*-benzyl ring (2-6H)₂), 7.17 (d, *J* = 8.3 Hz, 2H, Ar ring 3-H, 5-H), 6.78 (d, *J* = 8.6 Hz, 2H, Ar ring 2-H, 6-H), 4.84 (s, 1H, NH), 4.23 (d, *J* = 5.8 Hz, 2H, Ar ring 1-CCH₂), 4.16 (dq, *J* = 9.9, 5.2 Hz, 1H, chiral HC), 3.92 (d, *J* = 13.5 Hz, 2H, *N*-benzyl ring (CH_a)₂), 3.89 – 3.78 (m, 2H, Ar ring 4-COCH₂), 3.68 (dd, *J* = 13.4, 1.6 Hz, 20H, *N*-benzyl ring (C_b)₂), 2.91 – 2.60 (m, 2H, H₂CNH⁺), 1.46 (s, 1H, Boc (CH₃)₃).

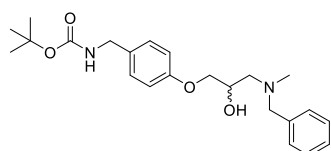
¹³C NMR (CDCl₃) δ_C 167.0 (C=O), 157.9 (HCOOH), 155.9 (Ar ring 4-C), 136.6 (*N*-benzyl ring 1-C), 131.4 (Ar ring 1-C), 129.6 (*N*-benzyl ring 2-C, 6-C), 128.8 (Ar ring 2-C, 6-C), 128.7 (*N*-benzyl ring 3-C, 5-C), 127.9 (*N*-benzyl ring 4-C), 114.6 (Ar ring 3-C, 5-C), 79.5 (Boc C(CH₃)₃), 70.2 (Ar ring 4-COCH₂), 66.1 (chiral C), 58.6, *N*-benzyl CH₂), 55.7 (H₂CNH⁺), 44.2 (Ar ring 1-CCH₂), 28.5 (Boc (CH₃)₃).

tert-Butyl-(4-(3-(benzyl(methyl)amino)-2-hydroxypropoxy)benzyl)carbamate (37I)

tert-Butyl-(4-(oxiran-2-ylmethoxy)benzyl)carbamate (**36**) (300 mg, 1.08 mmol) was dissolved in IPA (3 mL), stirred, and warmed to 70°C. *N*-methyl-1-phenylmethanamine (170 μl, 1.29 mmol, 1.2 eq) was added. After completion as determined by LC-MS the solvent was removed under vacuum and remaining residue purified by silica gel column chromatography (eluent DCM, 100, and MeOH[1M NH₃]:DCM, 2.5:7.5) to afford the title compound as a yellow oil (276 mg, 63%).

6. Experimental

LC-MS m/z calculated for $C_{23}H_{33}N_2O_4$ $[M+H]^+$: 401.2, found: 401.20, t_R = 2.76 mins (HPLC-method A)



1H NMR ($CDCl_3$) δ_H 7.37 – 7.22 (m, 5H, *N*-benzyl ring 2-6-H), 7.19 (d, J = 8.5 Hz, 2H, Ar ring 3-H, 5-H), 6.90 – 6.82 (m, 2H, Ar ring 2-H, 6-H), 4.77 (s, 1H, NH), 4.24 (d, J = 5.9 Hz, 2H, Ar ring 1-C CH_2), 4.11 (dq, J = 9.3, 4.7 Hz, 1H, chiral HC), 3.95 (d, J = 4.9 Hz, 2H, Ar ring 4-CO CH_2), 3.69 (d, J = 13.1 Hz, 1H, *N*-benzyl CH_a), 3.53 (d, J = 13.1 Hz, 1H, *N*-benzyl CH_b), 2.65 (dd, J = 12.3, 9.6 Hz, 1H, CH_aN), 2.54 (dd, J = 12.4, 4.1 Hz, 1H, CH_bN), 2.28 (s, 3H, *N*-methyl), 1.46 (s, 9H, Boc (CH_3) $_3$).

^{13}C NMR ($CDCl_3$) δ_C 158.1 (C=O), 155.9 (Ar ring 4-C), 138.3 (Ar ring 1-C), 131.3 (*N*-benzyl ring 1-C), 129.1 (Ar ring 2-C, 6-C), 128.8, (*N*-benzyl ring 4-C), 128.4 (*N*-benzyl ring 2-C, 6-C), 127.3 (*N*-benzyl ring 3-C, 5-C), 114.7 (Ar ring 3-C, 5-C), 77.2 (Boc $C(CH_3)_3$), 70.4 (Ar ring 4-CO CH_2), 66.2, (chiral C), 62.6 (*N*-benzyl CH_2), 59.7 (CH_2N), 44.2 (Ar ring 1-C CH_2), 42.2 (*N*-methyl), 28.4 (Boc (CH_3) $_3$).

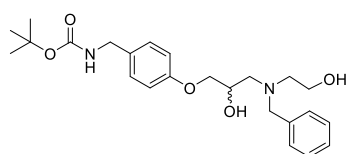
***tert*-Butyl-(4-(3-(benzyl(2-hydroxyethyl)amino)-2-hydroxypropoxy)benzyl)carbamate (37m)**

tert-Butyl-(4-(oxiran-2-ylmethoxy)benzyl)carbamate (**36**) (310 mg, 1.11 mmol) was dissolved in IPA (6 mL), stirred, and warmed to 75°C. 2-(Benzylamino)ethan-1-ol (240 μ L, 1.67 mmol, 1.5 eq) was added. After completion as determined by LC-MS the solvent was removed under vacuum and remaining residue purified by silica gel column

6. Experimental

chromatography (eluent MeOH[1M NH₃]:DCM, 4:6) to afford the title compound as a clear colourless oil (232 mg, 52%).

LC-MS *m/z* calculated for C₂₄H₃₅N₂O₅ [M+H]⁺: 431.3, found: 431.30, t_R = 2.22 mins (HPLC-method A)



¹H NMR (CDCl₃) δ_H 7.32 (d, *J* = 5.6 Hz, 5H, *N*-benzyl ring 2-6-H), 7.18 (d, *J* = 8.3 Hz, 2H, Ar ring 3-H, 5-H), 6.86 – 6.77 (m, 2H, Ar ring 2-H, 6-H), 4.78 (s, 1H, NH), 4.23 (d, *J* = 5.9 Hz, 2H, Ar ring 1-CCH₂), 4.06 (dq, *J* = 7.6, 5.0 Hz, 1H, chiral HC), 3.93 – 3.84 (m, 2H, Ar ring 4-COCH₂), 3.80 (d, *J* = 13.6 Hz, 1H, *N*-benzyl CH_a), 3.72 – 3.58 (m, 3H, *N*-benzyl CH_b, CH₂OH), 2.87 – 2.66 (m, 4H, H₂CNCH₂), 1.45 (s, 9H, Boc (CH₃)₃).

¹³C NMR (CDCl₃) δ_C 158.0 (Ar ring 4-C), 155.9 (C=O), 138.6 (*N*-benzyl ring 1-C), 131.5 (Ar ring 1-C), 129.0 (*N*-benzyl ring 2-C, 6-C), 128.9 (*N*-benzyl ring 4-C), 128.5 (*N*-benzyl ring 3-C, 5-C), 127.4 (Ar ring 2-C, 6-C), 114.6 (Ar ring 3-C, 5-C), 79.5 (Boc C(CH₃)₃), 70.3 (Ar ring 4-COCC₂H₂), 67.7 (chiral C), 59.8 (*N*-benzyl CH₂), 56.9 (H₂CN), 56.5 (NCH₂CH₂), 50.9 (NCH₂CH₂), 44.2 (Ar ring 1-CCH₂), 28.4 (Boc (CH₃)₃).

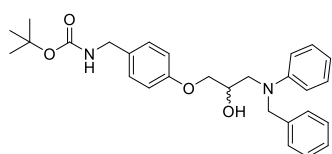
***tert*-Butyl-(4-(3-(benzyl(phenyl)amino)-2-hydroxypropoxy)benzyl)carbamate (37n)**

tert-Butyl-(4-(oxiran-2-ylmethoxy)benzyl)carbamate (**36**) (350 mg, 1.25 mmol) was dissolved in IPA (6 mL), stirred, and warmed to 75°C. *N*-Benzyaniline (300 µl, 1.88 mmol, 1.5 eq) was added. After completion as

6. Experimental

determined by LC-MS the solvent was removed under vacuum and remaining residue purified by RP flash chromatography (H₂O:MeCN, 0.1% formic acid, 100-10%) to afford the title compound as a clear residue (124 mg, 21%).

LC-MS *m/z* calculated for C₂₈H₃₅N₂O₄ [M+H]⁺: 463.3, found: 463.26, t_R = 2.17 mins (HPLC-method A)



¹H NMR (CDCl₃) δ_H 7.47 – 7.08 (m, 9H, Ar ring 3-H, 5-H, *N*-phenyl ring 2-6H, *N*-benzyl ring 2-H, 6-H), 7.04 – 6.78 (m, 4H, Ar ring 2-H, 6-H, *N*-benzyl ring 3-H, 5-H), 6.77 – 6.70 (m, 1H, *N*-benzyl ring 4-H), 4.82 (s, 1H, NH), 4.74 – 4.47 (m, 2H, *N*-benzyl CH₂), 4.35 (p, *J* = 7.0 Hz, 1H, chiral HC), 4.25 (d, *J* = 5.8 Hz, 2H, Ar 1-CCH₂), 4.03 (dd, *J* = 9.5, 4.1 Hz, 2H, 34), 3.96 (dd, *J* = 9.5, 5.4 Hz, 0H, 34), 3.70 (dd, *J* = 15.0, 5.6 Hz, 2H, Ar 1-COCH₂), 3.62 (dd, *J* = 15.0, 7.1 Hz, 2H, CH₂N), 1.47 (s, 9H, (Boc (CH₃)₃)).

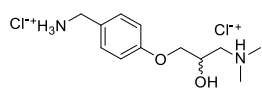
¹³C NMR (CDCl₃) δ_C 157.8 (C=O), 155.9 (Ar ring 4-C), 148.6 (*N*-phenyl ring 1-C), 138.4 (*N*-benzyl ring 1-C), 131.7 (Ar ring 1-C), 129.4 (Ar ring 2-C, 6-C), 128.9 (*N*-benzyl ring 4-C), 128.7 (*N*-phenyl ring 3-C, 5-C), 127.0 (*N*-benzyl ring 2-C 6-C), 126.7 (*N*-benzyl ring 3-C, 5-C), 117.3 (*N*-phenyl 4-C), 114.7 (Ar ring 3-C, 5-C), 113.1 (*N*-phenyl ring 2-C 6-C), 79.5 (Boc C(CH₃)₃), 69.8 (Ar 4-COCH₂), 68.3 (chiral C), 55.5 (CH₂N), 54.1 (*N*-benzyl CH₂), 44.2 (Ar ring 1-C), 28.5 (Boc (CH₃)₃).

6. Experimental

3-(4-(Ammoniomethyl)phenoxy)-2-hydroxy-*N,N*-dimethylpropan-1-aminium (38a)

tert-Butyl-(4-(3-(dimethylamino)-2-hydroxypropoxy)benzyl)carbamate (37a) (297 mg, 0.92 mmol) was dissolved in MeOH (0.2 mL), 4M HCl in 1, 4 dioxane (2 mL), and stirred. After completion as determined by LC-MS the solvent was removed under vacuum to afford the title compound as an off-white oil (250 mg, 93%), used without further purification.

LC-MS m/z calculated for $C_{12}H_{21}N_2O_2$ $[M+H]^+$: 225.2, found: 225.20, t_R = 0.40 mins (HPLC-method A)



1H NMR (DMSO) δ_H 10.28 (s, 1H, NH^+), 8.55 (s, 3H, NH_3^+), 7.44 (d, J = 8.4 Hz, 2H, Ar 2-H, 6-H), 6.98 (d, J = 8.5 Hz, 2H, Ar 3-H, 5-H), 6.05 (s, 1H, OH), 4.36 – 4.29 (m, chiral HC), 4.03 – 3.88 (m, 4H, Ar ring 1-CCH₂, Ar ring 4-COCH₂), 3.27 (s, 1H, H_aCNH^+), 3.23 – 3.13 (m, 1H, H_bCNH^+), 2.82 (d, J = 11.3 Hz, 6H, $NH^+(CH_3)_2$).

^{13}C NMR (DMSO) δ_c 158.8 (Ar ring 4-C), 131.1 (Ar ring 2-C, 6-C), 126.9 (Ar ring 1-C), 115.0 (Ar ring 3-C, 5-C), 70.6 (Ar ring 4-COCH₂), 64.3 (chiral C), 59.6, (H_2CNH^+), 44.2 (NH^+CH_3), 42.6 (NH^+CH_3), 42.0 (Ar ring 1-CCH₂).

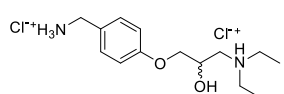
3-(4-(Ammoniomethyl)phenoxy)-*N,N*-diethyl-2-hydroxypropan-1-aminium (38b)

tert-Butyl-(4-(3-(diethylamino)-2-hydroxypropoxy)benzyl)carbamate (37b) (296 mg, 0.85 mmol) was dissolved in EtOAc (5 mL), 4M HCl in 1, 4 dioxane (2 mL), and stirred at 0°C allowing to come up to r.t. After

6. Experimental

completion as determined by LC-MS the solvent was removed under vacuum to afford the title compound as a white foam (275 mg, 106%), used without further purification.

LC-MS m/z calculated for $C_{14}H_{25}N_2O_2$ $[M+H]^+$: 253.2, found: 253.19, t_R = 0.42 mins (HPLC-method A)



1H NMR (DMSO) δ_H 10.15 (s, 1H, NH^+), 8.49 (s, 3H, NH_3^+), 7.47 – 7.41 (m, 2H, Ar 2-H, 6-H), 7.03 – 6.95 (m, 2H, Ar 3-H, 5-H), 6.01 (s, 1H, OH), 4.34 (td, J = 8.2, 4.1 Hz, 1H, chiral HC), 4.07 – 3.88 (m, 4H, Ar ring 1-CCH₂, Ar ring 4-COCH₂), 3.20 (ddt, J = 16.2, 9.4, 4.0 Hz, 4H, $H_2CNH^+(CH_2)_2$), 1.24 (t, J = 7.2 Hz, 6H, $(CH_3)_2$).

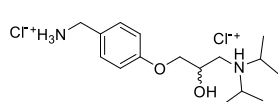
^{13}C NMR (DMSO) δ_c 158.8 (Ar ring 4-C), 131.1 (Ar ring 2-C, 6-C), 126.9 (Ar ring 1-C), 115.0 (Ar ring 3-C, 5-C), 70.4 (Ar ring 4-COCH₂), 54.2 ($H_2CNH^+(CH_2)_2$), 48.1 ($H_2CNH^+C_aH_2$), 47.4 ($H_2CNH^+C_bH_2$), 42.1 (Ar ring 1-CCH₂), 9.0 (C_aH_3), 8.9 (C_bH_3).

3-(4-(Ammoniomethyl)phenoxy)-2-hydroxy-*N,N*-diisopropylpropan-1-aminium (38c)

tert-Butyl-(4-(3-(diisopropylamino)-2-hydroxypropoxy)benzyl)carbamate (**37c**) (276 mg, 0.73 mmol) was dissolved in EtOAc (2 mL), 4M HCl in 1,4 dioxane (2 mL), and stirred. After completion as determined by LC-MS the solvent was removed under vacuum to afford the title compound as a white semi solid (240 mg, 93%), used without further purification.

6. Experimental

LC-MS m/z calculated for $C_{16}H_{28}N_2O_2$ $[M+H]^+$: 281.2, found: 281.22, t_R = 0.63 mins (HPLC-method A)



1H NMR (DMSO) δ_H 9.51 (s, 1H, NH^+), 8.45 (s, 3H, NH_3^+), 7.44 (d, J = 8.7 Hz, 2H, Ar 2-H, 6-H), 6.99 (d, J = 8.7 Hz, 2H, Ar 3-H, 5-H), 5.90 (d, J = 5.0 Hz, 1H, OH), 4.28 (s, 1H, chiral HC), 4.12 – 3.97 (m, 2H, Ar ring 4-COCH₂), 3.96 – 3.90 (m, 2H, Ar ring 1-CCH₂), 3.76 – 3.62 (m, 2H, $NH^+(CH_2)_2(CH_3CH_3)_2$), 3.34 – 3.24 (m, 1H, H_aCNH^+), 3.20 – 3.09 (m, 1H, H_bCNH^+), 1.40 – 1.31 (m, 9H, C_aH_3 , (C_bH_3)₂), 1.27 (d, J = 6.5 Hz, 3H, ($C_{aa}H_3$)).

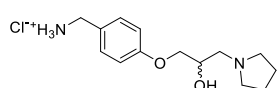
^{13}C NMR (DMSO) δ_c 58.8 (Ar ring 4-C), 131.1 (Ar ring 2-C, 6-C), 126.9 (Ar ring 1-C), 115.0 (Ar ring 3-C, 5-C), 69.9 (Ar ring 4-COCH₂), 66.1 (chiral C), 56.1, (NH^+C_aH), 55.1 (NH^+C_bH), 51.0 (H_2CNH^+), 42.1 (Ar ring 1-CCH₂), 18.9 (C_aH_3), 18.8 (C_bH_3), 17.5 ($C_{aa}H_3$), 16.5 ($C_{ba}H_3$).

(4-(2-Hydroxy-3-(pyrrolidin-1-yl)propoxy)phenyl)methanaminium (38d)

tert-Butyl-(4-(2-hydroxy-3-(pyrrolidin-1-yl)propoxy)benzyl)carbamate (37d) (365 mg, 1.04 mmol) was dissolved in EtOAc (6 mL), 4M HCl in 1, 4 dioxane (2 mL), and stirred. After completion as determined by LC-MS the solvent was removed under vacuum to afford a crude residue, purified by silica gel column chromatography (eluent MeOH[1M NH_3]:DCM, 18:82) to give the title compound as a white foam (167 mg, 56%).

6. Experimental

LC-MS m/z calculated for $C_{14}H_{23}N_2O_2$ $[M+H]^+$: 251.2, found: 251.20, t_R = 0.57 mins (HPLC-method A)



1H NMR (DMSO) δ_H 8.68 (s, 2H, NH_3^+), 7.47 – 7.37 (m, 1H, Ar 2-H, 6-H), 7.02 – 6.94 (m, 2H, Ar 3-H, 5-H), 5.59 (s, 1H, OH), 4.19 – 4.11 (m, 1H, chiral HC), 4.02 – 3.90 (m, 4H, Ar ring 1-CCH₂, Ar ring 4-COCH₂), 3.17 (s, 2H, piperidine ring 2-H_a, 5-H_a), 3.12 – 2.83 (m, 3H, H_2CNH^+ , piperidine ring 2-H_{aa}, 5-H_{aa}), 1.90 – 1.80 (m, 4H, piperidine ring 3-H, 4-H).

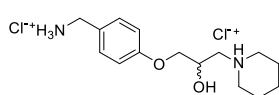
^{13}C NMR (DMSO) δ_c 159.0 (Ar ring 4-C), 131.0 (Ar ring 2-C, 6-C), 126.6 (Ar ring 1-C), 115.0 (Ar ring 3-C, 5-C), 70.7 (Ar ring 4-COCH₂), 66.0 (chiral C), 57.7 (H_2CNH^+), 54.4 (piperidine ring 2-C, 5-C), 42.3 (Ar ring 1-CCH₂), 23.2 (piperidine ring 3-C, 4-H).

1-(3-(4-(Ammoniomethyl)phenoxy)-2-hydroxypropyl)piperidin-1-ium (38e)

tert-Butyl-(4-(2-hydroxy-3-(piperidin-1-yl)propoxy)benzyl)carbamate (37e) (97 mg, 0.54 mmol) was dissolved in EtOAc (4 mL), 4M HCl in 1, 4 dioxane (2 mL), and stirred. After completion as determined by LC-MS the solvent was removed under vacuum to afford the title compound as a white foam (200 mg, 101%), used without further purification.

LC-MS m/z calculated for $C_{15}H_{25}N_2O_2$ $[M+H]^+$: 265.2, found: 269.20, t_R = 0.50 mins (HPLC-method A)

6. Experimental



$^1\text{H NMR}$ (DMSO) δ_{H} 10.17 (s, 1H, NH^+), 8.46 (s, 3H, NH_3^+), 7.43 (d, $J = 8.5$ Hz, 2H, Ar 2-H, 6-H), 6.99 (d, $J = 8.6$ Hz, 2H, Ar 3-H, 5-H), 5.98 (d, $J = 5.0$ Hz, 1H, OH), 4.41 (s, 1H, chiral HC), 3.96 (dt, $J = 7.7, 3.8$ Hz, 2H, Ar ring 4-COCH₂), 3.92 (s, 2H, Ar ring 1-CCH₂), 3.56 – 3.43 (m, 2H, H_2CNH^+), 3.25 (d, $J = 13.2$ Hz, 1H, piperidin-1-ium ring 2-H_a), 3.17 – 3.07 (m, 1H, piperidin-1-ium ring 2-H_b), 2.97 (s, 2H, piperidin-1-ium ring 6-H), 2.03 – 1.54 (m, 5H, piperidin-1-ium ring 3-H, 4-H_a, 5-H), 1.38 (d, $J = 12.6$ Hz, 1H, 4-H_b).

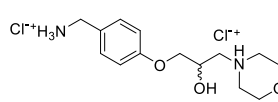
$^{13}\text{C NMR}$ (DMSO) δ_{C} 158.9 (Ar ring 4-C), 131.0 (Ar 2-C, 6-C), 127.0 (Ar ring 1-C), 115.1 (Ar 3-C, 5-C), 70.7 (Ar ring 4-COCH₂), 64.1 (chiral C), 59.4 (H_2CNH^+), 54.0 (piperidin-1-ium ring 2-C), 52.6 (piperidin-1-ium ring 6-C), 42.1 (Ar ring 1-CCH₂), 22.7, (piperidin-1-ium ring 3-C), 22.6 (piperidin-1-ium ring 3-C), 21.8 (piperidin-1-ium ring 4-C).

4-(3-(4-(Ammoniomethyl)phenoxy)-2-hydroxypropyl)morpholin-4-ium (38f)

tert-Butyl-(4-(2-hydroxy-3-morpholinopropoxy)benzyl)carbamate (**37f**) (292 mg, 0.80 mmol) was dissolved in EtOAc (4 mL), 4M HCl in 1, 4 dioxane (2 mL), and stirred. After completion as determined by LC-MS the solvent was removed under vacuum to afford the title compound as a white semi solid (239 mg, 86%), used without further purification.

LC-MS m/z calculated for $\text{C}_{14}\text{H}_{23}\text{N}_2\text{O}_3$ [$\text{M}+\text{H}$]⁺: 267.2, found: 267.17, $t_{\text{R}} = 0.50$ mins (HPLC-method A)

6. Experimental

**¹H NMR** (DMSO) δ_{H} 10.99 (s, 1H, NH⁺), 8.48 (s, 3H, NH₃⁺), 7.44 (d, J = 8.6 Hz, 2H, Ar 2-H, 6-H), 6.99 (d, J = 8.6 Hz, 2H, Ar 3-H, 5-H), 6.01 (s, 1H, OH), 4.50 – 4.41 (m, 1H, chiral HC), 4.09 – 3.74 (m, 9H, Ar ring 1-CCH₂, Ar ring 4-COCH₂, morpholin-4-ium ring 2-H, 6-H), 3.58 – 3.43 (m, 2H, morpholin-4-ium ring 3-H_a, 5-H_a), 3.35 (dt, J = 13.4, 3.2 Hz, 1H, H_bCNH⁺), 3.23 (dq, J = 7.9, 4.1 Hz, 3H, H_aCNH⁺, 3-H_b, 5-H_b).

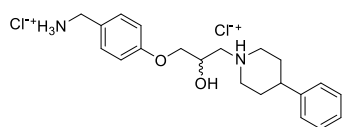
¹³C NMR (DMSO) δ_{C} 158.9 (Ar ring 4-C), 131.0 (Ar ring 2-C, 6-C), 126.9 (Ar ring 1-C), 115.1 (Ar ring 3-C, 5-C), 70.7 (Ar ring 4-COCH₂), 64.0 (chiral C), 63.6 (morpholin-4-ium ring 2-C), 63.5 (morpholin-4-ium ring 6-C), 59.4 (H₂CNH⁺), 53. morpholin-4-ium ring 3-C), 42.1 morpholin-4-ium ring (5-C).

1-(3-(4-(Ammoniomethyl)phenoxy)-2-hydroxypropyl)-4-phenylpiperidin-1-ium (38g)

tert-Butyl-(4-(2-hydroxy-3-(4-phenylpiperidin-1-yl)propoxy)benzyl) carbamate (**37g**) (322 mg, 0.73 mmol) was dissolved in MeOH (0.3 mL), 4M HCl in 1, 4 dioxane (2 mL), and stirred. After completion as determined by LC-MS the solvent was removed under vacuum to afford the title compound as a white semi-solid foam (303 mg, 101%), used without further purification.

LC-MS m/z calculated for C₂₁H₂₉N₂O₂ [M+H]⁺: 342.3, found: 342.33, t_{R} = 0.52 mins (HPLC-method A)

6. Experimental



$^1\text{H NMR}$ (DMSO) δ_{H} 10.62 (s, 1H, NH^+), 8.54 (s, 3H, NH_3^+), 7.49 – 7.41 (m, 2H, Ar 2-H, 6-H), 7.34 (dd, $J = 8.2, 6.9$ Hz, 2H, phenyl ring 2-H, 6-H), 7.28 – 7.18 (m, 3H, phenyl ring 3-H, 4-H, 5-H), 7.00 (d, $J = 8.7$ Hz, 2H, Ar 3-H, 5-H), 6.02 (s, 1H, OH), 4.49 (s, 1H, chiral HC), 4.07 – 3.96 (m, 2H, Ar ring 1- CCH_2), 3.92 (d, $J = 5.4$ Hz, 2H, Ar ring 4- COCH_2), 3.72 (d, $J = 12.3$ Hz, 1H, phenylpiperidin-1-ium ring 2- H_a), 3.63 (d, $J = 12.1$ Hz, 1H, phenylpiperidin-1-ium ring 6- H_a), 3.38 – 3.28 (m, 1H, phenylpiperidin-1-ium ring 2- H_b), 3.26 – 3.11 (m, 3H, H_2CNH^+ , phenylpiperidin-1-ium ring 6- H_b), 2.82 (t, $J = 3.7$ Hz, 1H, phenylpiperidin-1-ium ring 4-H), 2.27 – 2.08 (m, 2H, phenylpiperidin-1-ium ring 3-H), 1.94 (d, $J = 14.1$ Hz, 2H, phenylpiperidin-1-ium ring 5-H).

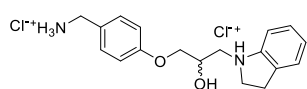
$^{13}\text{C NMR}$ (DMSO) δ_{C} 158.9 (Ar ring 4-C), 144.8 (phenylpiperidin-1-ium ring 1-C), 131.1 (Ar ring 2-C, 6-C), 129.0 (phenyl ring 2-C, 6-C), 127.1 (phenyl ring 3-C, 4-C, 5-C), 126.9 (Ar ring 1-C), 115.1 (Ar ring 3-C, 5-C), 70.7 (Ar ring 4- COCH_2), 64.3 (chiral C), 59.8 (H_2CNH^+), 53.9 (phenylpiperidin-1-ium ring 2-C), 52.9 (phenylpiperidin-1-ium ring 6-C), 42.0 (Ar ring 1- CCH_2), 39.1 (phenylpiperidin-1-ium ring 4-C), 30.2 (phenylpiperidin-1-ium ring 3-C), 30.1 (phenylpiperidin-1-ium ring 4-C).

6. Experimental

1-(3-(4-(Ammoniomethyl)phenoxy)-2-hydroxypropyl)indolin-1-ium (38h)

tert-Butyl-(4-(2-hydroxy-3-(indolin-1-yl)propoxy)benzyl)carbamate (37h) (98 mg, 0.25 mmol) was dissolved in MeOH (0.5 mL), 4M HCl in 1, 4 dioxane (0.4 mL), and stirred. After completion as determined by LC-MS the solvent was removed under vacuum to afford the title compound as a white semi solid foam (68 mg, 93%), used without further purification.

LC-MS *m/z* calculated for C₁₈H₂₃N₂O₂ [M+H]⁺: 299.2, found: 299.20, t_R = 0.75 mins (HPLC-method A)



¹H NMR (DMSO) δ_H 10.02 (s, 1H, NH₃⁺), 8.37 (s, 2H, NH⁺), δ_H 7.21 (d, *J* = 8.5 Hz, 2H, Ar ring 3-H, 5-H), 7.09 (ddd, *J* = 15.6, 7.7, 1.3 Hz, 2H, indolinyl ring 6-H, 7-H), 6.90 (dt, *J* = 8.6 Hz, 2H, Ar ring 2-H, 6-H), 6.71 (td, *J* = 7.4, 0.9 Hz, 1H, indolinyl ring 5-H), 6.56 (d, *J* = 7.8 Hz, 1H, indolinyl ring 4-H), 4.40 – 4.18 (m, 3H, Ar ring 1-CCH₂, chiral HC), 4.15 – 3.98 (m, 2H, Ar ring 4-COCH₂), 3.60 – 3.44 (m, 1H, indolinyl ring 2-H_a), 3.43 – 3.29 (m, 2H, CH_aN, indolinyl ring 2-H_b), 3.23 (dd, *J* = 13.8, 5.2 Hz, 1H, CH_bN), 3.01 (t, *J* = 8.3 Hz, 2H, indolinyl ring 2-H), 2.73 (s, 1H, OH).

¹³C NMR (DMSO) δ_C 157.9 (Ar ring 4-C), 155.9 (C=O), 152.7 (indolinyl ring 7_a-C), 131.6 (Ar ring 1-C), 129.8 (indolinyl ring 3_a-C), 128.9 (indolinyl ring 6-C), 127.4 (Ar ring 2-C, 6-C), 124.6 (indolinyl ring 4-C), 118.4 (indolinyl ring 5-C), 114.7 (Ar ring 3-C, 5-C), 107.2 (indolinyl ring 7-C), 79.5, 70.0 (Ar

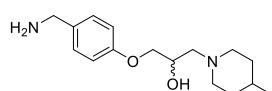
6. Experimental

ring 4-COCH₂), 68.4 (chiral C), 55.0 (CH₂N), 53.5 (indoliny ring 2-C), 44.2 (Ar ring 1-CCH₂), 28.8 (indoliny ring 3-C).

1-(4-(Aminomethyl)phenoxy)-3-(4-methylpiperidin-1-yl)propan-2-ol (38i)

1-(3-(4-(((*tert*-Butoxycarbonyl)amino)methyl)phenoxy)-2-hydroxypropyl)-4-methylpiperidin-1-ium (37i) (196 mg, 0.52 mmol) was dissolved in MeOH (0.5 mL), 4M HCl in 1, 4 dioxane (0.4 mL), and stirred. After completion as determined by LC-MS the solvent was removed under vacuum to adsorb crude residue onto isolate and purified by silica gel column chromatography (eluent MeOH[1M NH₃]:DCM, 1:9 and 1.5:8.5) to afford the title compound as a clear colourless oil (120 mg, 74%), used without further purification.

LC-MS *m/z* calculated for C₁₆H₂₇N₂O₂ [M+H]⁺: 279.2, found: 279.22, *t_R* = 0.55 mins (HPLC-method A)



¹H NMR (DMSO) δ_H 7.21 (d, *J* = 8.3 Hz, 2H, Ar 2-H, 6-H), 6.85 (d, *J* = 8.7 Hz, 2H, Ar 3-H, 5-H), 4.12 – 3.85 (m, 2H, Ar ring 4-COCH₂), 3.86 – 3.76 (m, 1H, chiral HC), 3.63 (s, 2H, Ar ring 1-CCH₂), 3.17 (s, 1H, OH), 3.01 – 2.71 (m, 2H, methylpiperidinyl ring 2-H), 2.39 (dd, *J* = 12.7, 6.0 Hz, H_bCN), 2.30 (dd, *J* = 12.6, 6.3 Hz, 1H, H_bCN), 1.95 (tdd, *J* = 11.6, 4.6, 2.6 Hz, 1H, methylpiperidinyl ring 6-H), 1.53 (dd, *J* = 10.0, 5.6 Hz, 2H, methylpiperidinyl ring 3-H), 1.38 – 1.20 (m, 1H, methylpiperidinyl ring 4-

6. Experimental

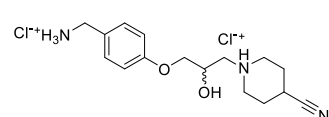
H), 1.11 (qd, $J = 11.9, 3.9$ Hz, 2H, methylpiperidinyl ring 5-H), 0.87 (d, $J = 6.4$ Hz, 3H, methylpiperidinyl ring 4-CCH₃).

¹³C NMR (DMSO) δ_c 157.8 (Ar ring 4-C), 136.6 (Ar ring 1-C), 128.6 (Ar ring 2-C, 6-C), 114.6 (Ar ring 3-C, 5-C), 71.7 (Ar ring 4-COCH₂), 67.1 (chiral C), 62.0 (H₂CN), 54.7 (methylpiperidinyl ring 2-C), 54.6 (methylpiperidinyl ring 6-C), 45.5 (Ar ring 1-CCH₂), 34.6 (methylpiperidinyl ring 3-C), 34.6 (methylpiperidinyl ring 5-C), 30.7 (methylpiperidinyl ring 4-C), 22.4 (methylpiperidinyl ring 4-CCH₃).

1-(3-(4-(Ammoniomethyl)phenoxy)-2-hydroxypropyl)-4-cyanopiperidin-1-ium (38j)

1-(3-(4(((*tert*-Butoxycarbonyl)amino)methyl)phenoxy)-2-hydroxypropyl)-4-cyanopiperidin-1-ium (**37j**) (239 mg, 0.52 mmol) was dissolved in MeOH (0.5 mL), 4M HCl in 1, 4 dioxane (0.4 mL), and stirred. After completion as determined by LC-MS the solvent was removed under vacuum to afford the title compound as a white semi solid foam (153 mg, 74%), used without further purification.

LC-MS m/z calculated for C₁₆H₂₄N₃O₂ [M+H]⁺: 290.2, found: 290.20, $t_R = 1.20$ mins (HPLC-method A)


¹H NMR (DMSO) δ_H 11.12 – 10.49 (m, 1H, NH⁺), 8.52 (s, 3H, NH₃⁺), 7.43 (d, $J = 7.3$ Hz, 2H, Ar 2-H, 6-H), 6.97 (dd, $J = 8.2, 4.1$ Hz, 2H, Ar 3-H, 5-H), 5.97 (s, 1H, OH), 4.46 – 4.32 (m, 1H, chiral HC), 4.23 – 3.79 (m, 4H, Ar ring 1-CCH₂, Ar ring 4-COCH₂), 3.74 – 3.57 (m, 1H, H_aCN), 3.49 – 3.33 (m, 1H,

6. Experimental

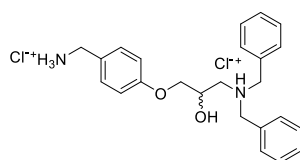
H_bCN), 3.34 – 2.97 (m, 5H, 4-cyanopiperidin-1-ium ring 2-H, 4-H, 6-H), 2.34 – 1.74 (m, 4H, 4-cyanopiperidin-1-ium ring 3-H, 5-H).

¹³C NMR (DMSO) δ_c 158.8, (HCOOH), 158.8 (Ar ring 4-C), 131.1 (Ar ring 2-C, 6-C), 126.9 (Ar ring 1-C), 121.9 (nitrile CN), 115.1 (Ar ring 3-C, 5-C), 70.7 (Ar ring 4-COCH₂), 64.3 (chiral C), 59.4 (H₂CN), 51.9 (4-cyanopiperidin-1-ium ring 2-C), 51.1 (4-cyanopiperidin-1-ium ring 6-C), 42.1 (Ar ring 1-CCH₂), 26.1 (4-cyanopiperidin-1-ium 3-C), 26.0 (4-cyanopiperidin-1-ium 5-C), 24.0 (4-cyanopiperidin-1-ium 4-C).

3-(4-(Ammoniomethyl)phenoxy)-*N,N*-dibenzyl-2-hydroxypropan-1-aminium (38k)

N,N-Dibenzyl-4-(4-(((*tert*-butoxycarbonyl)amino)methyl)phenoxy)-2-hydroxybutan-1-aminium (37k) (600 mg, 1.26 mmol) was dissolved in EtOAc (5 mL), 4M HCl in 1,4 dioxane (2 mL), and stirred. After completion as determined by LC-MS the solvent was removed under vacuum to afford the title compound as a semi-solid white foam (543 mg, 92%), used without further purification.

LC-MS m/z calculated for C₂₄H₂₉N₂O₂ [M+H]⁺: 377.2, found: 377.20, t_R = 1.17 mins (HPLC-method A)



¹H NMR (DMSO) δ_H 11.00 (m, 1H, NH⁺), 8.49 (s, 3H, NH₃⁺), 7.70 (t, *J* = 8.1 Hz, 4H, (*N*-benzyl ring (2-H, 6-H)₂), 7.45 (d, *J* = 5.0 Hz, 6H, *N*-benzyl ring (3-H, 4-H, 5H)₂), 7.41 (d, *J* = 8.2 Hz, 2H, Ar ring 3-H, 5-H), 6.84 (d, *J* = 8.1 Hz, 2H, Ar ring 2-H, 6-

6. Experimental

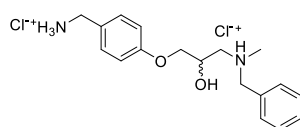
H), 6.15 (s, 1H, OH), 4.47 (q, $J = 10.6$ Hz, 5H, chiral HC, *N*-benzyl (CH₂)₂), 3.92 (d, $J = 6.0$ Hz, 2H, Ar 1-CCH₂), 3.82 (dd, $J = 10.1, 5.8$ Hz, 2H, Ar 4-COCH₂), 3.24 – 3.15 (m, 2H, H_{2a}CNH⁺), 3.04 (t, $J = 11.6$ Hz, 2H, H_{2b}CNH⁺).

¹³C NMR (DMSO) δ_c 158.1 (Ar ring 4-C), 131.9 (*N*-benzyl ring 1-C_a), 131.6 (*N*-benzyl ring 1-C_b), 130.5 (Ar ring 2-C, 6-C), 129.9 (*N*-benzyl ring 3-C_a, 5-C_a), 129.6, (*N*-benzyl ring 3-C_b, 5-C_b), 129.5 (*N*-benzyl ring 4-C_a, 4-C_b), 128.8 (*N*-benzyl ring 2-C_{aa}, 6-C_{aa}), 126.4 (Ar ring 1-C), 114.5 (Ar ring 3-C, 5-C), 69.7 (Ar ring 4-COCH₂), 63.7 (chiral C), 57.2 *N*-benzyl C_aH₂), 56.8 (*N*-benzyl C_bH₂), 53.8 (H₂CNH⁺), 41.6 (Ar ring 1-CCH₂).

3-(4-(Ammoniomethyl)phenoxy)-*N*-benzyl-2-hydroxy-*N*-methylpropan-1-aminium (38I)

tert-Butyl-(4-(3-(benzyl(methyl)amino)-2-hydroxypropoxy)benzyl) carbamate (37I) (209 mg, 0.52 mmol) was dissolved in EtOAc (4 mL), 4M HCl in 1, 4 dioxane (2 mL), and stirred. After completion as determined by LC-MS the solvent was removed under vacuum to afford the title compound as a white semi solid (190 mg, 98%), used without further purification.

LC-MS m/z calculated for C₂₄H₂₈N₂O₂ [M+H]⁺: 315.2, found: 315.21, $t_R = 1.02$ mins (HPLC-method A)



¹H NMR (DMSO) δ_H 10.94 – 10.19 (m, 1H, NH⁺), 8.40 (s, 1H, NH₃⁺), 7.69 – 7.57 (m, 4H, *N*-benzyl ring 2-H, 6-H), 7.55 – 7.36 (m, 5H, Ar 2-H, 6-H, *N*-benzyl ring 3-C, 4-H, 5-C), 6.94 (d, $J = 8.7$ Hz, 4H, Ar 3-H, 5-

6. Experimental

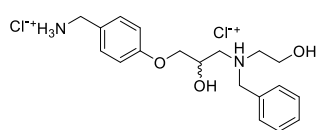
H), 6.04 (s, 1H, OH), 4.43 (d, $J = 17.5$ Hz, 1H, chiral HC), 4.05 – 3.77 (m, 4H, Ar ring 1-CCH₂, Ar ring 4-COCH₂), 3.34 (s, 3H, NH⁺CH₃), 3.24 – 3.04 (m, 2H, *N*-benzyl CH₂), 2.77 (d, $J = 8.0$ Hz, 2H, H₂CNH⁺).

¹³C NMR (DMSO) δ_c 158.8 (Ar ring 4-C), 131.9 (*N*-benzyl ring 2-C, 6-C), 131.0 (Ar ring 2-C, 6-C), 129.9 (*N*-benzyl ring 1-C), 129.2, (*N*-benzyl ring 3-C, 4-C, 5-C), 126.9 (Ar ring 1-C), 115.0 (Ar ring 3-C, 5-C), 70.5 (Ar ring 4-COCH₂), 59.8 (chiral C), 57.7 (NH⁺CH₃), 57.2 (*N*-benzyl CH₂), 42.1 (Ar ring 1-CCH₂), 41.0 (H₂CNH⁺).

3-(4-(Ammoniomethyl)phenoxy)-*N*-benzyl-2-hydroxy-*N*-(2-hydroxyethyl) propan-1-aminium (38m)

tert-Butyl-(4-(3-(benzyl(2-hydroxyethyl)amino)-2-hydroxypropoxy)benzyl) carbamate (37m) (200 mg, 0.47 mmol) was dissolved in 4M HCl in 1, 4 dioxane (2 mL) and stirred. After completion as determined by LC-MS the solvent was removed under vacuum to afford the title compound as a white semi-solid foam (190 mg, 101%), used without further purification.

LC-MS m/z calculated for C₁₉H₂₇N₂O₃ [M+H]⁺: 331.2, found: 331.20, $t_R = 1.24$ mins (HPLC-method A)



¹H NMR (DMSO) δ_H 10.02 (s, 1H, NH₃⁺), 8.37 (s, 2H, NH⁺), 7.64 (s, 2H, *N*-benzyl ring 2-H, 6-H), 7.48 – 7.37 (m, 5H, Ar 2-H, 6-H, *N*-benzyl ring 3-C, 4-H, 5-C), 6.93 (d, $J = 8.4$ Hz, 2H, Ar 3-H, 5-H), 6.04 (s, 1H, CH₂OH), 5.41 (s, 1H, OH), 4.76 – 4.23 (m, 3H, chiral HC, Ar ring 1-

6. Experimental

CCH₂), 4.11 – 3.65 (m, 6H, Ar ring 4-COCH₂, *N*-benzyl CH₂, CH₂OH), 3.37 – 3.04 (m, 2H, H₂CNH⁺CH₂OH).

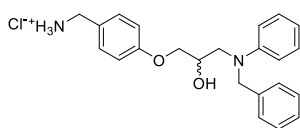
¹³C NMR (DMSO) δ_c 158.8 (Ar ring 4-C), 132.0 (*N*-benzyl ring 2-C, 6-C), 131.0 (Ar ring 2-C, 6-C), 130.0 (*N*-benzyl ring 1-C), 129.3 (*N*-benzyl ring 3-C, 4-C, 5-C), 126.8 (Ar ring 1-C), 115.0 (Ar ring 3-C, 5-C), 70.5 (Ar ring 4-COCH₂), 64.4 (chiral C), 58.0 (CH₂OH), 55.5 (H₂CNH⁺CH₂), 42.1 (Ar ring 1-CCH₂).

(4-(3-(Benzyl(phenyl)amino)-2-hydroxypropoxy)phenyl)

methanaminium (38m)

tert-Butyl-(4-(3-(benzyl(phenyl)amino)-2-hydroxypropoxy)benzyl) carbamate (37m) (24 mg, 0.05 mmol) was dissolved 4M HCl in 1, 4 dioxane (3 mL) and stirred. After completion as determined by LC-MS the solvent was removed under vacuum to afford the title compound as a white semi solid (17 mg, 94%), used without further purification.

LC-MS *m/z* calculated for C₂₄H₂₇N₂O₂ [M+H]⁺: 363.2, found: 363.22, t_R = 1.11 mins (HPLC-method A)



¹H NMR (DMSO) δ_H 8.36 (s, 3H, NH₃⁺), 7.41 (d, *J* = 8.3 Hz, 2H, Ar ring 2-H, 6-H), 7.33 – 7.24 (m, 2H, *N*-benzyl ring 2-H, 6-H), 7.20 (dd, *J* = 7.8, 5.7 Hz, 3H, *N*-benzyl 3-H, 4-H, 5-H), 7.10 (t, *J* = 7.7 Hz, 2H, *N*-phenyl 3-H, 5-H), 6.97 (d, *J* = 8.5 Hz, 2H, Ar ring 3-H, 5-H), 6.77 (d, *J* = 8.1 Hz, 2H, *N*-phenyl 2-H, 6-H), 6.65 – 6.55 (m, 1H, *N*-phenyl 4-H), 4.94 – 4.41 (m, 2H, *N*-benzyl CH₂), 4.13 (dq, *J* = 10.0, 5.3 Hz, 1H, chiral

6.Experimental

HC), 4.05 – 3.85 (m, 4H, Ar 1-CCH₂, Ar 4-OCH₂), 3.68 (dd, $J = 14.9, 5.1$ Hz, 1H, H_{2a}CN), 3.51 (dd, $J = 15.0, 6.9$ Hz, 1H, H_{2a}CN).

¹³C NMR (DMSO) δ_c 159.1 (Ar ring 4-C), 148. (N-phenyl ring 1-C), 137.4 (N-benzyl ring 1-C), 131.0 (Ar ring 2-C, 6-C), 129.5 (N-phenyl 3-C, 5-C), 128.9 (N-benzyl ring 2-C, 6-C), 127.2 (N-benzyl ring 3-C, 4-C, 5-C), 126.6 (Ar ring 1-C), 115.0 (Ar ring 3-C, 5-C), 70.8 (Ar 4-OCH₂), 67.4 (chiral C), 66.8, (H₂CN), 55.2, (N-benzyl CH₂), 42.1 (Ar 1-CCH₂).

7. References

- (1) Vaudry, H. Molecular Evolution of GPCRS: What We Know and What the Future Holds. *J. Mol. Endocrinol.* **2014**, *52* (3), 1–2.
- (2) Lefkowitz, R. J. Historical Review: A Brief History and Personal Retrospective of Seven-Transmembrane Receptors. *Trends Pharmacol. Sci.* **2004**, *25* (8), 413–422.
- (3) Hill, S. J. G-Protein-Coupled Receptors: Past, Present and Future. *Br. J. Pharmacol.* **2006**, *147 Suppl* (Suppl 1), S27-37.
- (4) Tuteja, N. Signaling through G Protein Coupled Receptors. *Plant Signal. Behav.* **2009**, *4* (10), 942–947.
- (5) Aghajanian, G. K.; Sanders-bush, E. 5-HT Receptor Subtypes: Molecular and Cellular Aspects. *Neuropharmacol. Fith Gener. Prog.* **2005**, *34*.
- (6) Lummis, S. C. R. 5-HT₃ Receptors. *J. Biol. Chem.* **2012**, *287* (48), 40239–40245.
- (7) Carhart-Harris, R. L.; Nutt, D. J. Serotonin and Brain Function: A Tale of Two Receptors. *J. Psychopharmacol.* **2017**, *31* (9), 1091–1120.
- (8) Roth, B. L.; Irwin, J. J.; Shoichet, B. K. Discovery of New GPCR Ligands to Illuminate New Biology. *Nat. Chem. Biol.* **2017**, *13* (11), 1143–1151.
- (9) Zalewska, M.; Siara, M.; Sajewicz, W. G Protein-Coupled Receptors:

7. References

- Abnormalities in Signal Transmission, Disease States and Pharmacotherapy. *Acta Pol. Pharm. Drug Res. Drug Res.* **2014**, *71* (2), 229–243.
- (10) Andrade, R.; Barnes, N, M.; Baxter, G.; Bockaert, J.; Branchek, T.; Butler, A.; Cohen, M, L.; Dumuis, A.; Eglen, R, M.; Göthert, M.; Hamblin, M.; Hamon, M.; Hartig, P, R.; Hen, R.; Hensler, J.; Herrick-Davis, K.; Hills, R.; Hoyer, D.; Humphrey, P, P, A.; Latté, K, P.; Maroteaux, L.; Martin, G, R.; Middlemiss, D, N.; Mylecharane, E.; Neumaier, J.; Peroutka, S, J.; Peters, J, A.; Roth, B.; Saxena, P, R.; Sharp, T.; Sleight, A.; Villalon, C, M.; Yocca, F. 5-Hydroxytryptamine Receptors (Version 2019.4). *IUPHAR/BPS Guid. to Pharmacol. Database* **2019**, No. (4).
- (11) Venkatakrishnan, A. J.; Deupi, X.; Lebon, G.; Heydenreich, F. M.; Flock, T.; Miljus, T.; Balaji, S.; Bouvier, M.; Veprintsev, D. B.; Tate, C. G.; Schertler, G. F. X.; Babu, M. M. Diverse Activation Pathways in Class A GPCRs Converge near the G-Protein-Coupling Region. *Nature* **2016**, *536* (7617), 484–487.
- (12) Nichols, D. E. Hallucinogens. *Pharmacol. Ther.* **2004**, *101* (2), 131–181.
- (13) Chan, H. C. S.; McCarthy, D.; Li, J.; Palczewski, K.; Yuan, S. Designing Safer Analgesics via μ -Opioid Receptor Pathways. *Trends Pharmacol. Sci.* **2017**, *38* (11), 1016–1037.
- (14) Hauser, A. S.; Attwood, M. M.; Rask-Andersen, M.; Schiöth, H. B.;

7. References

- Gloriam, D. E. Trends in GPCR Drug Discovery: New Agents, Targets and Indications. *Nat. Rev. Drug Discov.* **2017**, *16* (12), 829–842.
- (15) Sriram, K.; Insel, P. A. G Protein-Coupled Receptors as Targets for Approved Drugs: How Many Targets and How Many Drugs? *Mol. Pharmacol.* **2018**, *93* (4), 251–258.
- (16) Madsen, M. K.; Fisher, P. M. D.; Stenbæk, D. S.; Kristiansen, S.; Burmester, D.; Lehel, S.; Páleníček, T.; Kuchař, M.; Svarer, C.; Ozenne, B.; Knudsen, G. M. A Single Psilocybin Dose Is Associated with Long-Term Increased Mindfulness, Preceded by a Proportional Change in Neocortical 5-HT_{2A} Receptor Binding. *Eur. Neuropsychopharmacol.* **2020**, *33*, 71–80.
- (17) Kimura, K. T.; Asada, H.; Inoue, A.; Kadji, F. M. N.; Im, D.; Mori, C.; Arakawa, T.; Hirata, K.; Nomura, Y.; Nomura, N.; Aoki, J.; Iwata, S.; Shimamura, T. Structures of the 5-HT_{2A} Receptor in Complex with the Antipsychotics Risperidone and Zotepine. *Nat. Struct. Mol. Biol.* **2019**, *26* (2), 121–128.
- (18) Gray, J. A.; Roth, B. L. Paradoxical Trafficking and Regulation of 5-HT_{2A} Receptors by Agonists and Antagonists. *Brain Res. Bull.* **2001**, *56* (5), 441–451.
- (19) Matsumoto, I.; Inoue, Y.; Iwazaki, T.; Pavey, G.; Dean, B. 5-HT_{2A} and Muscarinic Receptors in Schizophrenia: A Postmortem Study. *Neurosci. Lett.* **2005**, *379* (3), 164–168.

7. References

- (20) Mintun, M. A.; Sheline, Y. I.; Moerlein, S. M.; Vlassenko, A. G.; Huang, Y.; Snyder, A. Z. Decreased Hippocampal 5-HT_{2A} Receptor Binding in Major Depressive Disorder: In Vivo Measurement with [¹⁸F]Altanserin Positron Emission Tomography. *Biol. Psychiatry* **2004**, *55* (3), 217–224.
- (21) Peroutka, S. J.; Snyder, S. H. Long-Term Antidepressant Treatment Decreases Spiroperidol-Labeled Serotonin Receptor Binding. *Science* (80-.). **1980**, *210* (4465), 88–90.
- (22) Moreno, J. L.; Muguruza, C.; Umali, A.; Mortillo, S.; Holloway, T.; Pilar-Cuéllar, F.; Mocci, G.; Seto, J.; Callado, L. F.; Neve, R. L.; Milligan, G.; Sealton, S. C.; López-Giménez, J. F.; Meana, J. J.; Benson, D. L.; González-Maeso, J. Identification of Three Residues Essential for 5-Hydroxytryptamine 2A-Metabotropic Glutamate 2 (5-HT_{2A}-mGlu₂) Receptor Heteromerization and Its Psychoactive Behavioral Function. *J. Biol. Chem.* **2012**, *287* (53), 44301–44319.
- (23) Adams, K. H.; Hansen, E. S.; Pinborg, L. H.; Hasselbalch, S. G.; Svarer, C.; Holm, S.; Bolwig, T. G.; Knudsen, G. M. Patients with Obsessive–Compulsive Disorder Have Increased 5-HT_{2A} Receptor Binding in the Caudate Nuclei. *Int. J. Neuropsychopharmacol.* **2005**, *8* (3), 391–401.
- (24) Pornnoppadol, C.; Friesen, D. S.; Haussler, T. S.; Gllaser, P. E. A.; Todd, R. D. No Difference Between Platelet Serotonin–5-HT_{2A} Receptors from Children With and Without ADHD. *J. Child Adolesc.*

7. References

- Psychopharmacol.* **1999**, 9 (1), 27–33.
- (25) Ballesteros, J. A.; Weinstein, H. [19] Integrated Methods for the Construction of Three-Dimensional Models and Computational Probing of Structure-Function Relations in G Protein-Coupled Receptors. In *Receptor Molecular Biology*; Sealfon, S. C. B. T.-M. in N., Ed.; Academic Press, 1995; Vol. 25, pp 366–428.
- (26) Quist, J. F.; Barr, C. L.; Schachar, R.; Roberts, W.; Malone, M.; Tannock, R.; Basile, V. S.; Beitchman, J.; Kennedy, J. L. Evidence for the Serotonin HTR2A Receptor Gene as a Susceptibility Factor in Attention Deficit Hyperactivity Disorder (ADHD). *Mol. Psychiatry* **2000**, 5 (5), 537–541.
- (27) Cho, S.-C.; Son, J.-W.; Kim, B.-N.; Kim, J.-W.; Yoo, H.-J.; Hwang, J.-W.; Cho, D.-Y.; Chung, U.-S.; Park, T.-W. Serotonin 2A Receptor Gene Polymorphism in Korean Children with Attention-Deficit/Hyperactivity Disorder. *Psychiatry Investig.* **2012**, 9 (3), 269–277.
- (28) Pitychoutis, P. M.; Belmer, A.; Moutkine, I.; Adrien, J.; Maroteaux, L. Mice Lacking the Serotonin HT2B Receptor Gene Present an Antipsychotic-Sensitive Schizophrenic-Like Phenotype. *Neuropsychopharmacology* **2015**, 40 (12), 2764–2773.
- (29) Bevilacqua, L.; Doly, S.; Kaprio, J.; Yuan, Q.; Tikkanen, R.; Paunio, T.; Zhou, Z.; Wedenoja, J.; Maroteaux, L.; Diaz, S.; Belmer, A.; Hodgkinson, C. A.; Dell’Osso, L.; Suvisaari, J.; Coccaro, E.; Rose, R.

7. References

- J.; Peltonen, L.; Virkkunen, M.; Goldman, D. A Population-Specific HTR2B Stop Codon Predisposes to Severe Impulsivity. *Nature* **2010**, *468* (7327), 1061–1066.
- (30) Ayme-Dietrich, E.; Lawson, R.; Côté, F.; de Tapia, C.; Da Silva, S.; Ebel, C.; Hechler, B.; Gachet, C.; Guyonnet, J.; Rouillard, H.; Stoltz, J.; Quentin, E.; Banas, S.; Daubeuf, F.; Frossard, N.; Gasser, B.; Mazzucotelli, J.-P.; Hermine, O.; Maroteaux, L.; Monassier, L. The Role of 5-HT_{2B} Receptors in Mitral Valvulopathy: Bone Marrow Mobilization of Endothelial Progenitors. *Br. J. Pharmacol.* **2017**, *174* (22), 4123–4139.
- (31) Rothman, R. B.; Baumann, M. H.; Savage, J. E.; Rauser, L.; McBride, A.; Hufeisen, S. J.; Roth, B. L. Evidence for Possible Involvement of 5-HT_{2B} Receptors in the Cardiac Valvulopathy Associated With Fenfluramine and Other Serotonergic Medications. *Circulation* **2000**, *102* (23), 2836–2841.
- (32) Wold, E. A.; Wild, C. T.; Cunningham, K. A.; Zhou, J. Targeting the 5-HT_{2C} Receptor in Biological Context and the Current State of 5-HT_{2C} Receptor Ligand Development. *Curr. Top. Med. Chem.* **2019**, *19* (16), 1381–1398.
- (33) Chagraoui, A.; Thibaut, F.; Skiba, M.; Thuillez, C.; Bourin, M. 5-HT_{2C} Receptors in Psychiatric Disorders: A Review. *Prog. Neuro-Psychopharmacology Biol. Psychiatry* **2016**, *66*, 120–135.
- (34) Demireva, E. Y.; Suri, D.; Morelli, E.; Mahadevia, D.; Chuhma, N.;

7. References

- Teixeira, C. M.; Ziolkowski, A.; Hersh, M.; Fifer, J.; Bagchi, S.; Chemiakine, A.; Moore, H.; Gingrich, J. A.; Balsam, P.; Rayport, S.; Ansorge, M. S. 5-HT_{2C} Receptor Blockade Reverses SSRI-Associated Basal Ganglia Dysfunction and Potentiates Therapeutic Efficacy. *Mol. Psychiatry* **2020**, *25* (12), 3304–3321.
- (35) Urban, J. D.; Clarke, W. P.; Von Zastrow, M.; Nichols, D. E.; Kobilka, B.; Weinstein, H.; Javitch, J. A.; Roth, B. L.; Christopoulos, A.; Sexton, P. M.; Miller, K. J.; Spedding, M.; Mailman, R. B. Functional Selectivity and Classical Concepts of Quantitative Pharmacology. *J. Pharmacol. Exp. Ther.* **2007**, *320* (1), 1–13.
- (36) Bohn, L.; Schmid, L. C. Serotonin Receptor Signaling and Regulation via β -Arrestins. *Crit. Rev. Biochem. Mol. Biol.* **2010**, *45* (6), 555–566.
- (37) Lin, S. L.; Setya, S.; Johnson-Farley, N. N.; Cowen, D. S. Differential Coupling of 5-HT₁ Receptors to G Proteins of the Gi Family. *Br. J. Pharmacol.* **2002**, *136* (7), 1072–1078.
- (38) Bockaert, J.; Claeysen, S.; Compan, V.; Dumuis, A. 5-HT₄ Receptors: History, Molecular Pharmacology and Brain Functions. *Neuropharmacology* **2008**, *55* (6), 922–931.
- (39) Marcos, B.; Cabero, M.; Solas, M.; Aisa, B.; Ramirez, M. J. Signalling Pathways Associated with 5-HT₆ Receptors: Relevance for Cognitive Effects. *Int. J. Neuropsychopharmacol.* **2010**, *13* (6), 775–784.

7. References

- (40) Guseva, D.; Wirth, A.; Ponimaskin, E. Cellular Mechanisms of the 5-HT7 Receptor-Mediated Signaling. *Front. Behav. Neurosci.* **2014**, *8* (OCT), 1–8.
- (41) Kim, K.; Che, T.; Panova, O.; DiBerto, J. F.; Lyu, J.; Krumm, B. E.; Wacker, D.; Robertson, M. J.; Seven, A. B.; Nichols, D. E.; Shoichet, B. K.; Skiniotis, G.; Roth, B. L. Structure of a Hallucinogen-Activated Gq-Coupled 5-HT_{2A} Serotonin Receptor. *Cell* **2020**, *182* (6), 1574–1588.e19.
- (42) Jerman, J. C.; Brough, S. J.; Gager, T.; Wood, M.; Coldwell, M. C.; Smart, D.; Middlemiss, D. N. Pharmacological Characterisation of Human 5-HT₂ Receptor Subtypes. *Eur. J. Pharmacol.* **2001**, *414* (1), 23–30.
- (43) Berg, K. A.; Clarke, W. P. Making Sense of Pharmacology: Inverse Agonism and Functional Selectivity. *Int. J. Neuropsychopharmacol.* **2018**, *21* (10), 962–977.
- (44) Wang, Y. qiang; Lin, W. wei; Wu, N.; Wang, S. yi; Chen, M. zi; Lin, Z. hua; Xie, X. Q.; Feng, Z. wei. Structural Insight into the Serotonin (5-HT) Receptor Family by Molecular Docking, Molecular Dynamics Simulation and Systems Pharmacology Analysis. *Acta Pharmacol. Sin.* **2019**, *40* (9), 1138–1156.
- (45) Kenakin, T. Theoretical Aspects of GPCR-Ligand Complex Pharmacology. *Chem. Rev.* **2017**, *117* (1), 4–20.
- (46) Kenakin, T. Efficacy at G-Protein-Coupled Receptors. *Nat. Rev. Drug*

7. References

- Discov.* **2002**, 1 (2), 103–110.
- (47) Baker, J. G.; Hill, S. J. Multiple GPCR Conformations and Signalling Pathways: Implications for Antagonist Affinity Estimates. *Trends Pharmacol. Sci.* **2007**, 28 (8), 374–381.
- (48) Leucht, C.; Kitzmantel, M.; Chua, L.; Kane, J.; Leucht, S. Haloperidol versus Chlorpromazine for Treatment of Schizophrenia. *Schizophr. Bull.* **2008**, 34 (5), 813–815.
- (49) Meltzer, H. Y. What's Atypical about Atypical Antipsychotic Drugs? *Curr. Opin. Pharmacol.* **2004**, 4 (1), 53–57.
- (50) Orzelska-Górka, J.; Mikulska, J.; Wiszniewska, A.; Biała, G. New Atypical Antipsychotics in the Treatment of Schizophrenia and Depression. *Int. J. Mol. Sci.* **2022**, 23 (18).
- (51) Abou-Setta, A. M.; Mousavi, S. S.; Spooner, C. *First-Generation Versus Second-Generation Antipsychotics in Adults: Comparative Effectiveness*, 63rd ed.; Agency for Healthcare Research and Quality (US), 2012.
- (52) Baldessarini, R. J.; Frankenburg, F. R. Clozapine - A Novel Antipsychotic Agent. *N. Engl. J. Med.* **1991**, 324 (11), 746–754.
- (53) Alvir, J. M. J.; Lieberman, J. A.; Safferman, A. Z.; Schwimmer, J. L.; Schaaf, J. A. Clozapine-Induced Agranulocytosis Incidence and Risk Factors in the United States. *N. Engl. J. Med.* **1993**, 329 (3), 162–167.

7. References

- (54) Hasnain, M.; Vieweg, W. V. R.; Hollett, B. Weight Gain and Glucose Dysregulation with Second-Generation Antipsychotics and Antidepressants: A Review for Primary Care Physicians. *Postgrad. Med.* **2012**, *124* (4), 154–167.
- (55) Fulton, B.; Goa, K. L. Olanzapine - A Review of Its Pharmacological Properties and Therapeutic Efficacy in the Management of Schizophrenia and Related Psychoses. *Drugs* **1997**, *53* (2), 281–298.
- (56) Bhana, N.; Foster, R. H.; Olney, R.; Plosker, G. L. Olanzapine - An Updated Review of Its Use in the Management of Schizophrenia. *Drugs* **2001**, *61* (1), 111–161.
- (57) Kirk, S. L.; Glazebrook, J.; Grayson, B.; Neill, J. C.; Reynolds, G. P. Olanzapine-Induced Weight Gain in the Rat: Role of 5-HT_{2C} and Histamine H₁ Receptors. *Psychopharmacology (Berl)*. **2009**, *207* (1), 119.
- (58) Rummel-Kluge, C.; Komossa, K.; Schwarz, S.; Hunger, H.; Schmid, F.; Lobos, C. A.; Kissling, W.; Davis, J. M.; Leucht, S. Head-to-Head Comparisons of Metabolic Side Effects of Second Generation Antipsychotics in the Treatment of Schizophrenia: A Systematic Review and Meta-Analysis. *Schizophr. Res.* **2010**, *123* (2), 225–233.
- (59) Harrison, T. S.; Scott, L. J. Ziprasidone - A Review of Its Use in Schizophrenia and Schizoaffective Disorder. *CNS Drugs* **2006**, *20*

7. References

- (12), 1027–1052.
- (60) Mattei, C.; Rapagnani, M. P.; Stahl, S. M. Ziprasidone Hydrochloride: What Role in the Management of Schizophrenia? *J. Cent. Nerv. Syst. Dis.* **2011**, *3*, 1–16.
- (61) Corena-McLeod, M. Comparative Pharmacology of Risperidone and Paliperidone. *Drugs R. D.* **2015**, *15* (2), 163–174.
- (62) Ochi, S.; Inoue, S.; Yoshino, Y.; Shimizu, H.; Iga, J.-I.; Ueno, S.-I. Efficacy of Asenapine in Schizophrenia Resistant to Clozapine Combined with Electroconvulsive Therapy: A Case Report. *Clin. Psychopharmacol. Neurosci.* **2019**, *17* (4), 559–563.
- (63) De Hert, M.; Yu, W.; Detraux, J.; Sweers, K.; van Winkel, R.; Correll, C. U. Body Weight and Metabolic Adverse Effects of Asenapine, Iloperidone, Lurasidone and Paliperidone in the Treatment of Schizophrenia and Bipolar Disorder. *CNS Drugs* **2012**, *26* (9), 733–759.
- (64) Weng, J.; Zhang, Y.; Li, H.; Shen, Y.; Yu, W. Study on Risk Factors of Extrapyramidal Symptoms Induced by Antipsychotics and Its Correlation with Symptoms of Schizophrenia. *Gen. Psychiatry* **2019**, *32* (1), 14–21.
- (65) Kroeze, W. K.; Hufeisen, S. J.; Popadak, B. A.; Renock, S. M.; Steinberg, S.; Ernsberger, P.; Jayathilake, K.; Meltzer, H. Y.; Roth, B. L. H1-Histamine Receptor Affinity Predicts Short-Term Weight Gain for Typical and Atypical Antipsychotic Drugs.

7. References

- Neuropsychopharmacology* **2003**, 28 (3), 519–526.
- (66) Awouters, L. H. F.; Lewi, J. P. Forty Years of Antipsychotic Drug Research—from Haloperidol to Paliperidone—with Dr. Paul Janssen. *Arzneimittelforschung* **2007**, 57 (10), 625–632.
- (67) Wei Xin Chong, J.; Hsien-Jie Tan, E.; Chong, C. E.; Ng, Y.; Wijesinghe, R. Atypical Antipsychotics: A Review on the Prevalence, Monitoring, and Management of Their Metabolic and Cardiovascular Side Effects. *Ment. Heal. Clin.* **2016**, 6 (4), 178–184.
- (68) Lyu, J.; Kapolka, N.; Gumper, R.; Alon, A.; Wang, L.; Jain, M. K.; Barros-Álvarez, X.; Sakamoto, K.; Kim, Y.; Diberto, J.; Kim, K.; Tummino, T. A.; Huang, S.; Irwin, J. J.; Tarkhanova, O. O.; Moroz, Y.; Skiniotis, G.; Kruse, A. C.; Shoichet, B. K.; Roth, B. L. AlphaFold2 Structures Template Ligand Discovery. *bioRxiv* **2023**, 2023.12.20.572662.
- (69) Cao, D.; Yu, J.; Wang, H.; Luo, Z.; Liu, X.; He, L.; Qi, J.; Fan, L.; Tang, L.; Chen, Z.; Li, J.; Cheng, J.; Wang, S. Supplementary Structure-Based Discovery of Nonhallucinogenic Psychedelic Analogs. *Science (80-.)*. **2022**, 375, 403–411.
- (70) Kaplan, A. L.; Confair, D. N.; Kim, K.; Barros-álvarez, X.; Rodriguiz, R. M.; Yang, Y.; Kweon, O. S.; Che, T.; Mccorvy, J. D.; Kamber, D. N.; Phelan, J. P.; Martins, L. C.; Pogorelov, V. M.; Diberto, J. F.; Slocum, S. T.; Huang, X.; Kumar, J. M.; Wetsel, W. C.; Irwin, J. J.; Skiniotis, G.; Shoichet, B. K. Bespoke Library Docking for 5-HT_{2A} Receptor

7. References

- Agonists with Antidepressant Activity. *Nature* **2022**, *610*, 582–591.
- (71) Chen, Z.; Fan, L.; Wang, H.; Yu, J.; Lu, D.; Qi, J.; Nie, F.; Luo, Z.; Liu, Z.; Cheng, J.; Wang, S. Structure-Based Design of a Novel Third-Generation Antipsychotic Drug Lead with Potential Antidepressant Properties. *Nat. Neurosci.* **2022**, *25* (1), 39–49.
- (72) McCorvy, J. D.; Wacker, D.; Wang, S.; Agegnehu, B.; Liu, J.; Lansu, K.; Tribo, A. R.; Olsen, R. H. J.; Che, T.; Jin, J.; Roth, B. L. Structural Determinants of 5-HT_{2B} Receptor Activation and Biased Agonism. *Nat. Struct. Mol. Biol.* **2018**, *25* (9), 787–796.
- (73) Ishchenko, A.; Wacker, D.; Kapoor, M.; Zhang, A.; Han, G. W.; Basu, S.; Patel, N.; Messerschmidt, M.; Weierstall, U.; Liu, W.; Katritch, V.; Roth, B. L.; Stevens, R. C.; Cherezov, V. Structural Insights into the Extracellular Recognition of the Human Serotonin 2B Receptor by an Antibody. *Proc. Natl. Acad. Sci. U. S. A.* **2017**, *114* (31), 8223–8228.
- (74) Denzinger, K.; Nguyen, T. N.; Noonan, T.; Wolber, G.; Bermudez, M. Biased Ligands Differentially Shape the Conformation of the Extracellular Loop Region in 5-HT_{2B} Receptors. *Int. J. Mol. Sci.* **2020**, *21* (24), 1–14.
- (75) Liu, W.; Wacker, D.; Gati, C.; Han, G. W.; James, D.; Wang, D.; Nelson, G.; Weierstall, U.; Katritch, V.; Barty, A.; Zatsepin, N. A.; Li, D.; Messerschmidt, M.; Boutet, S.; Williams, G. J.; Koglin, J. E.; Seibert, M. M.; Wang, C.; Shah, S. T. A.; Basu, S.; Fromme, R.; Kupitz, C.;

7. References

- Rendek, K. N.; Grotjohann, I.; Fromme, P.; Kirian, R. A.; Beyerlein, K. R.; White, T. A.; Chapman, H. N.; Caffrey, M.; Spence, J. C. H.; Stevens, R. C.; Cherezov, V. Serial Femtosecond Crystallography of G Protein–Coupled Receptors. *Science* (80-). **2013**, *342* (6165), 1521–1524.
- (76) Wacker, D.; Wang, C.; Katritch, V.; Han, G. W.; Huang, X.-P.; Vardy, E.; McCorvy, J. D.; Jiang, Y.; Chu, M.; Siu, F. Y.; Liu, W.; Xu, H. E.; Cherezov, V.; Roth, B. L.; Stevens, R. C. Structural Features for Functional Selectivity at Serotonin Receptors. *Science* (80-). **2013**, *340* (6132), 615–619.
- (77) Peng, Y.; McCorvy, J. D.; Harpsøe, K.; Lansu, K.; Yuan, S.; Popov, P.; Qu, L.; Pu, M.; Che, T.; Nikolajsen, L. F.; Huang, X. P.; Wu, Y.; Shen, L.; Bjørn-Yoshimoto, W. E.; Ding, K.; Wacker, D.; Han, G. W.; Cheng, J.; Katritch, V.; Jensen, A. A.; Hanson, M. A.; Zhao, S.; Gloriam, D. E.; Roth, B. L.; Stevens, R. C.; Liu, Z. J. 5-HT_{2C} Receptor Structures Reveal the Structural Basis of GPCR Polypharmacology. *Cell* **2018**, *172* (4), 719-730.e14.
- (78) Rovati, G. E.; Capra, V.; Shaw, V. S.; Malik, R. U.; Sivaramakrishnan, S.; Neubig, R. R. The DRY Motif and the Four Corners of the Cubic Ternary Complex Model. *Cell. Signal.* **2017**, *35* (January), 16–23.
- (79) Johnson, M. S.; Robertson, D. N.; Holland, P. J.; Lutz, E. M.; Mitchell, R. Role of the Conserved NPxxY Motif of the 5-HT_{2A} Receptor in Determining Selective Interaction with Isoforms of ADP-

7. References

- Ribosylation Factor (ARF). *Cell. Signal.* **2006**, *18* (10), 1793–1800.
- (80) Kristiansen, K.; Kroeze, W. K.; Willins, D. L.; Gelber, E. I.; Savage, J. E.; Glennon, R. A.; Roth, B. L. A Highly Conserved Aspartic Acid (Asp-155) Anchors the Terminal Amine Moiety of Tryptamines and Is Involved in Membrane Targeting of the 5-HT_{2A} Serotonin Receptor But Does Not Participate in Activation via a “Salt-Bridge Disruption.” *J. Pharmacol. Exp. Ther.* **2000**, *293* (3), 735–746.
- (81) Trzaskowski, B.; Latek, D.; Yuan, S.; Ghoshdastider, U.; Filipek, A. D. and S. Action of Molecular Switches in GPCRs - Theoretical and Experimental Studies. *Current Medicinal Chemistry.* 2012, pp 1090–1109.
- (82) Hulme, E. C. GPCR Activation: A Mutagenic Spotlight on Crystal Structures. *Trends Pharmacol. Sci.* **2013**, *34* (1), 67–84.
- (83) Wacker, D.; Wang, S.; McCorvy, J. D.; Betz, R. M.; Venkatakrishnan, A. J.; Levit, A.; Lansu, K.; Schools, Z. L.; Che, T.; Nichols, D. E.; Shoichet, B. K.; Dror, R. O.; Roth, B. L. Crystal Structure of an LSD-Bound Human Serotonin Receptor. *Cell* **2017**, *168* (3), 377-389.e12.
- (84) Wang, S.; Che, T.; Levit, A.; Shoichet, B. K.; Wacker, D.; Roth, B. L. Structure of the D₂ Dopamine Receptor Bound to the Atypical Antipsychotic Drug Risperidone. *Nature* **2018**, *555*, 269–273.
- (85) Yin, W.; Zhou, X. E.; Yang, D.; De Waal, P. W.; Wang, M.; Dai, A.; Cai, X.; Huang, C. Y.; Liu, P.; Wang, X.; Yin, Y.; Liu, B.; Zhou, Y.; Wang, J.;

7. References

- Liu, H.; Caffrey, M.; Melcher, K.; Xu, Y.; Wang, M. W.; Xu, H. E.; Jiang, Y. Crystal Structure of the Human 5-HT_{1B} Serotonin Receptor Bound to an Inverse Agonist. *Cell Discov.* **2018**, *4* (1).
- (86) Shimamura, T.; Shiroishi, M.; Weyand, S.; Tsujimoto, H.; Winter, G.; Katritch, V.; Abagyan, R.; Cherezov, V.; Liu, W.; Han, G. W.; Kobayashi, T.; Stevens, R. C.; Iwata, S. Structure of the Human Histamine H₁ Receptor Complex with Doxepin. *Nature* **2011**, *475*, 65–70.
- (87) Deupi, X.; Standfuss, J. Structural Insights into Agonist-Induced Activation of G-Protein-Coupled Receptors. *Curr. Opin. Struct. Biol.* **2011**, *21* (4), 541–551.
- (88) Casey, A. B.; Cui, M.; Booth, R. G.; Canal, C. E. “Selective” Serotonin 5-HT_{2A} Receptor Antagonists. *Biochem. Pharmacol.* **2022**, *200*, 115028.
- (89) Hunter, C.; Singh, J.; Thornton, J. Pi-pi Interactions: The Geometry and Energetics of Phenylalanine-phenylalanine Interactions in Proteins. *Journal of molecular biology*. London 1991, p 837.
- (90) Hunter, C. A.; Lawson, K. R.; Perkins, J.; Urch, C. J. Aromatic Interactions. *J. Chem. Soc. Perkin Trans. 2* **2001**, No. 5, 651–669.
- (91) Bhattacharyya, R.; Samanta, U. Aromatic-Aromatic Interactions in and around α -Helices. *Protein Eng.* **2002**, *15* (2), 91–100.
- (92) Huidobro-Toro, J. P.; Harris, R. A. Brain Lipids That Induce Sleep

7. References

- Are Novel Modulators of 5-Hydroxytryptamine Receptors. *Proc. Natl. Acad. Sci. U. S. A.* **1996**, 93 (15), 8078–8082.
- (93) Casey, A. B.; Mukherjee, M.; McGlynn, R. P.; Cui, M.; Kohut, S. J.; Booth, R. G. A New Class of 5-HT_{2A}/5-HT_{2C} Receptor Inverse Agonists: Synthesis, Molecular Modeling, in Vitro and in Vivo Pharmacology of Novel 2-Aminotetralins. *Br. J. Pharmacol.* **2021**.
- (94) Blake Hill, R.; Degrado, W. F. Solution Structure of A2d, a Nativelike de Novo Designed Protein. *J. Am. Chem. Soc.* **1998**, 120 (6), 1138–1145.
- (95) de Haan, H. W.; Tolokh, I. S.; Gray, C. G.; Goldman, S. Non-Equilibrium Molecular Dynamics Study of KcsA Gating VO - 80 RT. *Physical Review E.* 2006, p 030905(R).
- (96) Biggin, P. C.; Sansom, M. S. P. Open-State Models of a Potassium Channel. *Biophys. J.* **2002**, 83 (4), 1867–1876.
- (97) Sykes, D. A.; Charlton, S. J. Slow Receptor Dissociation Is Not a Key Factor in the Duration of Action of Inhaled Long-Acting B₂-Adrenoceptor Agonists. *Br. J. Pharmacol.* **2012**, 165 (8), 2672–2683.
- (98) Sykes, D. A.; Parry, C.; Reilly, J.; Wright, P.; Fairhurst, R. A.; Charlton, S. J. Observed Drug-Receptor Association Rates Are Governed by Membrane Affinity: The Importance of Establishing “Micro-Pharmacokinetic/Pharmacodynamic Relationships” at the B₂-Adrenoceptor. *Mol. Pharmacol.* **2014**, 85 (4), 608–617.

7. References

- o, T. D.; Gawrisch, K.; Pitman, M. C.; Reggio, P. H. A Lipid Pathway for Ligand Binding Is Necessary for a Cannabinoid G Protein-Coupled Receptor. *J. Biol. Chem.* **2010**, *285* (23), 17954–17964.
- (100) Hanson, M. A.; Roth, C. B.; Jo, E.; Griffith, M. T.; Scott, F. L.; Reinhart, G.; Desale, H.; Clemons, B.; Cahalan, S. M.; Schuerer, S. C.; Sanna, M. G.; Han, G. W.; Kuhn, P.; Rosen, H.; Stevens, R. C. Crystal Structure of a Lipid G Protein-Coupled Receptor. *Science* (80-). **2012**, *335*, 851–855.
- (101) Hildebrand, P. W.; Scheerer, P.; Park, J. H.; Choe, H. W.; Piechnick, R.; Ernst, O. P.; Hofmann, K. P.; Heck, M. A Ligand Channel through the G Protein Coupled Receptor Opsin. *PLoS One* **2009**, *4* (2), :e4382.
- (102) Cao, D.; Yu, J.; Wang, H.; Luo, Z.; Liu, X.; He, L.; Qi, J.; Fan, L.; Tang, L.; Chen, Z.; Li, J.; Cheng, J.; Wang, S. Structure-Based Discovery of Nonhallucinogenic Psychedelic Analogs. *Science* (80-). **2022**, *375*, 403–411.
- (103) Chen, J.; Garcia, E. J.; Merritt, C. R.; Zamora, J. C.; Bolinger, A. A.; Pazdrak, K.; Stafford, S. J.; Mifflin, R. C.; Wold, E. A.; Wild, C. T.; Chen, H.; Anastasio, N. C.; Cunningham, K. A.; Zhou, J. Discovery of Novel Oleamide Analogues as Brain-Penetrant Positive Allosteric Serotonin 5-HT_{2C} Receptor and Dual 5-HT_{2C}/5-HT_{2A} Receptor Modulators. *J. Med. Chem.* **2023**, *66* (14), 9992–10009.
- (104) Pottie, E.; Poulie, C. B. M.; Simon, I. A.; Harpsøe, K.; D'Andrea, L.;

7. References

- Komarov, I. V.; Gloriam, D. E.; Jensen, A. A.; Kristensen, J. L.; Stove, C. P. Structure–Activity Assessment and In-Depth Analysis of Biased Agonism in a Set of Phenylalkylamine 5-HT_{2A} Receptor Agonists. *ACS Chem. Neurosci.* **2023**, *14*, 2727–2742.
- (105) Cordes, F. S.; Bright, J. N.; Sansom, M. S. P. Proline-Induced Distortions of Transmembrane Helices. *J. Mol. Biol.* **2002**, *323* (5), 951–960.
- (106) S.P.Sansom, M.; Weinstein, H. Hinges, Swivels and Switches: The Role of Prolines in Signalling via Transmembrane α -Helices. *Trends Pharmacol. Sci.* **2000**, *21* (11), 445–451.
- (107) Shrivastava, I. H.; Sansom, M. S. P. Simulations of Ion Permeation through a Potassium Channel: Molecular Dynamics of KcsA in a Phospholipid Bilayer. *Biophys. J.* **2000**, *78* (2), 557–570.
- (108) Bright, J. N.; Shrivastava, I. H.; Cordes, F. S.; Sansom, M. S. P. Conformational Dynamics of Helix S6 from Shaker Potassium Channel: Simulation Studies. *Biopolymers* **2002**, *64* (6), 303–313.
- (109) Ulmschneider, M. B.; Tieleman, D. P.; Sansom, M. S. P. The Role of Extra-Membranous Inter-Helical Loops in Helix-Helix Interactions. *Protein Eng. Des. Sel.* **2005**, *18* (12), 563–570.
- (110) Deber, C. M.; Therien, A. G. Putting the β -Breaks on Membrane Protein Misfolding. *Nat. Struct. Biol.* **2002**, *9* (5), 318–319.
- (111) Li, S. C.; Deber, C. M. Glycine and β -Branched Residues Support and

7. References

- Modulate Peptide Helicity in Membrane Environments. *FEBS Lett.* **1992**, 311 (3), 217–220.
- (112) Jiang, Y.; Lee, A.; Chen, J.; Cadene, M.; Chait, B. T.; MacKinnon, R. The Open Pore Conformation of Potassium Channels. *Nature* **2002**, 417, 523–526.
- (113) Aarli J A; Avanzini, G.; Bertolote, M, J.; de Boer, H.; Breivik, H. *Neurological Disorders : Public Health Challenges*; Geneva, 1996.
- (114) Feigin, V. L.; Nichols, E.; Alam, T.; Bannick, M. S.; Beghi, E.; Blake, N.; Culpepper, W. J.; Dorsey, E. R.; Elbaz, A.; Ellenbogen, R. G.; Fisher, J. L.; Fitzmaurice, C.; Giussani, G.; Glennie, L.; James, S. L.; Johnson, C. O.; Kassebaum, N. J.; Logroscino, G.; Marin, B.; Mountjoy-Venning, W. C.; Nguyen, M.; Ofori-Asenso, R.; Patel, A. P.; Piccininni, M.; Roth, G. A.; Steiner, T. J.; Stovner, L. J.; Szoeki, C. E. I.; Theadom, A.; Vollset, S. E.; Wallin, M. T.; Wright, C.; Zunt, J. R.; Abbasi, N.; Abd-Allah, F.; Abdelalim, A.; Abdollahpour, I.; Aboyans, V.; Abraha, H. N.; Acharya, D.; Adamu, A. A.; Adebayo, O. M.; Adeoye, A. M.; Adsuar, J. C.; Afarideh, M.; Agrawal, S.; Ahmadi, A.; Ahmed, M. B.; Aichour, A. N.; Aichour, I.; Aichour, M. T. E.; Akinyemi, R. O.; Akseer, N.; Al-Eyadhy, A.; Al-Shahi Salman, R.; Alahdab, F.; Alene, K. A.; Aljunid, S. M.; Altirkawi, K.; Alvis-Guzman, N.; Anber, N. H.; Antonio, C. A. T.; Arabloo, J.; Aremu, O.; Ärnlov, J.; Asayesh, H.; Asghar, R. J.; Atalay, H. T.; Awasthi, A.; Ayala Quintanilla, B. P.; Ayuk, T. B.; Badawi, A.; Banach, M.; Banoub, J. A. M.; Barboza, M.

7. References

A.; Barker-Collo, S. L.; Bärnighausen, T. W.; Baune, B. T.; Bedi, N.; Behzadifar, M.; Behzadifar, M.; Béjot, Y.; Bekele, B. B.; Belachew, A. B.; Bennett, D. A.; Bensenor, I. M.; Berhane, A.; Beuran, M.; Bhattacharyya, K.; Bhutta, Z. A.; Biadgo, B.; Bijani, A.; Bililign, N.; Bin Sayeed, M. S.; Blazes, C. K.; Brayne, C.; Butt, Z. A.; Campos-Nonato, I. R.; Cantu-Brito, C.; Car, M.; Cárdenas, R.; Carrero, J. J.; Carvalho, F.; Castañeda-Orjuela, C. A.; Castro, F.; Catalá-López, F.; Cerin, E.; Chaiah, Y.; Chang, J. C.; Chatziralli, I.; Chiang, P. P. C.; Christensen, H.; Christopher, D. J.; Cooper, C.; Cortesi, P. A.; Costa, V. M.; Criqui, M. H.; Crowe, C. S.; Damasceno, A. A. M.; Daryani, A.; De la Cruz-Góngora, V.; De La Hoz, F. P.; De Leo, D.; Degefa, M. G.; Demoz, G. T.; Deribe, K.; Dharmaratne, S. D.; Diaz, D.; Dinberu, M. T.; Djalalinia, S.; Doku, D. T.; Dubey, M.; Dubljanin, E.; Duken, E. E.; Edvardsson, D.; El-Khatib, Z.; Endres, M.; Endries, A. Y.; Eskandarieh, S.; Esteghamati, A.; Esteghamati, S.; Farhadi, F.; Faro, A.; Farzadfar, F.; Farzaei, M. H.; Fatima, B.; Fereshtehnejad, S. M.; Fernandes, E.; Feyissa, G. T.; Filip, I.; Fischer, F.; Fukumoto, T.; Ganji, M.; Gankpe, F. G.; Garcia-Gordillo, M. A.; Gebre, A. K.; Gebremichael, T. G.; Gelaw, B. K.; Geleijnse, J. M.; Geremew, D.; Gezae, K. E.; Ghasemi-Kasman, M.; Gidey, M. Y.; Gill, P. S.; Gill, T. K.; Gnedovskaya, E. V.; Goulart, A. C.; Grada, A.; Grosso, G.; Guo, Y.; Gupta, R.; Gupta, R.; Haagsma, J. A.; Hagos, T. B.; Haj-Mirzaian, A.; Haj-Mirzaian, A.; Hamadeh, R. R.; Hamidi, S.; Hankey, G. J.; Hao, Y.; Haro, J. M.; Hassankhani, H.; Hassen, H. Y.; Havmoeller, R.; Hay, S. I.; Hegazy,

7. References

M. I.; Heidari, B.; Henok, A.; Heydarpour, F.; Hoang, C. L.; Hole, M. K.; Homaie Rad, E.; Hosseini, S. M.; Hu, G.; Igumbor, E. U.; Ilesanmi, O. S.; Irvani, S. S. N.; Islam, S. M. S.; Jakovljevic, M.; Javanbakht, M.; Jha, R. P.; Jobanputra, Y. B.; Jonas, J. B.; Józwiak, J. J.; Jürisson, M.; Kahsay, A.; Kalani, R.; Kalkonde, Y.; Kamil, T. A.; Kanchan, T.; Karami, M.; Karch, A.; Karimi, N.; Kasaeian, A.; Kassa, T. D.; Kassa, Z. Y.; Kaul, A.; Kefale, A. T.; Keiyoro, P. N.; Khader, Y. S.; Khafaie, M. A.; Khalil, I. A.; Khan, E. A.; Khang, Y. H.; Khazaie, H.; Kiadaliri, A. A.; Kiirithio, D. N.; Kim, A. S.; Kim, D.; Kim, Y. E.; Kim, Y. J.; Kisa, A.; Kokubo, Y.; Koyanagi, A.; Krishnamurthi, R. V.; Kuate Defo, B.; Kucuk Bicer, B.; Kumar, M.; Lacey, B.; Lafranconi, A.; Lansingh, V. C.; Latifi, A.; Leshargie, C. T.; Li, S.; Liao, Y.; Linn, S.; Lo, W. D.; Lopez, J. C. F.; Lorkowski, S.; Lotufo, P. A.; Lucas, R. M.; Lunevicius, R.; Mackay, M. T.; Mahotra, N. B.; Majdan, M.; Majdzadeh, R.; Majeed, A.; Malekzadeh, R.; Malta, D. C.; Manafi, N.; Mansournia, M. A.; Mantovani, L. G.; März, W.; Mashamba-Thompson, T. P.; Massenburg, B. B.; Mate, K. K. V.; McAlinden, C.; McGrath, J. J.; Mehta, V.; Meier, T.; Meles, H. G.; Melese, A.; Memiah, P. T. N.; Memish, Z. A.; Mendoza, W.; Mengistu, D. T.; Mengistu, G.; Meretoja, A.; Meretoja, T. J.; Mestrovic, T.; Miazgowski, B.; Miazgowski, T.; Miller, T. R.; Mini, G. K.; Mirrakhimov, E. M.; Moazen, B.; Mohajer, B.; Mohammad Gholi Mezerji, N.; Mohammadi, M.; Mohammadi-Khanaposhtani, M.; Mohammadibakhsh, R.; Mohammadnia-Afrouzi, M.; Mohammed, S.; Mohebi, F.; Mokdad, A.

7. References

H.; Monasta, L.; Mondello, S.; Moodley, Y.; Moosazadeh, M.; Moradi, G.; Moradi-Lakeh, M.; Moradinazar, M.; Moraga, P.; Moreno Velásquez, I.; Morrison, S. D.; Mousavi, S. M.; Muhammed, O. S.; Muruet, W.; Musa, K. I.; Mustafa, G.; Naderi, M.; Nagel, G.; Naheed, A.; Naik, G.; Najafi, F.; Nangia, V.; Negoï, I.; Negoï, R. I.; Newton, C. R. J.; Ngunjiri, J. W.; Nguyen, C. T.; Nguyen, L. H.; Ningrum, D. N. A.; Nirayo, Y. L.; Nixon, M. R.; Norrving, B.; Noubiap, J. J.; Nourollahpour Shiadeh, M.; Nyasulu, P. S.; Ogbo, F. A.; Oh, I. H.; Olagunju, A. T.; Olagunju, T. O.; Olivares, P. R.; Onwujekwe, O. E.; Oren, E.; Owolabi, M. O.; A, M. P.; Pakpour, A. H.; Pan, W. H.; Panda-Jonas, S.; Pandian, J. D.; Patel, S. K.; Pereira, D. M.; Petzold, M.; Pillay, J. D.; Piradov, M. A.; Polanczyk, G. V.; Polinder, S.; Postma, M. J.; Poulton, R.; Poustchi, H.; Prakash, S.; Prakash, V.; Qorbani, M.; Radfar, A.; Rafay, A.; Rafiei, A.; Rahim, F.; Rahimi-Movaghar, V.; Rahman, M.; Rahman, M. H. U.; Rahman, M. A.; Rajati, F.; Ram, U.; Ranta, A.; Rawaf, D. L.; Rawaf, S.; Reinig, N.; Reis, C.; Renzaho, A. M. N.; Resnikoff, S.; Rezaeian, S.; Rezai, M. S.; Rios González, C. M.; Roberts, N. L. S.; Roever, L.; Ronfani, L.; Roro, E. M.; Roshandel, G.; Rostami, A.; Sabbagh, P.; Sacco, R. L.; Sachdev, P. S.; Saddik, B.; Safari, H.; Safari-Faramani, R.; Safi, S.; Safiri, S.; Sagar, R.; Sahathevan, R.; Sahebkar, A.; Sahraian, M. A.; Salamati, P.; Salehi Zahabi, S.; Salimi, Y.; Samy, A. M.; Sanabria, J.; Santos, I. S.; Santric Milicevic, M. M.; Sarrafzadegan, N.; Sartorius, B.; Sarvi, S.; Sathian, B.; Satpathy, M.; Sawant, A. R.; Sawhney, M.; Schneider, I. J. C.;

7. References

Schöttker, B.; Schwebel, D. C.; Seedat, S.; Sepanlou, S. G.; Shabaninejad, H.; Shafieesabet, A.; Shaikh, M. A.; Shakir, R. A.; Shams-Beyranvand, M.; Shamsizadeh, M.; Sharif, M.; Sharif-Alhoseini, M.; She, J.; Sheikh, A.; Sheth, K. N.; Shigematsu, M.; Shiri, R.; Shirkoohi, R.; Shiue, I.; Siabani, S.; Siddiqi, T. J.; Sigfusdottir, I. D.; Sigurvinsdottir, R.; Silberberg, D. H.; Silva, J. P.; Silveira, D. G. A.; Singh, J. A.; Sinha, D. N.; Skiadaresi, E.; Smith, M.; Sobaih, B. H.; Sobhani, S.; Soofi, M.; Soyiri, I. N.; Sposato, L. A.; Stein, D. J.; Stein, M. B.; Stokes, M. A.; Sufiyan, M. B.; Sykes, B. L.; Sylaja, P.; Tabarés-Seisdedos, R.; Te Ao, B. J.; Tehrani-Banihashemi, A.; Temsah, M. H.; Temsah, O.; Thakur, J. S.; Thrift, A. G.; Topor-Madry, R.; Tortajada-Girbés, M.; Tovani-Palone, M. R.; Tran, B. X.; Tran, K. B.; Truelsen, T. C.; Tsadik, A. G.; Tudor Car, L.; Ukwaja, K. N.; Ullah, I.; Usman, M. S.; Uthman, O. A.; Valdez, P. R.; Vasankari, T. J.; Vasanthan, R.; Veisani, Y.; Venketasubramanian, N.; Violante, F. S.; Vlassov, V.; Vosoughi, K.; Vu, G. T.; Vujcic, I. S.; Wagnew, F. S.; Waheed, Y.; Wang, Y. P.; Weiderpass, E.; Weiss, J.; Whiteford, H. A.; Wijeratne, T.; Winkler, A. S.; Wiysonge, C. S.; Wolfe, C. D. A.; Xu, G.; Yadollahpour, A.; Yamada, T.; Yano, Y.; Yaseri, M.; Yatsuya, H.; Yimer, E. M.; Yip, P.; Yisma, E.; Yonemoto, N.; Yousefifard, M.; Yu, C.; Zaidi, Z.; Zaman, S. Bin; Zamani, M.; Zandian, H.; Zare, Z.; Zhang, Y.; Zodpey, S.; Naghavi, M.; Murray, C. J. L.; Vos, T. Global, Regional, and National Burden of Neurological Disorders, 1990–2016: A Systematic Analysis for the Global Burden of Disease Study 2016.

7. References

- Lancet Neurol.* **2019**, *18* (5), 459–480.
- (115) Fields, J. Z.; Reisine, T. D.; Yamamura, H. I. Biochemical Demonstration of Dopaminergic Receptors in Rat and Human Brain Using [3H]Spiroperidol. *Brain Res.* **1977**, *136* (3), 578–584.
- (116) Creese, I.; Snyder, S. H. 3H-Spiroperidol Labels Serotonin Receptors in Rat Cerebral Cortex and Hippocampus. *Eur. J. Pharmacol.* **1978**, *49* (2), 201–202.
- (117) Knight, A. R.; Misra, A.; Quirk, K.; Benwell, K.; Revell, D.; Kennett, G.; Bickerdike, M. Pharmacological Characterisation of the Agonist Radioligand Binding Site of 5-HT_{2A}, 5-HT_{2B} and 5-HT_{2C} Receptors. *Naunyn. Schmiedeberg's. Arch. Pharmacol.* **2004**, *370* (2), 114–123.
- (118) Bonhaus, D. W.; Bach, C.; DeSouza, A.; Salazar, F. H. R.; Matsuoka, B. D.; Zuppan, P.; Chan, H. W.; Eglen, R. M. The Pharmacology and Distribution of Human 5-hydroxytryptamine 2B (5-HT_{2B}) Receptor Gene Products: Comparison with 5-HT_{2A} and 5-HT_{2C} Receptors. *Br. J. Pharmacol.* **1995**, *115* (4), 622–628.
- (119) Yoshio, R.; Taniguchi, T.; Itoh, H.; Muramatsu, I. Affinity of Serotonin Receptor Antagonists and Agonists to Recombinant and Native A₁-Adrenoceptor Subtypes. *Jpn. J. Pharmacol.* **2001**, *86* (2), 189–195.
- (120) Newman-Tancredi, A.; Wootton, R.; Strange, P. G. High-Level Stable Expression of Recombinant 5-HT(1A) 5-Hydroxytryptamine

7. References

- Receptors in Chinese Hamster Ovary Cells. *Biochem. J.* **1992**, *285* (3), 933–938.
- (121) Krobert, K. A.; Bach, T.; Syversveen, T.; Kvingedal, A. M.; Levy, F. O. The Cloned Human 5-HT₇ Receptor Splice Variants: A Comparative Characterization of Their Pharmacology, Function and Distribution. *Naunyn. Schmiedeberg's Arch. Pharmacol.* **2001**, *363* (6), 620–632.
- (122) Leysen, J. E.; Gommeren, W.; Van Gompel, P.; Wynants, J.; Janssen, P. F.; Laduron, P. M. Receptor-Binding Properties in Vitro and in Vivo of Ritanserin: A Very Potent and Long Acting Serotonin-S₂ Antagonist. *Mol. Pharmacol.* **1985**, *27* (6), 600–611.
- (123) Metwally, K. A.; Dukat, M.; Egan, C. T.; Smith, C.; DuPre, A.; Gauthier, C. B.; Herrick-Davis, K.; Teitler, M.; Glennon, R. A. Spiperone: Influence of Spiro Ring Substituents on 5-HT_{2A} Serotonin Receptor Binding. *J. Med. Chem.* **1998**, *41* (25), 5084–5093.
- (124) Meloni, F.; Transi, M. G.; Sciacca, V.; De Felice, C.; Bagarone, A.; Sciacca, A. Therapeutic Efficacy of Ketanserin, a Selective Antagonist of the Serotonin (5-HT₂) Receptors, in Primary and Secondary Raynaud's Phenomenon. *Angiology* **1987**, *38* (7), 530–536.
- (125) Milei, J.; Lemus, J.; Finkielman, S.; Nahmod, V. E.; Bernardiner, E. Ketanserin in the Treatment of Essential Hypertension a Double Blind Trial against Metoprolol Followed by One-Year Open

7. References

- Treatment. *Clin. Exp. Hypertens. Part A Theory Pract.* **1989**, *11* (3), 371–389.
- (126) Sommer, I. E. C.; Kleijer, H.; Visser, L.; van Laar, T. *Successful Treatment of Intractable Visual Hallucinations with 5-HT_{2A} Antagonist Ketanserin*; 2018.
- (127) Hoyer, D.; Vos, P.; Closse, A.; Pazos, A.; Palacios, J. M.; Davies, H. [3H]Ketanserin Labels 5-HT₂ Receptors and A₁-Adrenoceptors in Human and Pig Brain Membranes. *Naunyn. Schmiedebergs. Arch. Pharmacol.* **1987**, *335* (3), 226–230.
- (128) Bucholtz, E. C.; Brown, R. L.; Tropsha, A.; Booth, R. G.; Wyrick, S. D. Synthesis, Evaluation, and Comparative Molecular Field Analysis of 1-Phenyl-3-Amino-1,2,3,4-Tetrahydronaphthalenes as Ligands for Histamine H₁ Receptors. *J. Med. Chem.* **1999**, *42* (16), 3041–3054.
- (129) López-Giménez, J. F.; Mengod, G.; Palacios, J. M.; Vilaró, M. T. Selective Visualization of Rat Brain 5-HT_{2A} Receptors by Autoradiography with [3H]MDL 100,907. *Naunyn. Schmiedebergs. Arch. Pharmacol.* **1997**, *356* (4), 446–454.
- (130) Leysen, J. E.; Niemegeers, C. J.; Nueten, J. M. Van; Laduron, P. M. [3H]Ketanserin (R 41 468), a Selective 3H-Ligand for Serotonin₂ Receptor Binding Sites. Binding Properties, Brain Distribution, and Functional Role. *Mol. Pharmacol.* **1982**, *21* (2), 301–314.
- (131) Liechti, M. E. *Role of the Serotonin 5-HT_{2A} Receptor in Mescaline-*

7. References

Induced Altered States of Consciousness (MDR); 2023.

- (132) Kraehenmann, R.; Pokorny, D.; Vollenweider, L.; Preller, K. H.; Pokorny, T.; Seifritz, E.; Vollenweider, F. X. Dreamlike Effects of LSD on Waking Imagery in Humans Depend on Serotonin 2A Receptor Activation. *Psychopharmacology (Berl)*. **2017**, *234* (13), 2031–2046.
- (133) Hadar, A.; David, J.; Shalit, N.; Roseman, L.; Gross, R.; Sessa, B.; Lev-Ran, S. The Psychedelic Renaissance in Clinical Research: A Bibliometric Analysis of Three Decades of Human Studies with Psychedelics. *J. Psychoactive Drugs* **2023**, *55* (1), 1–10.
- (134) Palfreyman, M. G.; Schmidt, C. J.; Sorensen, S. M.; Dudley, M. W.; Kehne, J. H.; Moser, P.; Gittos, M. W.; Carr, A. A. Electrophysiological, Biochemical and Behavioral Evidence for 5-HT₂ and 5-HT₃ Mediated Control of Dopaminergic Function. *Psychopharmacology (Berl)*. **1993**, *112* (1), S60–S67.
- (135) Kehne, J. H.; Baron, B. M.; Carr, A. A.; Chaney, S. F.; Elands, J.; Feldman, D. J.; Frank, R. A.; Giersbergen, P. L. van; McCloskey, T. C.; Johnson, M. P.; McCarty, D. R.; Poirot, M.; Senyah, Y.; Siegel, B. W.; Widmaier, C. Preclinical Characterization of the Potential of the Putative Atypical Antipsychotic MDL 100,907 as a Potent 5-HT_{2A} Antagonist with a Favorable CNS Safety Profile. *J. Pharmacol. Exp. Ther.* **1996**, *277* (2), 968–981.
- (136) Canal, C. E.; Cordova-Sintjago, T.; Liu, Y.; Kim, M. S.; Morgan, D.;

7. References

- Booth, R. G. Molecular Pharmacology and Ligand Docking Studies Reveal a Single Amino Acid Difference between Mouse and Human Serotonin 5-HT_{2A} Receptors That Impacts Behavioral Translation of Novel 4-Phenyl-2-Dimethylaminotetralin Ligands. *J. Pharmacol. Exp. Ther.* **2013**, *347* (3), 705–716.
- (137) Pucadyil, T. J.; Chattopadhyay, A. Cholesterol Modulates Ligand Binding and G-Protein Coupling to Serotonin_{1A} Receptors from Bovine Hippocampus. *Biochim. Biophys. Acta - Biomembr.* **2004**, *1663* (1), 188–200.
- (138) Barr, A. M.; Lehmann-Masten, V.; Paulus, M.; Gainetdinov, R. R.; Caron, M. G.; Geyer, M. A. The Selective Serotonin-2A Receptor Antagonist M100907 Reverses Behavioral Deficits in Dopamine Transporter Knockout Mice. *Neuropsychopharmacology* **2004**, *29* (2), 221–228
- (139) Canal, C. E.; Booth, R. G.; Morgan, D. Support for 5-HT_{2C} Receptor Functional Selectivity in Vivo Utilizing Structurally Diverse, Selective 5-HT_{2C} Receptor Ligands and the 2,5-Dimethoxy-4-Iodoamphetamine Elicited Head-Twitch Response Model. *Neuropharmacology* **2013**, *70*, 112–121.
- (140) Sorensen, S. M.; Kehne, J. H.; Fadayel, G. M.; Humphreys, T. M.; Ketteler, H. J.; Sullivan, C. K.; Taylor, V. L.; Schmidt, C. J. Characterization of the 5-HT₂ Receptor Antagonist MDL 100907 as a Putative Atypical Antipsychotic: Behavioral,

7. References

- Electrophysiological and Neurochemical Studies. *J. Pharmacol. Exp. Ther.* **1993**, 266 (2), 684–691.
- (141) Gründer, G.; Yokoi, F.; Offord, S. J.; Ravert, H. T.; Dannals, R. F.; Salzmann, J. K.; Szymanski, S.; Wilson, P. D.; Howard, D. R.; Wong, D. F. Time Course of 5-HT_{2A} Receptor Occupancy in the Human Brain after a Single Oral Dose of the Putative Antipsychotic Drug MDL 100,907 Measured by Positron Emission Tomography. *Neuropsychopharmacology* **1997**, 17 (3), 175–185.
- (142) de Paulis, T. M-100907 (Aventis). *Curr. Opin. Investig. Drugs* **2001**, 2 (1), 123–132.
- (143) Hacksell, U.; Burstein, E. S.; McFarland, K.; Mills, R. G.; Williams, H. On the Discovery and Development of Pimavanserin: A Novel Drug Candidate for Parkinson's Psychosis. *Neurochem. Res.* **2014**, 39 (10), 2008–2017.
- (144) Cummings, J.; Isaacson, S.; Mills, R.; Williams, H.; Chi-Burris, K.; Corbett, A.; Dhall, R.; Ballard, C. Pimavanserin for Patients with Parkinson's Disease Psychosis: A Randomised, Placebo-Controlled Phase 3 Trial. *Lancet* **2014**, 383, 533–540.
- (145) Ava, M.; Dirks, B.; Freeman, M. P.; Papakostas, G. I.; Shelton, R. C.; Thase, M. E.; Trivedi, M. H.; Liu, K.; Stankovic, S. A Phase 2, Randomized, Double-Blind, Placebo-Controlled Study of Adjunctive Pimavanserin in Patients With Major Depressive Disorder and an Inadequate Response to Therapy. *J Clin Psychiatry.* **2019**, 80 (6).

7. References

- (146) Meltzer, H. Y.; Mills, R.; Revell, S.; Williams, H.; Johnson, A.; Bahr, D.; Friedman, J. H. Pimavanserin, a Serotonin 2A Receptor Inverse Agonist, for the Treatment of Parkinson's Disease Psychosis. *Neuropsychopharmacology* **2010**, *35* (4), 881–892.
- (147) Ancoli-Israel, S.; Vanover, K. E.; Weiner, D. M.; Davis, R. E.; van Kammen, D. P. Pimavanserin Tartrate, a 5-HT_{2A} Receptor Inverse Agonist, Increases Slow Wave Sleep as Measured by Polysomnography in Healthy Adult Volunteers. *Sleep Med.* **2011**, *12* (2), 134–141.
- (148) Kao, H. T.; Adham, N.; Olsen, M. A.; Weinshank, R. L.; Branchek, T. A.; Hartig, P. R. Site-Directed Mutagenesis of a Single Residue Changes the Binding Properties of the Serotonin 5-HT₂ Receptor from a Human to a Rat Pharmacology. *FEBS Lett.* **1992**, *307* (3), 324–328.
- (149) Johnson, M. P.; Loncharich, R. J.; Baez, M.; Nelson, D. L. Species Variations in Transmembrane Region V of the 5-Hydroxytryptamine Type 2A Receptor Alter the Structure-Activity Relationship of Certain Ergolines and Tryptamines. *Mol. Pharmacol.* **1994**, *45* (2), 277–286.
- (150) Muneta-Arrate, I.; Diez-Alarcia, R.; Horrillo, I.; Meana, J. J. Pimavanserin Exhibits Serotonin 5-HT_{2A} Receptor Inverse Agonism for G_{ai}1- and Neutral Antagonism for G_{aq}/11-Proteins in Human Brain Cortex. *Eur. Neuropsychopharmacol.* **2020**, *36*, 83–

7. References

- 89.
- (151) Ma, M.; Yang, Y.; Du, G.; Dai, Y.; Zhu, X.; Wang, W.; Liu, W.; Ye, L.; Zhang, R.; Tian, J. Structure-Based Development of Novel 5-HT_{2A} Receptor Antagonists / Inverse Agonists. *Eur. J. Med. Chem.* **2022**, *234*, 114246.
- (152) Arnt, J.; Skarsfeldt, T. Do Novel Antipsychotics Have Similar Pharmacological Characteristics? A Review of the Evidence. *Neuropsychopharmacology* **1998**, *18* (2), 63–101.
- (153) Alex, D. K.; Pehek, A. E. Pharmacologic Mechanisms of Serotonergic Regulation of Dopamine Neurotransmission. *Pharmacol. Ther.* **2007**, *113* (2), 296–320.
- (154) Porras, G.; Matteo, V. Di; Ph, D.; Fracasso, C.; Lucas, G.; Spampinato, U. Modulate Dopamine Release Induced in Vivo by Amphetamine and Morphine in Both the Rat Nucleus Accumbens and Striatum. *Neuropsychopharmacology* **2002**, *26* (3), 311–324.
- (155) Vanover, K. E.; Weiner, D. M.; Makhay, M.; Veinbergs, I.; Gardell, L. R.; Lameh, J.; Del Tredici, A. L.; Piu, F.; Schiffer, H. H.; Ott, T. R.; Burstein, E. S.; Uldam, A. K.; Thygesen, M. B.; Schlienger, N.; Andersson, C. M.; Son, T. Y.; Harvey, S. C.; Powell, S. B.; Geyer, M. A.; Tolf, B.-R.; Brann, M. R.; Davis, R. E. Pharmacological and Behavioral Profile of (4-Fluorophenylmethyl)-(1-Methylpiperidin-4-Yl)-(4-(2-Methylpropyloxy)Phenylmethyl) Carbamide. *J. Pharmacol. Exp. Ther.* **2006**, *317* (2), 910–918.

7. References

- (156) Martin, P.; Gillen, M.; Millson, D.; Oliver, S.; Brealey, C.; Grossbard, E. B.; Baluom, M.; Lau, D.; Sweeny, D.; Mant, T.; Craven, K. Effects of CYP3A4 Inhibitors Ketoconazole and Verapamil and the CYP3A4 Inducer Rifampicin on the Pharmacokinetic Parameters of Fostamatinib: Results from In Vitro and Phase I Clinical Studies. *Drugs R. D.* **2016**, *16* (1), 81–92.
- (157) Shannon, M. W. Chapter 5 - Drug Interactions. In *Haddad and Winchester's Clinical Management of Poisoning and Drug Overdose*; W.B. Saunders: Philadelphia, 2007; pp 97–104.
- (158) Basheer, L.; Kerem, Z. Interactions between CYP3A4 and Dietary Polyphenols. *Oxid. Med. Cell. Longev.* **2015**, 2015.
- (159) Nichols, D. E. Structure-Activity Relationships of Serotonin 5-HT_{2A} Agonists. *Wiley Interdiscip. Rev. Membr. Transp. Signal.* **2012**, *1* (5), 559–579.
- (160) Burstein, E. S.; Olsson, R.; Jansson, K. E.; Skold, N. P.; Wahlstron, L. Y.; Von Wachenfeldt, H.; Bergner, M. G. W.; Dreisch, K.; Popov, K.; Kovalenko, O.; Klingstedt, P. T. *Compounds, Salts There of and Methods for Treatment of Diseases*, 2019.
- (161) Kim, M.; Hwang, I.; Pagire, H. S.; Pagire, S. H.; Choi, W.; Choi, W. G.; Yoon, J.; Lee, W. M.; Song, J. S.; Yoo, E. K.; Lee, S. M.; Kim, M. J.; Bae, M. A.; Kim, D.; Lee, H.; Lee, E. Y.; Jeon, J. H.; Lee, I. K.; Kim, H.; Ahn, J. H. Design, Synthesis, and Biological Evaluation of New Peripheral 5HT_{2A} Antagonists for Nonalcoholic Fatty Liver

7. References

- Disease. *J. Med. Chem.* **2020**, 63 (8), 4171–4182.
- (162) Ismaiel, A. M.; Amida, K.; Teitler, M.; Glennon, R. A. Ketanserin Analogues : The Effect of Structural Modification Serotonin Receptor Binding. **1995**, 1196–1202.
- (163) Albujuq, N. R.; Meana, J. J.; Diez-alarcia, R.; Muneta-arrate, I.; Naqvi, A.; Althumayri, K.; Alsehli, M. Design , Synthesis , Molecular Docking , and Biological Evaluation of Novel Pimavanserin-Based Analogues as Potential Serotonin 5-HT_{2A} Receptor Inverse Agonists. *J. Med. Chem.* **2023**, 66 (13), 9057–9075.
- (164) Herndon, J. L.; Ismaiel, A.; Glennon, R. A.; Ingher, S. P.; Teitler, M. Ketanserin Analogues: Structure-Affinity Relationships for 5-HT₂ and 5-HT_{1C} Serotonin Receptor Binding. *J. Med. Chem.* **1992**, 35 (26), 4903–4910.
- (165) Bielenica, A.; Kędzierska, E.; Koliński, M.; Kmiecik, S.; Koliński, A.; Fiorino, F.; Severino, B.; Magli, E.; Corvino, A.; Rossi, I.; Massarelli, P.; Koziół, A. E.; Sawczenko, A.; Struga, M. 5-HT₂ Receptor Affinity, Docking Studies and Pharmacological Evaluation of a Series of 1,3-Disubstituted Thiourea Derivatives. *Eur. J. Med. Chem.* **2016**, 116, 173–186.
- (166) Sykes, D. A.; Stoddart, L. A.; Kilpatrick, L. E.; Hill, S. J. Binding Kinetics of Ligands Acting at GPCRs. *Mol. Cell. Endocrinol.* **2019**, 485, 9–19.
- (167) Stoddart, L. A.; Kilpatrick, L. E.; Briddon, S. J.; Hill, S. J. Probing the

7. References

- Pharmacology of G Protein-Coupled Receptors with Fluorescent Ligands. *Neuropharmacology* **2015**, *98*, 48–57.
- (168) Vernall, A. J.; Hill, S. J.; Kellam, B. The Evolving Small-Molecule Fluorescent-Conjugate Toolbox for Class A GPCRs. *Br. J. Pharmacol.* **2014**, *171* (5), 1073–1084.
- (169) Stoddart, L. A.; White, C. W.; Nguyen, K.; Hill, S. J.; Pflieger, K. D. G. Fluorescence- and Bioluminescence-Based Approaches to Study GPCR Ligand Binding. *Br. J. Pharmacol.* **2016**, *173* (20), 3028–3037.
- (170) Alonso, D.; Vázquez-Villa, H.; Gamo, A. M.; Martínez-Esperón, M. F.; Tortosa, M.; Viso, A.; Fernández De La Pradilla, R.; Junquera, E.; Aicart, E.; Martín-Fontecha, M.; Benhamú, B.; López-Rodríguez, M. L.; Ortega-Gutiérrez, S. Development of Fluorescent Ligands for the Human 5-HT_{1A} Receptor. *ACS Med. Chem. Lett.* **2010**, *1* (6), 249–253.
- (171) Cornelius, P.; Lee, E.; Lin, W.; Wang, R.; Werner, W.; Brown, J. A.; Stuhmeier, F.; Boyd, J. G.; McClure, K. Design, Synthesis, and Pharmacology of Fluorescently Labeled Analogs of Serotonin: Application to Screening of the 5-HT_{2C} Receptor. *J. Biomol. Screen.* **2009**, *14* (4), 360–370.
- (172) Azuaje, J.; López, P.; Iglesias, A.; De La Fuente, R. A.; Pérez-Rubio, J. M.; García, D.; Stępniewski, T. M.; García-Mera, X.; Brea, J. M.; Selent, J.; Pérez, D.; Castro, M.; Loza, M. I.; Sotelo, E. Development

7. References

- of Fluorescent Probes That Target Serotonin 5-HT_{2B} Receptors. *Sci. Rep.* **2017**, 7 (1), 1–16.
- (173) Simonin, J.; Vernekar, S. K. V.; Thompson, A. J.; Hothersall, J. D.; Connolly, C. N.; Lummis, S. C. R.; Lochner, M. High-Affinity Fluorescent Ligands for the 5-HT₃ Receptor. *Bioorganic Med. Chem. Lett.* **2012**, 22 (2), 1151–1155.
- (174) Berque-Bestel, I.; Soulier, J. L.; Giner, M.; Rivail, L.; Langlois, M.; Sicsic, S. Synthesis and Characterization of the First Fluorescent Antagonists for Human 5-HT₄ Receptors. *J. Med. Chem.* **2003**, 46 (13), 2606–2620.
- (175) Vázquez-Villa, H.; González-Vera, J. A.; Benhamú, B.; Viso, A.; Fernández De La Pradilla, R.; Junquera, E.; Aicart, E.; López-Rodríguez, M. L.; Ortega-Gutiérrez, S. Development of Molecular Probes for the Human 5-HT₆ Receptor. *J. Med. Chem.* **2010**, 53 (19), 7095–7106.
- (176) Hello Bio Ltd. CA201019 CellAura fluorescent 5-HT_{2A/2B} receptor antagonist [4F4PP] <https://hellobio.com/ca201019-cellaura-fluorescent-5-ht2a-2b-receptor-antagonist-4f4pp.html> (accessed Dec 9, 2023).
- (177) Sykes, D.; Lochray, J.; Comfort, F. M. H.; Jain, P.; Charlton, J. S. Exploring the Kinetic Selectivity of Antipsychotics for Dopamine D₂ and 5-HT_{2A} Receptors: Implications for the Prevalence of EPS and Receptor Occupancy. *bioRxiv* **2021**, 2021.11.14.468520.

7. References

- (178) Ettrup, A.; Hansen, M.; Santini, M. A.; Paine, J.; Gillings, N.; Palner, M.; Lehel, S.; Herth, M. M.; Madsen, J.; Kristensen, J.; Begtrup, M.; Knudsen, G. M. Radiosynthesis and in Vivo Evaluation of a Series of Substituted ¹¹C-Phenethylamines as 5-HT_{2A} Agonist PET Tracers. *Eur. J. Nucl. Med. Mol. Imaging* **2011**, *38* (4), 681–693.
- (179) Congreve, M.; Andrews, S. P.; Dore, A. S.; Hollenstein, K.; Hurrell, E.; Langmead, C. J.; Mason, J. S.; Ng, I. W.; Tehan, B.; Zhukov, A.; Weir, M.; Marshall, F. H. Discovery of 1,2,4-Triazine Derivatives as Adenosine A_{2A} Antagonists Using Structure Based Drug Design. *J. Med. Chem.* **2012**, *55*, 1898–1903.
- (180) Wang, H. W.; Wang, J. W. How Cryo-Electron Microscopy and X-Ray Crystallography Complement Each Other. *Protein Sci.* **2017**, *26* (1), 32–39.
- (181) Barringer, R. Illuminating the Secrets of Crystals: Microcrystal Electron Diffraction in Structural Biology. *Biosci. Horizons* **2018**, *11*, 1–12.
- (182) Bachelard, H. NMR of Macromolecules. A Practical Approach Edited by G. C. K. Roberts (The Practical Approach Series; Series Editors, D. Rickwood and B. D. Hames). Oxford University Press, New York, 1993; 399 Pp., Cloth, ISBN 0-19-963225-1, \$68.00; Paperback, ISBN 0-19-. *J. Neurochem.* **1995**, *64* (1), 468–469.
- (183) Krieger, E.; Nabuurs, S. B.; Vriend, G. Chapter 25: Homology Modeling. *Struct. Bioinforma.* **2003**, *44*, 507–521.

7. References

- (184) Waterhouse, A.; Bertoni, M.; Bienert, S.; Studer, G.; Tauriello, G.; Gumienny, R.; Heer, F. T.; De Beer, T. A. P.; Rempfer, C.; Bordoli, L.; Lepore, R.; Schwede, T. SWISS-MODEL: Homology Modelling of Protein Structures and Complexes. *Nucleic Acids Res.* **2018**, *46* (W1), W296–W303.
- (185) Isberg, V.; Mordalski, S.; Munk, C.; Rataj, K.; Harpsøe, K.; Hauser, A. S.; Vroling, B.; Bojarski, A. J.; Vriend, G.; Gloriam, D. E. GPCRdb: An Information System for G Protein-Coupled Receptors. *Nucleic Acids Res.* **2016**, *44* (D1), D356–D364.
- (186) Runyon, S. P.; Mosier, P. D.; Roth, B. L.; Glennon, R. A.; Westkaemper, R. B. Potential Modes of Interaction of 9-Aminomethyl-9,10-Dihydroanthracene (AMDA) Derivatives with the 5-HT_{2A} Receptor: A Ligand Structure-Affinity Relationship, Receptor Mutagenesis and Receptor Modeling Investigation. *J. Med. Chem.* **2008**, *51* (21), 6808–6828.
- (187) Pecic, S.; Makkar, P.; Chaudhary, S.; Reddy, B. V.; Navarro, H. A.; Harding, W. W. Affinity of Aporphines for the Human 5-HT_{2A} Receptor: Insights from Homology Modeling and Molecular Docking Studies. *Bioorganic Med. Chem.* **2010**, *18* (15), 5562–5575.
- (188) Shah, U. H.; Gaitonde, S. A.; Moreno, J. L.; Glennon, R. A.; Dukat, M.; González-Maeso, J. Revised Pharmacophore Model for 5-HT_{2A} Receptor Antagonists Derived from the Atypical Antipsychotic

7. References

- Agent Risperidone. *ACS Chem. Neurosci.* **2019**, *10* (5), 2318–2331.
- (189) Benkert, P.; Tosatto, S. C. E.; Schomburg, D. QMEAN: A Comprehensive Scoring Function for Model Quality Assessment. *Proteins Struct. Funct. Genet.* **2008**, *71* (1), 261–277.
- (190) Benkert, P.; Biasini, M.; Schwede, T. Toward the Estimation of the Absolute Quality of Individual Protein Structure Models. *Bioinformatics* **2011**, *27* (3), 343–350.
- (191) Ramachandran, G. N.; Ramakrishnan, C.; Sasisekharan, V. Stereochemistry of Polypeptide Chain Configurations. *J. Mol. Biol.* **1963**, *7* (1), 95–99.
- (192) Wang, G.; Dunbrack, L. R., J. PISCES: A Protein Sequence Culling Server. *Bioinformatics* **2003**, *19*, 1589–1591.
- (193) Chen, V. B.; Arendall, W. B.; Headd, J. J.; Keedy, D. A.; Immormino, R. M.; Kapral, G. J.; Murray, L. W.; Richardson, J. S.; Richardson, D. C. MolProbity: All-Atom Structure Validation for Macromolecular Crystallography. *Acta Crystallogr. Sect. D Biol. Crystallogr.* **2010**, *66* (1), 12–21.
- (194) Halgren, T. A.; Murphy, R. B.; Friesner, R. A.; Beard, H. S.; Frye, L. L.; Pollard, W. T.; Banks, J. L. Glide: A New Approach for Rapid, Accurate Docking and Scoring. 2. Enrichment Factors in Database Screening. *J. Med. Chem.* **2004**, *47* (7), 1750–1759.
- (195) Friesner, R. A.; Murphy, R. B.; Repasky, M. P.; Frye, L. L.; Greenwood,

7. References

- J. R.; Halgren, T. A.; Sanschagrin, P. C.; Mainz, D. T. Extra Precision Glide: Docking and Scoring Incorporating a Model of Hydrophobic Enclosure for Protein-Ligand Complexes. *J. Med. Chem.* **2006**, *49* (21), 6177–6196.
- (196) Eldridge, M. D.; Murray, C. W.; Auton, T. R.; Paolini, G. V; Mee, R. P. Empirical Scoring Functions: I. The Development of a Fast Empirical Scoring Function to Estimate the Binding Affinity of Ligands in Receptor Complexes. *J. Comput. Aided. Mol. Des.* **1997**, *11* (5), 425–445.
- (197) McNutt, A. T.; Bisiriyu, F.; Song, S.; Vyas, A.; Hutchison, G. R.; Koes, D. R. Conformer Generation for Structure-Based Drug Design: How Many and How Good? *J. Chem. Inf. Model.* **2023**, *63* (21), 6598–6607.
- (198) Åqvist, J.; Medina, C.; Samuelsson, J.-E. A New Method for Predicting Binding Affinity in Computer-Aided Drug Design. *Protein Eng. Des. Sel.* **1994**, *7* (3), 385–391.
- (199) Kollman, P. A.; Massova, I.; Reyes, C.; Kuhn, B.; Huo, S.; Chong, L.; Lee, M.; Lee, T.; Duan, Y.; Wang, W.; Donini, O.; Cieplak, P.; Srinivasan, J.; Case, D. A.; Cheatham, T. E. Calculating Structures and Free Energies of Complex Molecules: Combining Molecular Mechanics and Continuum Models. *Acc. Chem. Res.* **2000**, *33* (12), 889–897.
- (200) Lyne, P. D.; Lamb, M. L.; Saeh, J. C. Accurate Prediction of the

7. References

- Relative Potencies of Members of a Series of Kinase Inhibitors Using Molecular Docking and MM-GBSA Scoring. *J. Med. Chem.* **2006**, *49* (16), 4805–4808.
- (201) Kollman, P. Free Energy Calculations: Applications to Chemical and Biochemical Phenomena. *Chem. Rev.* **1993**, *93* (7), 2395–2417.
- (202) Wan, S Tresadern, G.; Pérez-Benito, L.; van Vlijmen, H.; Coveney, P, V. Accuracy and Precision OfAlchemical Relative Free Energy Predictions with and without Replica-Exchange. 2020, p 1900195.
- (203) Ngo, S. T.; Vu, K. B.; Bui, L. M.; Vu, V. V. Effective Estimation of Ligand-Binding Affinity Using Biased Sampling Method. *ACS Omega* **2019**, *4* (2), 3887–3893.
- (204) Gilson, M. K.; Given, J. A.; Bush, B. L.; McCammon, J. A. The Statistical-Thermodynamic Basis for Computation of Binding Affinities: A Critical Review. *Biophys. J.* **1997**, *72* (3), 1047–1069.
- (205) Srinivasan, J.; Cheatham, T. E.; Cieplak, P.; Kollman, P. A.; Case, D. A. Continuum Solvent Studies of the Stability of DNA, RNA, and Phosphoramidate-DNA Helices. *J. Am. Chem. Soc.* **1998**, *120* (37), 9401–9409.
- (206) Pearlman, D. A. Evaluating the Molecular Mechanics Poisson-Boltzmann Surface Area Free Energy Method Using a Congeneric Series of Ligands to P38 MAP Kinase. *J. Med. Chem.* **2005**, *48* (24), 7796–7807.

7. References

- (207) Adler, M.; Beroza, P. Improved Ligand Binding Energies Derived from Molecular Dynamics: Replicate Sampling Enhances the Search of Conformational Space. *J. Chem. Inf. Model.* **2013**, *53* (8), 2065–2072.
- (208) Xu, L.; Sun, H.; Li, Y.; Wang, J.; Hou, T. Assessing the Performance of MM/PBSA and MM/GBSA Methods. 3. the Impact of Force Fields and Ligand Charge Models. *J. Phys. Chem. B* **2013**, *117* (28), 8408–8421.
- (209) Sadiq, S. K.; Wright, D. W.; Kenway, O. A.; Coveney, P. V. Accurate Ensemble Molecular Dynamics Binding Free Energy Ranking of Multidrug-Resistant HIV-1 Proteases. *J. Chem. Inf. Model.* **2010**, *50* (5), 890–905.
- (210) Sahil, M.; Sarkar, S.; Mondal, J. Long-Time-Step Molecular Dynamics Can Retard Simulation of Protein-Ligand Recognition Process. *Biophys. J.* **2023**, *122* (5), 802–816.
- (211) Bhati, A. P.; Hoti, A.; Potterton, A.; Bieniek, M. K.; Coveney, P. V. Long Time Scale Ensemble Methods in Molecular Dynamics: Ligand-Protein Interactions and Allostery in SARS-CoV-2 Targets. *J. Chem. Theory Comput.* **2023**, *19* (11), 3359–3378.
- (212) Caves, D. S.; EVANSECK, D. J.; KARPLUS, M. Locally Accessible Conformations of Proteins: Multiple Molecular Dynamics Simulations of Crambin. *Protein Sci.* **1998**, *7*, 649–666.
- (213) Maffucci, I.; Contini, A. Explicit Ligand Hydration Shells Improve the

7. References

- Correlation between MM-PB/GBSA Binding Energies and Experimental Activities. *J. Chem. Theory Comput.* **2013**, 9 (6), 2706–2717.
- (214) Hou, T.; Wang, J.; Li, Y.; Wang, W. Assessing the Performance of the MM/PBSA and MM/GBSA Methods. 1. The Accuracy of Binding Free Energy Calculations Based on Molecular Dynamics Simulations. *J. Chem. Inf. Model.* **2011**, 51 (1), 69–82.
- (215) Hayes, J. M.; Archontis, G. *MM-GB(PB)SA Calculations of Protein-Ligand Binding Free Energies*; IntechOpen: Rijeka, 2012.
- (216) Gohlke, H.; Homeyer, N. Free Energy Calculations by the Molecular Mechanics Poisson Boltzmann Surface Area Method. *Mol. Inform.* **2012**, 31, 114–122.
- (217) Honig, B.; Nicholls, A. Classical Electrostatics in Biology and Chemistry. *Science* **1995**, 268, 1144–1149.
- (218) Gohlke, H.; Kiel, C.; Case, D. A. Insights into Protein-Protein Binding by Binding Free Energy Calculation and Free Energy Decomposition for the Ras-Raf and Ras-RalGDS Complexes. *J. Mol. Biol.* **2003**, 330 (4), 891–913.
- (219) Huang, N.; Kalyanaraman, C.; Bernacki, K.; Jacobson, M. P. Molecular Mechanics Methods for Predicting Protein-Ligand Binding. *Phys. Chem. Chem. Phys.* **2006**, 8 (44), 5166–5177.
- (220) Genheden, S.; Ryde, U. How to Obtain Statistically Converged

7. References

- MM/GBSA Results. *J. Comput. Chem.* **2009**, *31*, 837–846.
- (221) Genheden, S.; Ryde, U. The MM/PBSA and MM/GBSA Methods to Estimate Ligand-Binding Affinities. *Expert Opin. Pharmacother.* **2015**, *10* (5), 449–461.
- (222) Tan, C.; Tan, Y. H.; Luo, R. Implicit Nonpolar Solvent Models. *J. Phys. Chem. B* **2007**, *111* (42), 12263–12274.
- (223) Gouda, H.; Kuntz, I. D.; Case, D. A.; Kollman, P. A. Free Energy Calculations for Theophylline Binding to an RNA Aptamer Comparison of MM-PBSA and Thermodynamic Integration Methods. *Biopolymers* **2003**, *68*, 16–34.
- (224) Ohtaka, H.; Velázquez-Campoy, A.; Xie, D.; Freire, E. Overcoming Drug Resistance in HIV-1 Chemotherapy: The Binding Thermodynamics of Amprenavir and TMC-126 to Wild-type and Drug-resistant Mutants of the HIV-1 Protease. *Protein Sci.* **2002**, *11* (8), 1908–1916.
- (225) Velazquez-campoy, A.; Todd, M. J.; Freire, E. HIV-1 Protease Inhibitors: Enthalpic versus Entropic Optimization of the Binding Affinity. **2000**, 2201–2207.
- (226) Lafont, V.; Armstrong, A. A.; Ohtaka, H.; Kiso, Y.; Mario Amzel, L.; Freire, E. Compensating Enthalpic and Entropic Changes Hinder Binding Affinity Optimization. *Chem. Biol. Drug Des.* **2007**, *69* (6), 413–422.

7. References

- (227) Tarcsay, Á.; Keseru, G. M. Is There a Link between Selectivity and Binding Thermodynamics Profiles? *Drug Discov. Today* **2015**, *20* (1), 86–94.
- (228) Agarwal, A.; Pearson, P. P.; Taylor, E. W.; Li, H. B.; Dahlgren, T.; Herslöf, M.; Yang, Y.; Lambert, G.; Nelson, D. L.; Regan, J. W.; Martin, A. R. Three-Dimensional Quantitative Structure-Activity Relationships of 5-HT Receptor Binding Data for Tetrahydropyridinylindole Derivatives: A Comparison of the Hansch and CoMFA Methods. *J. Med. Chem.* **1993**, *36* (25), 4006–4014.
- (229) Gandhimathi, A.; Sowdhamini, R. Molecular Modelling of Human 5-Hydroxytryptamine Receptor (5-HT_{2A}) and Virtual Screening Studies towards the Identification of Agonist and Antagonist Molecules. *J. Biomol. Struct. Dyn.* **2016**, *34* (5), 952–970.
- (230) Sterling, T.; Irwin, J. J. ZINC 15 - Ligand Discovery for Everyone. *J. Chem. Inf. Model.* **2015**, *55* (11), 2324–2337.
- (231) Shan, J.; Khelashvili, G.; Mondal, S.; Mehler, E. L.; Weinstein, H. Ligand-Dependent Conformations and Dynamics of the Serotonin 5-HT_{2A} Receptor Determine Its Activation and Membrane-Driven Oligomerization Properties. *PLOS Comput. Biol.* **2012**, *8* (4), e1002473.
- (232) Perez-Aguilar, J. M.; Shan, J.; Levine, M. V.; Khelashvili, G.; Weinstein, H. A Functional Selectivity Mechanism at the Serotonin-

7. References

- 2A GPCR Involves Ligand-Dependent Conformations of Intracellular Loop 2. *J. Am. Chem. Soc.* **2014**, *136* (45), 16044–16054.
- (233) Martí-Solano, M.; Iglesias, A.; Fabritiis, G. de; Sanz, F.; Brea, J.; Loza, M. I.; Pastor, M.; Selent, J. Detection of New Biased Agonists for the Serotonin 5-HT_{2A} Receptor: Modeling and Experimental Validation. *Mol. Pharmacol.* **2015**, *87* (4), 740–746.
- (234) Lyu, J.; Wang, S.; Balias, T. E.; Singh, I.; Levit, A.; Moroz, Y. S.; O'Meara, M. J.; Che, T.; Alga, E.; Tolmachova, K.; Tolmachev, A. A.; Shoichet, B. K.; Roth, B. L.; Irwin, J. J. Ultra-Large Library Docking for Discovering New Chemotypes. *Nature* **2019**, *566* (7743), 224–229.
- (235) Consortium, T. U. UniProt : The Universal Protein Knowledgebase in 2021. **2021**, *49*, 480–489.
- (236) Altschul, S. F.; Gish, W.; Miller, W.; Myers, E. W.; Lipman, D. J. Basic Local Alignment Search Tool. *J. Mol. Biol.* **1990**, *215* (3), 403–410.
- (237) Remmert, M.; Biegert, A.; Hauser, A.; Söding, J. HHblits: Lightning-Fast Iterative Protein Sequence Searching by HMM-HMM Alignment. *Nat. Methods* **2012**, *9* (2), 173–175.
- (238) Steinegger, M.; Meier, M.; Mirdita, M.; Vöhringer, H.; Haunsberger, S. J.; Söding, J. HH-Suite3 for Fast Remote Homology Detection and Deep Protein Annotation. *BMC Bioinformatics* **2019**, *20* (1), 1–15.

7. References

- (239) Mirdita, M.; Von Den Driesch, L.; Galiez, C.; Martin, M. J.; Soding, J.; Steinegger, M. Uniclust Databases of Clustered and Deeply Annotated Protein Sequences and Alignments. *Nucleic Acids Res.* **2017**, *45* (D1), D170–D176.
- (240) Abeln, S.; Feenstra, K. A.; Heringa, J. *Protein Three-Dimensional Structure Prediction*; Elsevier Ltd., 2018; Vol. 1–3.
- (241) Studer, G.; Tauriello, G.; Bienert, S.; Biasini, M.; Johner, N.; Schwede, T. ProMod3 - A Versatile Homology Modelling Toolbox. *PLoS Comput. Biol.* **2021**, *17* (1), 1–18.
- (242) Shelley, J. C.; Cholleti, A.; Frye, L. L.; Greenwood, J. R.; Timlin, M. R.; Uchimaya, M. Epik: A Software Program for PKa Prediction and Protonation State Generation for Drug-like Molecules. *J. Comput. Aided. Mol. Des.* **2007**, *21* (12), 681–691.
- (243) Greenwood, J. R.; Calkins, D.; Sullivan, A. P.; Shelley, J. C. Towards the Comprehensive, Rapid, and Accurate Prediction of the Favorable Tautomeric States of Drug-like Molecules in Aqueous Solution. *J. Comput. Aided. Mol. Des.* **2010**, *24* (6–7), 591–604.
- (244) Lu, C.; Wu, C.; Ghoreishi, D.; Chen, W.; Wang, L.; Damm, W.; Ross, G. A.; Dahlgren, M. K.; Russell, E.; Von Bargen, C. D.; Abel, R.; Friesner, R. A.; Harder, E. D. OPLS4: Improving Force Field Accuracy on Challenging Regimes of Chemical Space. *J. Chem. Theory Comput.* **2021**, *17* (7), 4291–4300.
- (245) Emtage, A. L.; Mistry, S. N.; Fischer, P. M.; Kellam, B.; Laughton, C.

7. References

- A. GPCRs through the Keyhole: The Role of Protein Flexibility in Ligand Binding to β -Adrenoceptors. *J. Biomol. Struct. Dyn.* **2017**, 35 (12), 2604–2619.
- (246) Roth, B. L.; Shoham, M.; Choudhary, M. S.; Khan, N. Identification of Conserved Aromatic Residues Essential for Agonist Binding and Second Messenger Production at 5-Hydroxytryptamine_{2A} Receptors. *Mol. Pharmacol.* **1997**, 52 (2), 259–266.
- (247) Kolakowski, L. F. J. GCRDb: A G-Protein-Coupled Receptor Database. *Receptors Channels* **1994**, 2 (1), 1–7.
- (248) Madhavi Sastry, G.; Adzhigirey, M.; Day, T.; Annabhimoju, R.; Sherman, W. Protein and Ligand Preparation: Parameters, Protocols, and Influence on Virtual Screening Enrichments. *J. Comput. Aided. Mol. Des.* **2013**, 27 (3), 221–234.
- (249) Li, J.; Abel, R.; Zhu, K.; Cao, Y.; Zhao, S.; Friesner, R. A. The VSGB 2.0 Model: A next Generation Energy Model for High Resolution Protein Structure Modeling. *Proteins Struct. Funct. Bioinforma.* **2011**, 79 (10), 2794–2812.
- (250) Jacobson, M. P.; Pincus, D. L.; Rapp, C. S.; Day, T. J. F.; Honig, B.; Shaw, D. E.; Friesner, R. A. A Hierarchical Approach to All-Atom Protein Loop Prediction. *Proteins Struct. Funct. Genet.* **2004**, 55 (2), 351–367.
- (251) Pantzar, T.; Poso, A. Binding Affinity via Docking: Fact and Fiction. *Molecules* **2018**, 23, 1899.

7. References

- (252) Bender, B. J.; Gahbauer, S.; Lutten, A.; Lyu, J.; Webb, C. M.; Stein, R. M.; Fink, E. A.; Balius, T. E.; Carlsson, J.; Irwin, J. J.; Shoichet, B. K. A Practical Guide to Large-Scale Docking. *Nat. Protoc.* **2021**, *16* (10), 4799–4832.
- (253) Bressa, G. M.; Marini, S.; Gregori, S. Serotonin S₂ Receptors Blockage and Generalized Anxiety Disorders. A Double-Blind Study on Ritanserin and Lorazepam. *Int. J. Clin. Pharmacol. Res.* **1987**, *7* (2), 111–119.
- (254) Weisstaub, N. V.; Zhou, M.; Lira, A.; Lambe, E.; González-Maeso, J.; Hornung, J.-P.; Sibille, E.; Underwood, M.; Itohara, S.; Dauer, W. T.; Ansorge, M. S.; Morelli, E.; Mann, J. J.; Toth, M.; Aghajanian, G.; Sealfon, S. C.; Hen, R.; Gingrich, J. A. Cortical 5-HT_{2A} Receptor Signaling Modulates Anxiety-Like Behaviors in Mice. *Science* (80-). **2006**, *313*, 536–540.
- (255) González-Maeso, J.; Ang, R. L.; Yuen, T.; Chan, P.; Weisstaub, N. V.; López-Giménez, J. F.; Zhou, M.; Okawa, Y.; Callado, L. F.; Milligan, G.; Gingrich, J. A.; Filizola, M.; Meana, J. J.; Sealfon, S. C. Identification of a Serotonin/Glutamate Receptor Complex Implicated in Psychosis. *Nature* **2008**, *452*, 93–97.
- (256) Daly, C. J.; McGrath, J. C. Fluorescent Ligands, Antibodies, and Proteins for the Study of Receptors. *Pharmacol. Ther.* **2003**, *100* (2), 101–118.
- (257) Conroy, S.; Kindon, N. D.; Glenn, J.; Stoddart, L. A.; Lewis, R. J.; Hill,

7. References

- S. J.; Kellam, B.; Stocks, M. J. Synthesis and Evaluation of the First Fluorescent Antagonists of the Human P2Y₂ Receptor Based on AR-C118925. *J. Med. Chem.* **2018**, *61* (7), 3089–3113.
- (258) Lacivita, E.; Masotti, A. C.; Jafurulla, M.; Saxena, R.; Rangaraj, N.; Chattopadhyay, A.; Colabufo, N. A.; Berardi, F.; Perrone, R.; Leopoldo, M. Identification of a Red-Emitting Fluorescent Ligand for in Vitro Visualization of Human Serotonin 5-HT_{1A} Receptors. *Bioorganic Med. Chem. Lett.* **2010**, *20* (22), 6628–6632.
- (259) Stoddart, L. A.; Vernall, A. J.; Briddon, S. J.; Kellam, B.; Hill, S. J. Direct Visualisation of Internalization of the Adenosine A₃ Receptor and Localization with Arrestin3 Using a Fluorescent Agonist. *Neuropharmacology* **2015**, *98*, 68–77.
- (260) Cottet, M.; Faklaris, O.; Zwier, J. M.; Trinquet, E.; Pin, J. P.; Durroux, T. Original Fluorescent Ligand-Based Assays Open New Perspectives in G-Protein Coupled Receptor Drug Screening. *Pharmaceuticals* **2011**, *4* (1), 202–214.
- (261) Sexton, M.; Woodruff, G.; Horne, E. A.; Lin, Y. H.; Muccioli, G. G.; Bai, M.; Stern, E.; Bornhop, D. J.; Stella, N. NIR-Mbc94, a Fluorescent Ligand That Binds to Endogenous CB₂ Receptors and Is Amenable to High-Throughput Screening. *Chem. Biol.* **2011**, *18* (5), 563–568.
- (262) Stoddart, L. A.; Vernall, A. J.; Denman, J. L.; Briddon, S. J.; Kellam, B.; Hill, S. J. Fragment Screening at Adenosine-A₃ Receptors in Living Cells Using a Fluorescence-Based Binding Assay. *Chem.*

7. References

- Biol.* **2012**, *19* (9), 1105–1115.
- (263) Casella, B. M.; Farmer, J. P.; Nesheva, D. N.; Williams, H. E. L.; Charlton, S. J.; Holliday, N. D.; Laughton, C. A.; Mistry, S. N. Design, Synthesis, and Application of Fluorescent Ligands Targeting the Intracellular Allosteric Binding Site of the CXC Chemokine Receptor 2. *J. Med. Chem.* **2023**, *66* (18), 12911–12930.
- (264) Glennon, R. A.; Seggel, M. R.; Soine, W. H.; Herrick-Davis, K.; Lyon, R. A.; Titeler, M. Iodine-125 Labeled 1-(2,5-Dimethoxy-4-Iodophenyl)-2-Aminopropane: An Iodinated Radioligand That Specifically Labels the Agonist High-Affinity State of 5-HT₂ Serotonin Receptors. *J. Med. Chem.* **1988**, *31* (1), 5–7.
- (265) Canal, C. E.; Morgan, D. Head-Twitch Response in Rodents Induced by the Hallucinogen 2,5-Dimethoxy-4-Iodoamphetamine: A Comprehensive History, a Re-Evaluation of Mechanisms, and Its Utility as a Model. *Drug Test. Anal.* **2012**, *4* (7–8), 556–576.
- (266) Cho, A. K.; Segal, D. S. *Amphetamine and Its Analogs: Psychopharmacology, Toxicology, and Abuse*; Academic Press: San Diego, 1994.
- (267) C, Sheehan, J.; P, Hess, G. A New Method of Forming Peptide Bonds. *J. Am. Chem. Soc.* **1955**, *77* (4), 1067–1068.
- (268) Rosenkranz, R. P.; Hoffman, B. B.; Jacobson, K. A.; Verlander, M. S.; Klevans, L.; O'Donnell, M.; Goodman, M.; Melmon, K. L. Conjugates of Catecholamines. II. In Vitro and in Vivo Pharmacological Activity

7. References

- of N-Alkyl-Functionalized Carboxylic Acid Congeners and Amides Related to Isoproterenol. *Mol. Pharmacol.* **1983**, *24* (3), 429–435.
- (269) Jacobson, K. A.; Kirk, K. L.; Padgett, W. L.; Daly, J. W. Functionalized Congeners of Adenosine: Preparation of Analogs with High Affinity for A1-Adenosine Receptors. *J. Med. Chem.* **1985**, *28* (9), 1341–1346.
- (270) Comeo, E.; Kindon, N. D.; Soave, M.; Stoddart, L. A.; Kilpatrick, L. E.; Scammells, P. J.; Hill, S. J.; Kellam, B. Subtype-Selective Fluorescent Ligands as Pharmacological Research Tools for the Human Adenosine A2A Receptor. *J. Med. Chem.* **2020**, *63*, 2656–2672.
- (271) Jacobson, K. A.; Ukena, D.; Padgett, W.; Kirk, K. L.; Daly, J. W. Molecular Probes for Extracellular Adenosine Receptors. *Biochem. Pharmacol.* **1987**, *36* (10), 1697–1707.
- (272) Jacobson, K. A. Functionalized Congener Approach to the Design of Ligands for G Protein-Coupled Receptors (GPCRs). *Bioconjug. Chem.* **2009**, *20* (10), 1816–1835.
- (273) Comeo, E.; Kindon, N. D.; Stoddart, L. A.; Laura, E.; Scammells, P. J.; Hill, S. J.; Kellam, B. Supporting Information Subtype-Selective Fluorescent Ligands as Pharmacological Research Tools for the Human Adenosine A2AAR Receptor. *J. Med. Chem.* **2020**, *63*, S1–S9.
- (274) Baker, J. G.; Middleton, R.; Adams, L.; May, L. T.; Briddon, S. J.;

7. References

- Kellam, B.; Hill, S. J. Influence of Fluorophore and Linker Composition on the Pharmacology of Fluorescent Adenosine A₁ Receptor Ligands: Themed Section: Imaging in Pharmacology Research Paper. *Br. J. Pharmacol.* **2010**, *159* (4), 772–786.
- (275) Dale, C. L.; Hill, S. J.; Kellam, B. New Potent, Short-Linker BODIPY-630/650TM Labelled Fluorescent Adenosine Receptor Agonists. *Medchemcomm* **2012**, *3* (3), 333–338.
- (276) Comeo, E.; Trinh, P.; Nguyen, A. T.; Nowell, C. J.; Kindon, N. D.; Soave, M.; Stoddart, L. A.; White, J. M.; Hill, S. J.; Kellam, B.; Halls, M. L.; May, L. T.; Scammells, P. J. Development and Application of Subtype-Selective Fluorescent Antagonists for the Study of the Human Adenosine A₁ Receptor in Living Cells. *J. Med. Chem.* **2021**, *64* (10), 6670–6695.
- (277) Vernall, A. J.; Stoddart, L. A.; Briddon, S. J.; Ng, H. W.; Laughton, C. A.; Doughty, S. W.; Hill, S. J.; Kellam, B. Conversion of a Non-Selective Adenosine Receptor Antagonist into A₃-Selective High Affinity Fluorescent Probes Using Peptide-Based Linkers. *Org. Biomol. Chem.* **2013**, *11* (34), 5673–5682.
- (278) Invitrogen. Chapter 01 - Fluorophores and Their Amine-Reactive Probes Derivatives. *Mol. Probes Handbook- A Guid. to Fluoresc. Probes Labeling Technol. 11th Ed.* **2010**, 1–88.
- (279) Kulkarni, P. P.; Kadam, A. J.; Mane, R. B.; Desai, U. V.; Wadgaonkar, P. P. Demethylation of Methyl Aryl Ethers Using Pyridine

7. References

- Hydrochloride in Solvent-Free Conditions under Microwave Irradiation. *J. Chem. Res. - Part S* **1999**, No. 6, 394–395.
- (280) Lord, R. L.; Korich, A. L.; Conrad, H. A.; Kosak, T. M.; Conrad, H. A.; Korich, A. L.; Lord, R. L. Ether Cleavage Re-Investigated: Elucidating the Mechanism of BBr₃-Facilitated Demethylation of Aryl Methyl Ethers. *European J. Org. Chem.* **2015**, 7460–7467.
- (281) Mathew, A. E.; Stella, V. J.; Mejillano, M. R.; Nath, J. P.; Himes, R. H.; Mathew, A. E.; Nath, J. P. Synthesis and Evaluation of Some Water-Soluble Prodrugs and Derivatives of Taxol with Antitumor Activity. *J. Med. Chem.* **1992**, 35 (1), 145–151.
- (282) Attie, A. D.; Raines, R. T. Analysis of Receptor – Ligand Interactions. **2017**, 72 (2), 119–124.
- (283) David, A.; Vannice, M. A. Control of Catalytic Debenzylation and Dehalogenation Reactions during Liquid-Phase Reduction by H₂. *J. Catal.* **2006**, 237 (2), 349–358.
- (284) Dale, N. C.; Johnstone, E. K. M.; White, C. W.; Pflieger, K. D. G. NanoBRET: The Bright Future of Proximity-Based Assays. *Front. Bioeng. Biotechnol.* **2019**, 7 (MAR), 1–13.
- (285) Alcobia, D. C.; Ziegler, A. I.; Kondrashov, A.; Comeo, E.; Mistry, S.; Kellam, B.; Chang, A.; Woolard, J.; Hill, S. J.; Sloan, E. K. Visualizing Ligand Binding to a GPCR In Vivo Using NanoBRET. *iScience* **2018**, 6, 280–288.

7. References

- (286) Finkelstein, H. Darstellung Organischer Jodide Aus Den Entsprechenden Bromiden Und Chloriden. *Berichte der Dtsch. Chem. Gesellschaft* **1910**, 43 (2), 1528–1532.
- (287) Motulsky, H. J.; Mahan, L. C. The Kinetics of Competitive Radioligand Binding Predicted by the Law of Mass Action. *Mol. Pharmacol.* **1984**, 25 (1), 1–9.
- (288) Sykes, D. A.; Moore, H.; Stott, L.; Holliday, N.; Javitch, J. A.; Robert Lane, J.; Charlton, S. J. Extrapiramidal Side Effects of Antipsychotics Are Linked to Their Association Kinetics at Dopamine D2 Receptors. *Nat. Commun.* **2017**, 8 (1), 1–11.
- (289) Sykes, D. A.; Dowling, M. R.; Charlton, S. J. Measuring Receptor Target Coverage: A Radioligand Competition Binding Protocol for Assessing the Association and Dissociation Rates of Unlabeled Compounds. *Curr. Protoc. Pharmacol.* **2010**, 50 (1), 9.14.1-9.14.30.
- (290) Yung-Chi, C.; Prusoff, W. H. Relationship between the Inhibition Constant (KI) and the Concentration of Inhibitor Which Causes 50 per Cent Inhibition (I50) of an Enzymatic Reaction. *Biochem. Pharmacol.* **1973**, 22 (23), 3099–3108.
- (291) Willcott, M. R. MestRe Nova. *J. Am. Chem. Soc.* **2009**, 131 (36), 13180–13180.